EXPERIMENTAL STUDIES OF SOIL BEHAVIOR SUBJECTED TO DRYING

A Thesis

by

DUAA ABDULRAZZAQ FALIH AL-JEZNAWI

Submitted to the Office of Graduate and Professional Studies of
Texas A&M University
in partial fulfillment of the requirements for the degree of

MASTER OF SCIENCE

Chair of Committee,	Marcelo Sanchez
Committee Members,	Charles Aubeny
	Eduardo Gildin
Head of Department,	Robin Autenrieth

May 2015

Major Subject: Civil Engineering

ABSTRACT

Expansive soils (also known as shrink/swell soils) are encountered in different regions of the world. The behavior of this type of soils is quiet complex. They fall in the category of 'problematic soils'. One a typical characteristics of this material is the formation of cracks during drying and shrinkage. The presence of cracks in soils is very detrimental as its affects the hydraulic behavior (e.g. providing pathways for water flow and pollutant transport) and the mechanical behavior (e.g. impacting on soil strength and other mechanical properties). As a consequence, the presence of cracks in soils may, amongst other: trigger landslides, increase the infiltration capacity of soils, and induce differential settlement in buildings. One of the aims of this thesis is to improve our current understanding on crack formation and propagation. Soil curling is another phenomenon associated with soil drying. The goal of this study is to enhance the understanding of the behavior of soils under drying conditions. This would expand our capabilities in dealing with a wide spectrum of geotechnical and geologic problems related to the modeling of shrink-swell soils.

The literature review performed in this thesis detected significant gaps in the knowledge regarding factors and parameters that control the development and propagation of desiccation cracks in soils and also curling deformation in soils. In this research, these phenomena associated with soil drying were studied through laboratory experiments using different mixtures of artificial soils.

This thesis includes experimental and theoretical investigations of drying soil under different conditions. For this purpose, a total of thirteen tests related to cracking and shrinking were carried out; considering: i) different soil mixtures; ii) different environmental conditions at controlled relative humidity (i.e. testing at the lab atmosphere versus testing inside a desiccator under controlled relative humidity conditions); iii) different roughness of the soil-plate interface (i.e. rough versus smooth surfaces); and iv) different water salinity (i.e. distilled water versus saturated salt solutions). Additionally, the effect of wetting and drying cycles on soil cracking pattern was also investigated. The results of these tests were analyzed based on both visual inspection and via image analysis techniques (using the *image j* software). This technique facilitates the process of determining the location and severity of cracked areas and it also provides useful information to determine the width, length, and shape of the cracks.

The soil shear parameters (i.e. cohesion and friction angle) and the soil-interface strength parameters (i.e. soil-interface adhesion and interface friction angle) for the kaolinite/ bentonite mixture were obtained from the direct shear test. A total of fifty tests were carried out while varying the drainage conditions (i.e. drained or undrained conditions), soil water content, soil-plate contact surface (i.e. smooth or rough), and the normal load. Since curling phenomenon was visually observed in some samples, a set of additional eleven drying tests were carried out to study in more detail this feature of soil behavior.

The effect of two main factors influencing soil curling was investigated: soil mixture (i.e. percentage of different soils) and initial water content.

The results show that the contact surface has a significant effect on soil behavior during drying. In particular, cracked and uncracked areas, average width of cracks, and the crack intensity factor (CIF) were obtained to determine the development of crack patterns. In general, these parameters are critical when modeling the formation and propagation of cracks. Furthermore, experimental results showed that the maximum shearing resistance is controlled by the drainage conditions, the roughness of the interface material, the water content of the soil, and the normal stress. For a specific soil mixture, the maximum interface shear stress (i.e. maximum shear stress of the soil-grooved plate interface) was observed just before the initiation of the desiccation cracks. Moreover, soil fabric and soil water content have significant effects on soil behavior during drying. It has been observed that particles sizes distribution has a significant effect of soil curling deformation. It was concluded that the particle size distribution of soil samples prepared at high water content (e.g. 2.75× LL and 3× LL; where LL is the soil's liquid limit) is governed by sedimentation phenomenon at early stages of drying.

ACKNOWLEDGEMENTS

I would like to thank my advisor, Dr. Marcelo Sanchez, for his patience, valuable guidance, and support throughout my research, my course work and my residence in the city of college station. He made this university home away from home for me and my colleagues. I would also like to thank Dr. Charles Aubeny and Dr. Eduardo Gildin for serving as my committee members. Furthermore, I would like to thank the Higher Committee for Education Development in Iraq (HCED) for helping me financially to get the great opportunity of studying in the United States of America. I would further like to acknowledge the support of my friends, Ajay, Ghassan, Sola, Kierstyn, Thomas, Dong, Tam, Mojdeh,, Jumanah, Layal, Mabel, Lorena, Rasha, Shwan , Fawaz, Dema, Hussam "Abu Fatima" and his wife, and Raghad. You made it a happier journey for me.

Special thanks go out to my old brother, Hussam "Abu Adam", for his love, support and kindness. You have been my voice, my strength and you made this happen for me. Also, I would like to thank my sister, Marwa, and my brother, Husham, for their endless love. My father figure, my dearest uncle, Ala'a Hussain, thank you for being there for me and my grandmother for her kindness and blessing.

Like I began with you, I am ending this with you, my dearest mother. This is all for you, and because of you and every beautiful thing you have ever been for me. I am the luckiest little girl for having you, my strength and my reason for everything.

TABLE OF CONTENTS

Page

LIST OF FIGURES

Page

LIST OF TABLES

Page

INTRODUCTION

1.1 BACKGROUND

Swelling and shrinkage in soils occur as a result of the seasonal variations in climatic conditions which affect the water retention in soils. Shrinkage deformations, in general, take place due to the drying. Which may be divided in two main types intra-deformations (among the soil particles), and/or global deformations (noticeably change in a soil sample volume); the latter one can be cracking, shrinkage, and/or curling deformation (Zielinski et al., 2014). Cracks on the surface develop in soils as they dry and under conditions of restrained shrinkage. Formation of cracks in the field is generally related to the soil shrinkage during droughts. Intact soils behave totally different from cracked soils because the presence of desiccation cracks in the soil mass changes the behavior of soils in different ways (Lakshmikantha, 2009). Cracks are a common phenomenon in soils in general, and in clayey or expansive soils specifically. Cracks provide routes for water infiltration into soils. The curling phenomenon is defined as a natural soil deformation which is the upward (concave-up) or downward (convex-up) moving of the edges of the soil sample during drying (Zielinski et al., 2014).

Studying how cracks develop can enhance the understanding of a wide spectrum of geotechnical and geological problems. Complex networks of cracks create problems by facilitating the formation of pollutant pathways to the subsoil (Drumm et al., 1997). The

deeper cracks, the more threat we expect because the infiltration capacity of the soil increases during intense drought with deep cracks. Sometimes, horizontal cracks join the vertical cracks and create a network of discontinuities (Konrad and Ayad, 1997; Lakshmikantha, 2009; and Dyer et al., 2009). According to Berney et al. (2008), one of the main factors affect on the development and propagation of subhorizontal cracks in soils is the curling deformation, which is commonly associated with desiccation cracks. Obviously, the subhorizontal cracks increase cracks connectivity inside the soil mass, affecting the soil permeability. The rate at which microorganisms and solutes are transported in the soil is governed by the length, width, depth, tortuosity, spatial distribution and connectivity of cracks (Horgan and Young, 2000). Also, hydraulic properties of soils are directly governed by the networks of the desiccation crack (Chertkov, 2000; Chertkov and Ravina, 1999).

According to Corte and Higashi (1960), cracks generally begin in the center of the soil layer and propagate with non-uniform speed to the surface or to the bottom. Lachenbruch (1961) stated that cracks are usually initiated at the surface of great stress and sometimes at or near the surface and then propagated toward the interior of the medium where the tension decreases. However, according to Towner (1987b), cracks occur as a result of different conditions and they cannot be explained in the same way.. Morris et al. (1994) stated that soil suction and the properties of soil such as modulus of compressibility, Poisson's ratio, tensile strength, shear strength, and specific surface energy control the cracking in soils subjected to drying. Fang (1997) referred that cracks

occur as a result of imbalance of the internal energy in the soil mass which is caused by non-uniform distribution of moisture, temperature, or compaction energy during construction. Weinberger (1999) stated that cracks initiated and propagated from the bottom and move vertically upward to the surface and move laterally outward to the adjacent cracks that occurred during desiccation. Prat et al. (2002) explained the initiation and propagation of cracks in soils is a complicated problem including the mechanics of strain localization and the hydraulic of water flow in both saturated and unsaturated media. According to Nahlawi and Kodikara (2002), when the soil restrains against the change in volume, cracks start to develop as a result of the suction generated in a desiccating soil mass.

Desiccation cracks in soils has become a subject of increasing interest in soil mechanics and geotechnical engineering, with a very large number of publications looking at different aspects of this problem and proposing different theories and ideas to explain and model this complex phenomenon. It is virtually impossible to summarize all of these contributions in a document. Table 1 present some key ideas used to explain the phenomenon of drying cracks in soils and some relevant papers associated with them.

Table 1. 1: Some common hypotheses for development of cracks.

Name	Schematic	Description	Reference
Tensile failure	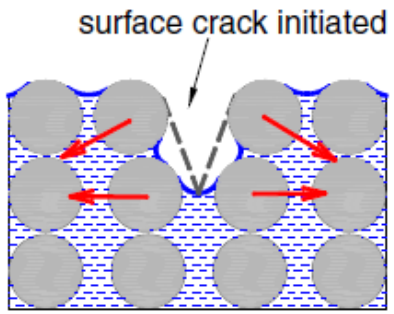	If the initial state of the soil is fully saturated, then water–air interface meniscus develops between soil particles, the tensile stress develops in the upper layer; so the cracks start at the soil surface because of the shrinkage distortion and/or because the tensile stress overcomes the tensile strength of the soil.	Tang et al., 2011; Lachenbruch, 1962; Allen, 1982; Morris et al., 1992; Naser Abu-Hejleh and Znidarcic, 1995; Konrad and Ayad, 1997; Hallett and Newson, 2005; Rodriguez et al., 2007; Sanchez et al., 2014.
Air invasion	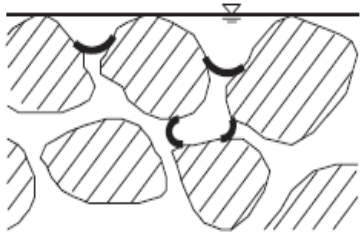	Air invasion is the starting point for desiccation cracks formation.	Childs, 1969; Brinker and Scherer, 1990; Herrera et al., 2007, Shin_ and Santamarina, 2011.

Table 1. 1. Continued.

Name	Schematic	Description	Reference
Irregular drying front	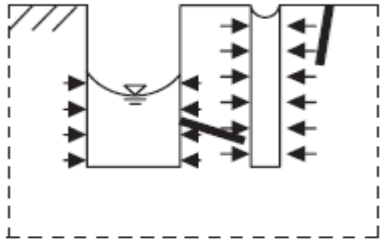	As a result of the difference in capillary pressure, the pore walls fail.	Zarzycki et al., 1982.
Circumferential tension	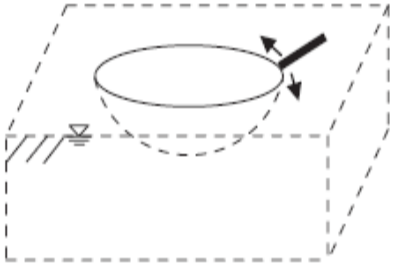	Developing of radial cracks as a results of hoop stress (tension).	Scherer, 1990.
Packing collapse	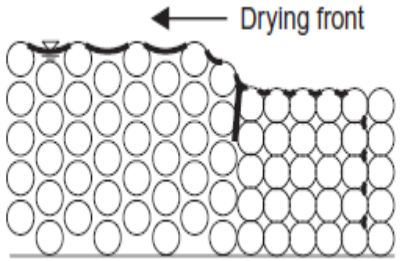	Collapse of soil particles due to the capillary pressure.	Holmes et al., 2006.

1.2 MOTIVATION

For many decades, the phenomenon of cracking in clayey soils has been of interest (e.g. Stirling, Davie, and Glendinning, 2013). The motivation for studying desiccation cracks and the apparent increase in permeability of cracked soils have been increased because of the cracking affects many earth structures including liners (e.g. Philip et al., 2002), foundations (e.g. Silvestri et al 1992), cuttings and embankments (e.g. Smethurst et al 2006). Also, soils can cause damage to the foundations of building during shrinking and swelling that creates a problem for the housing insurance industry (Building Research Establishment-BRE, 1990). Most studies have not been focused on the cracking process (crack formation and propagation), but only focused on soils which already have cracks (Lakshmikantha, 2009). Finally, it is important to mention that the desiccation cracking phenomenon is likely to increase in the future because if the predictions about climate change are confirmed. Therefore, it is necessary to improve our knowledge on the development and propagation of desiccation cracks in soils.

When stresses transfer between the superstructure and the unsaturated soil, the contact surface, should be called 'unsaturated soil interface' (Tariq et al., 2009). This situation can be found in foundations, retaining walls and any other geo-structure that is contact with a unsaturated soil. Therefore, studying soil interface strength can enhance the understanding of soil performance in these cases. Additionally, this study helps to understand the behavior of the soil samples in desiccation tests in the laboratory (i.e.

typically using plates); where the effect of the bottom and lateral contact surface between sample and container can be relevant during shrinkage.

The present work focuses on the better understanding the behavior of clayey soils under drying. This work deals with artificial soil samples investigated in the lab via different type of desiccation tests. Digital photos were regularly taken during the test evolution to learn about the changes in the soil sample during drying. These photos were then processed using image analysis technique to determine the location and severity of cracked areas, and to gather useful information associated with the crack morphology and pattern (e.g. determination of width, length, and shape of the cracks). Furthermore, in this research to study the behavior of the interface soil/container a direct shear tests was modified to investigate the behavior of clay- rough surface and clay-smooth surface interfaces.

1.3 OBJECTIVE OF THIS RESEARCH

Although several works were done in the past to investigate the behavior of soils under drying conditions, significant gaps were found in the literature. The study of how cracks start and develop is complicated and detailed tests are necessary to improve our understanding, which will in turn assist to enhance a wide spectrum of geotechnical and geologic problems.

The main following objectives can be mentioned:

- To achieve a better understanding of initiation and propagation of desiccation cracks in soils.
- To investigate how the restriction conditions (during shrinkage) affect the formation and propagation of cracks in soils.
- To obtain key strength parameters related to soil-interface behavior.
- To explore the effect of water salinity on soil shrinkage and crack formation.
- To acquire a better understanding of the curling phenomenon and key aspects related to it, like, soil graduation and water content.

1.4 ACTIVITIES

Six tasks were accomplished in order to reach the objectives of this research stated above. These tasks can be described as follows:

- Task 1- Literature review: as mentioned previously, many researchers have already investigated the behavior of soils subjected to drying. A comprehensive literature review of previous work was accomplished.

- Task 2 - Determination of soil properties: index properties of soils used in this research, as well as the soil-water retention curve were determined by using different techniques.

- Task 3: Experiments on soil samples in the lab: desiccation tests under the lab atmosphere by using artificial soils were performed. Then, the effect of osmotic technique on clayey soils was studied by using a saturated salt solution of calcium nitrate tetrahydrate ($Ca(NO_3)_2.4H_2O$).

- Task 4-Image analysis techniques: digital cameras were used for capturing the soil behavior under drying conditions by programming these cameras to take a time-lapsed series of photos. Afterwards, by applying image analysis techniques using *image j* software, these images were analyzed for multiple proposes. The most important parameters such as cracked and uncracked areas, average width of cracks, and the crack intensity factor (CIF) were obtained in order to determine the development of cracks patterns.

- Task 5-Soil-plate interface investigation: the direct shear box was modified to investigate the behavior of clay- rough surface and clay-smooth surface interfaces under drained and undrained conditions. That was done by creating plates with grooves in one side and smooth surface in the other side, and the traditional device was modified to be able to obtain the interface shear strength of soils.

- Task 6: Soil surface curling investigation: several laboratory experiments were performed to explore the effect of material properties (i.e. soil grain size

distribution, mineralogy and soil microstructure), and soil water content in curling phenomenon.

1.5 LAYOUT OF THE THESIS

This thesis is composed of 7 chapters. In chapter 2, a comprehensive literature review on desiccation cracks and behavior of soils under drying is presented. In chapter 3, a number of drying tests on thin soil layers are presented with details, and then the effect of wetting-drying cycles is studied on thin soil layers. In chapter 4, interface direct shear tests are described with presenting the results of several tests by considering different conditions. In chapter 5, a comprehensive literature review on image analysis technique is presented, and the results are analyzed and described in chapter three. Furthermore, the results are discussed in details regarding the effects of boundary conditions. In chapter 6, soil surface curling is studied in the lab on thin soil layers and the results are discussed at the end of this chapter and compared with the previous works. Finally, chapter 7 presents conclusions of this research and recommendations for future work.

LITERATURE REVIEW

2.1 INTRODUCTION

In this chapter, soil behavior under drying has been discussed in detail. Also, a literature review of the behavior of thin soil layers under drying has been done comprehensively. Also, a brief description of the total suction, water retention curve, and WP4-T with pressure plate devices were presented at the end of this chapter.

2.2 INTRODUCTION TO DESICCATION CRACKS

Since many years ago, many laboratory experiments and field studies have been carried out to investigate the initiation and development of desiccation cracks in soils (Corte and Higashi, 1960; Kleppe and Olson, 1985; Konrad and Ayad, 1997; Miller et al., 1998; Morris et al., 1992; Nahlawi and Kodikara, 2006; Tang et al., 2008, 2010; Velde, 1999). All these investigations were very qualitative, and the majority of them are limited to the description of desiccation cracking phenomena. Generally, soils are highly complex materials; the desiccation cracking behavior is controlled by several factors such as, composition of the mineral, clay content, relative humidity, degree of temperature, thickness of the layer, boundary conditions. (Albrecht and Benson, 2001; Fang, 1997; Nahlawi and Kodikara, 2006; Rodríguez et al., 2007; Tang et al., 2007, 2008, 2010).

Due to loss of water, desiccation cracks form on the soil surface, and this is a common natural phenomenon. This phenomenon can significantly affect the performance of soil

in geotechnical, agricultural and environmental applications. As a result, mechanical strength is weakened due to the presence of cracks; the cracked soil is more compressible than the intact one at the same water content (Morris et al., 1992).

When soil shrinkage because of the moisture reduction takes place and cracks form, the internal tensile stresses develop due to the restriction of the shrinkage. Subsequently, when the tensile strength is equal to the tensile stresses, cracks begin to develop. Several factors control the rate of water evaporation for example, relative humidity, temperature, wind velocity, solar radiation, soil suction, salt concentration, soil pore size and layer thickness. (Kayyal, 1995; Cui et al., 2005; Prat et al., 2006; Rodríguez et al., 2007). As mentioned previously, the capillary pressure and the tensile strength of the soil control the desiccation cracking.

According to Zhang (2011), the developing of desiccation cracks can be concluded in three stages: the initial stage, the primary stage, and the steady state stage. The evaporation of the soil water would be in one dimension from the soil matrix and the evaporation rate would be small when there are no or few cracks in the soil initially. Then, after some cracks appear in the soil, the soil water would evaporate from the crack walls in a horizontal direction and the water loss from the soil matrix in vertical direction. Therefore, in the primary stage cracks grew much faster because the evaporation rate in two dimensions is larger than that in only one dimension (Zhang, 2011).

Generally, desiccation cracks will develop in the zones where internal defects exist (Trabelsi et al., 2011). Figure 2.1 shows a picture of cracks. The whole land shown in the figure was cracked in the same way that was observed in the lower left side of the figure. These cracks probably result only from the desiccation phenomena, which cause a significant drooping in the material mechanical properties. Mainly, properties related to the shear resistance, which lead to the landslide shown in the right side of the figure (Trabelsi et al., 2011).

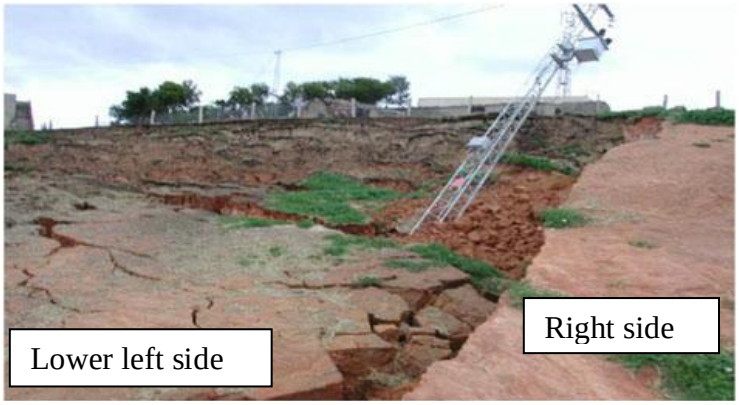

Figure 2. 1. The effect of desiccation cracks on structure (Trabelsi et al., 2011).

2.3 SOME PREVIOUS WORKS ON DESICCATION CRACKING

In this section, a comprehensive literature review of desiccation cracks have done including field investigations, modeling, and laboratory studies.

2.3.1 Field investigations

The reasons of material fracturing are mostly dependent on the tensile stresses and the brittleness of the dry material (Andersen et al., 1994). Andersen et al. (1994) studied the patterns of cracks due to an external stress field, and the results showed possible patterns on the material surface. More recently, techniques for determining some features of cracks patterns have been developed from a field measurement to a more advanced analysis by image processing (Miller et al., 1998; Velde, 1999; Vogel et al., 2005a, b). The water molecule motion velocity and kinetic energy are increased with increasing temperature. Konrad and Ayad (1997) have conducted a field experiment in a clayey soil in order to investigate the geometry of cracks on the soil surface, and they found the shape of the cracks as polygons as shown in figure 2.2.

Figure 2. 2. Polygonal cracking with protuberance (after Konrad and Ayad, 1997).

Dyer, Utili and Zielinski (2009), carried out a laboratory and field experiments on a clayey embankment in the UK. Their work was divided into two parts, which were

providing actual field data by making deep trenches in the embankment and some laboratory tests such as small scale model and soil sample analysis. They found some deep cracks with subhorizontal ones and some very deep cracks (around 1.1 m) but without subhorizontal cracks as shown in figure 2.3.

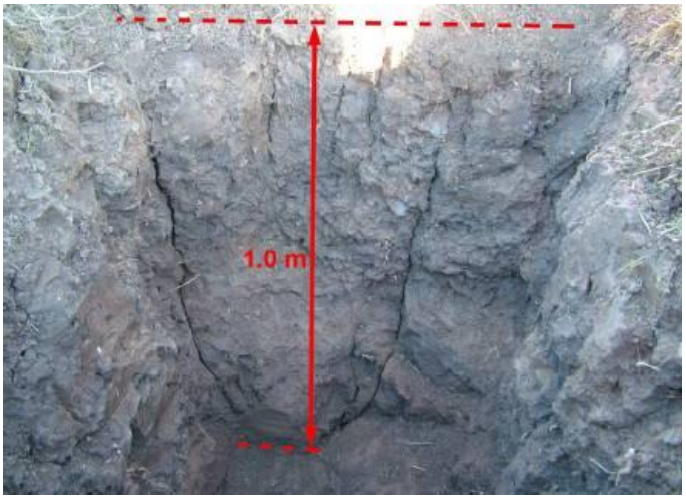

Figure 2. 3. Cracks to the depth of 1m (2006) (Dyer, Utili and Zielinski).

Laboratory tests would more reasonable for engineering applications; however, the conditions of the test may not be ideal because field tests carried out on in-situ soils under atmosphere conditions. Dasog et al. (1988) concluded that cracking is more pronounced in cultivated soils and in sub-arid areas.

2.3.2 Modeling

Modeling and predicting the formation of desiccation cracks has advantages in a number of applications including earth dam construction and crop science. Nevertheless, most studies have worked on statistical analysis of the patterns of crack and the qualitative study of contributing factors to crack propagation rather than prediction. Most models handle the formation of cracks without regarding differentiation of material properties with time that because it is complicated to work on the nonlinear processes during desiccation in an analytical modeling. Aoki et al. (2002) and Aoki et al. (2007) used similar spring model to visualize the crack generation. Additionally, Abu-Hejleh and Znidarčić (1995); Ayad et al. (b1997); Chertkov (2000) and (2002); Chertkov and Ravina (1998); Deng and Shen (2006); Konrad and Ayad (1997); Péron (2008); and Péron et al. (2009a) worked on some modeling and theoretical studies on desiccation cracking. Another work was done by Rodriguez et al. (2007), which was basically analyzing the desiccation process in mining materials based on physical laws, they have been done some laboratory drying tests with numerical analyses to simulate some laboratory tests. The modeling carried out by using CODE_BRIGHT finite element program. Furthermore, Chertkov and Ravina (1998), created a physically based probabilistic model for the prediction of cracks in swelling soil by considering the effect of the soil depth on crack concentration. Also, Trabelsi et al., (2011) did a new model developed by using a CODE_BRIGHT finite element program, this model related the porosity evaluation to the suction and to the tensile strength. This model showed the initiation and propagation of desiccation cracks in a thin layer soil and predicted the

crack patterns in terms of average crack length and other Minkowski densities. Bronswijk (1988), developed a procedure to model water balance and cracking in clay soil, it helps to direct calculation the effect of moisture transport on volume change and consequently creating cracks. Kodikara and Choi (2006) have done analytical model for desiccation cracking of a clay layer and this model showed the maximum tensile strength developed at mid-section of the layer, also this model was applied to predict the laboratory desiccation test for a long and thin layer. Kodikara et al. (2011) developed a model was able to simulate some physical aspects of cracks evaluation in soil sample with different height, and length in terms of number of cracks formed and width of cracks. In this model, the required properties were obtained from laboratory experiments.

2.3.3 Laboratory studies

Some laboratory experiments were performed to understand the development of desiccation cracks using small-size slurry clay (Shorlin et al., 2000; Mizuguchi et al., 2005; Kodikara and Choi, 2006; Peron et al., 2006). The formation of cracks and crack patterns with different directions of drying, sample sizes, and sample thicknesses have been investigated (e.g. Shorlin et al., 2000; Peron et al., 2006). Another paper was done by Li and Zhang (2010) to differentiate the desiccation cracks pattern and geometric parameters of them in natural silty clay at a constant moisture condition with time. Zieliski et al. (2014) have done a paper to present a 2D profile laser which allows to scan the overall surface of a drying soil and to measure the losing in water during desiccation.

Lecocq and Vandewalle (2002) have done a practical experiment to study the dynamical formation of cracks and the statistical properties of final cracks and they compared their results with the existing models. It showed that the drying process has a significant effect on the way of cracks appear and propagate. Nahlawi and Kodikara (2004) have done some tests in the lab on thin clay layers to show the quantitative relationship between the properties of cracks and the current controlling conditions. Also, a series of lab tests on thin soil layers was done by Lakshmikantha (2009) on circular specimens, and rectangular specimens with different dimensions, different geometry, and different conditions to examine the initiation and propagation of cracks and the finial pattern of desiccation cracks. Also, Peron et al. (2009) have done some experimental studies on the desiccation cracks in fine grained soils.

In the paper, which was done by Tang et al. (2010), experimental tests were carried out on a fully saturated soil to investigate the behavior of desiccation cracking at three degrees of temperature (22, 60 and 105 ℃). A digital camera was used to monitor the cracks initiation and developing. The results are collected in table 2.1.

Table 2. 1: The results of experiments conducted on saturated slurry (Tang et al., 2010)

The summary of the results for each test at various temperatures.

Specimen No.	Initial water content (%)	Temperature (°C)	Initial evaporation rate (g/min)	Surface crack ratio R_{SC} (%)	Initial critical water content w_{IC} (%)	Final critical water content w_{FC} (%)	Final void ratio e
S1	170	22	0.021	13.9	35.7	15.3	0.431
S2	170	22	0.022	13.8	40.1	9.9	0.430
S3	170	22	0.022	14.2	38.2	12.3	0.430
S4	170	60	0.252	17.3	79.1	8.7	0.465
S5	170	60	0.255	16.9	74.8	14.3	0.461
S6	170	60	0.250	16.9	72.3	11.2	0.457
S7	170	105	0.507	23.1	96.1	13.1	0.470
S8	170	105	0.501	21.5	87.1	10.1	0.471
S9	170	105	0.499	22.3	89.5	7.6	0.473

2.4 BOUNDARY CONDITIONS

Corte and Higashi (1960) worked on the effect of contact surface and they used wood and glass. At the end, it has been observed that cracked area is much smaller with glass surfaces than the one with wood surfaces, showing that the less friction on surfaces leads to smaller cracked area. According to Towner (1987), clays experience anisotropically shrinkage during a drying process when they are being restricted in any direction. Basically, boundary conditions have significant influences on soil behavior that have been proven by some experiments which have been done in the lab. The two main types of boundary conditions are: a restrained movement and unrestrained movement of soil, which can be explained in other words like control soil shrinkage by some ways or allow to free shrinkage occurs during drying process. In reality, the first boundary condition is more applicable one in the field because each element in the soil is already restrained by other elements from different sides as shown in figure 2.4. However, the one with

smooth plate is used more in laboratories to allow free shrinkage occurs in the soil sample.

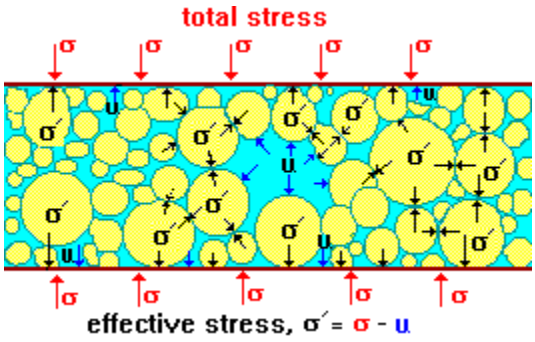

Figure 2. 4. Stresses on each element inside a soil (Wikipedia).

The water evaporation is higher at the surface and the cracks initiation start to appear at the surface and their depth increase with time. Nahlawi and Kodikara (2006) presented this equation to mathematically describe the rate of desiccation:

$$(w - wr) = (wi - wr) * e^{-kt}$$

Thus,

$$\left(\frac{dw}{dt}\right) = -k(w - wt)$$

Where,

t is the desiccation time;

w is the water content at time t;

wi is the initial water content;

wr is the residual water content at final stage of desiccation;

k is the parameter for the desiccation rate (1/[T]);

dw/dt is the desiccation rate.

Corte and Higashi (1960) have developed the same definition with a minor difference which is excluding the residual water content.

2.5 OVERVIEW OF CRACKS PROPAGATION LOCATION

The location of cracks has been widely debated this is because shrinkage cracks may appear on the surface (upper part of the soil sample) or at any arbitrary point inside the sample. Starting with the experiments, which were done by Corte and Higashi (1960), cracks was developed at the center of the soil, then started to spread to the bottom surface or the upper part of the soil and their rate was not the same. On the other hand, Morris et al, (1992) illustrated that the behavior of soils in drying process is downward where the matric suction increases in general. Furthermore, according to some studies of Weinberger (1999) showed that cracks start at the bottom of the soil surface and move upward. Desiccation cracks generally start at the upper part of the soil and they may appear inside the sample in some specific conditions, (Lakshmikantha, 2009). Also, it has been discussed that, since the inter-particle voids usually exit at the top surface of soils, cracks initiation is more likely to be there. Thus, the matric suction and the inter-particles voids may not perfectly show that cracks start at the bottom surface. After all,

crack initiation influences by several factors which should be considered such as boundary conditions, type of soil and so on.

2.6 INTRODUCTION TO CURLING DEFORMATION

Significant curling of polygonal clay blocks was observed in the field by Konrad and Ayad (1997), this curling was lifting off of the polygons edges due to desiccation cracking (Kodikara et al., 2004). Curling of clayey soils was observed and studied in the lab by Nahlawi and Kodikara (2002). Deformations of stiff materials are fairly small in comparison with curling deformations, this is because of the small failure strains (Kodikara et al., 2004). The surface of the soil may curl up or down during drying and this became a typical phenomenon; different stages of curling deformation have been observed by using a precise non-contact electro-optical technique with proposed a simple theoretical model (Zielinski et al., 2014). It has been stated that soils curl toward the fine particles and the curling rate is controlled by the grain size distribution (Bradley, 1933; Valentin and Bresson, 1992). Berney, et al. (2008) were observed that the development of sub-horizontal cracks in soils affected by curling. Lab experiments are generally performed under constrained condition to look at curling in soils by using a slurry paste with circular or rectangular molds (Kindle, 1923; Kodikara et al., 2004; Nahlawi and Kodikara, 2002). However, Peron et al. (2009) studied the curling in soils with constrained condition by using a metallic grooved bottom plate.

2.7 TOTAL SUCTION AND WATER RETENTION BEHAVIOR

Generally, water potential governs water flow and it consists of four components: Matrix potential (ψ_c), Osmotic potential (ψ_o), Gas potential (ψ_g), and Gravitational potential (ψ_z) (Panel, 1965). Hence, the equation of the total water potential is:

$$\psi = \psi_c + \psi_o + \psi_g + \psi_z$$

Where:

$\psi_c = u_w - u_a$;

u_w = pore water pressure, and u_a = air pressure;

$\psi_0 = c_m * R * T$;

R = gas constant = 8.314 J/mol °K, and T = Temperature;

$\psi_g = (u_a - u_{atm})$, it depends on the hydrostatic pressure on the water;

u_{atm} = atmosphere pressure;

$\psi_z = \Upsilon_w * z$, it depends on the position of the water in the field;

Υ_w = water unit weight.

It has been accepted that the total suction is a matrix suction plus osmotic suction and there is an equation was derived by Dao et al., (2008). Total suction is directly related to relative humidity (Panel, 1965). In this paper, we are interested in these two major components of the total suction.

Matrix suction in soil (Capillary) is governed by surface tension and the surface tension is controlled by the cohesive forces which exist between liquid molecules, as shown in figures 2.5 and 2.6.

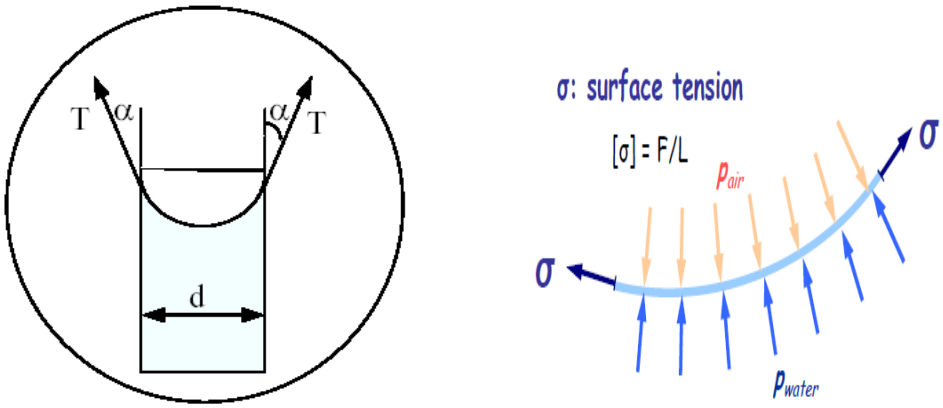

(a) (b)

Figure 2. 5. (a) Surface tension in tube, and (b) showing the effect of water pressure and air pressure, (Dr. Sanchez notes from course 673).

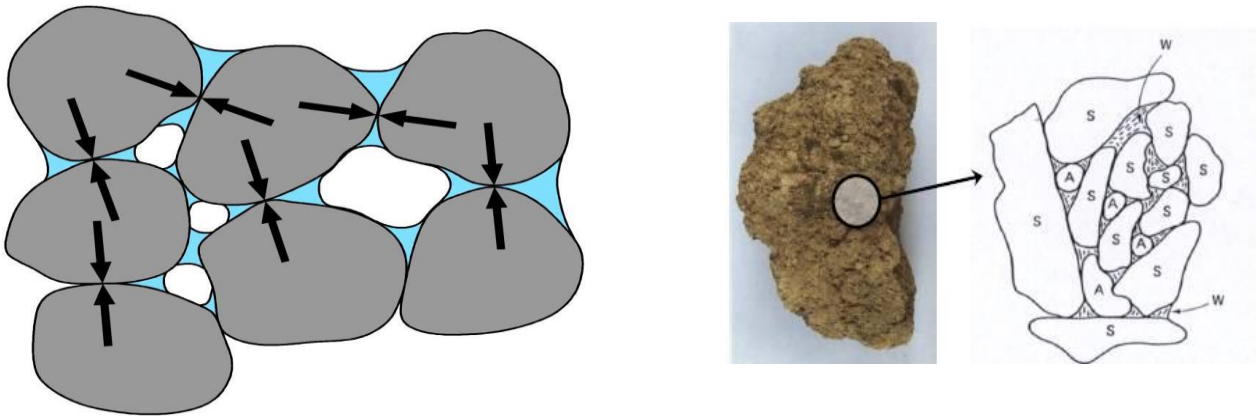

Figure 2. 6. Water inside the soil pores (capillary water rises in porous media), (Dr. Sanchez notes from course 673).

Because these molecules do not have molecules from all sides, they stick robustly with those directly connected with them on the surface. This phenomenon depends mainly on the type of liquid and degree of temperature as well, for example water has a surface tension of 72.8 dynes/cm, ethyl alcohol has 22.3 dynes/cm, and mercury has 465 dynes/cm all @ 20 ℃, and water has a surface tension of 67.5 dynes/cm @ 60 ℃. This surface tension generates negative pressure called capillary pressure or matrix suction (ψ_c). As mentioned previously, the matrix suction may lead to soil contraction and that ends in shrinkage (sometimes associated with curling) and/or cracking in soils as shown in figure 2.7.

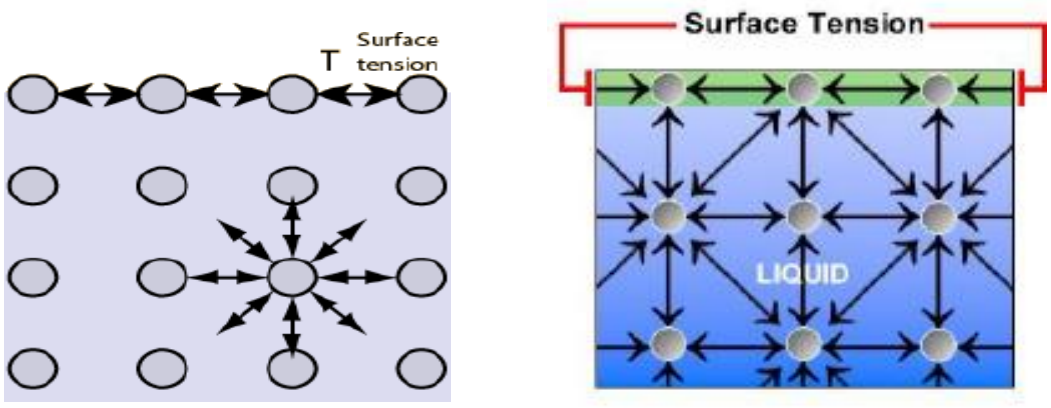

Figure 2. 7. Surface tension phenomenon (Dr. Sanchez notes from course 673).

Pore geometry controls water rise inside the soil such that the smaller pore's diameter, the higher the capillary water. Since clayey soils which are fine grained soils usually have very small pores comparing with sands, they have high capillary pressure as shown in figures 2.8 and 2.9.

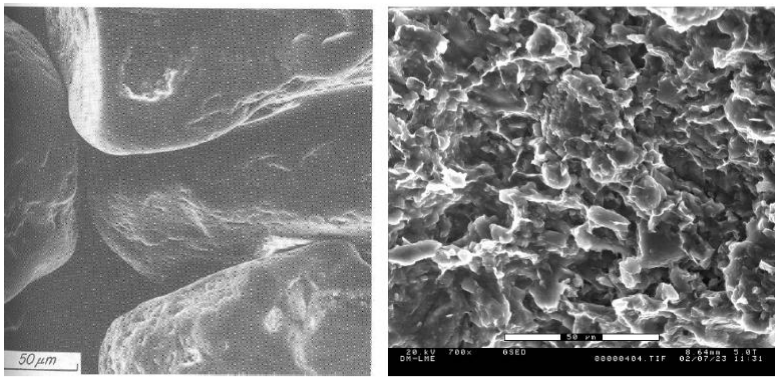

Figure 2. 8. Capillary effects in (a) clays and (b) sands.

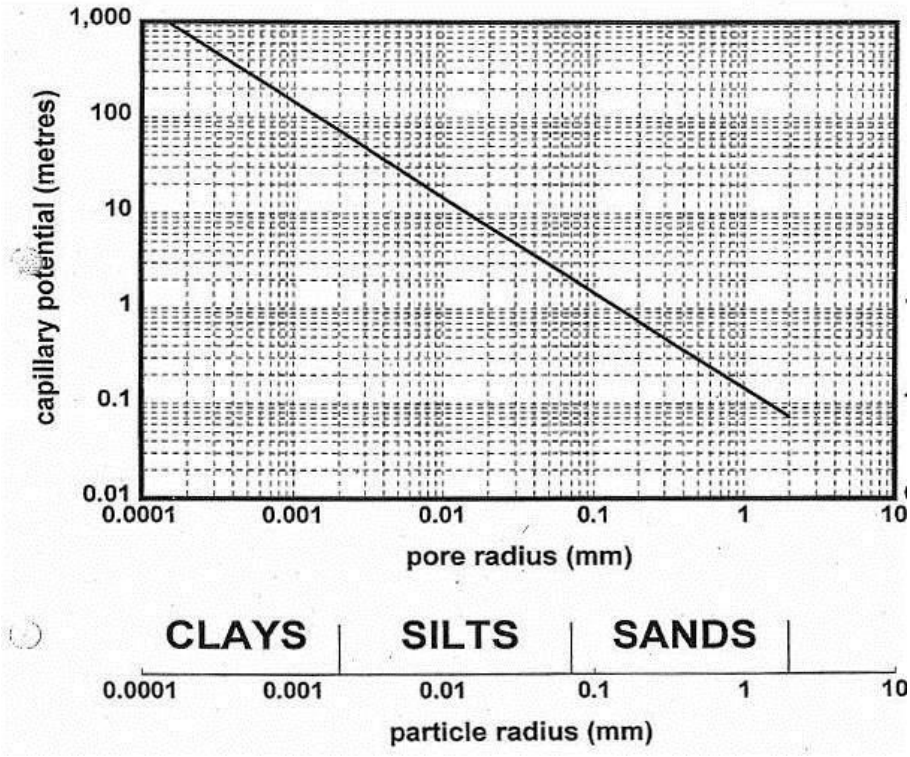

Figure 2. 9. Capillary potential vs. pore radius.

In partially saturated soils, suction with degree of saturation has a significant effect on soil characterization. Graphically, it has been represented the relationship between these factors for each soil with a specific density by a chart called (water retention curve). Fredlund and Xing (1994) gave empirical equations to describe this phenomenon which is also called soil-water retention curve (soil-water characteristic curve). The water retention curve is represented in both wetting and drying path as shown in figure 2.10. This is because of a phenomenon called hysteresis, which was noticed between the results of the water retention curve that obtained from wetting- drying path; also the value of suction can be estimated from different water content.

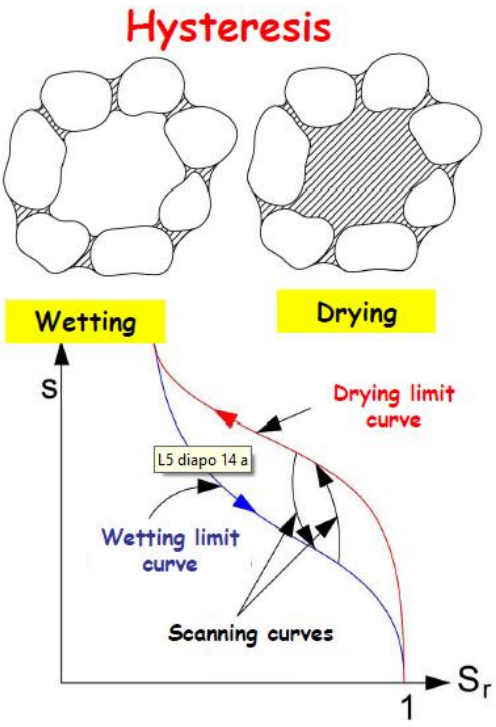

Figure 2. 10. Soil-water retention curve in wetting-drying paths.

Another term called air entry value (AEV), which is defined as the pressure at which water starts to penetrate into the soil as shown in figure 2.11. It is worth mentioning that the retention curve can be expressed in terms of suction vs. degree of saturation, suction vs. volumetric water content, and suction vs. water content.

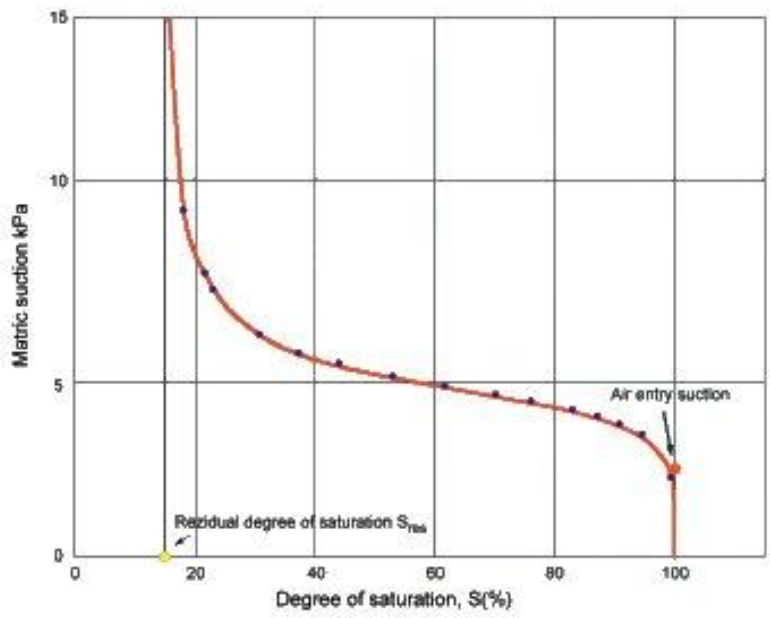

Figure 2. 11. Point of the air entry value in the soil-water retention curve.

Van Genuchten (1980) has developed a model for soil-water retention curve, which is the most common one:

$$Se = \frac{Sl - Slr}{Sls - Srl} = \left(1 + \left(\frac{Pg - Pl}{P}\right)^{\frac{1}{1-\lambda}}\right)^{-\lambda}$$

Where:

Se = effective degree of saturation;

Sl or Se = degree of saturation;

Sls = maximum degree of saturation;

Slr = limit (or minimum, or residual) degree of saturation;

P_g-P_l = capillary pressure (= suction‘s’);

P = Air Entry Values (AEV) (P large = fine grained soils and P small = coarse grained soils);

λ = parameter related to the slope of the curve (λ small = uniform grading and λ large = well graded).

Osmotic suction is defined as the movement of water molecules from low to high concentration region through a semipermeable membrane as shown in figure 2.12. However, osmotic suction is considered as a part of the total suction just when the flow has reactive species.

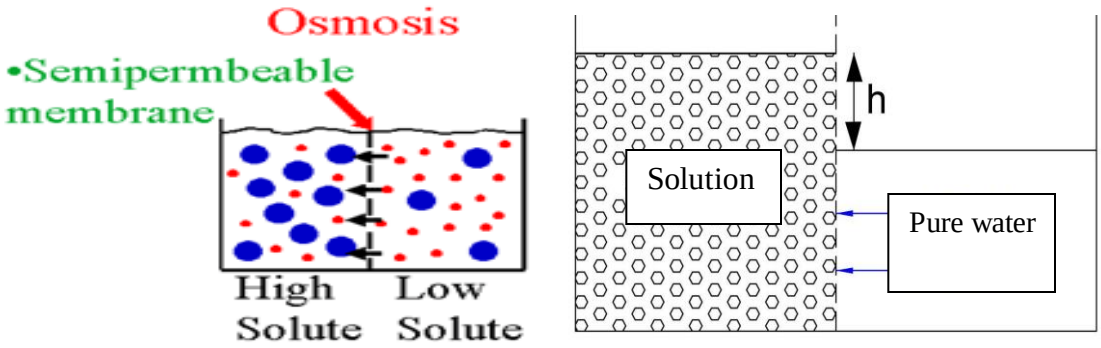

Figure 2. 12. Osmotic suction with semipermeable membrane (Dr. Sanchez notes in course 673).

Some experiments were carried out by Fleureau et al. (1993) in order to notice the effect of suction on saturated soils; it has been realized that a huge decreasing in the degree of saturation existed with a constant void ratio when the water contents of soils become less than the air entry value.

2.8 WP4-T AND PRESSURE PLATE DEVICES TO MEASURE THE SUCTION

WP4-T device has been used for measuring water potential (Range 0 to -300 MPa) which is a measurement of the water energy in the system. Figures 2.13 and 2.14 show the WP4-T device with its details.

Figure 2. 13. WP4-T, Dewpoint PotentiaMeter.

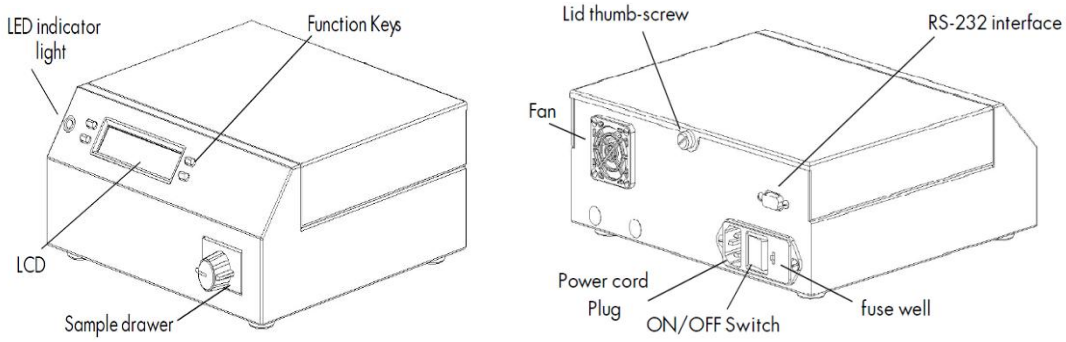

(a) (b)

Figure 2. 14. (a) Front view and (b) Back view of WP4-T.

Basically, WP4-T measures the water potential of any sample by using the technique of the chilled-mirror dewpoint. WP4 measures the summation of matric and osmotic potential by using this equation:

$$\psi = \left(R * \frac{T}{M}\right) * \ln\left(\frac{p}{p_0}\right)$$

Where:

R = gas constant (8.31 J/mol °K);

T = sample temperature in Kelvin;

M= molecular mass of water;

p = air vapor pressure, it can be obtained by using a chilled mirror;

p_0 = saturation vapor pressure at the sample temperature, it can be calculated from sample temperature.

Thus, by a few simple steps we can measure the water potential of any soil sample. After putting the sample in the chamber, this device starts to adjust the sample temperature with the chamber temperature. In the small screen we can follow the difference in temperature (Ts-Tb) until it gets close enough (around 0 to 0.5) to give more precise results. As mentioned previously, temperature has a significant effect on the water potential. By equilibrating the liquid phase of the sample (water) with the vapor phase in the chamber, water potential can be measured and the vapor pressure as well. At the end, water potential and the temperature appear in the small screen (LCD). However, the shortcoming of this device is the accuracy of its results when the sample suction is low (between 0 to 10 MPa). Therefore, pressure plate (figure 2.15) was used to measure the suction of soil samples with the values of the equilibrium moisture content at higher RH levels (≈ 95 to 100%). This test was conducted according to ASTM C1699-09 (Standard Test Method for Moisture Retention Curves of Porous Building Materials Using Pressure Plates). The values of equilibrium water content can be determined. Each

pressure applied corresponds to a matric suction and to the corresponding water content in equilibrium under this suction. Thus, each pressure applied corresponds to a point on the water retention curve. The results of equilibrium water content at each matric suction can be used to characterize the soil or to provide factors to computer models that can reproduce wetting or drying potential of soil materials with particular environmental conditions. These results can be used directly in research or a report; they are reliable, but carefulness needs to be considered during performing the test.

Figure 2. 15. Pressure chamber.

DESICCATION TESTS

3.1 INTRODUCTION

In this chapter, overview of osmotic flow and vapor transfer have been presented. In addition, a number of lab experiments were carried out and described thoroughly. Also, all material properties were discussed briefly. Finally, a conclusion was written at the end of this chapter.

3.2 OSMOTIC FLOW

Osmotic is defined as a term used to illustrate a phenomenon of water passing through a semi-permeable membrane from a lower solute concentration into a solution of higher solute concentration. A semi-permeable membrane is defined as a membrane allowing certain molecules to pass but it does not allow all molecules to pass through it. For instance, in figure 3.1 the yellow wall, which represents a semi-permeable membrane, allows some small molecules to pass through it such as white, purple, and green ones. Also their movement is from high concentration (left side) to the lower one (right side). However, the large particles (red and blue) are not allowed to pass through the membrane.

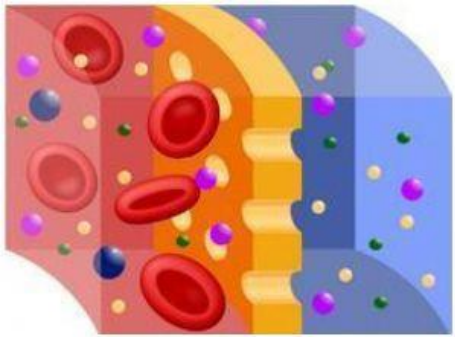

Figure 3. 1. Illustration of a semi-permeable membrane, (Dr. Sanchez, Transport phenomena in porous media, Lec. #11).

This technique was first introduced by Lagerwerff et al. (1961), who were biologists, and then developed by Zur (1966). Then, it was introduced to geotechnical engineering by Kassiff and Ben-shalom (1971). In particular, they used a solution of Polyethyleneglycol (PEG) and the soil sample was connected with it by a semi-permeable membrane. In this case, water could pass through this membrane but PEG molecules could not pass. Thus, the semi-permeable membrane applied an osmotic suction to the soil sample and this suction increased with the concentration of PEG solution. The osmotic technique might control the matric suction but not the osmotic suction of the soil sample because water in the liquid phase could pass through the semi-permeable membrane freely (Tarantino et al., 2008).

Generally, the osmotic pressure is calculated by using thermodynamic principles (Robinson and Stokes, 1968). Approximately, the osmotic pressure can be calculated by the Van't Hoff equation (Metten, 1966):

$$\pi = R * T * C$$

Where: π = osmotic pressure (KPa), C = sum of the molar concentrations in solution (mol/L), R = universal gas constant = 8.314 J/mol °K, and T = absolute temperature (°K). Also, the osmotic flow of water in soil can be calculated by using a flow law which has a similar form to Darcy's law:

$$q\pi = K\pi * \frac{\Delta\pi}{\Delta X} = \sigma * Kh * \frac{\Delta\pi}{\Delta X}$$

Where: q = water flux (m/s), K = coefficient of osmotic permeability (m/s), Kh = coefficient of (hydraulic) permeability (m/s), π = osmotic pressure head = $\pi/\rho_f.g$ (m), ρ_f = pore fluid density (kg/m^3), g = gravitational acceleration (m/s^2), σ = osmotic efficiency, and X = distance (m).

When the coefficient of osmotic permeability equals the coefficient of hydraulic permeability, the soil acts as a perfect semi-permeable membrane. Only pure water can flow in this case with respect to osmotic gradients. On the other hand, when the osmotic permeability equals the hydraulic permeability multiplied by the osmotic efficiency, the membrane is "leaky", so the water can flow with respect to osmotic gradients carrying with it some dissolved salts. Therefore, the osmotic efficiency could be defined as a measure of the degree to which the soil behaves as a perfect semi-permeable membrane. Many studies about the osmotic efficiency of clays were already done by Kemper and Rollins (1966), Bresler (1973), Olsen (1972), and others. Figure 3.2 shows the results of

these studies; it illustrates that in an unsaturated soil the osmotic efficiency is dependent on pore fluid concentration, pore fluid chemistry, and fluid film thickness between soil particles. To get the thickness of the fluid film, divide the volumetric water content by half the area of the soil surface. At low void ratio or low pore fluid concentration, high osmotic efficiency has been observed.

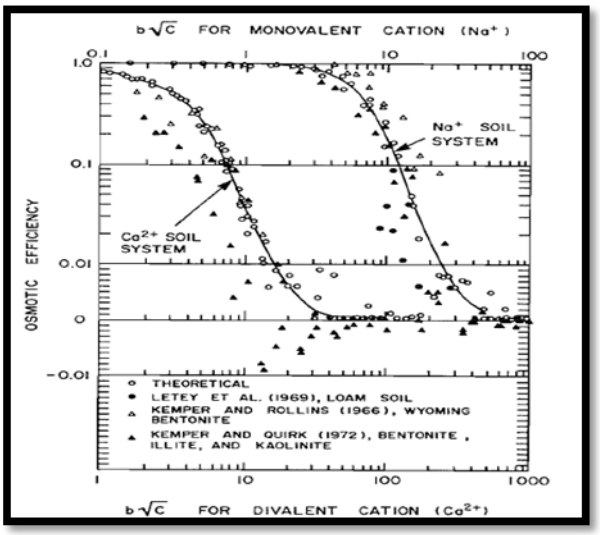

Figure 3. 2. The efficiency of osmotic unsaturated soil system, as a function of b√c (C is the concentration of pore fluid in normality, 2b is the thickness of a film in angstroms, Bresler 1973).

3.3 VAPOR EQUILIBRIUM TECHNIQUE OR VAPOR TRANSFER (CONTROLLING THE SUCTION BY IMPOSING RELATIVE HUMIDITY)

Vapor equilibrium technique (VET) is defined as creating environment of constant suction by using osmotic potential of salt solutions (chemical solutions) inside perfectly closed containers (Tang and Cui, 2005; Tang and Cui, 2007; Delage et al., 1998;

Romero, 1999; Delage and Cui, 2000; Blatz, Yu-Jun Cui and Luciano Oldecop, 2008). The idea of controlling the suction by imposing relative humidity was primarily developed by Esteban and Saez (1988). They recognized that the vapor exchange was somewhat slow and it may take several weeks. They ran the test by putting an odometer in a chamber containing sulphuric acid solution with a known concentration. Not long ago, a system governing the mass of water exchanged was proposed by Dineen and Burland (1995). However, Marcial et al. (2002) presented a method to decrease the equilibrium time. They worked with two methods: the first one, putting a sample inside a perfectly closed desiccator which has saturated salt solution at the bottom; the second one, is using a pneumatic pump to ensure humid air distribution which is obtained from a bottle has saturated salt solution at the bottom. In the second one, air was distributed inside the chamber of the soil sample. Thus, they compared these two methods and the later one took shorter time (2-4 weeks) to reach the equilibrium state than the first one (several months). Basically, the idea of using fully saturated solution is keeping the suction constant. Since the suction is associated with the molar fraction of water and the molar fraction stays constant when humidity exchanges between liquid and gaseous phases, the suction does not change. The chemical potential of different forms of aqueous solutions may control the relative humidity of the reference system (Delage et al., 1998, Tang and Cui, 2005). In this research, a saturated solution of calcium nitrate tetrahydrate $Ca(NO_3)_2.4H_2O$ was used.

To show the relationship between relative humidity and suction, Kelvin's law may be used:

$$u_a - u_w = \left(\frac{R * T}{Mg}\right) * \ln\left(\frac{P}{P0}\right)$$

Where:

u_a is the air pressure;

u_w is the water pressure;

R is the gas constant (8.314 J/mol °K);

T is the degree of temperature in kelvin (T= 293 °K @ 20 °C);

M is the molar mass of water (18.02 g/mol);

g is the acceleration of gravity (9.81 m/sec^2);

P is the partial pressure vapor;

P0 is the saturated vapor pressure;

P/P0 is the relative humidity.

3.4 RESEARCH METHODOLOGY

To study the initiation and propagation of desiccation cracks, a number of experiments were carried out in the lab. This chapter presents several drying tests with the results of desiccation cracking tests conducted on thin layers (1/2" to 1") of clayey soils. Two conditions were considered in these tests; open plates in the lab and plates inside a desiccator glass with controlled relative humidity and temperature. In both cases, the relative humidity of the air surrounding the sample was monitored and roughly constant

during the test. An aqueous solution of chemical compound was put inside a desiccator. Therefore, water was allowed to be exchanged by means of vapor transferring between the salt solution and the soil sample, and then under an equilibrium condition (which was reached after 45-50 days) a known suction (~75 MPa) was applied to the sample. The salt solution used in this research is calcium nitrate tetrahydrate $Ca(NO_3)_2.4H_2O$,; it has a density of 1.41 Mg/m^3 and can impose a relative humidity of 58.1%, which is corresponding to a suction of 75 MPa (which was calculated in the lab at 24.5 °C).

In general, cracks are formed during the process of desiccation due to shrinkage of the soil as a result of a reduction of the moisture content. Tensile stresses are developed inside the soil sample due to the restriction of the shrinkage. As soon as these tensile stresses equal the tensile strength of the soil, cracks start to develop.

3.5 MATERIALS, SPECIMENS PREPARATION

Three types of artificial clays (kaolinite, bentonite, and porcelain) were used in this research. Temperature and relative humidity were both monitored during the tests. Generally, all types of clays were passed through sieve #200. Mixtures were prepared by mixing soil powder with the distilled water, then tapped carefully to remove any entrapped air and to ensure uniformity in density and moisture conditions. Thus, the soil was fully saturated. Cylindrical molds were used with diameters of 4.33" (11 cm) and 5.9" (15 cm), and two different thicknesses: 0.5" (1.27 cm) and 1" (2.54 cm). Then, the mixtures were left covered by using tightly sealed containers for 24 hours prior to testing

to allow the redistribution of moisture uniformly and guarantee homogenization before distributing them into the molds. The molds were cleaned and the samples were prepared by gradually placing soil until it reached the required thickness. The air bubbles were removed by slightly tapping the sides of the molds. Then, in order to obtain an even surface, samples were leveled with a ruler and weighed by using a small scale to an accuracy of 0.01 g. Finally, samples were put on the surface by using levels which are shown in the figure 3.3. Thus, the same previous procedure was repeated for all the samples.

Figure 3. 3. These two rulers with bubbles (levels) which have been used in the lab.

3.6 ATTERBERG LIMITS

The Atterberg Limits determination was carried out according to American Society for Testing and Materials (ASTM) D 4318-00 “Standard Test Method for Liquid Limit, Plastic Limit, and Plasticity Index of Soils” (ASTM, 2000). The soil sample was mixed with distilled water. Then it was kept in a plastic bag and placed in a humid chamber for around 24 hours for homogenization. When the soil tempered, the soil sample was spread on a standard glass plate, and it was divided into two parts. Around 30 grams of soil was required to perform the Plastic Limit test.

The liquid limit was obtained by performing trials in which a part of the specimen was spread in a brass cup (Casagrande Cup). Then, the soil sample was divided into two parts by using a specific tool; and then by repeatedly dropping the cup in a standard mechanical device, it was allowed to flow together. Three separate water content determinations were needed; two were performed at blow counts less than 25 blows and the other one was performed at blow counts more than 25 blows. The water contents were plotted versus the number of blows in logarithmic scale. Thus, the Liquid Limit was determined as the water content of the soil sample at 25 blows, and the plastic limit was determined by rolling the soil threads on a standard glass plate to a diameter of 3.18 mm (1/8 in) until the soil specimen crumbled and could not be rolled to that diameter. Three to six threads were rolled and the water contents were determined. The average of these values represents the Plastic Limit of the soil.

3.7 EXPERIMENTAL SET-UP

In this section the main discussion will be about two mixtures: bentonite with kaolinite and porcelain with kaolinite. However, all other mixtures presented in appendix 1.

3.7.1 Kaolinite and bentonite

This sample was a mixture of 75% kaolinite and 25% bentonite (the percentage in terms of sample mass). The initial dry density (ρ_d) of this soil was 800.69 Kg/m^3, initial dry unit weight (Υ_d) was 7.85 KN/m^3, the wet bulk density (ρ_T) was 1522.81 Kg/m^3, and the saturated unit weight (Υ_T) was 14.94 KN/m^3. Also, other properties of this mixture were obtained such as specific gravity (G_s) = 2.61, void ratio (e) = 2.36, and porosity (n) = 0.7. Water content was measured by taking small amount of soil from the mold, then using a small can with a known mass to weight this piece by using a sensitive balance before putting it inside the oven with a temperature of 110 ℃ for 24 hours. After that, the dry sample was determined to calculate the difference before and after drying. Thus, the water content of this mixture was obtained and it turned out to be around 90.19%. Also, water content of the soil before mixing it with water was obtained and it found to be around 5.09%. Therefore, the net water content was approximately 85.09%. Finally, Atterberg limits (Liquid and Plastic Limits) of this sample was obtained in the lab and they found to be 67.5% Liquid Limit, 38.1% Plastic Limit, and 29.4% Plasticity Index.

3.7.1.A Under the lab atmosphere

The temperature of the lab was (24 ± 1 °C) and relative humidity, RH (52 ± 5%). A constant suction of 90 MPa was measured during these tests.

1) Using a circular mold of diameter 5.9" (150 mm) with a thickness of 0.5" (12.7 mm), and small circular grooves (1.5 mm deep and 2 mm width) were created at the bottom (figure 3.4). The idea of creating grooves at the bottom is to avoid sliding at the contact between the plate and the clay (creating adhesion with soil). After preparing the soil and making the surface of the sample is roughly smooth, the sample left under the lab atmosphere for around 6 days to allow water evaporation.

Figure 3. 4. Spiral grooves which created at the bottom of the mold.

Figure 3.5 shows the initiation and the propagation of desiccation cracks with time.

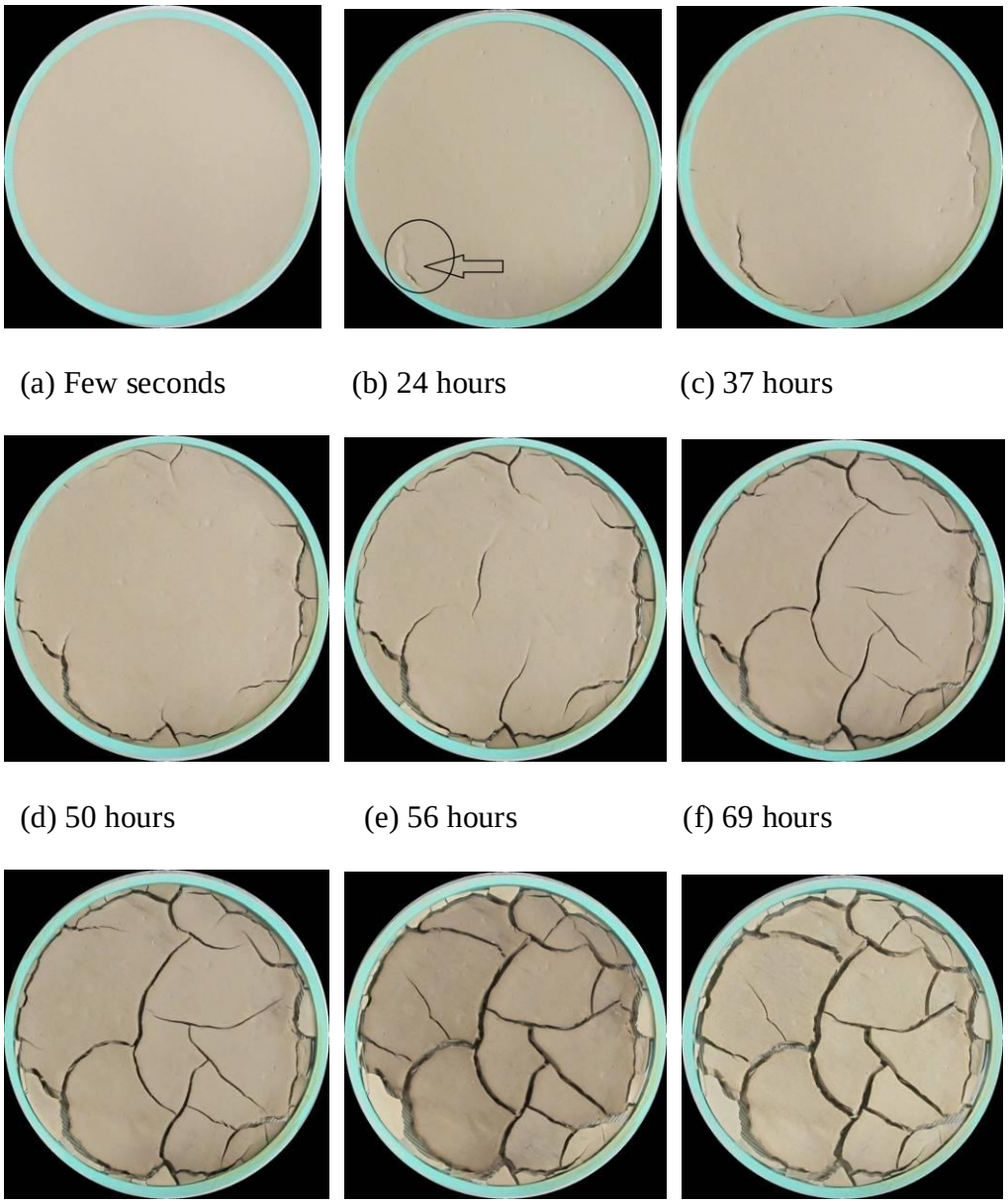

(a) Few seconds (b) 24 hours (c) 37 hours

(d) 50 hours (e) 56 hours (f) 69 hours

(g) 76 hours (h) 84 hours (i) 100 hours

Figure 3. 5. Photos were taken during the experiment, notice case (a) was just taken after preparing the sample, and case (j) was at the final stage of drying.

(j) 146 hours

Figure 3. 5. Continued.

For sake of measuring the loss of water content with time, the mold was weighted empty and with the soil sample respectively. Then, by using a Canon camera and a small scale connected to the computer, photos were taken each 30 minutes and the weight of the sample was recorded continuously. Thus, it is possible to calculate the water content after the first crack, second crack, and so on, until the end of the test. However, the water content at the time of the first crack appeared, was considered as the cracking water content.

2) Using identical circular holding tray to the previous one except two things: the thickness was changed to 1" (25.4 mm), and small holes were created at the bottom plate of diameter 2.5 mm (figure 3.6). The idea of creating holes in addition to the circular grooves is to allow water to penetrate through the soil sample. In this case the height of the sample was 0.5" (12.7 mm) and exposed the soil to 0.5" (12.7 mm) depth of distilled water as shown in figure 2.7.

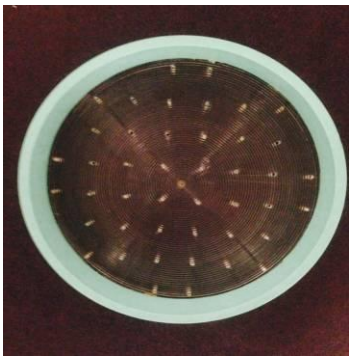

Figure 3. 6. A mold with thickness of 1" (25.4 mm) and small grooves with holes at the bottom.

Figure 3. 7. Monitoring the soil sample during drying by using a camera to take a series of photos (one each 30 minutes).

Figures 3.8 and 3.9 show the behavior of the soil sample under distilled water.

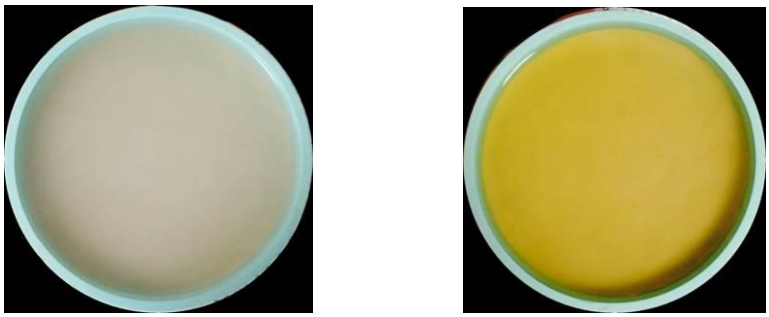

(a) (b)

Figure 3. 8. Photos were taken at (a) initial state and (b) 100 hours.

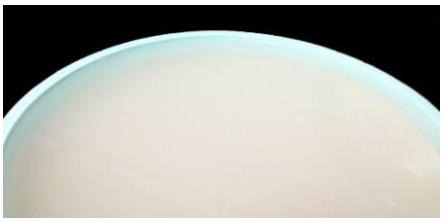

Figure 3. 9. "Zoom in" to show the water level above the soil.

3) Using a circular mold of diameter 5.9" (150 mm) with a thickness of 0.5" (12.7 mm) with a smooth bottom. In this case, the bottom and the sides of the mold were greased with Vaseline before putting the soil in. The idea of greasing the mold was to decrease the friction between the soil and the mold as much as possible to allow free shrinkage (zero adhesion) as shown in figure 3.10.

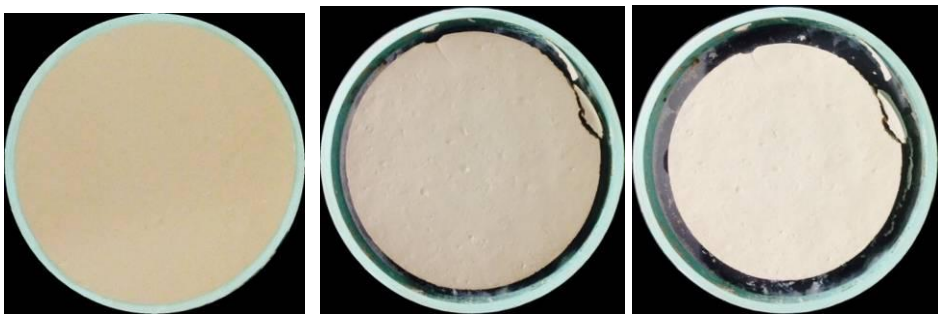

(a) (b) (c)

Figure 3. 10. Photos were taken at (a) 0 hour, (b) 48 hours, and (c) 96 hours.

4) Since this mixture was a little sticky, the mold was divided into two pieces each 0.5" (12.7 mm). This mold has small grooves and holes at the bottom. Thus, after preparing the sample and making sure that the surface was fairly smooth, the other piece of the mold was fixed above it by using a metal worm drive clamp with water resistant anti-slip tape. Sequentially, the sample was exposed to the salt solution. However, time was a considerable issue while working on these steps to avoid changing the water content of the sample. Therefore, all these steps were done in a few seconds and photos were taken during the work for more illustration of them, as shown in figure 3.11.

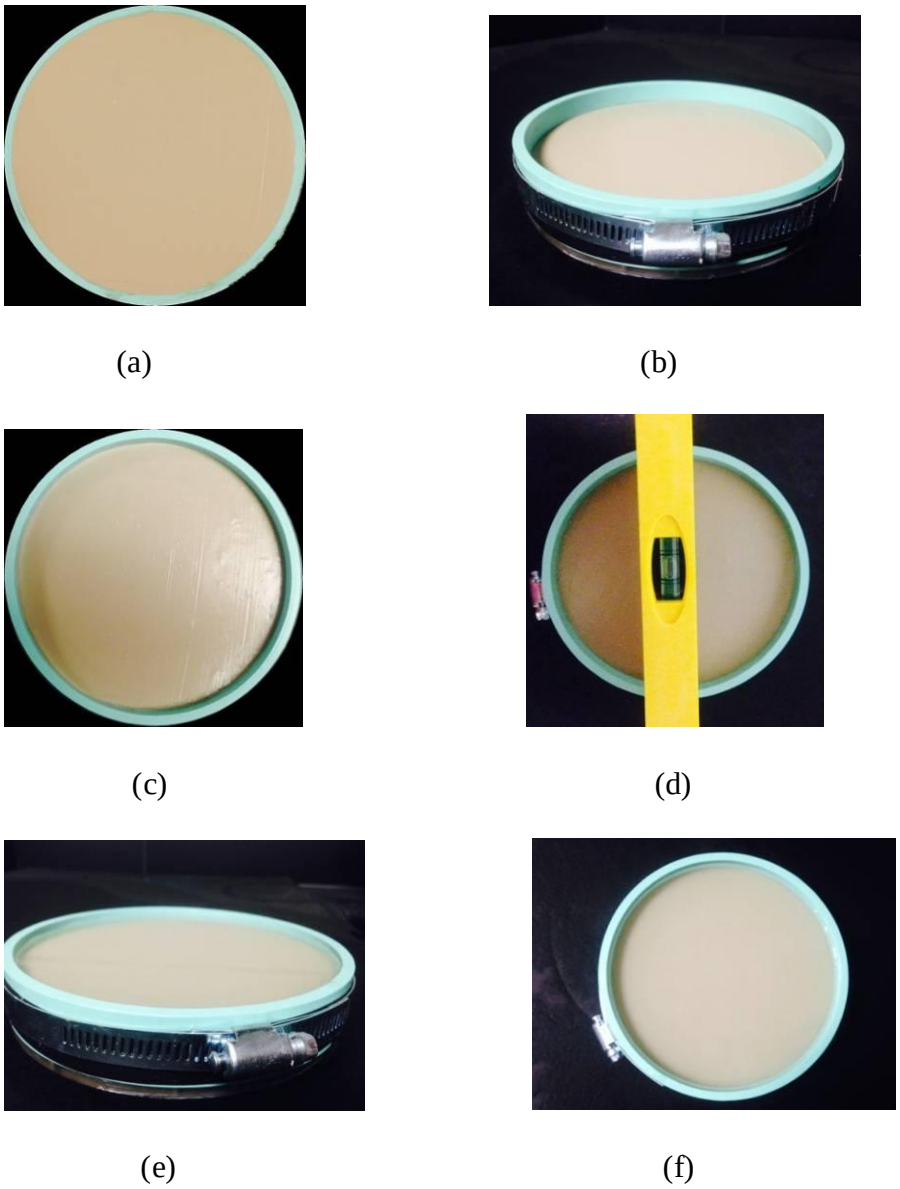

Figure 3. 11. Shows the details of this test: (a) preparing the sample with smooth surface in 0.5"thick mold, (b) using metal worm drive clamp with water resistant anti-slip tape to fix the other 0.5" ring above the original one, (c) showing the sample after placing the extra ring, (d) checking the horizontal level of the surface, (e) and (f) photos were taken directly after exposing the sample to the salt solution, (g) this photo was taken after few minutes (around half an hour), and (h) just for visualization, a small red piece put in the solution to show its surface level.

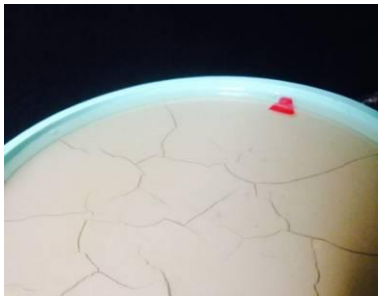

(g) (h)

Figure 3. 11. Continued.

5) An identical test to the previous one was performed except using a smooth bottom instead of using a grooved one. This test ended with no crack initiation and no shrinkage but the depth of the sample was changed from 12.7 mm to around 11 mm, which was measured manually after carefully removing the solution from the sample surface. Figure 3.12 shows the behavior of the soil sample under salt solution with smooth surface.

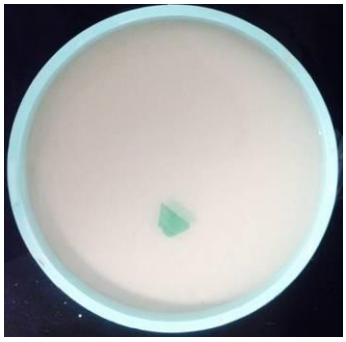

(a) (b)

Figure 3. 12. Shows the details of this test: (a) initial state before adding the solution, (b) after adding the solution, (c) and (d) for showing the level of the solution, a small green piece put in the solution.

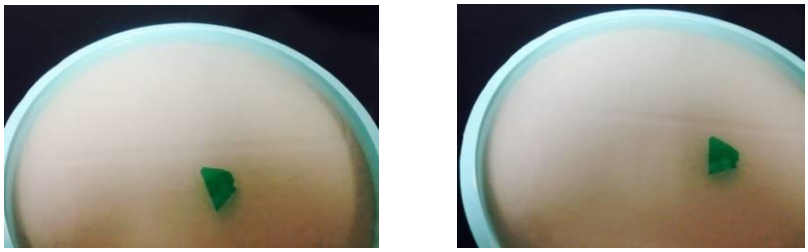

(c) (d)

Figure 3. 12. Continued.

3.7.1.B Inside the desiccator

A relative humidity of 58.1% was imposed by means of salt solution $Ca(NO_3)_2.4H_2O$ with a total suction of 75 MPa (measured by using the WP4-T device). Two desiccators were used for this research. These desiccators had covers and porcelain plates with 300 mm inner diameter, 365 mm outer diameter, and 340 mm height as shown in figure 3.13.

A hypothesis of using a closed chamber is the water evaporation in this case governed by water vapor diffusion in the gas phase from the soil sample to the salt solution (Rodriguez et al., 2007). The diffusion of the water is slower than the liquid water flow in the soil. Therefore, to reach an equilibrium condition, longer time needs to be considered (more than the one under the lab atmosphere). As a result, suction is distributed uniformly over the vertical dimension of the soil sample inside the desiccator. This theory is true when the thickness of the sample is small in comparison with the distance between the plate surface and the salt solution, which controls the relative humidity inside the desiccator (Rodriguez et al., 2007).

Figure 3. 13. The glass desiccator with the porcelain plate.

1) Using a mold of thickness 0.5" (12.7 mm) with small circular grooves at the bottom, and the sample was left inside the desiccator on the porcelain plate for 49 days. To avoid closing the holes of the plate (figure 3.13), small plastic pieces put under the mold to rise it few millimeters that is because these holes are needed for water vapor transfer. The salt solution (calcium nitrate tetrahydrate $Ca(NO_3)_2.4H_2O$) poured into the bottom of the desiccator under the plate. Thus, the suction uniformly distributed over the vertical dimension of the soil sample inside the desiccator. Also, a small camera (Gopro camera) was used inside the desiccator to take a series of photos (one each 30 minutes) in order to monitor crack patterns that was analyzed by using *image j* software. By using a level (a ruler with a bubble), the direction of the camera with the sample was controlled (the camera was fixed exactly perpendicular to the sample) as shown in figures 3.14 and 3.15. The chamber was closed for 49 days.

Figure 3. 14. Using a level bubble after fixing the camera inside the cap to make sure the camera is perpendicular to the sample.

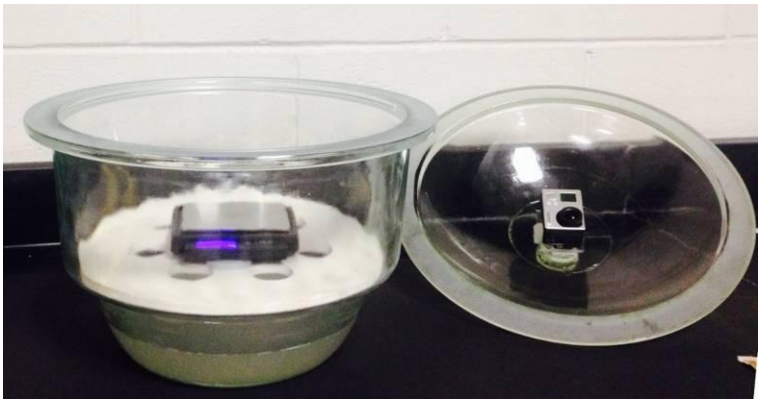

Figure 3. 15. Putting the solution at the bottom of the desiccator, and using a small scale to measure the weight of the sample at the beginning and at the end of the test.

Figure 3.16 and 3.17 show the setting up of the experiment and show the initiation and the propagation of desiccation cracks with time.

Figure 3. 16. Setting up the experiment.

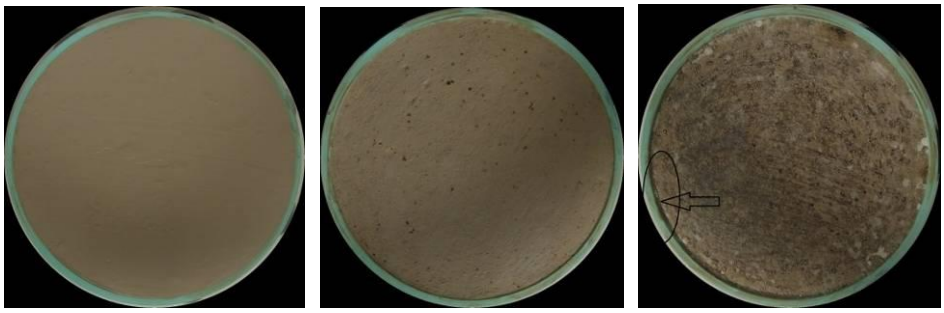

(a) Initial state (b) 20 days (c) 28 days

Figure 3. 17. Photos were taken during the experiment, notice case (a) was showing sample initial state before closing the chamber, and case (k) was taken at the end of 49 days when the sample was taken out of the chamber.

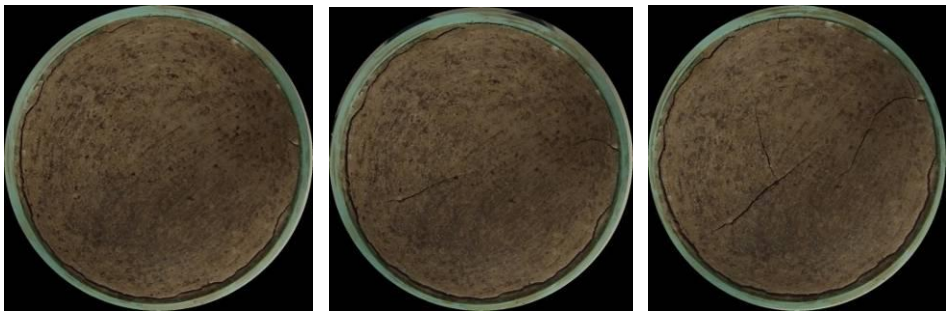

(d) 35 days (e) 38 days (f) 41 days

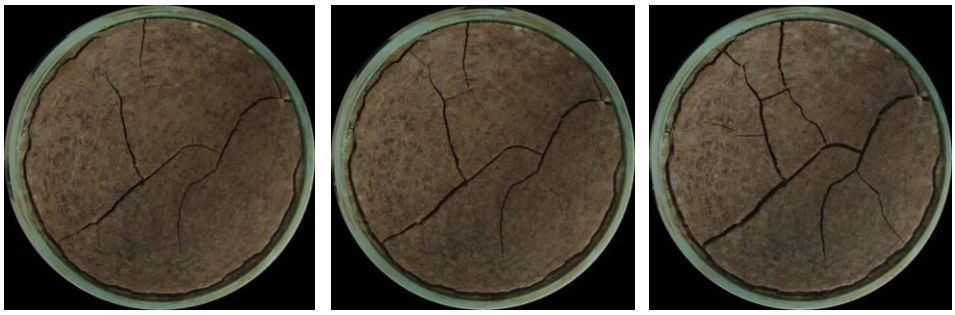

(g) 43 days (h) 44 days (i) 46 days

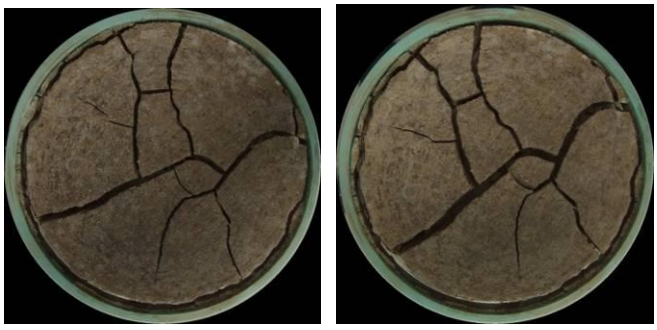

(j) 47 days (k) 49 days

Figure 3. 17. Continued.

As shown in figure 3.17, there were no cracks development till around 28 days. After that, the cracked areas increased with time, and they increased rapidly for a period

between 44 days and 47 days. Then, at the end of 47 days, the number of cracks approached a steady state situation.

2) Using a mold of thickness 0.5" (12.7 mm) with a smooth surface (without grooves). In this case, the bottom and the sides of the mold were greased with Vaseline before placing the mixture. Additionally, the salt solution poured into the bottom of the desiccator. The chamber was closed for 49 days, the sample was monitored each few hours, and photos were taken manually each few days. Over time, the cross section area and the volume of the sample were gradually changed because of the shrinkage due to water evaporation and the depth of the sample decreased from 12.7 mm to 8.5 mm as shown in figure 3.18.

(a) Initial state (b) 30 days (c) 35 days

Figure 3. 18. Shrinkage stages inside the desiccator.

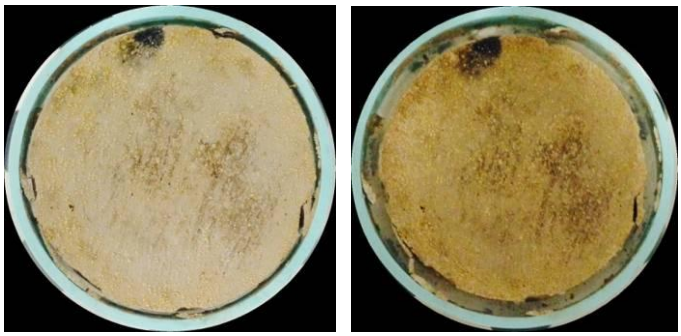

(d) 40 days (e) 49 days

Figure 3. 18. Continued.

3.7.2 Porcelain and kaolinite

This mixture consists of 50% porcelain and 50% kaolinite (the percentage in terms of sample mass). Initial water content before mixing with water was measured and found to be around 1.43%, and the total water content of the sample was 75.3%. Therefore, the net water content was 73.75%.The liquid limit of the mixture was 50%. The initial dry density (ρ_d) of this soil was 878.19 Kg/m^3, initial dry unit weight (Υ_d) was 8.62 KN/m^3, wet bulk density (ρ_T) was 1536.83 Kg/m^3, and the saturated unit weight (Υ_T) was 15.08 KN/m^3. Also, other properties of this mixture were obtained such as specific gravity (G_s) was 2.5, void ratio (e) of fully saturated soil was 1.88, and porosity (n) was 0.65. Basically, all tests were done with this mixture were identical to the previous ones. Therefore, to avoid repetition, only the images of these tests are attached below to show the results.

3.7.2.A Under the lab atmosphere

A mold of thickness 0.5" (12.7 mm) with small circular grooves at the bottom. Figure 3.19 shows the initiation and the propagation of cracks development with time.

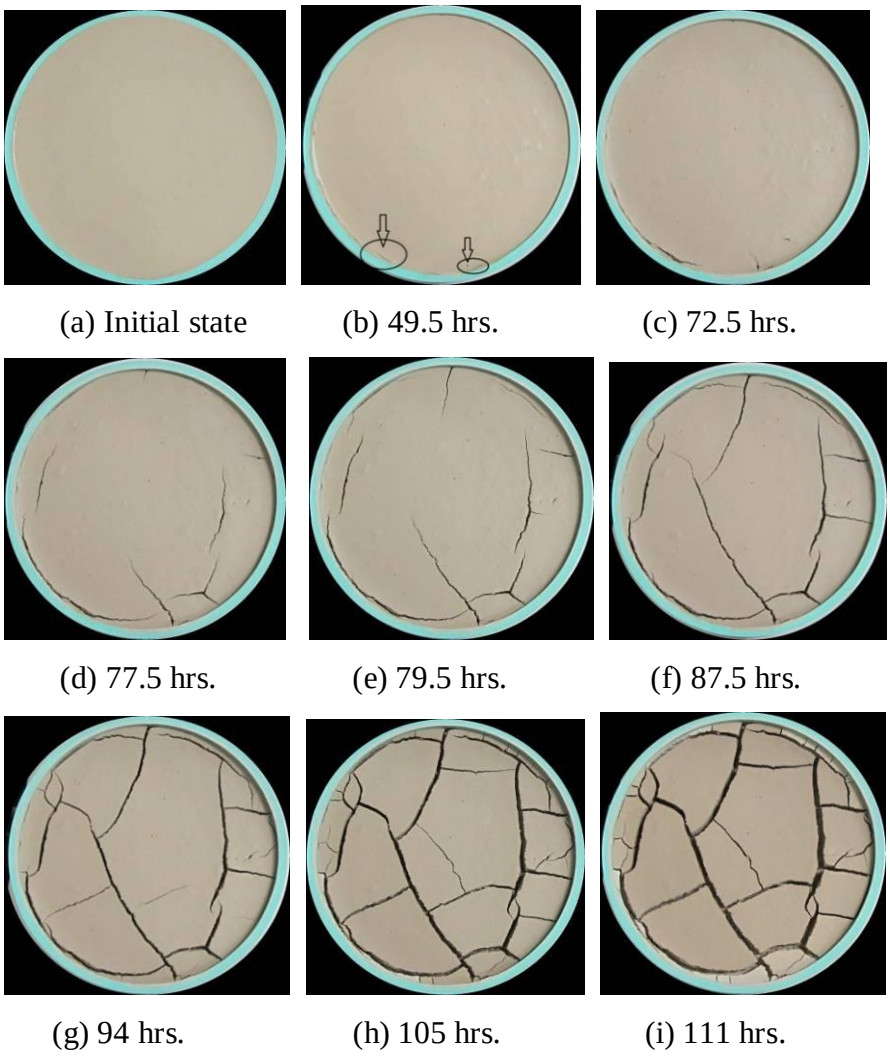

(a) Initial state (b) 49.5 hrs. (c) 72.5 hrs.

(d) 77.5 hrs. (e) 79.5 hrs. (f) 87.5 hrs.

(g) 94 hrs. (h) 105 hrs. (i) 111 hrs.

Figure 3. 19. Photos were taken during the experiment, notice case (a) was taken just after preparing the sample, and case (k) at the end of the test.

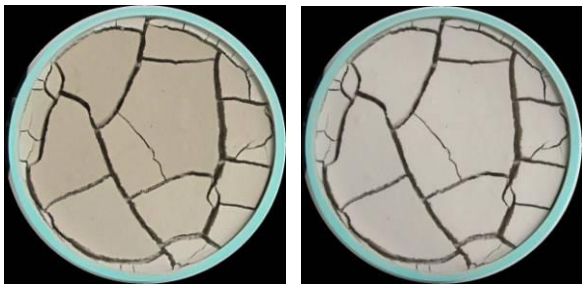

(j) 113.5 hrs. (k) 117 hrs.

Figure 3. 19. Continued.

1) A mold of thickness 1" (25.4 mm) with small circular grooves and holes (2.5 mm diameter) at the bottom. Exposing the soil sample to a distill water directly as shown in figure 3.20.

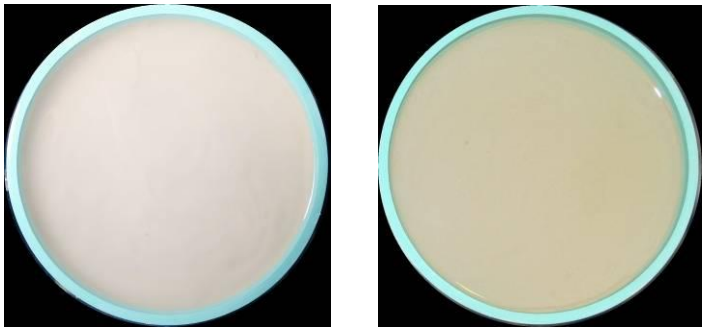

(a) (b)

Figure 3. 20. Photos were taken to the sample (a) initial state and (b) after 96 hours.

2) A mold 0.5" thick mold with smooth bottom surface. Figure 3.21 shows the behavior of the soil sample under drying with smooth surface.

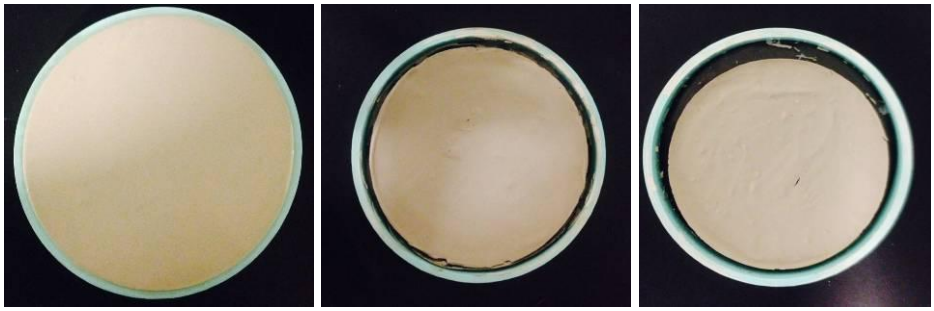

(a) (b) (c)

Figure 3. 21. Photos were taken to the sample (a) initial state, (b) after 48 hours, and (c) after 96 hours from the time of setting up the test.

3) A mold of thickness 1" (25.4 mm) with small circular grooves and holes. Exposing the sample to the salt solution as shown in figure 3.22.

(a) (b) (c)

Figure 3. 22. Photos were taken to the sample (a) initial state, (b) during the test; the sample was monitored by capturing a series of photos, and (c) after few hours from the time of setting up the test.

3.7.2.B Inside the desiccator

A mold of thickness 0.5" (12.7 mm) with small circular grooves at the bottom. Figure 3.23 shows the initiation and the propagation of desiccation cracks with time.

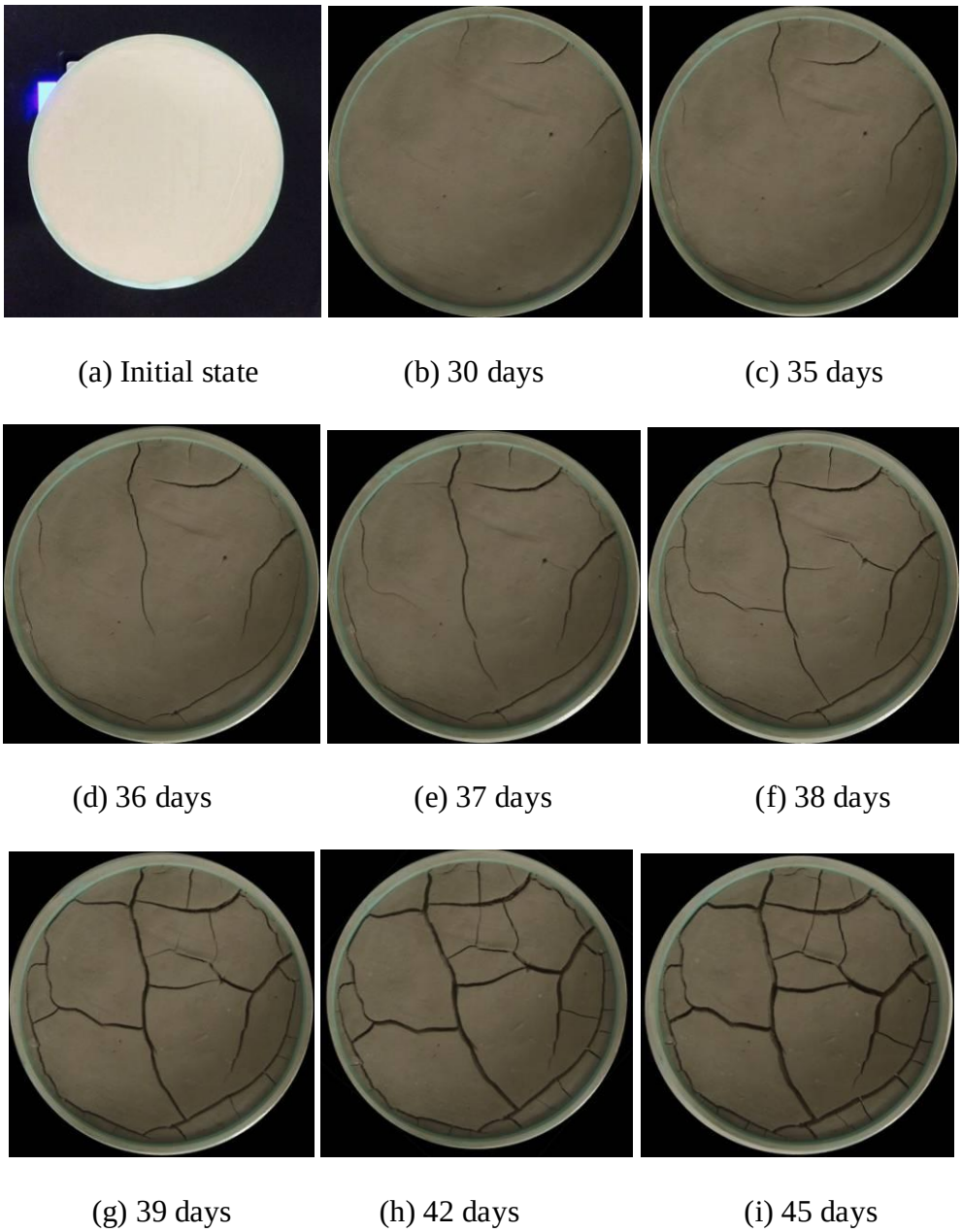

(a) Initial state (b) 30 days (c) 35 days

(d) 36 days (e) 37 days (f) 38 days

(g) 39 days (h) 42 days (i) 45 days

Figure 3. 23. Photos were taken during the experiment, notice case (a) was just to weight the sample with the mold before closing the chamber, and case (i) at the end of the experiment when the sample was taken out of the chamber.

1) A mold of 0.5" (12.7 mm) thickness with a smooth bottom surface.

At the end of this test, only the volume of the sample was changed because the depth of the sample decreased from 12.7 mm to 10.2 mm as shown in figure 3.24.

(a) (b) (c)

Figure 3. 24. Photos were taken to the sample (a) initial state, (b) after setting up the experiment, and (c) after 45 days inside the desiccator.

3.9 DESICCATION AND CRACKING BEHAVIOR OF CLAY UNDER WETTING-DRYING (W-D) CYCLES

According to Tang et al. (2011), several researchers worked on the hydro-mechanical behavior of clayey soils under wetting-drying cycles (e.g. Audiguier et al., 2007; Laribi et al., 2008; Geremew et al., 2009; and Tang et al., 2009). Few studies have researched the effect of wetting-drying cycles on desiccation cracks (Tang et al., 2011). The effect of multiple wetting-drying cycles in the cracking behavior was investigated in this research by doing several wetting-drying cycles on the initially saturated samples of pure kaolinite and a mixture of kaolinite with bentonite. These experiments were conducted under the lab atmosphere (24 ± 1 ℃, and 52 ± 2% of RH), and the weight of each

sample was monitored by using a small scale (with an accuracy of 0.01 g) connected to the computer. A Canon camera also was fixed directly above the sample (perpendicularly) to take a series of photos regularly (one each 30 minutes) during drying as shown in figure 3.25. In each cycle, the drying test was ended when the weight of the sample was roughly stabilized with (±0.05 g). The subsequent wetting was done by carefully adding distilled water to the sample using a spray bottle as shown in figure 3.26. Then, the sample was left covered for 24 hours to ensure that water was spread through the all soil particles (to obtain a fully saturated sample). After that, the sample was subjected to the lab atmosphere again and the whole process was repeated until it ended with four to five wetting-drying cycles.

Figure 3. 25. Monitoring the sample weight and the cracking surface during drying process.

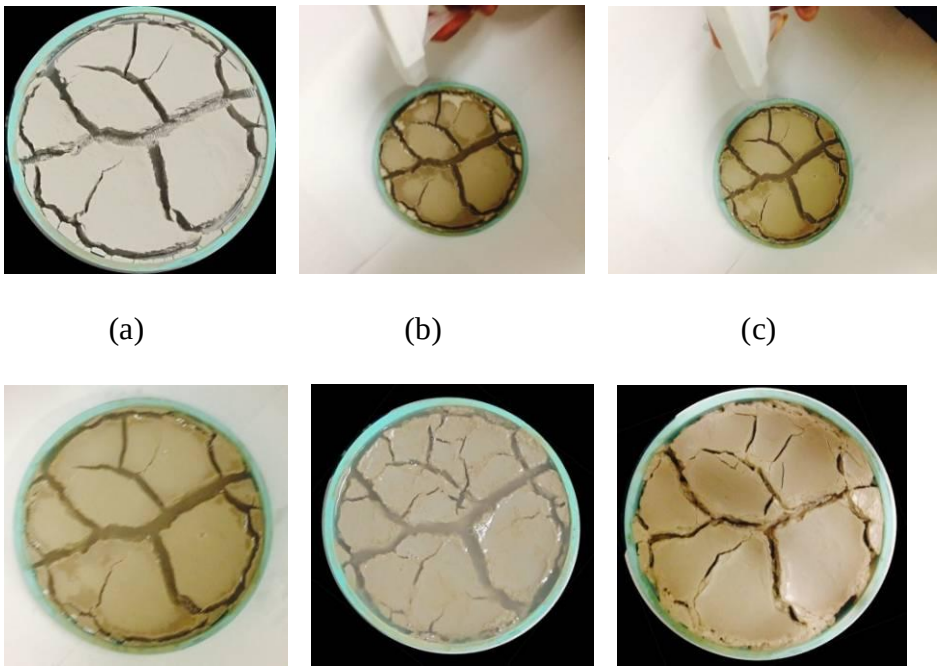

(a) (b) (c)

(d) (e) (f)

Figure 3. 26. (a) Initial state before the 2nd wetting process; (b) and (c) during wetting process by using a spray bottle; (d) and (e) final state of wetting process (before covering the sample); and (f) initial state before the 2nd drying path.

3.9.1 Kaolinite and bentonite

An identical mixture, which was used in the previous tests, was also used for wetting-drying tests. Figure 3.27 shows the final crack patterns after each wetting-drying cycle. For more details, photos of all wetting-drying cycles are attached in appendix 3.

At the end of each wetting-drying cycle, the image analysis technique was applied (by using *image j* software) to obtain the main parameters which are CIF, $(CIF)_{tot}$, cracked area, and shrinkage area.

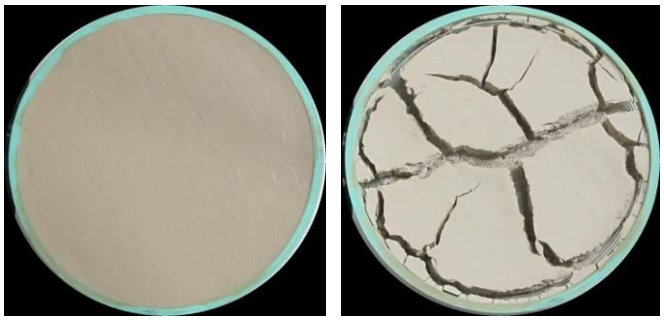

(a) Initial state (b) After 1st drying

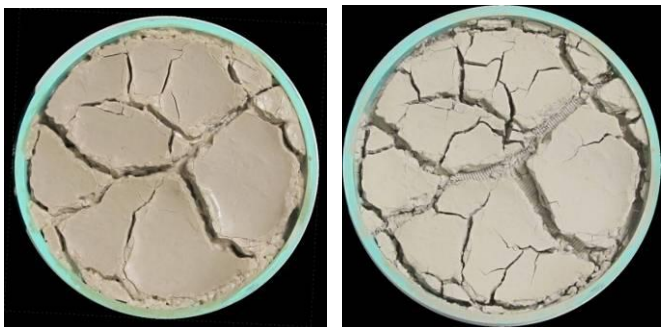

(c) After 2nd wetting (d) After 2nd drying

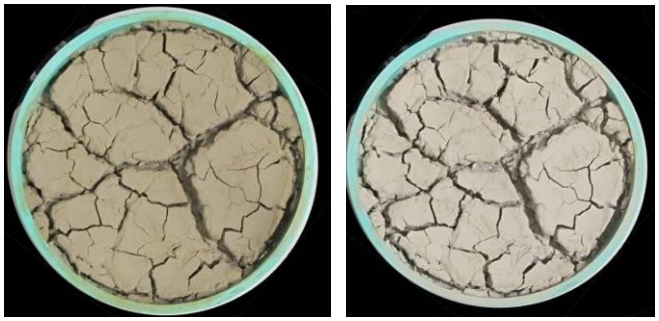

(e) After 3rd wetting (f) After 3rd wetting

Figure 3. 27. Final pattern at the end of each wetting-drying cycle.

(g) After 4th wetting (h) After 4th drying

(i) After 5th wetting (j) After 5th drying

Figure 2. 27. Continued.

3.9.2 Kaolinite with 100% water content

Another mixture of pure kaolinite was used for doing wetting-drying cycles. However, the results were quite different from the previous mixture. The crack patterns (CIF and $(CIF)_{tot}$) changed dramatically between the first and the second cycles, and then they were roughly constant with minor changes during the third and fourth cycles. Figure 3.28 shows the final crack patterns after each wetting-drying cycle. For more details, photos of all wetting-drying cycles are attached in appendix 3.

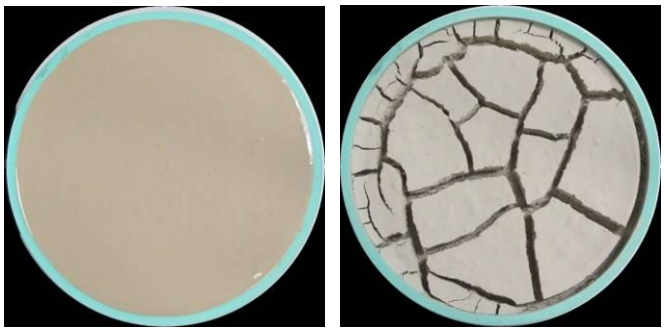

(a) Initial state (b) After 1st drying

(c) After 2nd wetting (d) After 2nd drying

(e) After 3rd wetting (f) After 3rd wetting

Figure 3. 28. Final patterns at the end of each wetting-drying cycle.

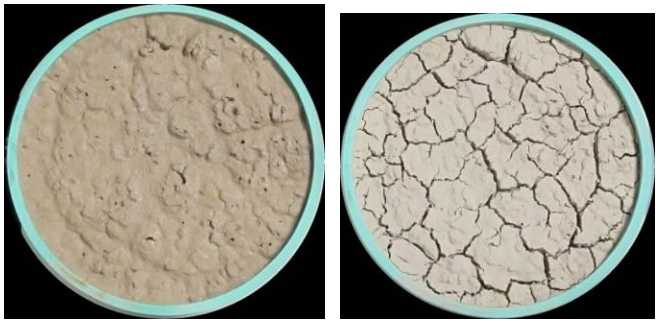

(g) After 4th wetting (h) After 4th drying

Figure 3. 28. Continued.

A series of 6 images, which were taken in the lab while the sample was drying after the 2nd wetting process, are as shown in figure 3.29. These images show the development of surface cracks and fissures with time after the wetting process. After the second wetting process the edges of the cracks segments became jagged more than the ones observed after the first wetting-drying cycle. Also, the main cracks were virtually closed after a few minutes of the second wetting process, and then some micro-cracks (fissures) developed on the surface while the sample was drying. Additionally, uncracked cells were broken into a large number of small pieces during the second wetting-drying cycle.

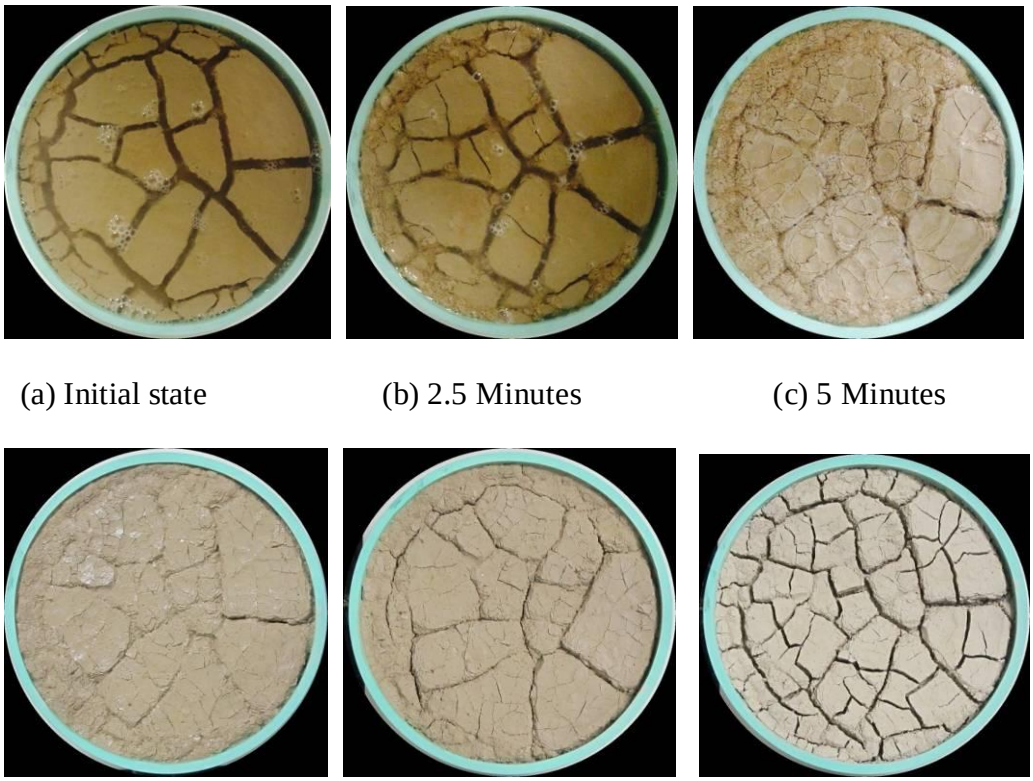

(a) Initial state (b) 2.5 Minutes (c) 5 Minutes

(d) 10 Minutes (e) 5 Hours (f) 3 Days

Figure 3. 29. Development of crack patterns during the 2nd wetting-drying cycle.

3.10 SALT SOLUTION PROPERTIES

Calcium nitrate tetrahydrate ($Ca(NO_3)_2.4H_2O$) was used in this research. It is white, deliquescent mass, and soluble in water, alcohol and acetone (Lewis Richard, 2007). This salt has many applications, but its main purpose is working as a component in fertilizers. Table 3.1 presents the main properties of this salt.

There were two problems related to this kind of salt: first, it takes too long in order to arrive after it is ordered online; second, it is too expensive comparing with Anhydrous

calcium nitrate ($Ca(NO_3)_2$). Therefore, for saving time and money, calcium nitrate tetrahydrate was obtained in this way:

$$Ca(NO_3)_2 + 4H_2O = Ca(NO_3)_2.4H_2O$$

by obtaining the molecular mass of water (which is 18.02 g/mol) and multiplying it by 4. Then, adding it to the molecular mass of $Ca(NO_3)_2$ (which is 164.088 g/mol). Thus, the $Ca(NO_3)_2.4H_2O$ was obtained. For example:

$$100 \text{ g of } (Ca(NO_3)_2) + 43.93 \text{ g of } (H_2O) = 143.93 \text{ g of } (Ca(NO_3)_2.4H_2O)$$

Then, the solubility of this salt is dependent on temperature. For instance, at 20 ℃, for each 129 g of ($Ca(NO_3)_2.4H_2O$) add 100 g of (H_2O) to obtain a fully saturated solution.

Table 3. 1. Properties of calcium nitrate tetrahydrate ($Ca(NO_3)_2.4H_2O$)

Properties	
Molar Mass	236.15
Density	1.896 g/cm^3 @25℃
Melting point	42.7 ℃
Boiling point	132 ℃
Solubility in water	195 g/100 g @ 0 ℃
	129 g/100 g @ 20 ℃
	156 g/ 100 g @ 30 ℃
	363 g/100 g @ 100 ℃
PH	5-7.5 @ 25 ℃

3.11 KAOLINITE, PORCELAIN, AND BENTONITE PROPERTIES

Basically, individual particles of clay are mixed together to form clay bodies. Different types of clay contribute with their properties to the clay body - color, texture, plasticity and so on. Thus, clay types are: Residual Clays, Sedimentary Clays, Kaolin, Ball Clay, Stoneware Clays, Fireclay, Earthenware Clays, and Porcelain (which is known as china). In this research, kaolinite, porcelain, and bentonite were used.

Kaolinite is kind of a clay mineral with chemical composition $Al_2Si_2O_5(OH)_4$. Generally, kaolinite has a considerably small shrink-swell capacity and a small cation- exchange capacity (Jolyon Ralph, mindat.org, 2014).

Porcelain is Warm Brown Stoneware Clay. It has some particular properties such as: low permeability and elasticity, but it has high resistance to chemical attack and thermal shock.

Bentonite has a complicated chemical composition $2[(Al_{1.67}Mg_{0.33})(Si_{3.5}\,Al_{0.5})O_{10}(OH)_2]$. Also, it has some particular characteristics such as: the ability to create viscosity with very low concentration in water, to absorb very large amount of water, to swell when contacts with water. It also has low permeability, has a high cation- exchange capacity which is opposite to the kaolinite, and cheaper than other types of clay.

3.12 CONCLUSION

This chapter presented three sets of experiments, which were done in the lab on artificial clays to provide insight into the crack patterns of thin soil layers. The first set of tests was composed of seven samples; a total of five samples were associated with the tests which were done under the lab atmosphere; and the other two samples were associated with the tests which were done inside the desiccators. The other set of tests was similar to the first one except the mixture was different. The third set of tests was composed of two samples for testing the soils under wetting-drying cycles. For the first two sets, two main mixtures were used for these experiments with circular specimens, each one with a diameter of 5.9" (150 mm). The effect of bottom contact was studied effectively by using two different surface textures (grooved and smooth plates). Another boundary condition, which was considered, is the effect of different environmental conditions (lab atmosphere and desiccator). A series of photos was taken during the tests and analyzed by using *image j* software; the main parameters were obtained and discussed in chapter 5.

To reach the equilibrium condition inside the desiccator took too long (around 45 to 49 days); that is probably because of the exchanging of liquid water between the soil sample and the salt solution by means of water diffusion in the gas phase. Since the water vapor diffusion is slower than the water flow in the sample, it takes a long time to reach the equilibrium condition.

As for the samples exposed directly to the salt solution, an osmotic suction was applied to them by using the salt solution ($Ca(NO_3)_2.4H_2O$). Cracks were developed on the sample surface after few minutes of exposing the sample to the solution.

The results of drying tests are not beyond the presented literature. The effect of bottom contact surface on the strength of the soil during drying is studied effectively in chapter 4. In general, this work helps to develop a model which predicts formation of desiccation cracks in soil under different boundary conditions.

The effects of wetting-drying cycles on the behavior of thin soil layers were investigated in the lab with a mixture of pure kaolinite and another mixture of kaolinite with bentonite. During the test, the water evaporation path with the development of surface cracks and volume shrinkage were monitored. *Image j* software was used for quantitatively analyzing cracks patterns after each wetting-drying cycle. The results of these two mixtures were slightly different. However, the behavior of soil sample of pure kaolinite was in acceptable agreement with existing literature of Tang et al. (2011). There was an equilibrium state in the third and fourth wetting-drying cycles, which was stated by Tang et al. (2011). Additionally, as shown in figure 3.29 the main cracks formed in the first dry path were virtually closed after 10 minutes of the second wetting path; at the meantime, small cracks (fissures) were initiated after this wetting process, which was also stated by Tang et al. (2011). Furthermore, figure 3.29 clearly showed that destruction initially started on the edges and the corners of the main cells, which

were developed after the first wetting-drying cycle, which is probably because the main cracks offered free spaces for clay swelling (Tang et al., 2011). As for the results of soil sample with a mixture of kaolinite and bentonite, were rather difficult to interpret. After the second wetting path, the main cracks were not totally closed; however, a number of micro-cracks (fissures) were initiated on the surface. The effect of high plasticity value of bentonite clay was considered by doing five wetting-drying cycles to reach the equilibrium state. In general, when clayey soils have high plasticity, more wetting-drying cycles required to reach the equilibrium condition than the normal ones (Al-Wahab and El-Kedrah, 1995; Omidi et al., 1996; and Yesiller et al., 2000). After all, the results of these lab experiments are useful for understanding the effect of different seasons on soil behavior. It is worth mentioning that swelling was observed in both samples, so more attention should be paid to soil swelling during wetting path.

Note: results are presented in detail in chapter five.

INTERFACE DIRECT SHEAR TESTING AND SOIL-WATER RETENTION CURVE

4.1 INTRODUCTION

In this chapter, the intention was to modify the conventional direct shear device in order to simulate identical interface conditions of those tests that were discussed in chapter three. The main objective is to investigate the behavior of clay- rough surface and clay-smooth surface interfaces and show how to modify the traditional direct shear box. Therefore, general information about the interface direct shear test and how to modify the conventional direct shear box have been described. In addition, a number of lab experiments have been carried out and described in detail. Also, the soil-water retention curve was obtained in the lab to investigate the behavior of the soil in terms of suction during drying. Finally, a comprehensive conclusion has been written at the end of this chapter to discuss the results and summarize them.

4.2 SHEAR STRENGTH OF SOILS

Soil shear strength could be defined as the ability of soil to resist shear stresses, so the strength of any soil represents the greatest stress this soil can tolerate. In general, interaction between soil particles controls the soil shear strength, as shown in figure 4.1.

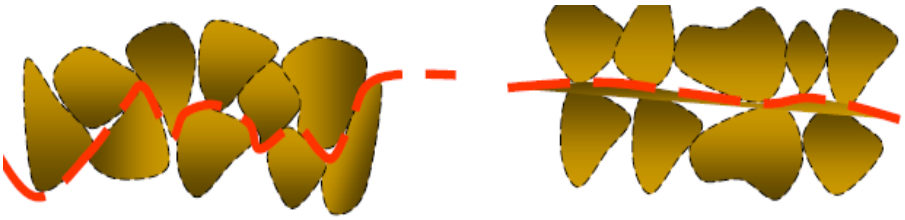

Figure 4. 1. Interactions between particles (particles slide or roll past each other).

In geotechnical major, the safety of any structure is governed by the strength of the soil because the structure may collapse when its soil (the soil exists below the structure) fails. Figure 4.2 shows an example of the shear failure in soils and figure 4.3 shows slope failure in soils.

Figure 4. 2. Shear failure in soils.

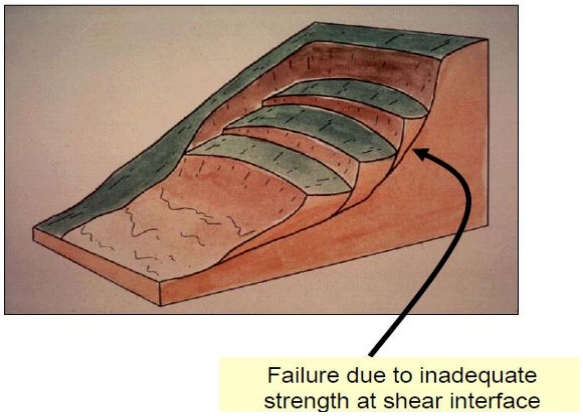

Figure 4. 3. Slope failure in soils.

A particular case of the undrained strength is relevant to a clayey soil that in the short term remains undrained. In this case, pore pressures cannot be estimated, so effective stresses cannot be determined from undrained tests. Also, undrained strengths may become unreliable in case of using low shearing rate because it would be impossible to prevent localized drainage.

The direct shear test is the oldest strength tests for soils (cohesive and non-cohesive), and used to obtain their shear strength. This strength is a significant engineering characteristic of any soil because it is required for determining the slopes stability, the foundations bearing capacity, and retaining walls. Shibuya et al. (1997) have provided the best explanation of the shear box for determining soil strength in the direct shear device. Figure 4.4 shows a commercially available direct shear apparatus and figure 4.5 shows the conventional shear boxes.

Figure 4. 4. Conventional direct shear apparatus.

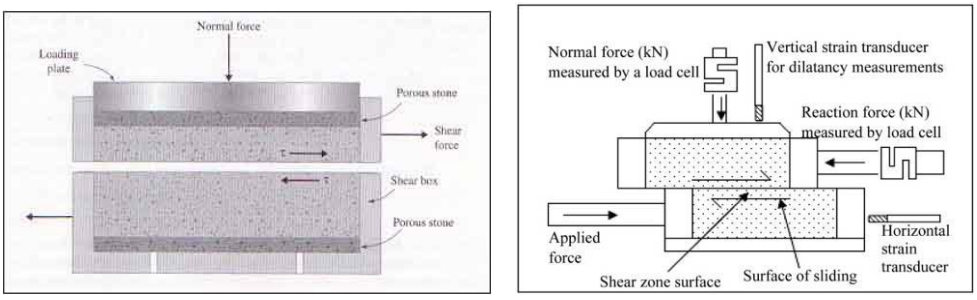

(a) (b)

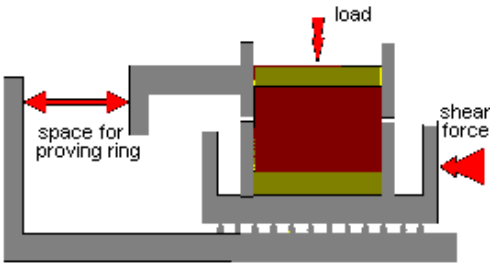

(c)

Figure 4. 5. Conventional direct shear boxes.

In the present work, the traditional test (in accordance with ASTM standard D 3080 (American Society for Testing and Materials, 2007)) was carried out to measure the shear strength parameters of saturated and dry samples, and then the device was modified for interface testing under drained and undrained conditions (slow and high shear rates respectively).

4.3 SHEARING RATE

Although the conventional direct shear device is used to measure parameters of drained shear strength, some researchers were interested in modifying this device to replicate the undrained condition by keeping the sample volume constant during the test (Bro et al., 2013). These investigations were done by adjusting the normal load while the test was running (Taylor, 1952; O'Neil, 1962; Takada, 1993). These adjustments provided reasonable approximations of undrained shear strength from simple shear test of constant volume (Hanzawa et al., 2007). After all, the present study is intended to modify the traditional direct shear device for interface shearing, and also to provide reasonable estimates of drained and undrained soil strength parameters. In present study, both undrained and drained conditions have been considered with shear rate of 0.5 mm/min and 0.018 mm/min, respectively. For undrained condition, a shear rate of 0.5 mm/min was selected depending on some text books, which suggested that undrained shear strength of saturated sample can be estimated by using the direct shear test at high shear rate (e.g., Bowles, 1992; Carter, 1983; Lambe, 1951; Liu and Evett, 1997). These studies suggested that if the saturated soil sample has low permeability and the direct shear test

was run at fast shear rates, the sample would shear with no considerable volume change. As for the drained condition, a shear rate of 0.018 mm/min was used. That is considered as a slow shear rate and the pore pressure generation was ignored inside the sample. However, shearing rate of 0.005 mm/min was used in some previous works (Miller et al., 2007 and Khoury et al., 2012). Although there was no test carried out to evaluate the effect of shearing rate on the behavior of soil, the value of shearing rate in the present study is considered practically reasonable for the mixture of kaolinite and bentonite; that is because two different tests (soil- plate interface) were carried out with shearing rate of 0.005 mm/min; and then the results were compared with those of shearing rates 0.018 mm/min and 0.5 mm/min. It has been shown that the values of the maximum shear strength of the soil-grooved surface of both shearing rates (0.005 mm/min and 0.018 mm/min) were roughly close together; conversely, the maximum shear strength of 0.5 mm/min shear rate was far from them as shown in figure 4.6. As a result, a shearing rate of 0.018 mm/min was selected in this research due to the time factor; the time of running the test (which was around 10 hours) was reasonable in comparison with the time of running the test at 0.005 mm/min (which was around 36 hours); since multiple tests were needed to be performed, time was a significant factor in this research.

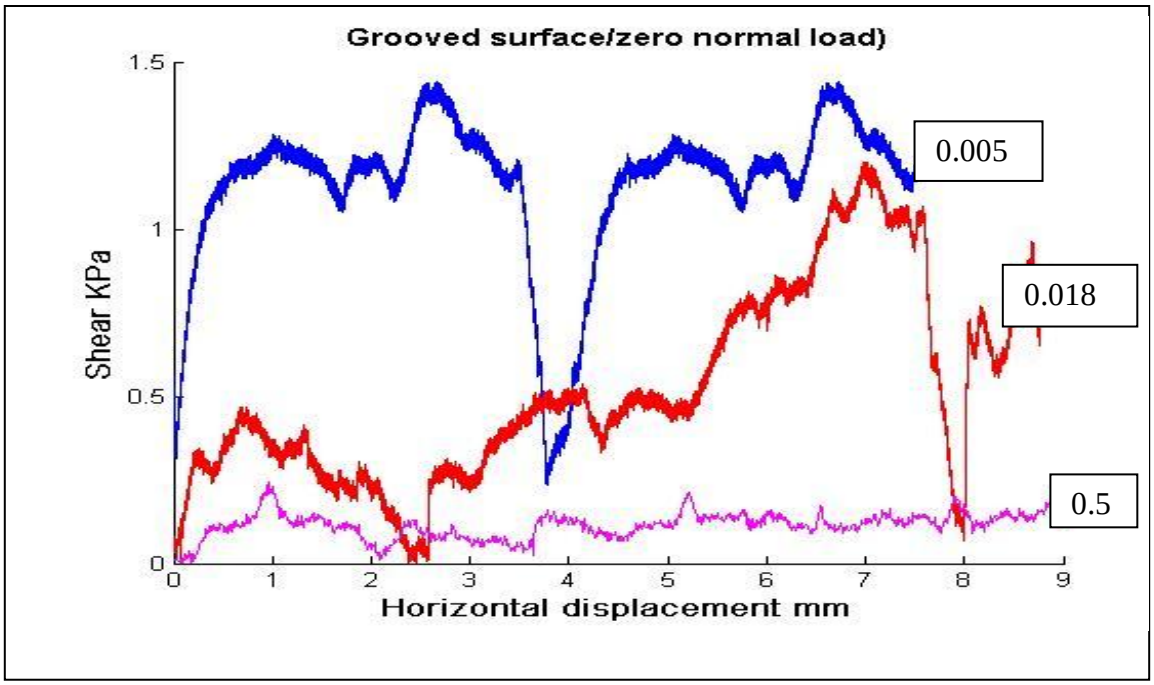

(a) Shear stress (KPa) vs. horizontal displacement (mm).

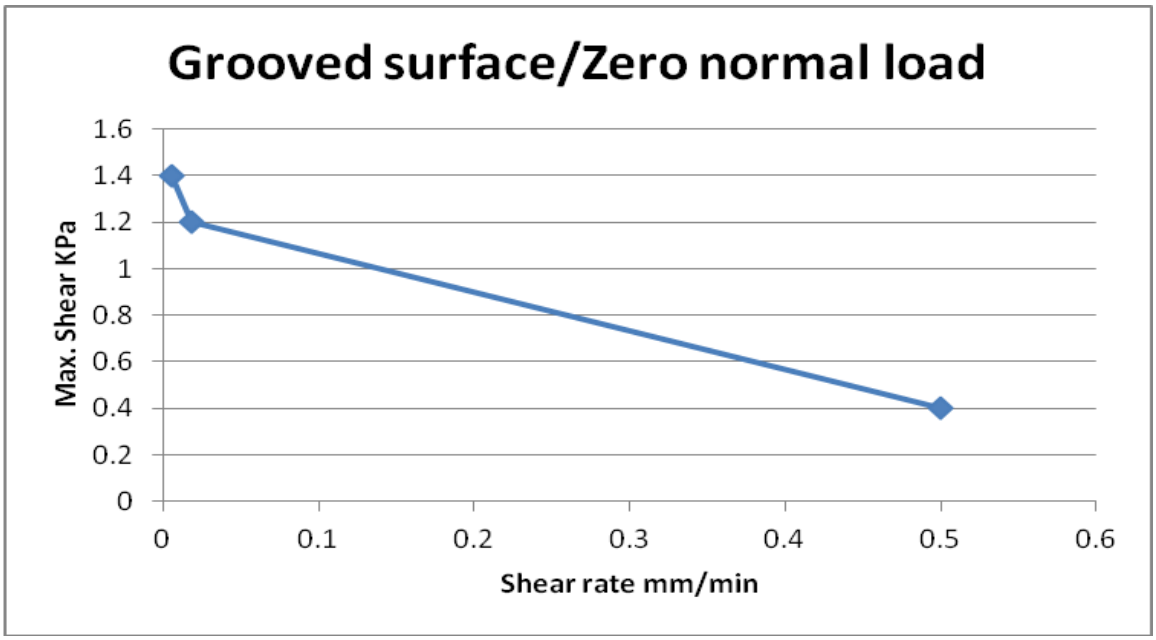

(b) Maximum shear stress (KPa) vs. shearing rate (mm/min).

Figure 4. 6. Effect of the shearing rate on the soil maximum shear stress.

4.4 INTERFACE SHEAR STRENGTH

Interface friction was studied by some researchers (e.g. Potyondy, 1961; Tsubakihara and Kishida, 1993; Fakharian and Evgin, 1996; Akhtar Hossain et al., 2012, Hamid et al., 2009, and Miller et al., 2007). These studies were done by using different devices like the direct shear, torsion, and the simple shear device. Generally, these apparatus were helpful to obtain different features of soil in interface behavior; for instance, Subba Rao et al. (2000) studied the effect of over-consolidation ratio on interface behavior. Since the direct shear device is simple to use and its results are not complicated to interpret, this device was used in this research to study soil interface behavior. In the present research, the original device has been modified in order to measure the shear strength of saturated and the unsaturated soils interface. Since there was very little water passed through the holes which exist at the bottom of the molds (Chapter Three), both undrained and drained conditions were considered. Identical circular grooves (1 mm in thickness and 1.5 mm in width) were created in a square plate (6 mm in thickness and 88.9 mm in width) with the same material of the bottom plates of the molds which were used in this research (Chapter Three). So, in this case it would be possible to test the interfaces in saturated and unsaturated samples. Furthermore, in order to simulate both conditions (with smooth and grooved surface), this plate was grooved on one side and smooth on the other side as shown in figure 4.7. This plate set between the two squared shear boxes and it was fixed by creating holes on the two opposite corners to use bolts which were able to hold the plate with the lower part of the shear box. Finally, a gap of 0.6 mm was provided between the plate and the upper part of the box by using two other

screws in the opposite corners (ASTM D3080). Figure 4.8 shows the modified direct shear device in detail.

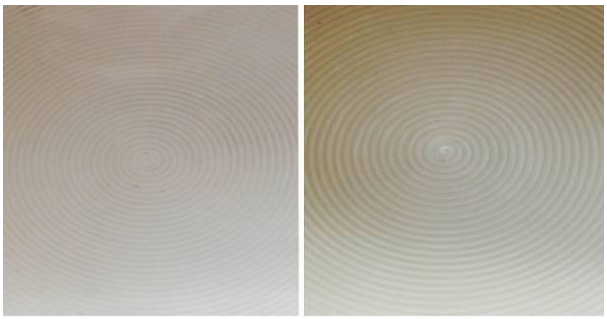

Figure 4. 7. The smooth surface to the left and the grooved one to the right.

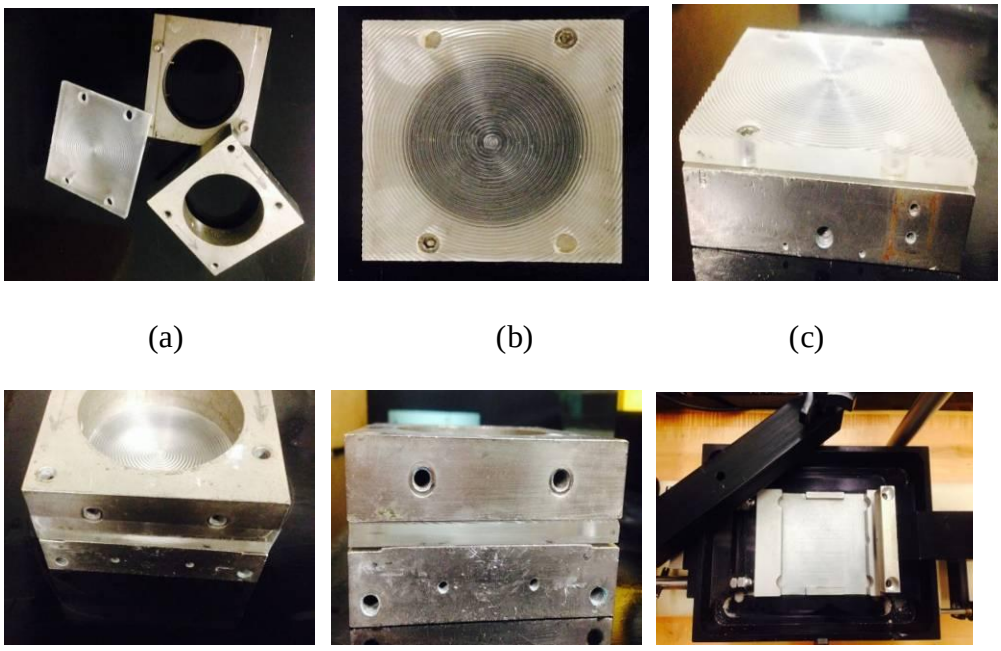

(a) (b) (c)

(d) (e) (f)

Figure 4. 8. Modified direct shear box with details.

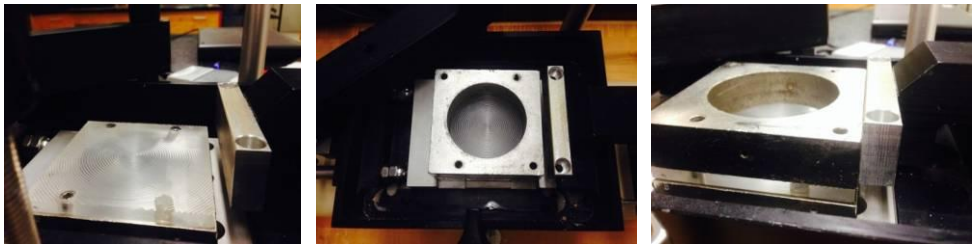

(g) (h) (i)

(j) (k) (l)

Figure 4. 8. Continued.

The purpose of this work is to study the behavior of the clay- (rough and smooth) plate interface and compare the results with the soil-soil interface. This investigation was done through laboratory experiments.

4.4 EXPERIMENTAL SET UP

First of all, a saturated case (water content around 90.19% and 0 MPa matric suction) was studied with different conditions: the soil-grooved plate interface, the soil-smooth plate interface, and the soil-soil interface. The mold was weighted before and after placing the soil to obtain the dry density which was around 0.800 g/cm^3. Thus, soil was sheared under drained condition with a constant shearing rate of 0.018 mm/min.

Shearing was continued until the peak value of shear force was visibly observed (or when shear force becomes almost constant or decreasing with time). Consequently, shearing tests were done to a maximum displacement of 8 to 10 mm. Before doing the tests, the coefficients of friction between grooved and smooth surfaces with the upper part of the shear box (steel) were obtained. The results were turn out to be 0.22 for the grooved plate and 0.17 for the smooth plate. To overcome this problem, a small gap (0.6 mm) was provided between the plate and the upper part of the shearing box (ASTM D3080). Thus, the coefficient of friction was measured again and it found to be around zero for both grooved and smooth surface.

4.4.1 Drained condition with shearing rate of 0.018 mm/min

Under a drained condition, soil was sheared directly. During the shearing process, the horizontal shear load with the vertical and horizontal displacements were recorded automatically via transducers, as shown in figures 4.9.a, b, and c.

(a) (b) (c)

Figure 4. 9. Shearing soil under drained condition, (a) without applying a normal load, (b) & (c) by applying a normal load and measuring the vertical displacement.

Thus, the first attempt was done without using a normal load (zero normal stress), and the saturated soil sample (w ~ 90.19%) was sheared under the lab atmosphere. However, sample water content was measured after shearing the sample and it found to be around 84.42%. The results are shown in figure 4.10.

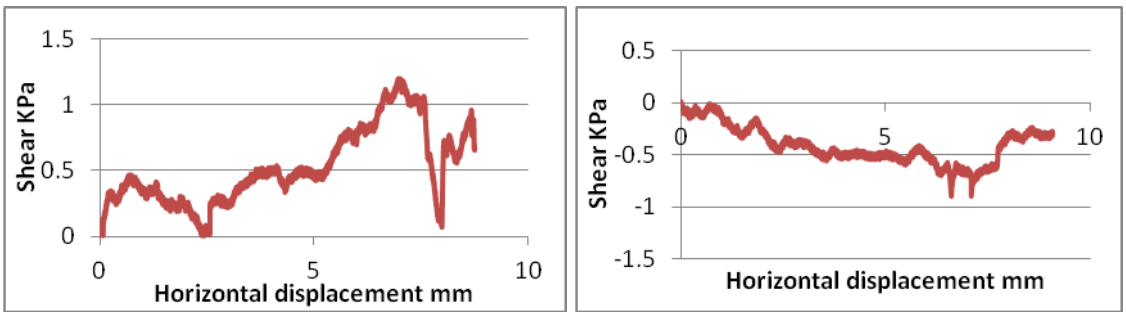

(a) (b)

Figure 4. 10. Saturated sample and zero normal stress under drained condition with (a) grooved surface, and (b) smooth surface.

All negative values in figure 4.10 (b) were considered as zeros. These results probably go back to the sensitivity of the force transducer to very small numbers. Nevertheless, negative values indicate having tensile stresses and these tensile stresses should not appear under these experimental conditions.

After that, by using a normal load of 5 kg which is given a normal stress of 15.5 KPa, the results are presented in figure 4.11. Soil initial water content was around 90.1% and after running the test it found to be around 88.71%.

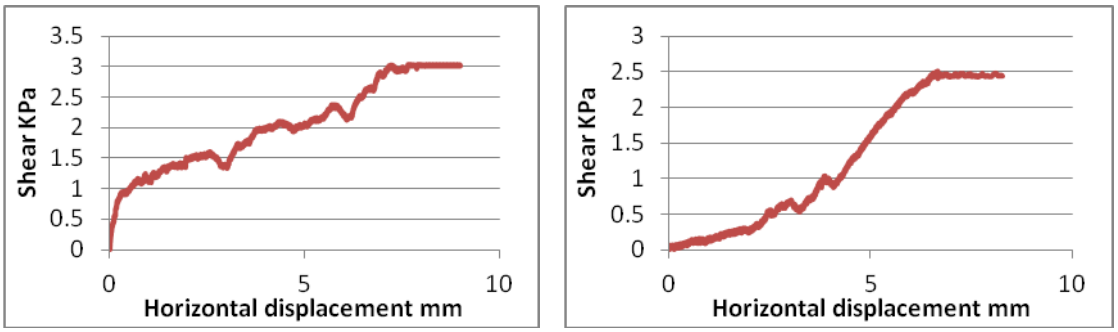

(a) (b)

Figure 4. 11. Saturated sample and 15.5 KPa normal stress under drained condition with (a) grooved surface, and (b) smooth surface.

Subsequently, by using a normal load of 2 kg which is given a normal stress of 6.2 KPa, the results are presented in figure 4.12.

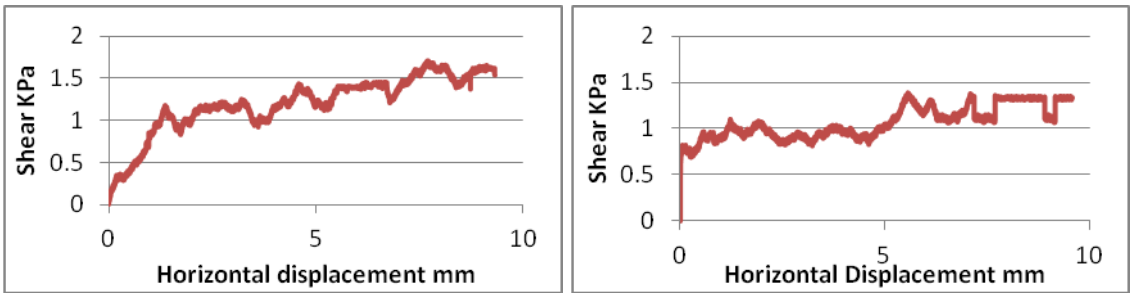

(a) (b)

Figure 4. 12. Saturated sample and 6.2 KPa normal stress under drained condition with (a) grooved surface, and (b) smooth surface.

These results were used to identify failure envelopes for soil interfaces having grooved and smooth surfaces as shown in figure 4.13 and table 4.1.

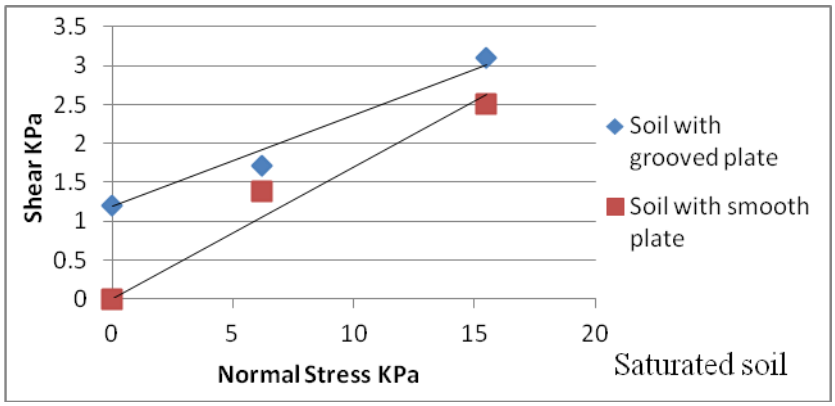

Figure 4. 13. Maximum interface shear stress vs. normal stress of saturated samples under drained condition.

Table 4. 1. Results of the interface shearing tests (drained condition)

Grooved surface			
Saturated sample	**Normal Stress 0.0 KPa**	**Normal Stress 6.2 KPa**	**Normal Stress 15.5 KPa**
Shear KPa	1.2	1.71	3.1
Adhesion KPa	1.2		
Friction angle	6.67°		
Smooth surface			
Saturated sample	**Normal Stress 0.0 KPa**	**Normal Stress 6.2 KPa**	**Normal Stress 15.5 KPa**
Shear KPa	0.0	1.38	2.5
Adhesion KPa	0.0		
Friction angle	9.09°		

A traditional direct shear test was carried out to obtained soil parameters (cohesion and friction angle) under drained condition for both saturated and dry soil samples. Figure 4.14 and table 4.2 show the results of these tests.

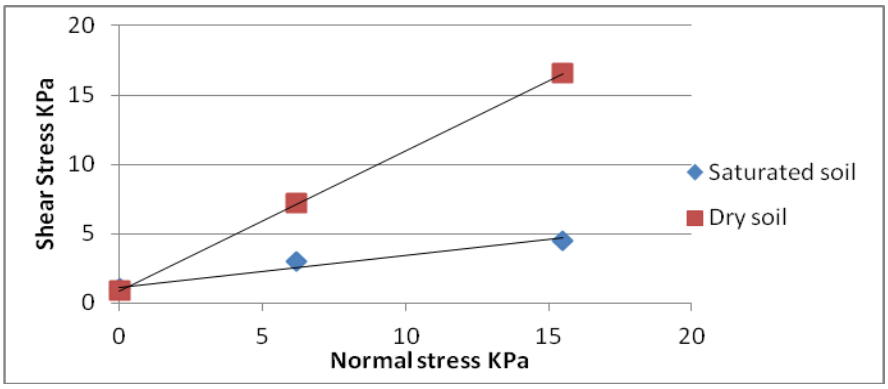

Figure 4. 14. Maximum shear stress vs. normal stress of saturated and dry samples under drained condition.

Table 4. 2. Results of the soil-soil shearing tests (drained condition)

Soil-Soil shear test			
Saturated sample	**Normal Stress 0.0 KPa**	**Normal Stress 6.2 KPa**	**Normal Stress 15.5 KPa**
Shear KPa	1.1	3.0	4.53
Cohesion KPa	1.1		
Friction angle	13.12°		
Dry sample	**Normal Stress 0.0 KPa**	**Normal Stress 6.2 KPa**	**Normal Stress 15.5 KPa**
Shear KPa	0.87	7.2	16.54
Cohesion KPa	0.87		
Friction angle	45.29°		

4.4.2 Undrained condition with shear rate of 0.5 mm/min

In order to test the soil under undrained condition, some adjustments need to be considered. A clear plastic wrap was used to cover the bottom of the shear box to make sure water is not going out, as shown in figure 4.15 (a and b). Furthermore, water

resistant anti-slip tape was used to close the two small holes located on the sides of the box as shown in figure 4.15 c. Then, after preparing the soil sample inside the box and placing the box inside the direct shear device with its cap, a clear plastic wrap was also used to cover the entire box as shown in figure 4.15 (d and e).

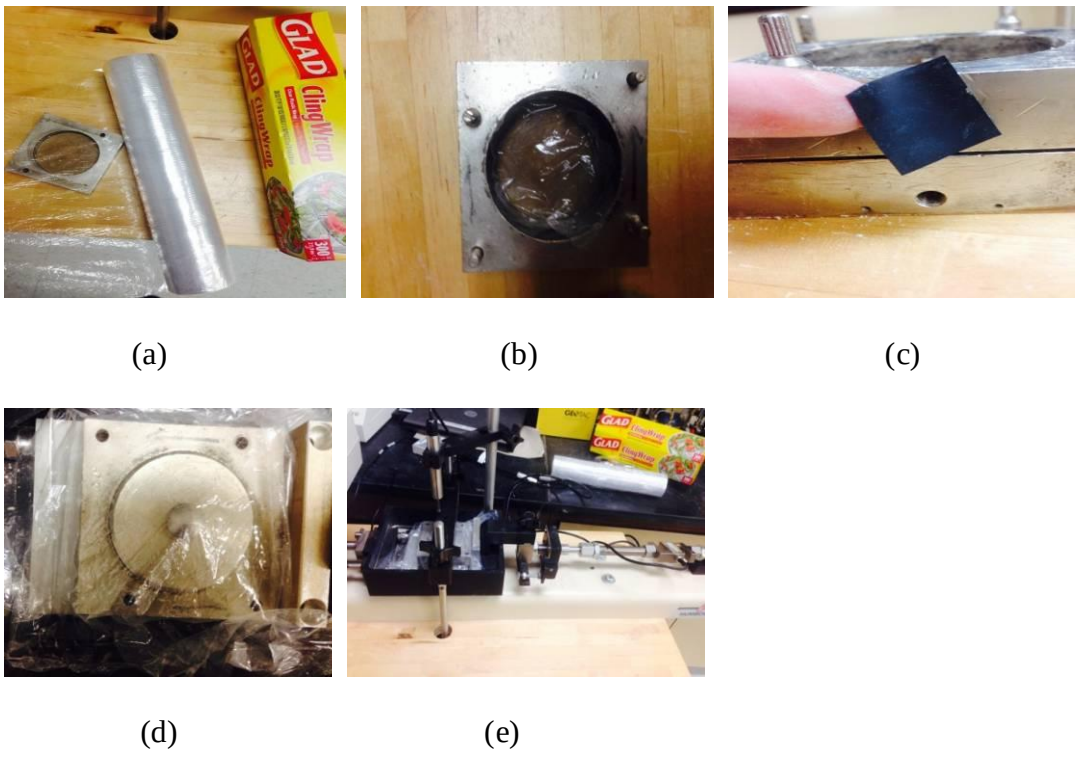

(a) (b) (c)

(d) (e)

Figure 4. 15. (a) And (b) using a clear plastic wrap, (c) using water resistant anti-slip tape to close the holes, (d) and (e) covering the whole box to prevent water evaporation.

Identical soil samples were prepared, but these samples were placed under a shear rate of 0.5 mm/min. The results are provided in figures 4.16, 4.17, and 4.18.

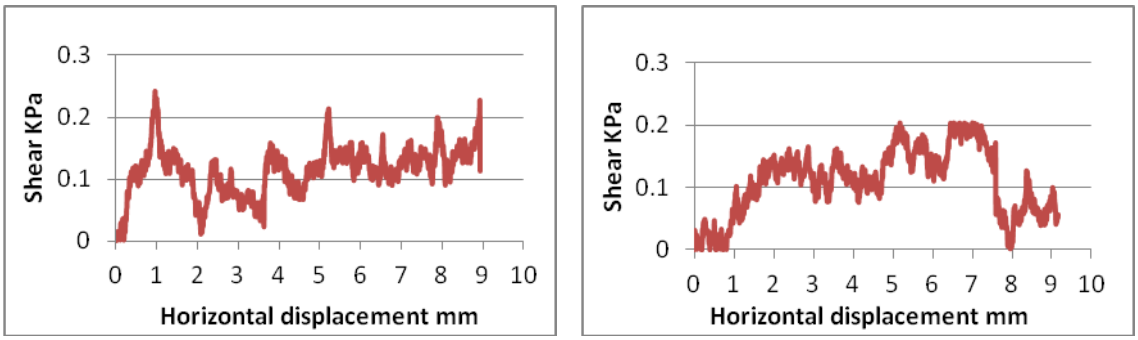

(a) (b)

Figure 4. 16. Saturated sample and zero normal load under undrained condition with (a) grooved surface, and (b) smooth surface.

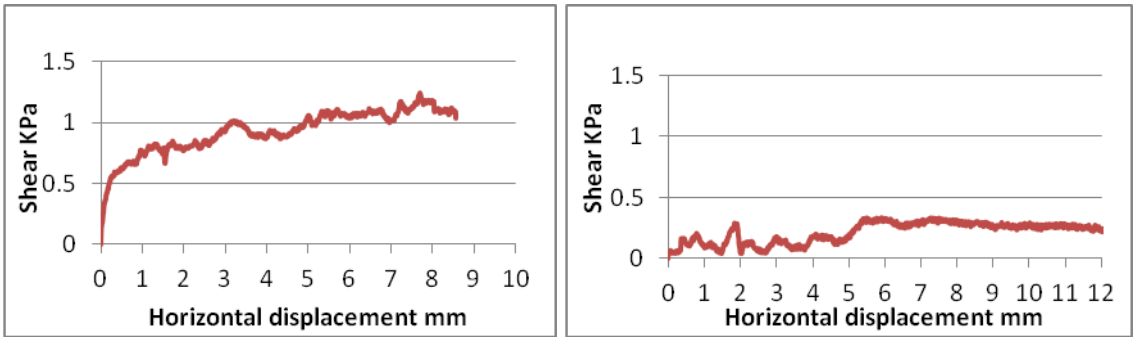

(a) (b)

Figure 4. 17. Saturated sample and 15.5 KPa normal stress under drained condition with (a) grooved surface, and (b) smooth surface.

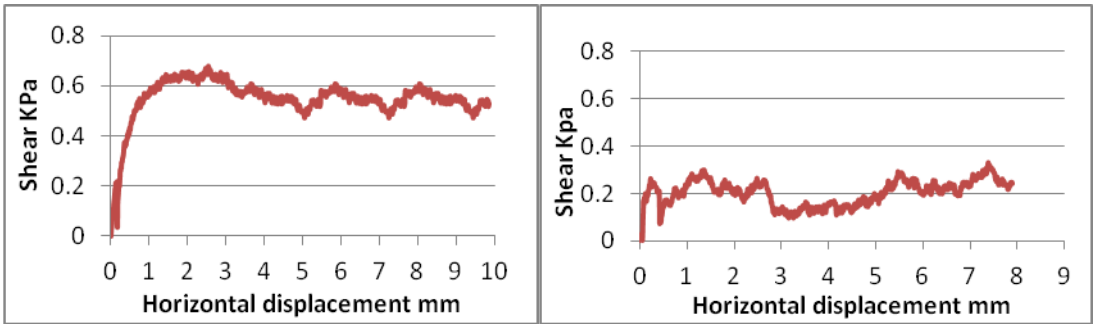

(a) (b)

Figure 4. 18. Saturated sample and 6.2 KPa normal stress under drained condition with (a) grooved surface, and (b) smooth surface.

Thus, Adhesion and the friction angle were obtained as shown in figures 4.19, 4.20, and table 4.3.

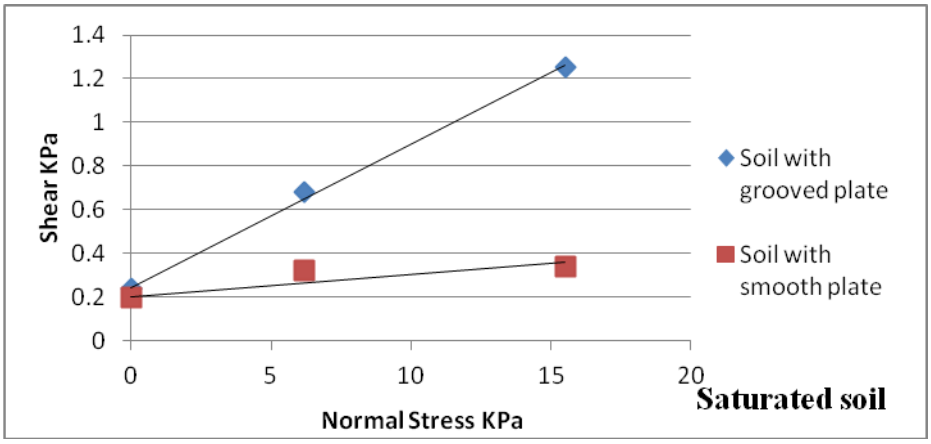

Figure 4. 19. Maximum shear stress vs. normal stress of saturated samples under undrained condition.

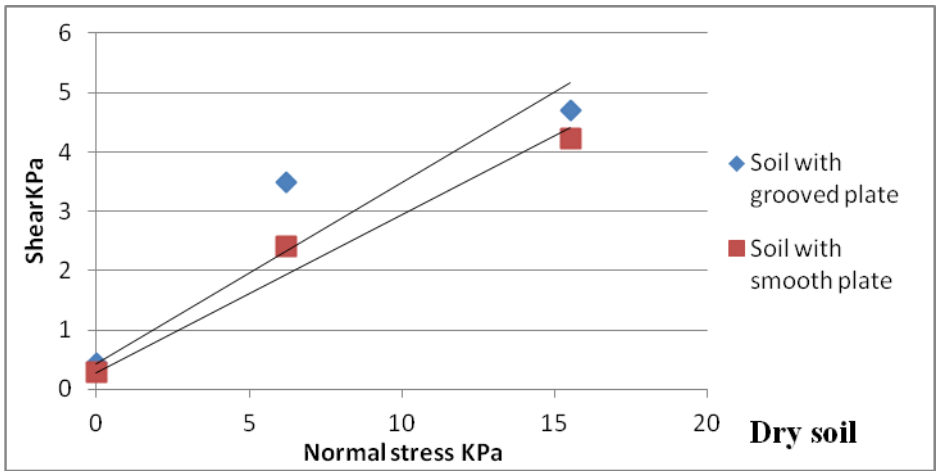

Figure 4. 20. Maximum shear stress vs. normal stress dry samples under undrained condition.

Table 4. 3. Results of the interface shearing tests (undrained condition)

Grooved surface			
Dry sample	**Normal Stress 0.0 KPa**	**Normal Stress 6.2 KPa**	**Normal Stress 15.5 KPa**
Shear KPa	0.43	3.49	4.7
Adhesion KPa	0.43		
Friction angle	17°		
Saturated sample	**Normal Stress 0.0 KPa**	**Normal Stress 6.2 KPa**	**Normal Stress 15.5 KPa**
Shear KPa	0.24	0.68	1.25
Adhesion KPa	0.24		
Friction angle	3.8°		
Smooth surface			
Dry sample	**Normal Stress 0.0 KPa**	**Normal Stress 6.2 KPa**	**Normal Stress 15.5 KPa**
Shear KPa	0.28	2.4	4.22
Adhesion KPa	0.28		
Friction angle	14.9°		
Saturated sample	**Normal Stress 0.0 KPa**	**Normal Stress 6.2 KPa**	**Normal Stress 15.5 KPa**
Shear KPa	0.2	0.32	0.34
Adhesion KPa	0.2		
Friction angle	0.6°		

A traditional direct shear test was carried out to obtained soil parameters (cohesion and friction angle) under undrained condition for both saturated and dry soil samples. Figure 4.21 and table 4.4 show the results of these tests.

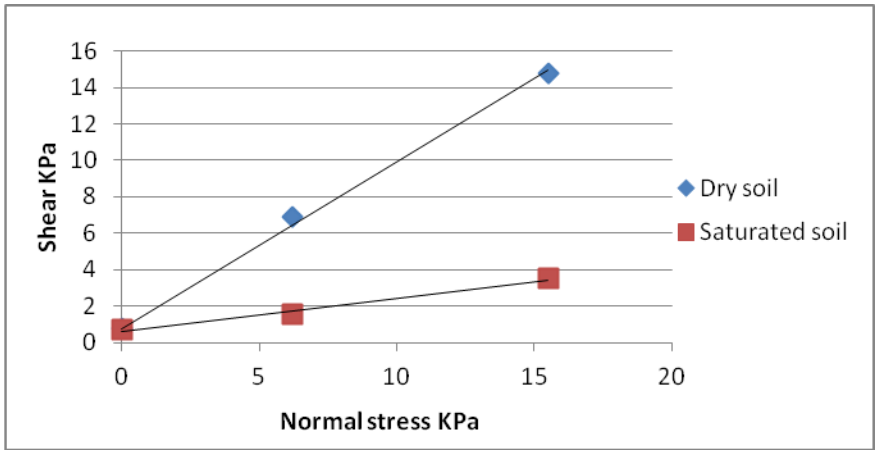

Figure 4. 21. Maximum shear stress vs. normal stress of saturated and dry samples under undrained condition.

Table 4. 4. Results of the soil-soil shearing tests (undrained condition)

Soil-Soil shear test			
Saturated sample	**Normal Stress 0.0 KPa**	**Normal Stress 6.2 KPa**	**Normal Stress 15.5 KPa**
Shear KPa	0.72	1.54	3.5
Cohesion KPa	0.7		
Friction angle	10.30°		
Dry sample	**Normal Stress 0.0 KPa**	**Normal Stress 6.2 KPa**	**Normal Stress 15.5 KPa**
Shear KPa	0.774	6.89	14.76
Cohesion KPa	0.774		
Friction angle	42.43°		

4.5 SHEAR STRESS VERSUS SOIL WATER CONTENT

Tests on fourteen samples were carried out to obtain the soil shear stress versus different water contents. Samples with different water contents were prepared and sheared under zero normal load (zero normal stress). Moreover, the conditions of allowing water to evaporate under the lab atmosphere and cracks develop without applying any load were simulated by using the shear box. The box was cleaned and the sample (with identical water content to the previous drying tests, 90.19%, chapter three) was prepared by gradually placing soil into the box, and the air bubbles were removed by slightly tapping the sides of the box. Then, the sample with the box was weighed by using a small scale to an accuracy of 0.01 g. Also, a Canon camera was used to take a series of photos in order to capture the time of the initiation of the first crack. The main idea of this test is to obtain the soil shear stress at the time of (and slightly before the time of) the initiation of the first crack. Thus, the water content and the time of the initiation of the first crack were known. Subsequently, two identical samples were prepared and allowed water to evaporate under the lab atmosphere. This procedure has been repeated twice in order to test the sample with low and high shear rates.

4.5.1 Drained condition with shear rate of 0.018 mm/min

The first sample was sheared at time of slightly before the initiation of the first crack, which was around 22 hours and the water content was around 70.32%. The other sample was sheared after developing of the first crack (the time was around 22.5 hours and the

water content was around 66.12%), as shown in figure 4.22. As a result, the maximum shear stress was found at the time of slightly after the development of the first crack.

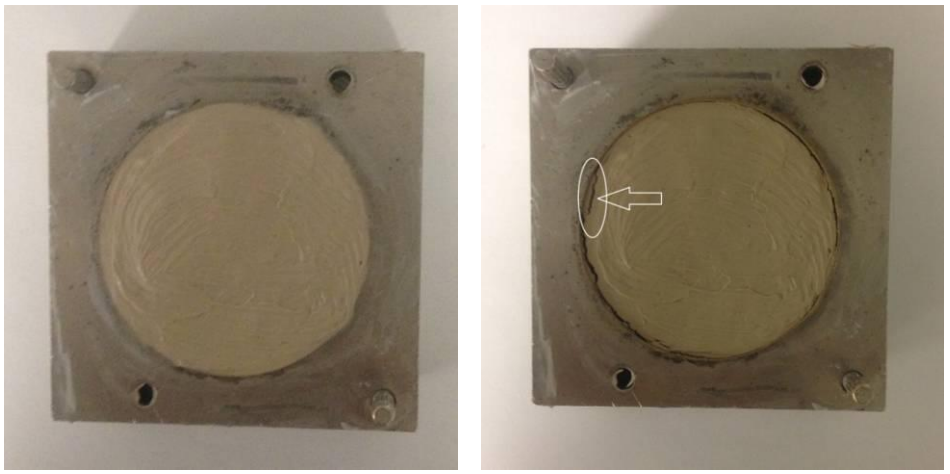

(a) Initial state (b) After 22.5 hours

Figure 4. 22. Crack initiation inside the modified shear box by using a grooved bottom plate.

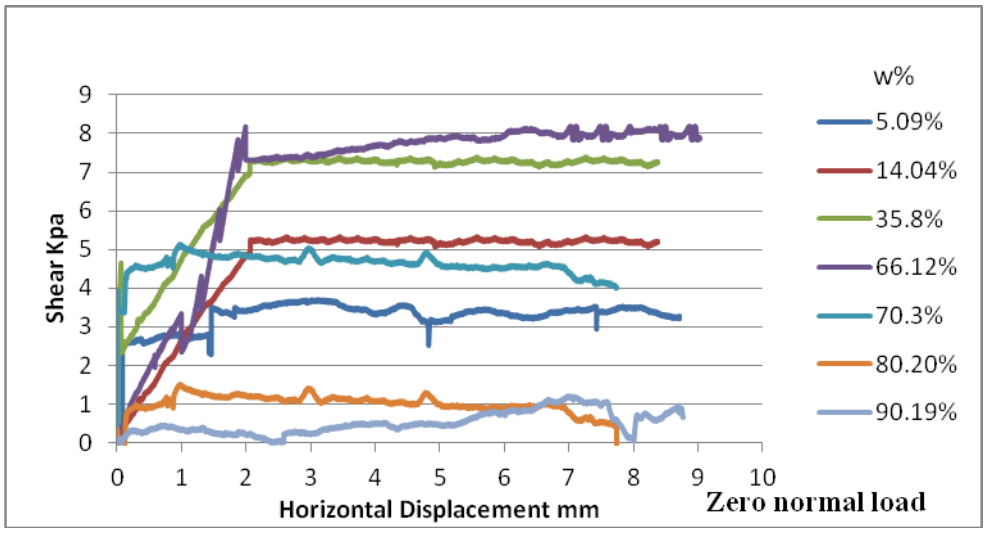

(a)

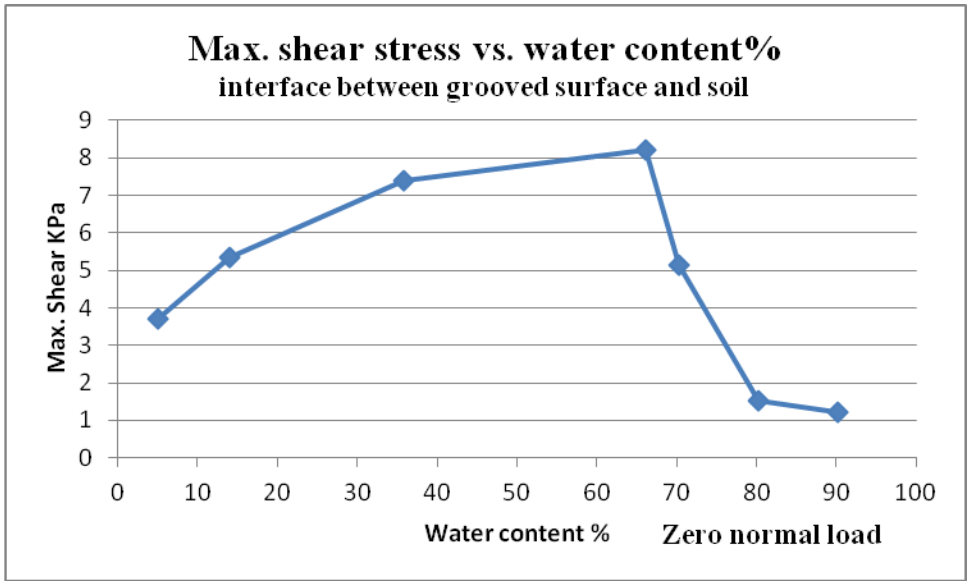

(b)

Figure 4. 23. Drained condition (a) shear stress vs. horizontal displacement of different water contents, (b) maximum shear stress (KPa) vs. water content (%).

4.5.2 Undrained condition with shear rate of 0.5 mm/min

In this case, the same steps of the drained condition were repeated. However, since the temperature and relative humidity were not constant in the lab, the time and the sample water content of the first crack initiation were different. Therefore, the sample was sheared after 23.5 hours (that time was slightly before the initiation of the first crack) and the sample water content was around 75.2%. Then, the sample was sheared after 25 hours (that time was slightly after the initiation of the first crack), and the sample water content was 70.4%.

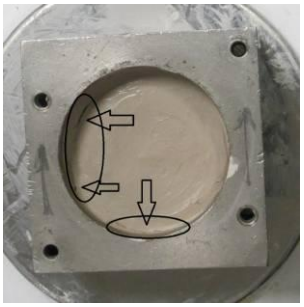

Figure 4. 24. Cracks initiation inside the modified shear box.

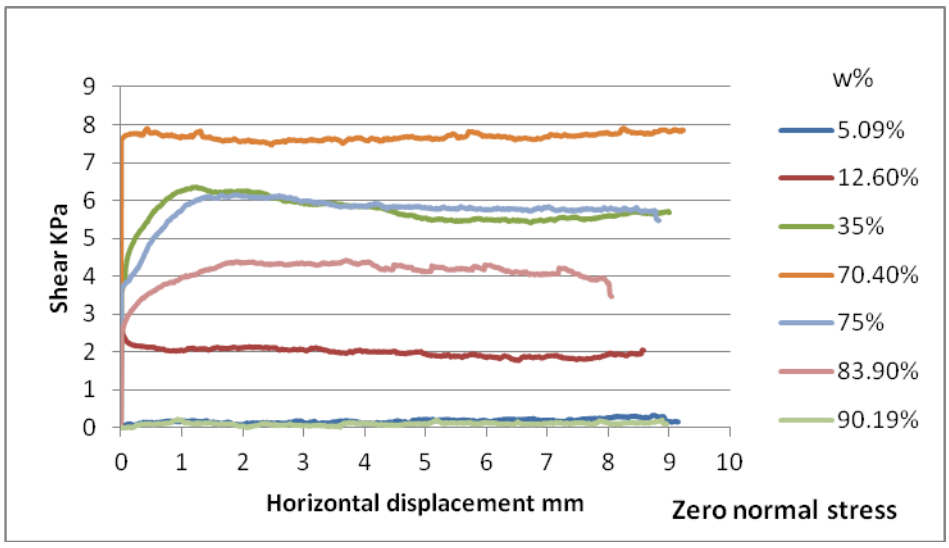

(a)

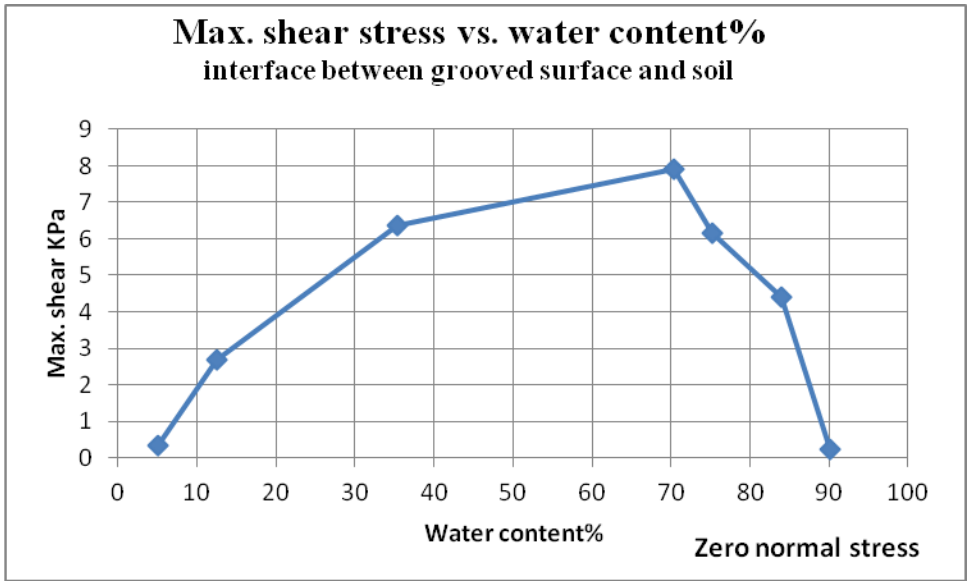

(b)

Figure 4. 25. Undrained condition (a) shear stress vs. horizontal displacement of different water content, and (b) maximum shear stress vs. water content%.

Note: Some other results are attached in appendix 4.

4.6 SOIL-WATER RETENTION CURVE

The soil-water retention curve represents the relationship between the soil suction and the degree of saturation (Sl)/ mass water content (w %) / volume water content (Ø). In the present work, the retention curve had been determined by using WP4-T and pressure plates devices (to obtain the suction of soil samples with different water contents). More details about these devices were discussed in section 2.8. An identical mixture of kaolinite and bentonite (7.5:2.5 respectively) was used with a dry density around 0.80

g/cm^3. Soil suction was obtained at a temperature of (24±1) °C. In order to calculate the degree of saturation with different water content, this equation has been used:

$$Sl = \frac{w * \rho d}{\rho w - \frac{\rho d}{Gs}}$$

Where:

Sl is the sample degree of saturation;

w is the sample water content;

ρ_d is the sample dry density;

ρ_w is the density of water;

G_s is the sample specific gravity (which is around 2.61).

At the beginning, the soil-water retention curve was obtained by using the WP4-T device. Then, three points of this curve were re-checked by using pressure plate's device. These points were selected depending on two things: (1) it was anticipated that the accuracy of WP4-T device decreases with small suctions (e.g. lower than 1 MPa) and (2) the limitations of pressure plates measurements (0 to 1.5 MPa). Thus, three different points were selected below 1.5 MPa. In the pressure plates, suction was imposed by means of air pressure with a corresponding sample water content depending on WP4-T. Thus, the original curve (the one obtained via WP4-T) was corrected with the new results (which obtained via pressure plates), as shown in table 4.5.

Table 4. 5. Shows the results of these tests

W%	Suction MPa	PF	density of mixture g/cm^3	Dry density g/cm^3	Sl
4.06	88.6	5.96	0.83	0.798	0.05
5.23	86.44	5.95	0.84	0.796	0.06
5.77	84.97	5.94	0.85	0.800	0.07
7.32	57.4	5.77	0.86	0.801	0.08
22.19	10.47	5.04	0.98	0.800	0.26
33.44	2.96	4.48	1.07	0.801	0.39
45.79	1.38	4.16	1.17	0.802	0.53
~~65.20~~ 56.75	1.02	3.97	1.32	0.801	~~0.75~~ 0.66
76.2	0.91	3.89	1.41	0.803	0.88
~~84.5~~ 67.28	0.71	3.75	1.47	0.799	~~0.98~~ 0.78
~~90.19~~ 74.58	0.47	3.69	1.52	0.800	~~1.04~~ 0.86

Where:

1 PF = 10 cm of suction;

2 PF = 100 cm of suction.

Figures 4.26, 4.27, and 4.28 are showing the experimental results for determining the soil-water retention curve.

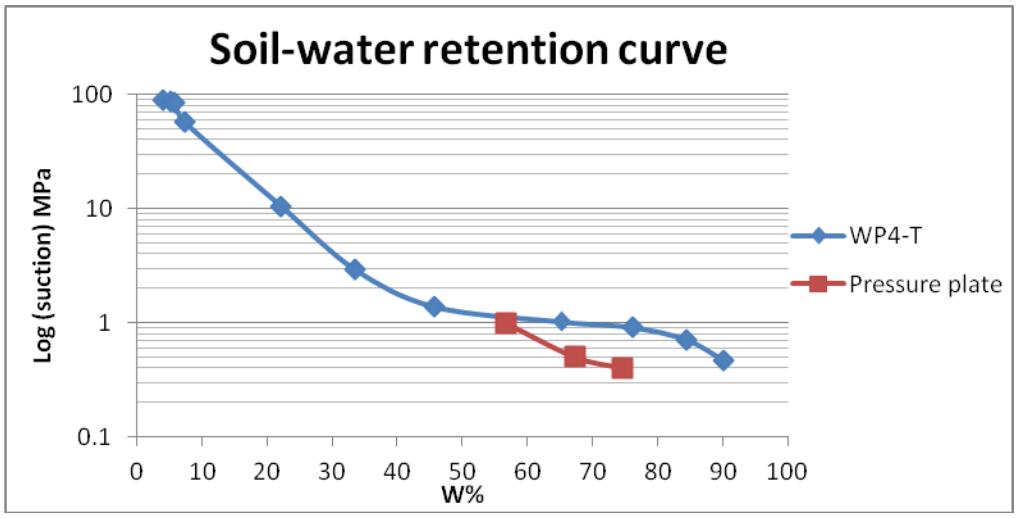

Figure 4. 26. Retention curve represented by w% vs. s.

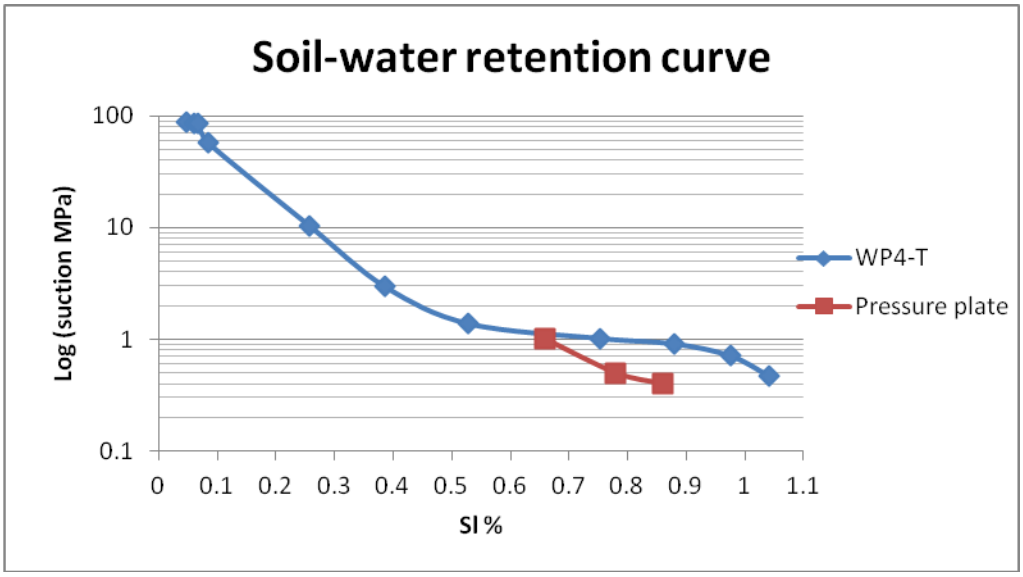

Figure 4. 27. Retention curve represented by Sl vs. s.

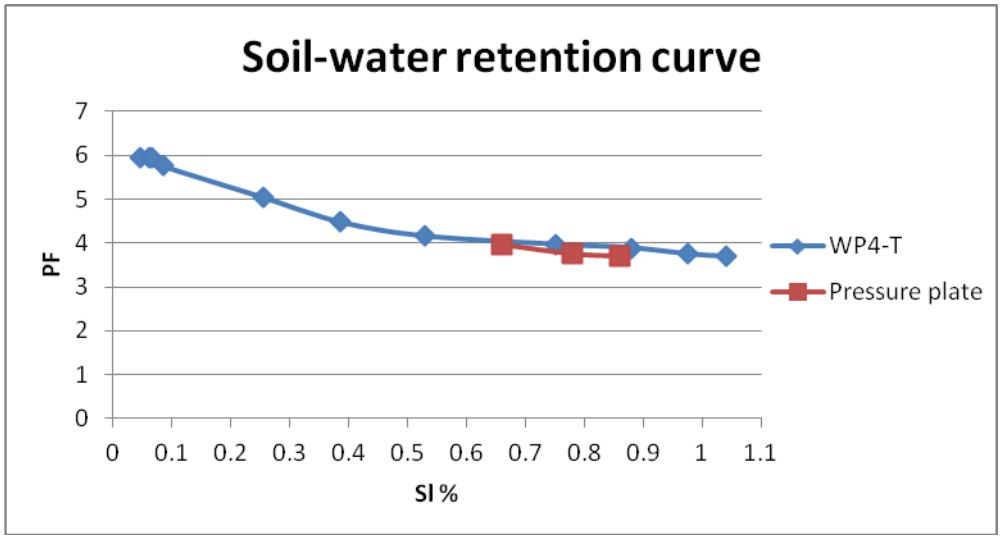

Figure 4. 28. Retention curve represented by Sl vs. PF.

4.6 DISCUSSION AND CONCLUSION

A conventional direct shear device was adapted to test interfaces of saturated and unsaturated soils. Experimental results have been analyzed, and they showed that the maximum shearing resistance controlled by the drainage conditions, the roughness of the interface material, water content of the soil, and the value of the normal stress. Thus, a series of tests on twelve samples was performed to develop the failure envelopes of soil interfaces having grooved and smooth surfaces under drained and undrained conditions. Further, tests on other twelve samples were carried out to develop the failure envelopes of soil-soil interface for saturated (w = 90.1%) and dry (w = 5.09%) samples under both drained and undrained conditions. Additionally, tests on fourteen other samples were performed to obtained the behavior of the soil interface having grooved surface with different water contents before and after cracks initiation; the applied normal load in

these cases was zero (samples were sheared under their self-weight). Thus, tests were carried out in this chapter giving a total of thirty eight tests; however, a set of twelve other tests were performed for different purposes and the results are presented in appendix 4.

Internal friction angle is one of most important parameters. It was obtained for soil interfaces having grooved and smooth surfaces. In the drained condition (shear rate = 0.018 mm/min), the results showed that the internal friction angle is higher with smooth surface (9.09°) than with the grooved one (6.67°); further, for saturated soil-soil interface, the friction angle was 13.12° which was much lower than the internal friction of the dry soil-soil interface (45.29°). In the undrained condition (shear rate = 0.5 mm/min), the results showed that the internal friction angle is higher with grooved surface (3.8°) than with the smooth one (0.6°); in addition, for saturated soil-soil interface, the friction angle (10.3°) was much lower than the internal friction angle of dry soil-soil interface (42.43°). These results of drained condition were somewhat contradicted with the results of Tariq et al. (2009); they worked on low plasticity fine grained soil with shearing rate of 0.005 mm/min, and the grooves shape was such the peak to valley height = 0.38 mm for the rough surface and was 0.0025 mm for the smooth surface. Their results showed that there is no difference between the soil-rough surface interface and soil-soil interface in terms of internal friction angle; however, the friction angle of the soil-smooth surface was considered lower in comparison with them. In this research, it was found that friction angle of soil-soil interface is higher than the

soil-plate interface under both conditions (drained and undrained). As a result, these differences may go back to the grooves dimensions, degree of saturation, and the soil fabric because the interaction between the interface surface (plate) and the contact soil has a considerable effect on the interface shearing behavior.

Moreover, the results of the drained condition showed that the adhesion intercept of the soil-grooved surface (1.2 KPa) was roughly similar to the cohesion intercept of the soil (1.1 KPa). Therefore, cracks may develop either from the bottom of the sample or on the surface. In addition, it was anticipated that the adhesion of the soil-smooth surface interface was negligible due to grease the plate with Vaseline; the data which were collected via LVDT were showing all negative values. As mentioned previously, the shear stress should not be negative values (e.g. tensile force), but the results may go back to the transducer sensitivity. Therefore, these values were considered as zeros. In this case, the failure plane may develop inside the soil particles, which has considerably lower shearing resistance. However, the results of the undrained condition showed that the cohesion (0.7 KPa) of the soil was greater than the adhesion of the rough and smooth interfaces (0.24 KPa and 0.2 KPa respectively). This divergence in the results of the drained and the undrained condition because they are shear-rate-dependent.

As for the normal load, two different normal loads (5 Kg and 2 Kg) were used in this research, and the behavior of the interface was roughly similar for drained and undrained conditions. Also, the soil was sheared with zero normal load under different conditions.

The results were practically acceptable; the shear stresses were much higher with grooved plate than with the smooth one, and the shearing with soil-soil interface was higher than the soil-plate interfaces. Besides, the relationship between the shear stress and the normal load (or normal stress) was roughly acceptable; the shear stress increased as the normal stress increased. It is worth mentioning that the average vertical displacement of these tests was around 8.2 mm under drained condition.

In addition, the results of the shear stress with different water contents under zero normal load were reasonably matched to what was expected, as shown in figures 4.23 and 4.25. The specimens were sheared slightly before the initiation of the first crack when the water contents were 70.32% (for the drained condition) and 75.2% (for the undrained condition); the shear stresses were found to be 5.13 MPa and 6.82 MPa respectively. Then, it was observed that the shear stresses were increasing with time until the cracks developed in the soil. These samples were sheared slightly after the initiation of the first crack when the water contents were 66.12% and 70.4%; the shear stresses were reached the maximum value around that time and were found to be 8.2 MPa and 7.9 MPa respectively. Subsequently, shear stresses started to decrease with decreasing water contents. However, the results of the shear stress with different water contents under the normal load of 5 Kg were different to a certain extent, as shown in appendix 4. In this case, shear stress reached the maximum (17.8 MPa) after the initiation of several cracks. Thus, the shear stress was increasing with decreasing water content until it reached the maximum value at a water content of 40%, then started to decrease with decreasing

water content. Therefore, further studies with different normal stress and different water contents may need to be studied in order to be able to describe the behavior of the soil under this condition.

IMAGE ANALYSIS TECHNIQUE

5.1 INTRODUCTION

This section starts with an overview of the image analysis technique, followed by a brief discussion of its main steps. Subsequently, calculations of the main parameters of soil cracks were described as well. In addition, the main experiments, which were discussed in chapter three, were analyzed using *image j* software. Finally, the results were discussed at the end of this chapter.

5.2 HISTORICAL OVERVIEW OF IMAGE ANALYSIS TECHNIQUE

Image analysis is defined as taking out useful information from collected visual data through what is called digital image analysis technique. This idea was developed in 1920 for cable transmission of pictures, and the first computer processing began in 1967. Subsequently, this technique has been developed for mariner space missions in order to correct geometries and data transmission errors. This processing was carried out by using large mainframe computers. The first book, which is written by A. Rosenfeld, is titled "Picture Processing by Computer," Academic Press (1969).

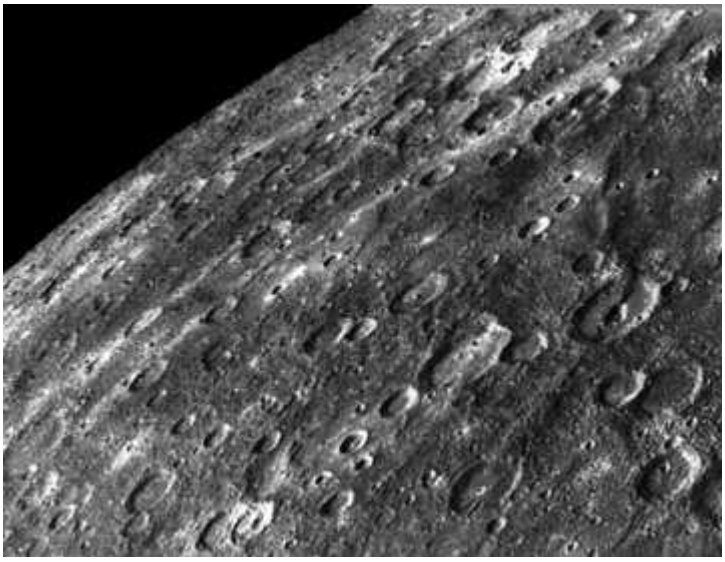

Figure 5. 1. Image from Mercury Mariner in 1974, (University of Edinburgh, theory of image analysis).

Since computer systems were very expensive at that time, the image analysis technique was limited to space projects. However, in the early 1980s, this technique became more accessible to people due to the increasing affordability of personal computers. It spread from research labs to companies in various industries. Thus, image analysis has evolved over time.

The general idea of using image analysis is to remove the obscure details in an image, use collected data to rebuild the best image from them, and display an image for visual inspection. Also, it is carried out with quantitative measurements, so it is easy to determine image properties such as dimensions, color, counts of particles by size, and path length. Therefore, it analyzes an image for multiple things and the test performance of computer-based image analysis enables multiple images to be processed rapidly. In

geotechnical engineering, there is a significant potential of using image analysis technique to study cracking soils by quantifying the characteristics of the crack network. In particular, this technique facilitates the process of determining the location and severity of cracked areas and getting useful information to determine the width, length, and shape of the cracks. Since the characterization of cracks is represented as an indicator of the state of soil structure, this information is valuable in different engineering fields such as soil mechanics, agriculture studies, and geotechnical engineering. Thus, when crack patterns are not similar among the soil treatments, other structural characteristics of the soil are probably different as well, but not vice versa (Lakshmikantha, 2009). Recently, image analysis technique has been used in various applications to assess soil characteristics such as crack monitoring (Horgan, 1998; Sarmah et al., 1996, Preston et al., 1997; Puppala et al., 2004; Sarmah et al., 1996; Velde, 1999; Velde, 2001; and Vogel et al., 2005).

5.3 IMAGE ANALYSIS PROCESS

Basically, the image analysis process is described in two main steps that need to be performed on the required image to prepare it for analyzing. First, converting the colored image to a gray-scale image, and then converting the latter one to a binary image (black and white). Also, there are some options such as Erode, Dilate, and Outline that are used to clarify the areas of interested as much as possible. It is important to mention that these stages should be performed respectively before moving to the next one. Figure 5.2 shows the order of the main steps.

Figure 5. 2. The main steps for image analysis process.

Second, the required parameters including the cracked and un-cracked areas, perimeter of each piece, average crack length and width, and crack intersection angle are obtained. Moreover, the main parameter is the evolution of the crack density factor (surface shrinkage), which is equal to the cracked area divided by the original sample cross section area (Miller et al., 1998).

To clarify the previous processes, an example of *Java* image processing program, *Image j*, can be used for illustration. Generally, in most digital cameras, RGB color space is used to represent all colors by combining different amounts of red, green, and blue. Furthermore, 8 bits of data in each channel are considered. This representation of data is valid in most applications, so 2^8=256, and 256^3= 16777216 colors can be represented (Person, 2005). Then, converting the original image (RGB image) to the gray-scale image means that the resultant image is shaded in gray. The gray color represents the three colors (red, green, blue) with equal intensity. The gray-scale image has two major processes: subtract background by using the rolling ball algorithm, and un-sharpen mask

which subtracts a blurred version of the image from the original. However, the first process in gray-scale image (subtract background) has been used in this research. The main aspect of it is that the radius of the rolling ball should be larger than the radius of the largest object in the original image (Sternberg, 1983). After that, the gray-scale image was converted to the binary image (black and white) by pressing the following series of buttons: Process >Binary >Make Binary, this operation has multiple options: Erode, Dilate, Open, and Close. Figures 5.3 and 5.4 show these steps in order.

(a) (b) (c)

Figure 5. 3. Converting original image (a) to a gray-scale image, and then (b) to a binary one (c).

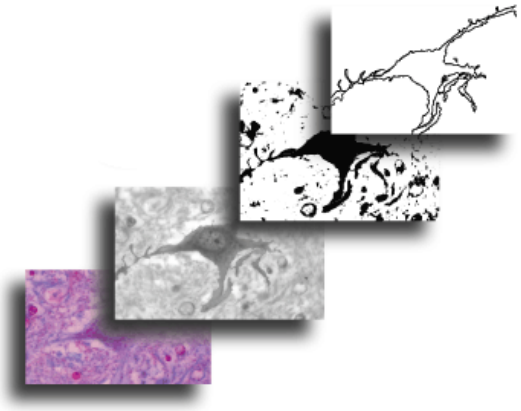

Figure 5. 4. Converting the original image to a gray scale and to a binary image then using outline option (which is defined at the end of this section).

Additionally, some other options were used in this research in order to count the number of cells with their areas and some other valuable outputs. First, *analyze* which is working by inspecting the image until finding the edge of an object, and the main goals of using it are counting and measuring objects in binary images. Second, *skeletonize,* which is calling from Process >Binary >Skeletonize, works by taking out pixels from the edges of an object in the binary image to reduce them to single-pixel-wide shapes. Thus, this process is repeated until no pixel can be removed. Third, *angle tool* which appears in the status bar and by pressing Analyze >Measure to see the results, helps to measure any angle defined by three points. Finally, *Outline*, which is calling from Process >Binary >Outline, draws a line inside the object and this line is represented as a one pixel wide outline in a binary image.

5.4 CALCULATION OF SHRINKAGE AREA

In this research two different ways have been used to determine the cross section area of the samples during drying:

5.4.1 Segmentation

Image segmentation is helped to separate the shrinkage area from the cracks. It divides the image into different regions. In particular, the cracks and shrinkage area are considered as darker pixels and the uncracked area is the brighter pixels, so the segmentation compares each pixel of the gray-scale image to the threshold. Thus, the value of the pixel becomes 0 when its color is darker than the threshold, and it becomes 255 for a white one. Consequently, the gray-scale image becomes a binary image (segmented image). However, some white or black spots come out in the shrinkage area which may affect the evaluation of this area; to solve this problem there are some binary operators work to enhance the image by removing these spots (Serra, 1982). In this research, different binary options were used to calibrate the images and remove some undesirable points.

5.4.2 Average of different diameters

Basically, different diameters were considered to determine shrinkage areas. These diameters were selected manually by using a straight line tool from *Image j* software, as shown in figure 5.5. Then, the average of these diameters was taken to calculate the cross section area. Although it is not a 100% accurate method, it provided us with

reasonable values comparing with previous methods (for samples experience only shrinkage without cracking).

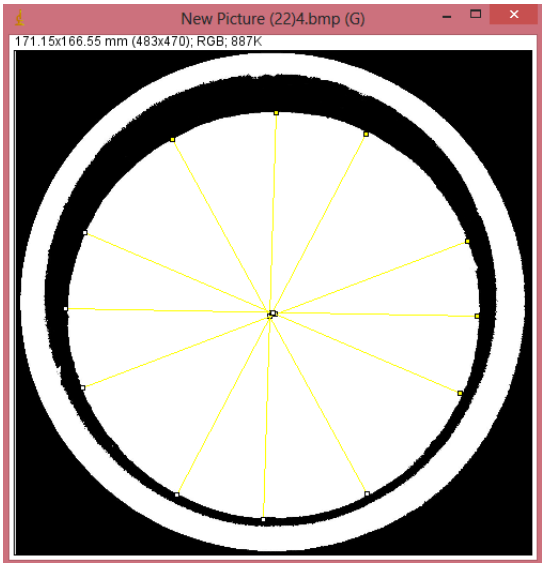

Figure 5. 5. Measuring the sample diameter from different locations to estimate its shrinkage area.

5.5 CRACK-INTENSITY-FACTOR (CIF) AND CRACK INTERSECTION ANGLES

Crack intensity factor (CIF), or crack density factor (CDF), is defined as the time variable ratio of the crack area (Miller et al., 1998). This factor provides an explanation of how the cracks extend and the ratio of the cracks or shrinkage areas to the original ones. It is known that the soil hydraulic and mechanical properties are affected by length, width, and depth of the cracks. On the one hand, some studies consider the cracking area including the shrinkage area, so CIF in this case is equal to $(CIF)_{tot}$, which is the total crack intensity factor. On the other hand, in this research, CIF and $(CIF)_{tot}$

were determined separately. The first one is equal to the cracking area divided by the original sample area; however, the second one is equal to the cracking area plus the shrinkage area divided by the original sample area, (Auvray et al., 2013).

$$\mathrm{CIF} = \frac{\text{Crack area}}{\text{Specimen area}} * 100\%$$

And;

$$(\mathrm{CIF})_{\mathrm{tot}} = \frac{(\text{Crack area}) + (\text{Shrinkage area})}{\text{Specimen area}} * 100\%$$

Since the CIF and $(CIF)_{tot}$ were needed to be determined with time, a series of photos was selected while the tests were running. These calculations were performed for this series of photos of each test. The main idea of plotting CIF or $(CIF)_{tot}$ versus the sample water content with time is to obtain the general idea of the evolution of cracks, crack initiation, the time of severe cracking, and cracking rate.

Crack intersection angles could be considered as one of the important factors that describe a crack network because they provide an idea of principal stress directions during the development of individual cracks (Lakshmikantha et al., 2009). In this research, crack intersection angles were calculated; interestingly, the significant range was (80°-100°) which may call orthogonal intersection. According to Hartge and Bachmann (2000), tensile failure may create orthogonal crack intersections and the other

angles which are less than 80° or higher than 100° are more likely to be associated with shear failure. Thus, since the orthogonal intersections are more dominant than others (they have higher range than non-orthogonal ones), it could be observed that the tensile stresses have a significant effect on desiccation cracks.

5.6 ANALYZING OF THE MAIN EXPERIMENTS WHICH DESCRIBED IN CHAPTER THREE

In the present work, *image j* software is used to characterize the 2D crack network and to determine the final cross section area of the samples. While the camera was programmed to gain and store images at a specific time frequency, a series of images was selected during the test for characterization of the soil behavior.

5.6.1 Kaolinite: bentonite 7.5:2.5 and 90.19% water content

1. A half-inch thick mold with grooved bottom under the lab atmosphere (GA1) is used. Figure 5.6 (a) shows the final stage image when the cracks developed in the soil sample under the lab atmosphere and reached the final shape. Figures 5.6 (b), (c), (d), and (e) show the main processes used to analyze the final pattern of cracks.

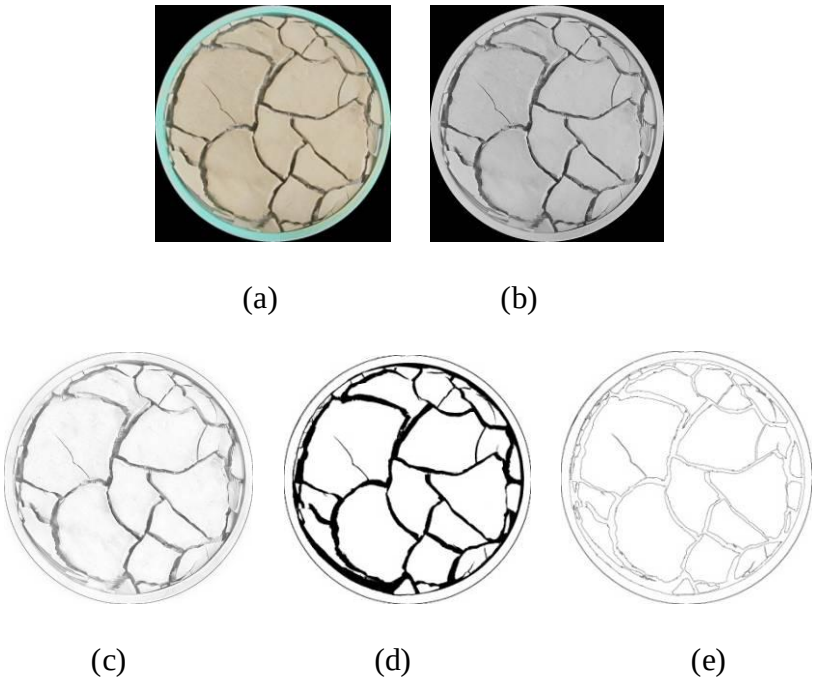

Figure 5. 6. Final pattern of the soil sample (kaolinite-bentonite)/ 0.5" thick under the lab atmosphere. (a) Original image, (b) converting the original image to a gray scale, (c) using subtract background option, (d) converting to a binary image, and (e) using outline option.

Water loss and water content were measured during the test by using a small scale. This scale was programmed to measure the sample weight every 30 minutes and the sample water content was measured by using the following equation:

$$w\% = 100 * \frac{w_i - w_t}{w_t}$$

Where:

w% is the percentage of the water content of the sample;

w_i is the initial weight of the sample (g);

w_t is the weight of the sample related to the time (g).

Figure 5.7 shows the plot of the water loss% with time.

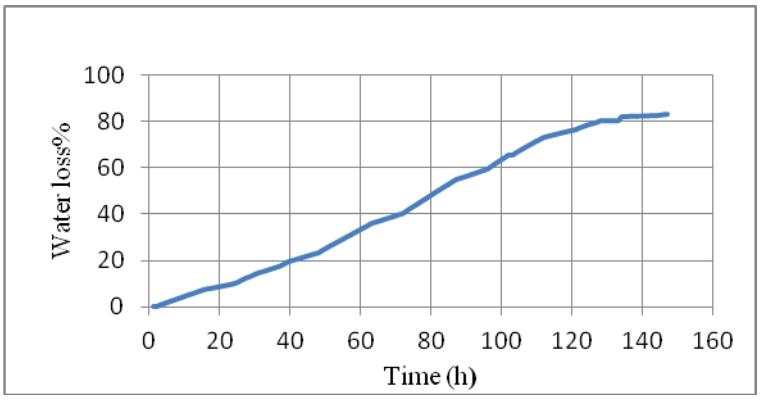

Figure 5. 7. Plot of the amount of water loss (percentage) versus time (hours)/ a mixture of kaolinite-bentonite.

Figure 5.8 shows the plot of the sample water content% with time. As shown in this plot, the initial water content was 90.19% (saturated sample) and it was ended up with 5.7% (dry sample).

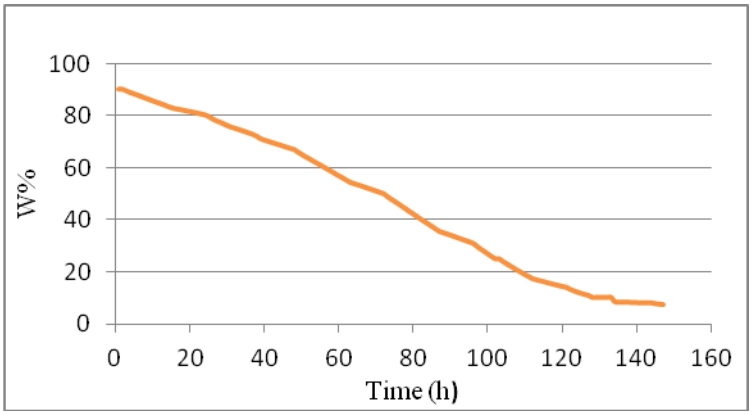

Figure 5. 8. Plot of the water content (percentage) versus time (hours)/ a mixture of kaolinite-bentonite.

The main parameter (CIF) was plotted against the time to enhance the understanding of the behavior of the desiccation cracks during drying process. Figure 5.9 shows the plots of CIF and $(CIF)_{tot}$ against the time. Figure 5.10 show the plot of the sample water content % against the $(CIF)_{tot}$ %.

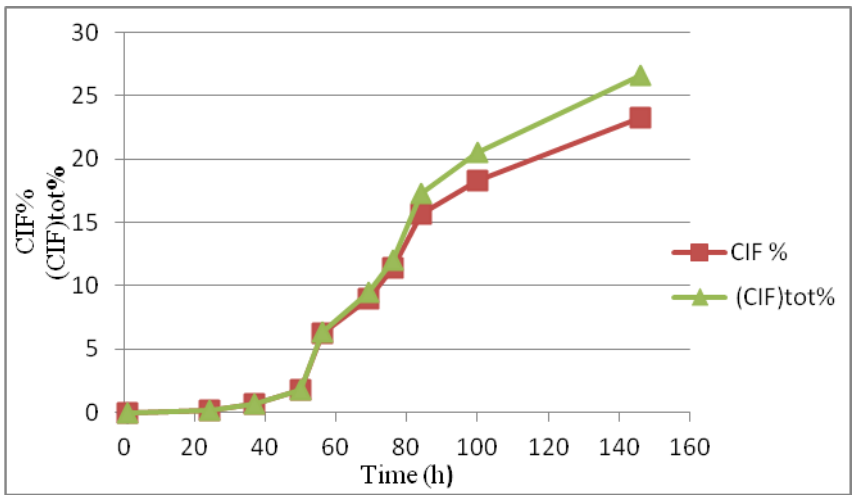

Figure 5. 9. Plot of the CIF and $(CIF)_{tot}$ (percentage) versus time (hours)/ a mixture of kaolinite-bentonite.

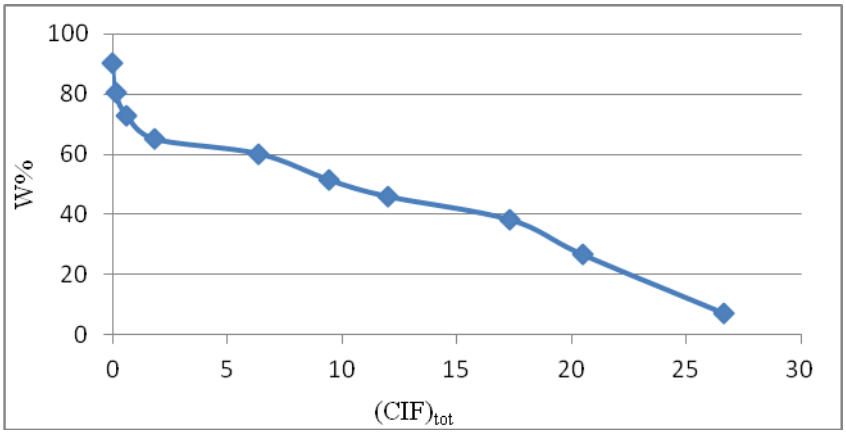

Figure 5. 10. Plot of the water content (percentage) versus the $(CIF)_{tot}$/ a mixture of kaolinite-bentonite.

2. A half-inch thick mold with a smooth bottom under the lab atmosphere (SA1) is used. Figure 5.11(a) shows the final stage image after the soil sample experiencing shrinkage during drying under the lab atmosphere. Figures 5.11 (b), (c), and (d) show the main processes which were used to analyze figure 11 (a).

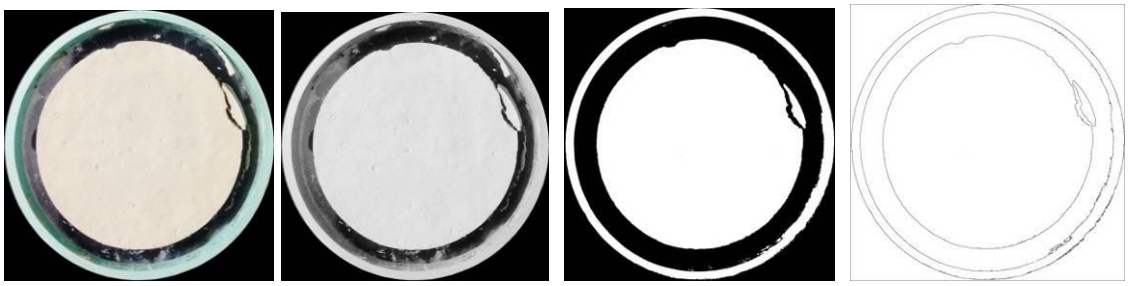

(a) (b) (c) (d)

Figure 5. 11. Applying image analysis technique for determining the shrinkage area of the soil sample (kaolinite-bentonite). (a) Original image, (b) converting the original image to a gray scale, (c) converting to a binary image, and (d) using outline option.

3. A 1" thick mold with small grooves and holes (1.5 mm diameter) at the bottom is used. The sample was exposed directly to a salt solution (GAsalt). Figure 5.12 (a) shows the final stage image after developing the cracks on the surface of the soil sample. Figures 5.12 (b), (c), and (d) show the main processes used to analyze the final pattern of cracks.

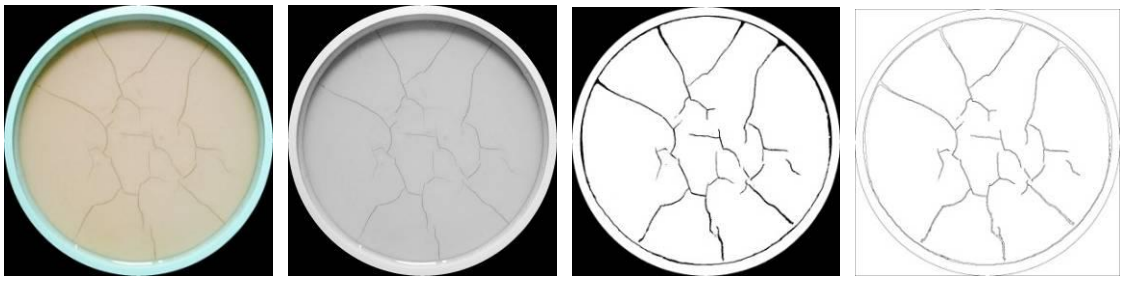

(a) (b) (c) (d)

Figure 5. 12. Final pattern of the soil sample (kaolinite-bentonite) under the salt solution. (a) Original image, (b) converting the original image to a gray scale, (c) converting to a binary image, and (d) using outline option.

4. Inside the desiccator, a half-inch thick mold with small grooves (GDsalt1) is used. Figure 5.13 (a) shows the final stage image after developing the cracks on the soil sample inside a desiccator with a salt solution (calcium nitrate tetrahydrate $Ca(NO_3)_2.4H_2O$). Figures 5.13 (b), (c), (d), and (e) show the main processes used to analyze the final pattern of cracks.

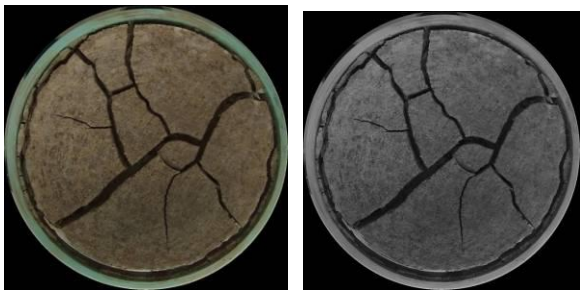

(a) (b)

Figure 5. 13. Final pattern of the soil sample (kaolinite-bentonite) inside the desiccator. (a) Original image, (b) converting the original image to a gray scale, (c) using subtract background option, (d) converting to a binary image, and (e) using outline option.

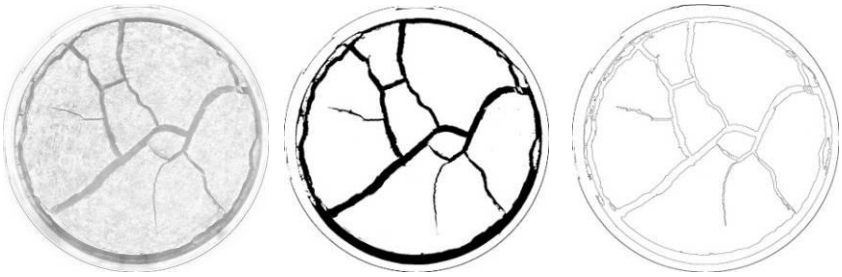

(c) (d) (e)

Figure 5. 13. Continued.

For this test, $(CIF)_{tot}$ was calculated for a series of images starting from the one taken when the first crack appeared until the one taken at the end of the test; it was plotted versus time as shown in figure 5.14.

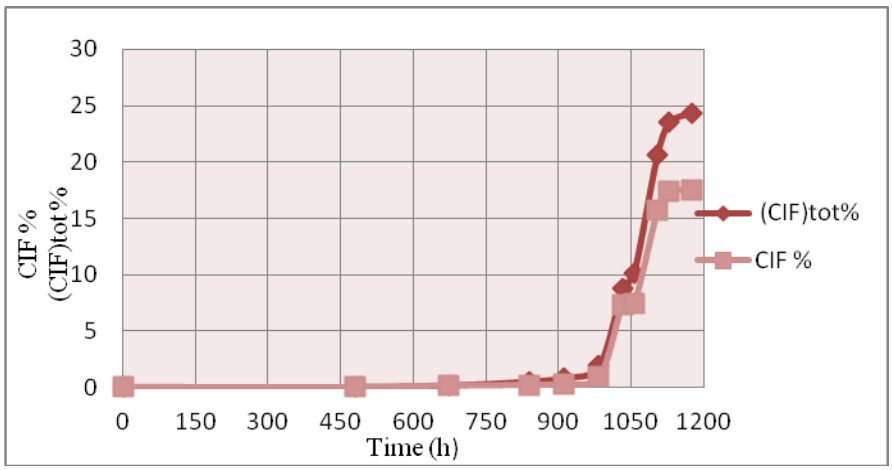

Figure 5. 14. Chart of $(CIF)_{tot}$ (percentage) versus time (hours)/ a mixture of bentonite-kaolinite.

5. Inside the desiccator, a half-inch thick mold with smooth surface (SDsalt) is used.

In this test, the sample experienced shrinkage without showing any cracks because of using a smooth surface (zero friction between the soil sample and the bottom surface). Since fungi were grown on the surface of this sample (unknown reasons), it was quite difficult to apply image analysis technique. Although several ways were used to remove the undesirable spots, none of them were proper and accurate because some details were disappeared during these processes. Therefore, the shrinkage area of this sample was calculated manually by using a straight line option and measuring the diameter of the sample from different locations, and there was no significant crack to be considered in this sample as shown in figure 5.15.

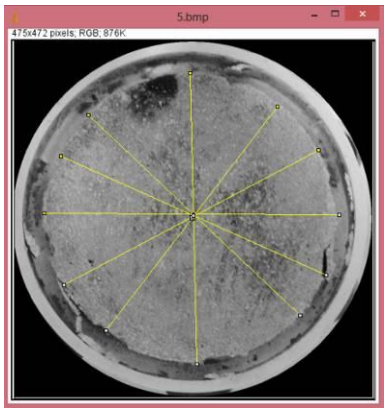

Figure 5. 15. Determining the diameter of a sample by using a straight line option (*image j*).

5.6.2 Porcelain: kaolinite 5:5 and 74% water content

1. A half-inch thick mold with grooved bottom under the lab atmosphere (GA2) is used.

Figure 5.16 (a) shows the final stage image after the sample reaching the final shape. Figures 5.16 (b), (c), and (d) show how *image j* analyzed this photo by applying three processes in order.

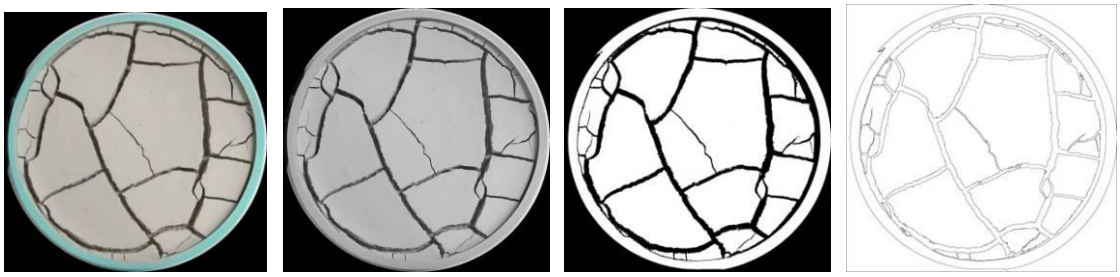

(a) (b) (c) (d)

Figure 5. 16. Final pattern of the soil sample (porcelain-kaolinite)/0.5" thick under the lab atmosphere. (a) Original image, (b) converting the original image to a gray scale, (c) converting the gray-scale image to a binary image, and (d) using outline option.

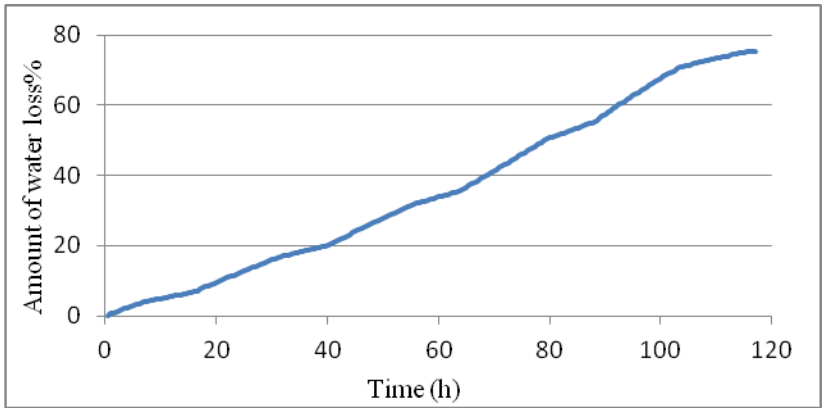

Figure 5. 17. Plot of the amount of water loss (percentage) versus time (hours)/a mixture of porcelain-kaolinite.

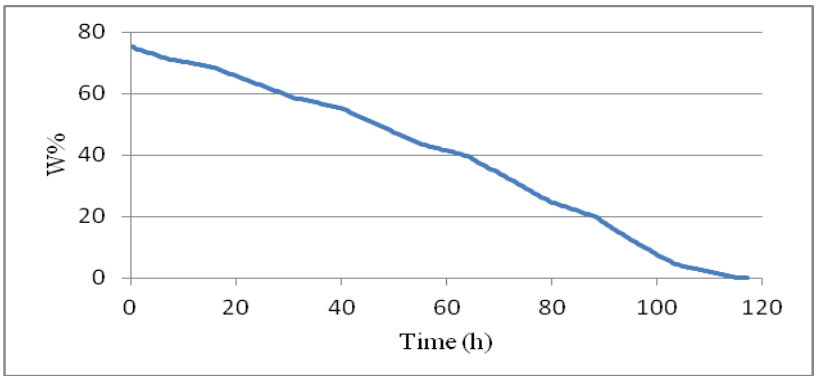

Figure 5. 18. Plot of the water content (percentage) versus time (hours)/ a mixture of porcelain-kaolinite.

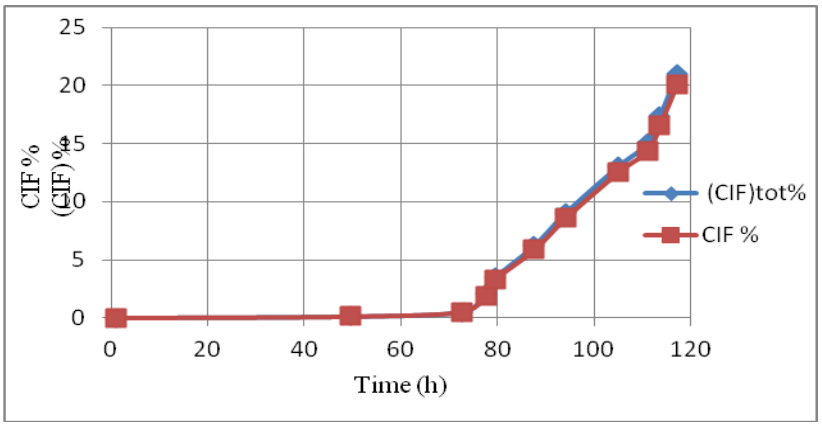

Figure 5. 19. Plot of CIF and $(CIF)_{tot}$ (percentage) versus time (hours)/ a mixture of porcelain-kaolinite.

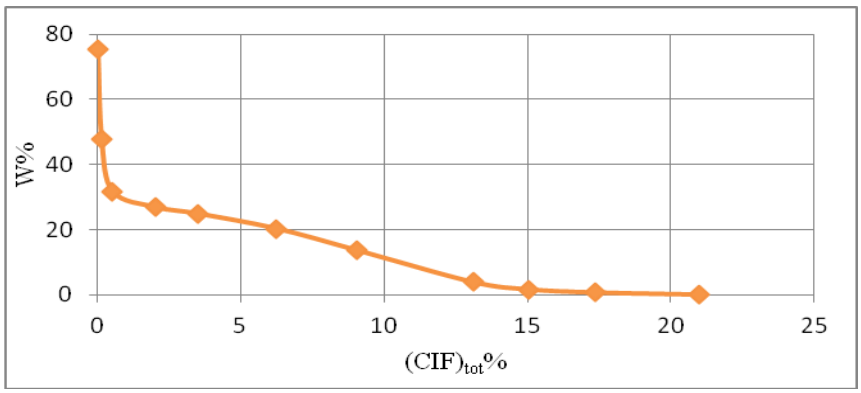

Figure 5. 20. Plot of water content (percentage) versus $(CIF)_{tot}$ (percentage)/ a mixture of porcelain-kaolinite.

2. A half-inch thick mold with a smooth bottom under the lab atmosphere (SA2) is used.

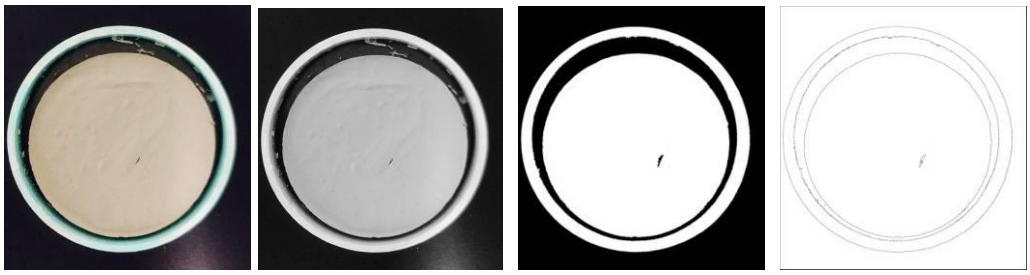

(a) (b) (c) (d)

Figure 5. 21. Applying image analysis technique for determining the shrinkage area of the soil sample (porcelain-kaolinite). (a) Original image, (b) converting the original image to a gray scale, (c) converting the gray-scale image to a binary image, and (d) using outline option.

3. Inside the desiccator, a half-inch thick mold with small grooves (GDsalt2) is used.

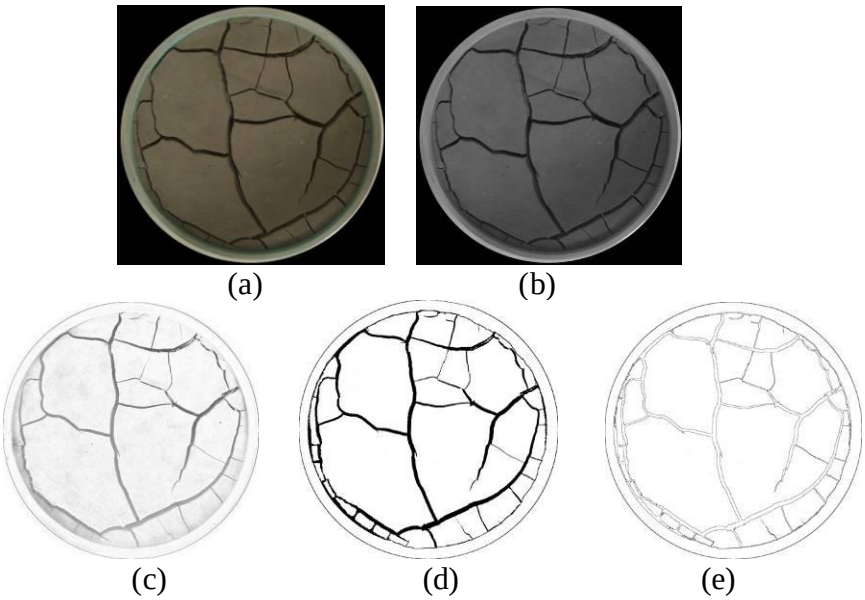

(a) (b)

(c) (d) (e)

Figure 5. 22. Final pattern of the soil sample (porcelain-kaolinite) inside the desiccator. (a) Original image, (b) converting the original image to a gray scale, (c) using subtract background option, (d) converting to a binary image, and (e) using outline option.

For this test, $(CIF)_{tot}$ was calculated for a series of images (which are shown in chapter 3) starting from the one taken when the first crack appeared until the one taken at the final stage. Since the sample did not experience any shrinkage, the CIF was equal to the $(CIF)_{tot}$.

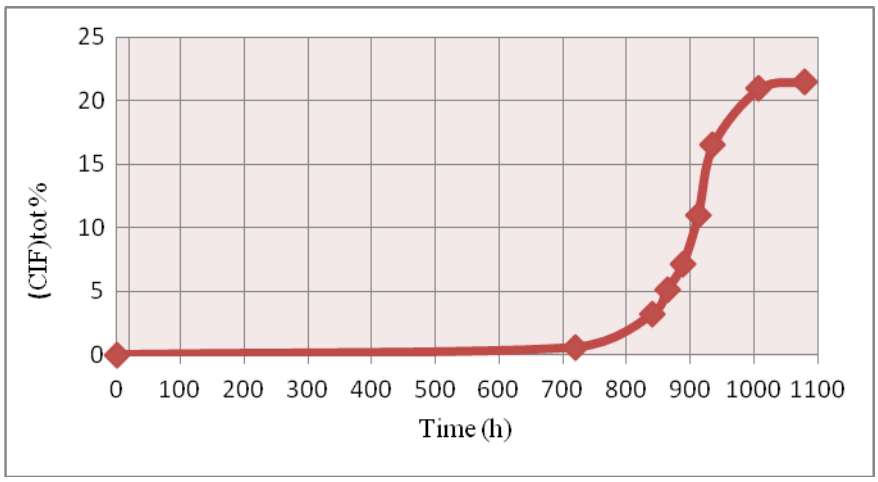

Figure 5. 23. Chart of $(CIF)_{tot}$ (percentage) versus time (hours)/ a mixture of porcelain-kaolinite.

Table 5. 1. The geometry of the samples with the main results of image analysis technique

Sample No.	GA1	SA1	GAsalt	GDsalt1	SDsalt	GA2	SA2	GDsalt2
Initial sample Area (mm^2)	17662.5	17662.5	17662.5	17662.5	17662.5	17662.5	17662.5	17662.5
Initial thickness (mm)	12.7	12.7	12.7	12.7	12.7	12.7	12.7	12.7
Initial sample volume(cm^3)	224.31	224.31	224.31	224.31	224.31	224.31	224.31	224.31
Final thickness (mm)	8	8	10.8	8.5	8.5	8.4	8.6	8.5
Final sample volume(cm^3)	103.67	92.53	184.84	113.53	111.38	117.19	117.64	117.86

Table 5. 1. Continued

Sample No.	GA1	SA1	GAsalt	GDsalt1	SDsalt	GA2	SA2	GDsalt2
Percentage of the volume change %	53.8	58.7	17.6	49.4	50.3	47.8	47.6	47.5
Area of uncracked material (mm^2)	12958.7	11566.2	17114.6	13356.29	13103.7	13951.054	13679.57	13865.36
Shrinkage area (mm^2)	590.82	6035.17	0	1205.02	4558.77	163.40	3977.228	41.67
Total Cracked area (mm^2)	4112.98	61.08	547.866	3101.19	0	3548.04	5.7	3755.47
CIF %	23.29	0.35	3.10	17.56	0.00	20.09	0.032	21.26
$(CIF)_{tot}$%	26.63	34.52	3.10	24.38	25.81	21.01	22.550	21.50
Total length of pieces (mm)	2243.18	494.26	-	1355.02	405.69	2463.25	442.01	2604.5
Length per unit area (1/mm)	0.17	0.03	-	0.10	-	0.14	0.025	0.15
Avg. width of cracks (mm) (measured manually)	1.97	11.74*	-	3.104	9.85*	1.63	8.89*	1.87
Avg. width of cracks (mm) (Equation)	2.10	12.33*	-	3.18	11.24	1.51	9.01*	1.46
Final vertical strain (ΔH/H)	0.37	0.37	0.15	0.33	0.33	0.34	0.32	0.33

Note the star (*) is used for the average width of shrinkage area.

The above table show the geometry of the samples with the results of image analysis technique for the main tests were described in chapter three.

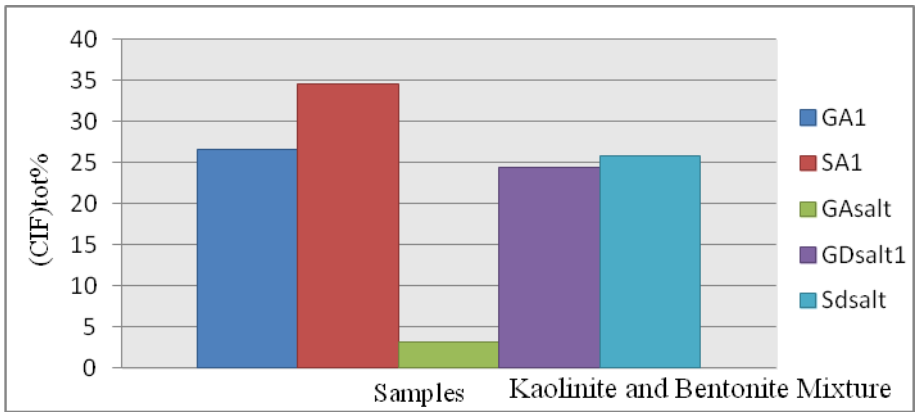

Figure 5. 24. Comparing the $(CIF)_{tot}$% of the (kaolinite-bentonite) samples.

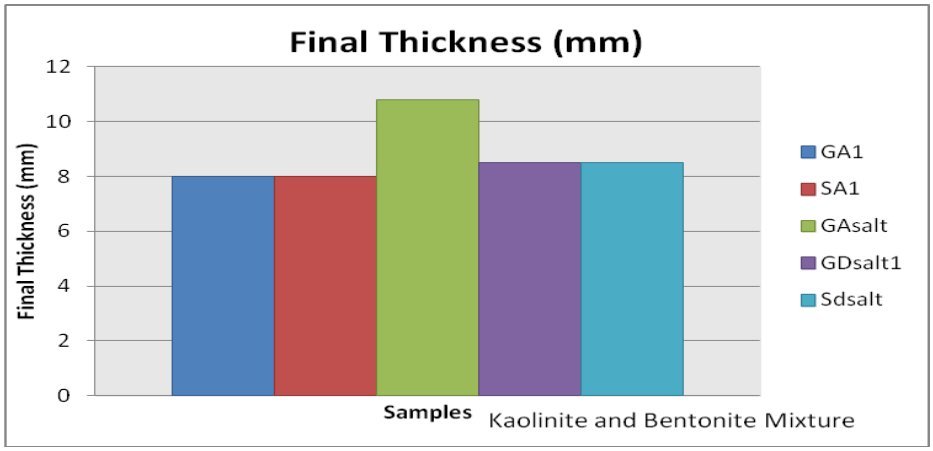

Figure 5. 25. Comparing the final thickness of the (kaolinite-bentonite) samples.

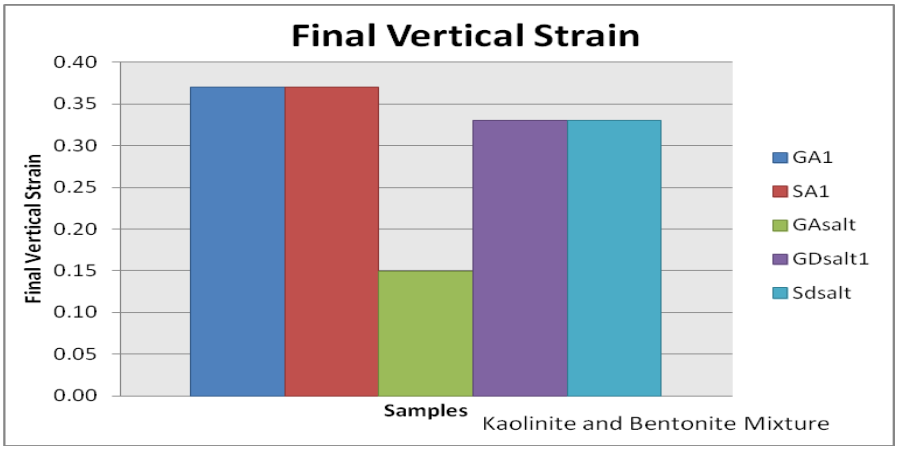

Figure 5. 26. Comparing the final vertical strain of the (kaolinite-bentonite) samples.

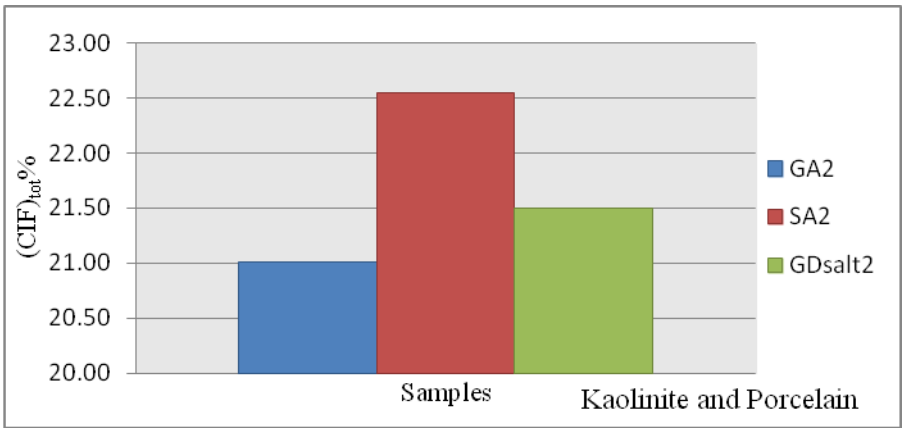

Figure 5. 27. Comparing the $(CIF)_{tot}$% of the (porcelain-kaolinite) samples.

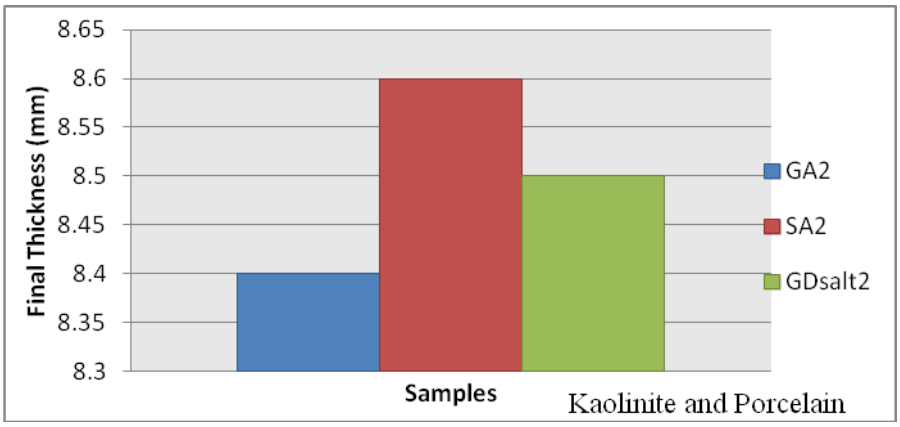

Figure 5. 28. Comparing the final thickness of the (porcelain-kaolinite) samples.

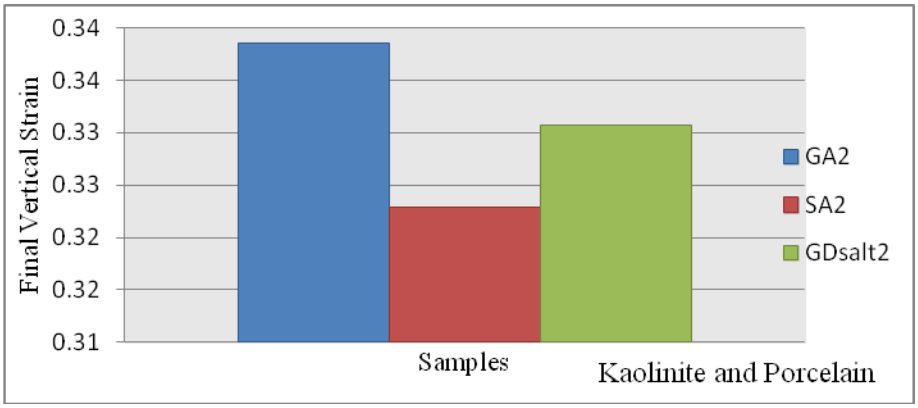

Figure 5. 29. Comparing the final vertical strain of the (porcelain-kaolinite) samples.

Table 5. 2. Crack intersection angles

No. of angles	Sample #	GA1	SA1	GAsalt	GDsalt1	SDsalt	GA2	SA2	GDsalt2
	➡		Shrinkage			Shrinkage		Shrinkage	
1		114.3	-	63.8	103.7	-	84.13	-	108.02
2		89.4	-	92.9	95.4	-	97.4	-	11.7
3		69.8	-	99.12	77.5	-	71.4	-	96.83
4		72.4	-	92.49	53.9	-	88.6	-	89.01
5		59.7	-	77.72	104.9	-	83.3	-	121.8
6		89.04	-	96.7	99.9	-	82.9	-	79.88
7		114.6	-	75.2	85.05	-	99.6	-	89.64
8		74.1	-	109.71	86.9	-	66.1	-	85.4
9		142.8	-	88.3	98.5	-	113.7	-	95.3
10		105.6	-	131.82	91.4	-	64.6	-	77.1
11		69.6	-	97.23	90.6	-	98.5	-	89.4
12		89.9	-	*93.18*	77.6	-	84.12	-	96.3
13		78.6	-		100	-	99.4	-	92.1
14		100.34	-		82.2	-	100	-	89.5
15		105.4	-		89.8	-	67.4	-	96.7
16		64.2	-		90.8	-	89.1	-	88.1
17		79.24	-		*89.26*	-	93.14	-	72.6
18		49.6	-			-	75.7	-	79.9
19		75.1	-			-	87.03	-	88.4
20		*86.51*	-			-	100.4	-	99.23
21			-			-	105.9	-	76.15
22			-			-	99.2	-	84.6
23			-			-	103.9	-	126.5
24			-			-	85.2	-	62
25			-			-	101.81	-	77.03
26			-			-	91.9	-	92.98
27			-			-	68.5	-	*87.16*
28			-			-	95.3	-	
29		-	-			-	*89.22*	-	

Table 5. 2. Continued.

Note: the last number of each column represents the average value of intersection angles of that sample.

These angles were summarized depending on their values in table 5.3. The table showed that the major angles were in range of 80.1 to 100.

Table 5. 3. Summary of intersection angles

Range	0°-80°	80.1°-100°	100.1°-180°
No. of cells	23	51	17
Average	70.91°	90.15°	106.38°

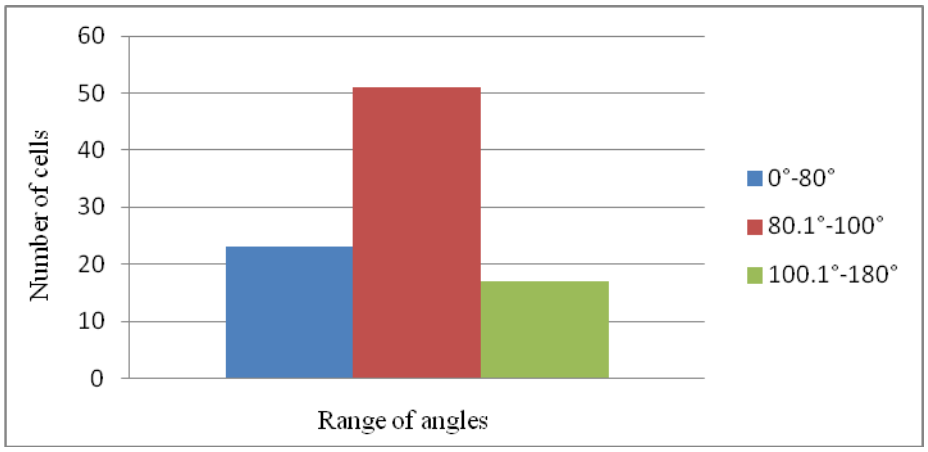

Figure 5. 30. Range of angles values versus the number of cells.

5.7 WETTING-DRYING CYCLES

In this section, the results of wetting-drying cycles are analyzed by using the final stage image after reaching the sample the final shape.

5.7.1 Kaolinite with bentonite

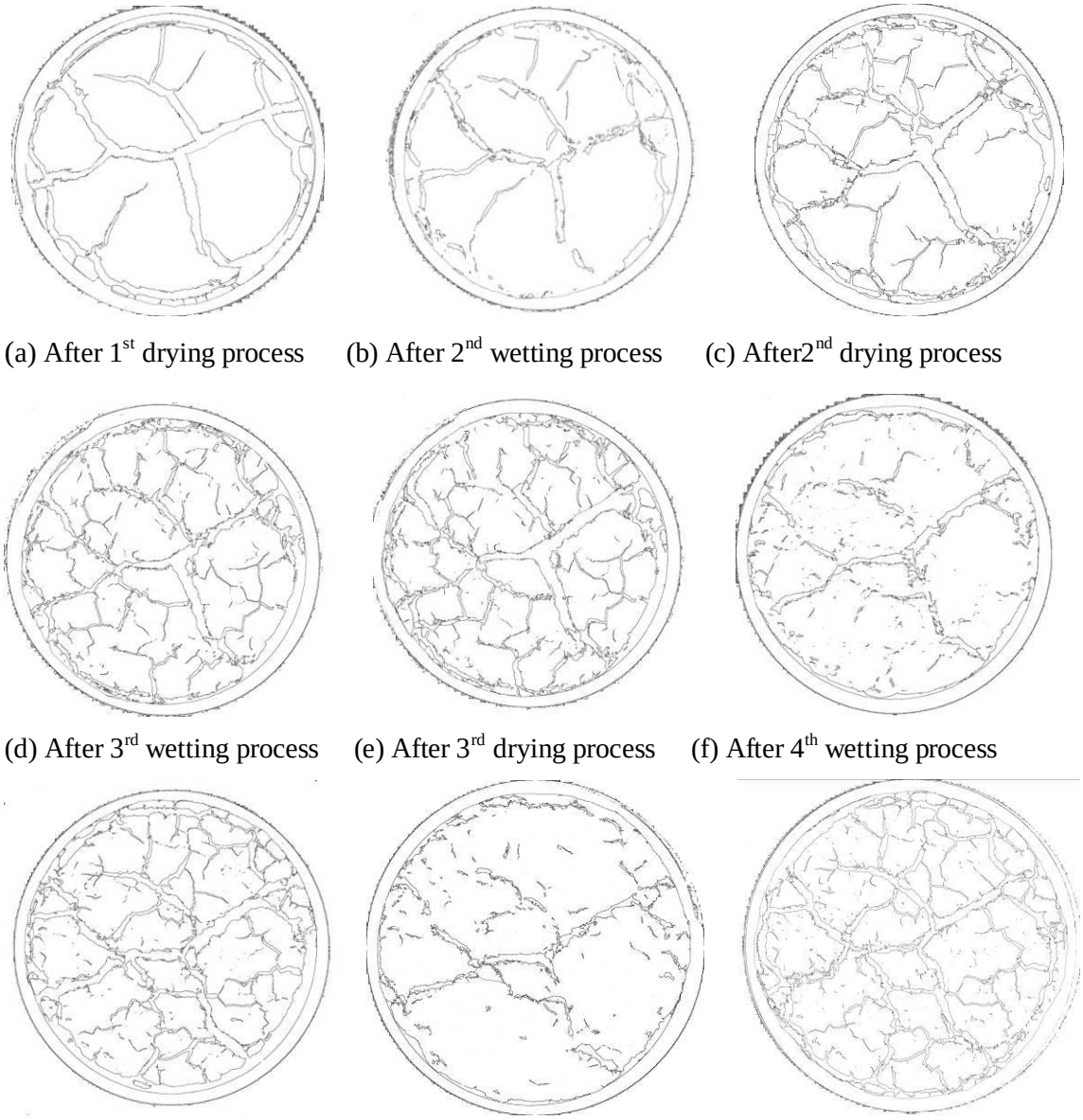

(a) After 1st drying process (b) After 2nd wetting process (c) After2nd drying process

(d) After 3rd wetting process (e) After 3rd drying process (f) After 4th wetting process

(g) After 4th drying process (h) After 5th wetting process (i) After 5th drying process

Figure 5. 31. Final cracks pattern after each cycle/ a mixture of kaolinite-bentonite.

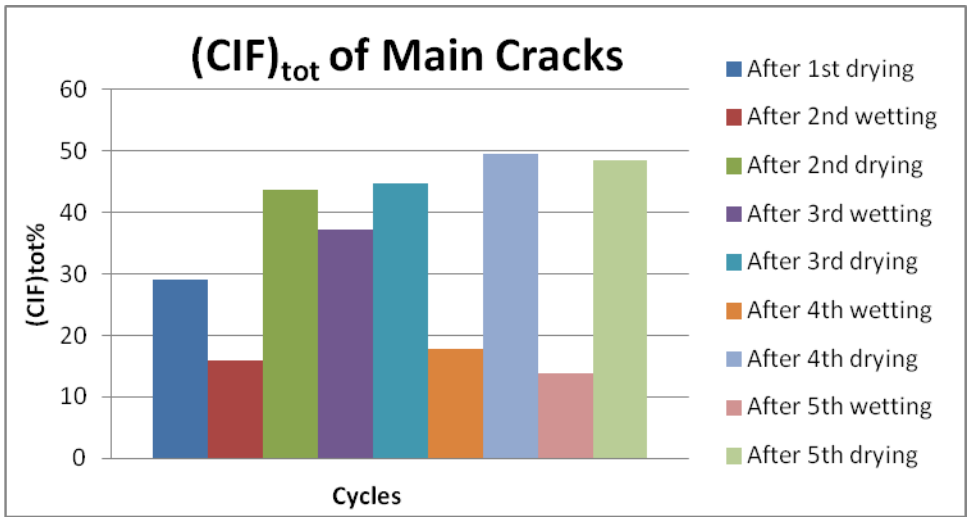

Figure 5. 32. $(CIF)_{tot}$% at the end of each cycle for the only main cracks/ a mixture of kaolinite-bentonite.

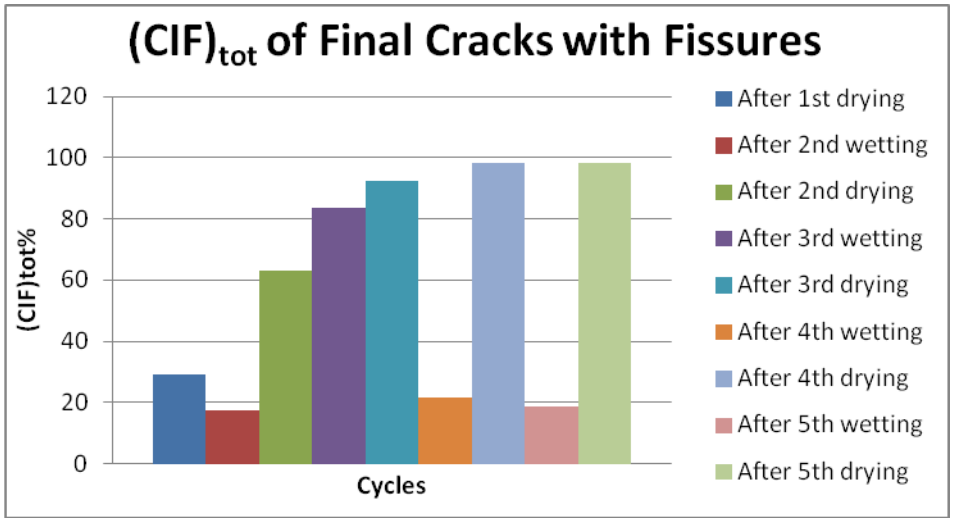

Figure 5. 33. $(CIF)_{tot}$% at the end of each cycle including the fissures/ a mixture of kaolinite-bentonite.

Note: for more details, a table of calculations has been attached in appendix 3.

5.7.2 Kaolinite with 100% water content

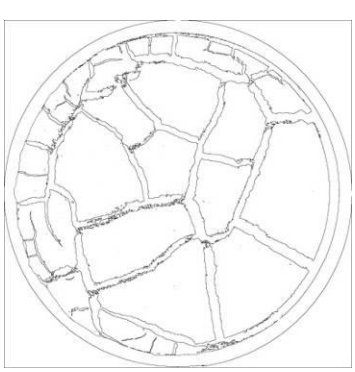

(a) After 1st drying process

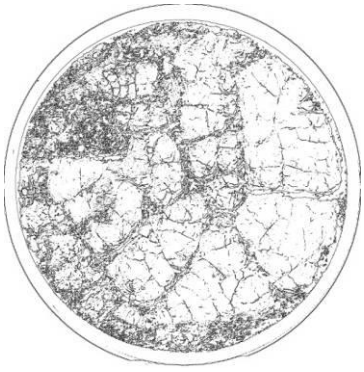

(b) After 2nd wetting process

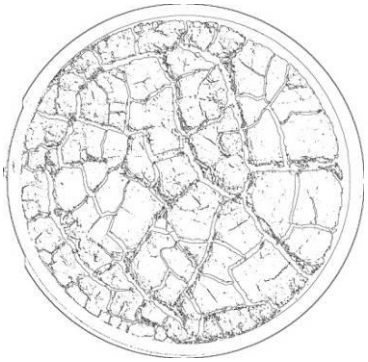

(c) After 2nd drying process

(d) After 3rd wetting process

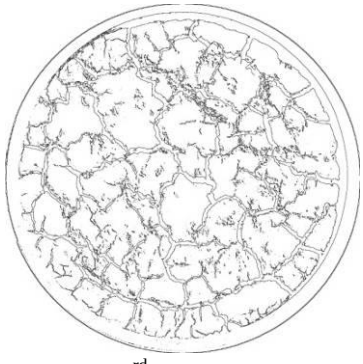

(e) After 3rd drying process

(f) After 4th wetting process

(g) After 4th drying process

Figure 5. 34. Final cracks pattern after each wetting-drying cycle/ a mixture of pure kaolinite.

Note: for more details, a table of calculations has been attached in appendix 3.

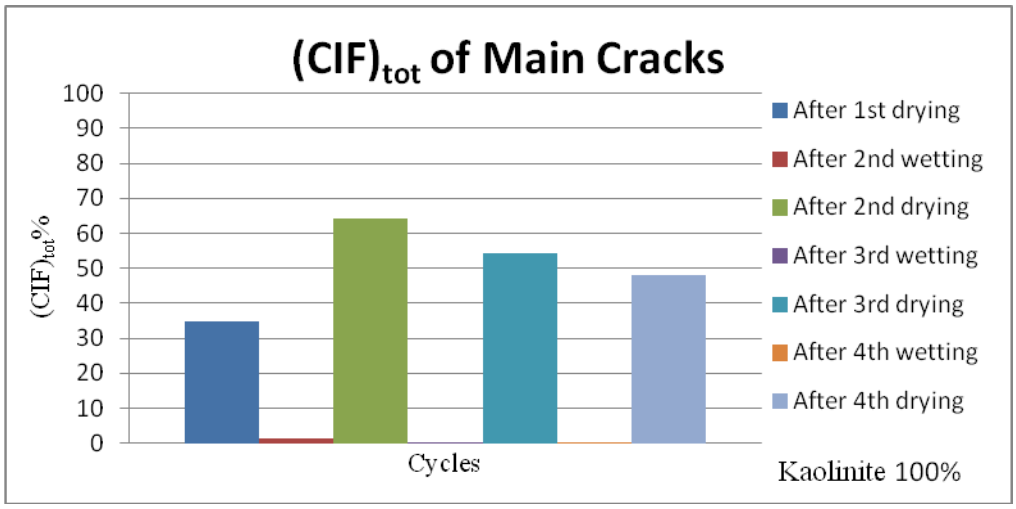

Figure 5. 35. $(CIF)_{tot}$% at the end of each cycle for the only main cracks/ a mixture of pure kaolinite.

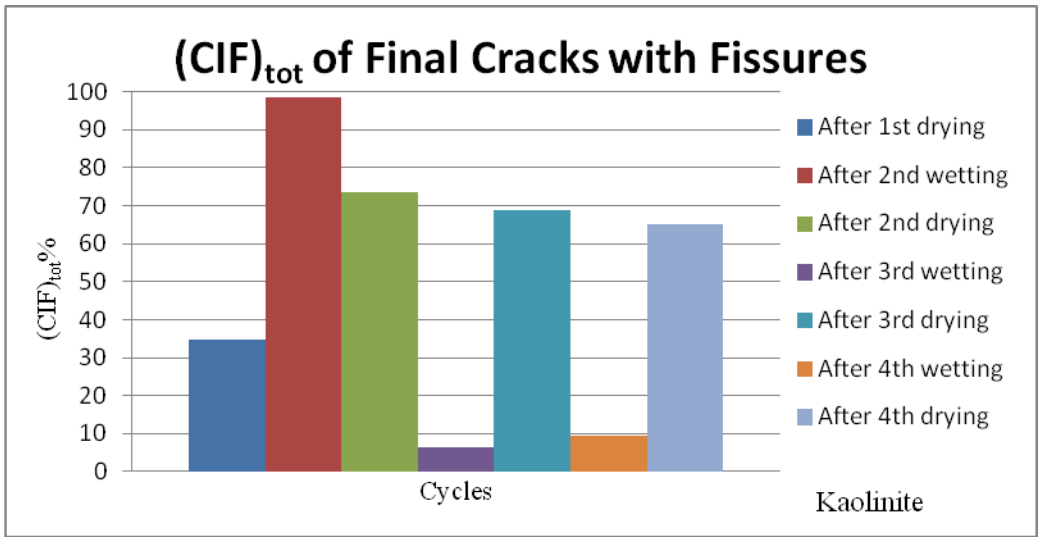

Figure 5. 36. $(CIF)_{tot}$% at the end of each cycle including the fissures/ a mixture of pure kaolinite.

5.8 EFFECT OF BOUNDARY CONDITIONS ON SOIL BEHAVIOR DURING DRYING PROCESS

Image analysis process (*Image j*, Rashband, 2005) was used in this research to obtain comprehensive information about the cracking mechanism during drying. Photos were taken with digital cameras, and then processed with *image j* software to characterize the crack patterns.

5.8.1 Bottom contact surface

In the present work, boundary conditions were simulated in the lab by using a plate that has very small (V-shape) grooves with 1 mm depth and 1.5 mm width by using a very smooth (flat) plate at the bottom of the mold. Thus, the smooth surface represents the condition of less friction whereas the grooved plate represents the most; and both surfaces have the same material properties. Consequently, these two boundary conditions showed significantly different results at the end. Since a sample can move on the smooth surface without restrictions, it was anticipated that the sample experiences shrinkage during drying (water evaporation) without cracking because the smooth surface offers less friction. However, the grooved surface offers higher friction, so it restricts the soil from moving easily during drying. The smooth plate with applied grease allows for free movement of the soil samples during shrinkage because the cohesion (~ 1.1 KPa, measured by using the direct shear device) of the soil particles is much higher than the adhesion (~ 0, measured by the direct shear device) between the soil and the mold. However, by using a grooved plate, soil samples try to shrink while water

evaporates, but these small grooves impede the soil from moving; and after testing the soil sample (in a saturated case) by the direct shear device, it turned out the adhesion (1.2 KPa, measured by the modified direct shear device) between the soil particles and the grooved bottom plate is roughly the same as the cohesion (1.1 KPa, measured by the direct shear device) of the soil particles. So that may increase the stresses inside the soil during drying and it ends up developing cracks. For example, there were obvious differences between the two samples, the kaolinite and bentonite mixture, under the lab atmosphere. The one with the grooved plate had high cracked area (4113 mm^2) in comparison with the other one with the smooth plate (61.09 mm^2), although both of them have identical conditions and the same initial surface area (17662.5 mm^2), except the bottom contact surface was different. Conversely, shrinkage area with the grooved plate (590.82 mm^2) was quite smaller than the one with the smooth plate (6035.17 mm^2). As a result, the less friction at the bottom surface, the less cracked area or the less crack formation.

5.8.2. Under opened and closed environment

This condition was simulated by using a desiccator glass for closed environment and the lab atmosphere for the opened environment. Temperature and relative humidity were almost controlled by continuously measuring them with a hygro-thermometer instrument, which were around (24 ±1) °C and (52 ± 2%) respectively. However, the relative humidity of 58.1% was imposed by means of salt solution $Ca(NO_3)_2.4H_2O$ inside the desiccator with a constant suction of 75 MPa (measured). The relative

humidity of the lab atmosphere was (52 ±2) % with a constant suction of 90 MPa. In particular, comparing the two tests with the mixture of kaolinite and porcelain, the crack intensity factor was approximately the same by using a grooved plate. That means the difference between the value of suction under the lab atmosphere (90 MPa) and the one (75 MPa) imposed in terms of relative humidity inside the desiccator may not have an effect on the results, and also the cracks pattern did not differ that much. However, by using a smooth plate, the results were relatively different. The sample shrank significantly under the lab atmosphere, so the surface area changed from 17662.5 mm^2 to 13679.6 mm^2 and the thickness also changed from 12.7 mm to 8.6 mm. On the other hand, the surface area of the first sample, which was placed inside the desiccator, did not change except the depth was decreased from 12.7 mm to 8.5 mm. The reason of that difference is probably because of a development of a layer of mold (fungal growth) on the upper surface of the sample inside the desiccator which might prevent the sample from shrinking. Another possibility is the soil may need a longer time to allow water evaporation and reach the equilibrium condition, but a layer of mold was developed above the sample surface in less than 20 days which may have restricted the sample from shrinking by decreasing the water evaporation rate. The latter one may consider as the main reason because the soil water content was measured at the end of 45 days and it was 69.2%, which is higher than the one with a grooved surface (55%). Therefore, for better understanding the behavior of a clayey soil under this condition, two different tests were performed; the first one was done by adding a small amount of clorox disinfecting spray to the salt solution and the test was going for a longer time which

around 55 days; the other one was done by adding small amount of clorox disinfecting spray to the mixture itself and also the test was going on for around 55 days. It is worth mentioning that the sample water content and the suction of the salt solution were measured and controlled to be identical to the previous tests. After all, the results were behind what was expected; layers of mold (fungal growth) were developed on the surface of these samples, and the volume of each sample was measured and it turned out to be roughly similar to the previous one. Therefore, more studies are needed to investigate the effect of temperature, which may be the main reason for growing a layer of mold on the sample surface.

As for the mixture of kaolinite and bentonite, the same observations were noticed except with the sample of the smooth surface, where shrinkage was observed without using clorox disinfection spray. Shrinkage area was determined in terms of $(CIF)_{tot}$. Even so, it was (25.81%) which is smaller than the $(CIF)_{tot}$ of the sample under the lab atmosphere (34.52%). This could be related to three factors which are: time, temperature, and the difference in the values of the total suction.

5.9 SAMPLE VOLUME CHANGE DURING DRYING

During drying, a number of stages were identified. At the beginning, desiccation cracks develop on the sample surface due to using a grooved bottom plate which impeded the soil movement and limited the changing of sample cross section area during water evaporation. As the water evaporated from the soil, the volume of the sample decreased

due to cracks initiation (cracks develop when the shear stress equals the shear strength of the soil). Over time, the sample reached the stage of shrinkage limit, which is defined as the reduction of the soil water content without resulting in volumetric change. Thus, this stage could be defined as a zero shrinkage stage, which was considered as the last stage of the drying process. These stages were proposed by Konrad and Ayad (1997b). They stated that cracks start to appear in the first stage while soil is still fully saturated. However, this is not the case with these experiments because it turned out that the first crack appeared under the lab atmosphere when the degree of saturation was around 93% and 65% in the kaolinite : bentonite and kaolinite : porcelain mixtures respectively.

Thickness of these samples was measured manually at the end of each test. The sample thickness changed in range of 15% to 37% of the original state during drying. The big change was with the samples left under the lab atmosphere. As for the cross section areas, they changed gradually during drying. However, changing in the cross section areas was dramatic at the end of some tests. The sample's cross section area depends on whether the sample experience shrinkage or cracking, which are depending on the roughness of the bottom contact surface. Basically, that change may express in terms of $(CIF)_{tot}$, which represents the summation of shrinkage and cracked area divided by the sample original area. The results are shown in table 5.1. Consequently, volumes of the samples change by depending on their cross section areas and their thicknesses. As shown in table 5.1, the maximum volumetric change (54%) occurred in the case of using a grooved contact surface and leaving the sample under the lab atmosphere.

When the soil samples exposed to a fully saturated salt solution (calcium nitrate tetrahydrate, $Ca(NO_3)_2.4H_2O$), a number of cracks were showing up just after few minutes of starting the test, as described in chapter three. Photos were taken when the soil sample was under the solution, which made the photos blurred and not as clear as the normal images. Although it was hard to measure the dimensions of these cracks, it found that the $(CIF)_{tot}$ was around 3.1% (for kaolinite and bentonite sample) by doing some corrections with the *image j* software. However, the sample's thickness and the sample's water content were measured after removing the solution. The average changes among the thicknesses and also the water contents were in range of 15% and 26% respectively. These changes could be described in terms of osmotic flow. When a salt solution added directly to the soil sample with a suction of 75 MPa, which was calculated in the lab by using the WP4-T device, the volume of the soil changed due to fluid flow (diffusion) that develops through the soil sample as a result of osmotic gradients. Thus, water moved out of the clay to the solution due to the gradient of fluid pressure needs to be in equilibrium condition. Eventually, these outward flows result in creating negative pore fluid pressures which increase the effective stress. Thus, the soil volume changes in response to these changes. According to Barbouar and Fredlund (1989), this volumetric change in soil is called osmotically induced consolidation.

5.10 SUMMARY

In this chapter, image analysis technique was discussed with presenting the results of some experiments were done in the lab. For these experiments, two main mixtures were

used and different conditions were considered. The results showed that the surface of the mold has a significant effect on cracks formation. For instance, with the kaolinite-porcelain mixture and a mold of a smooth surface under the lab atmosphere, the sample had no cracks and the CIF was about 0%. However, the same mixture under the lab atmosphere but with the mold of a grooved surface, there were significant cracks and the CIF was about 20.1%.

It has been proved that the image analysis technique is a useful tool for describing a set of images. *Image j* software is a basic tool with less cost in comparison with the traditional ways of determining the crack characteristics because it is available online for free and anyone can download it. Also, it is possible to solve almost any image processing because of the user-written plugins (Tiago Ferreira, and Wayne Rasband, 2012). In this research, a set of images were taken for each experiment which was done in the lab, and then the image analysis technique was applied to obtain the most important parameters required to describe the crack patterns (Lakshmikantha et al., 2009). In particular, cracked and uncracked areas, average width of cracks, and the crack intensity factor (CIF) were obtained to determine the development of crack patterns. In general, these parameters are used to adjust the numerical modeling which concerns the formation of cracks.

SOIL CURLING

6.1 OVERVIEW OF THE SECTION

The aim of this chapter is to investigate soil surface curling phenomenon that takes place when a thin layer of soil experiences desiccation. A series of experiments, which was carried out in the lab, had been described and the results were analyzed and discussed in this section. At the end, a comprehensive conclusion has been written to discuss the results and summarize them.

6.2 INTRODUCTION

Drying clayey soils may show development of cracks, shrinkage, or curling deformation and sometimes show combinations of them. In this research, a number of laboratory experiments were performed depending on the effect of material properties (soil grain size distribution, mineralogy and soil microstructure), and soil water content. However, there are other factors governing the curling deformation in soils such as hydraulic boundary conditions and chemical interactions (Zielinski et al., 2014). Furthermore, the elevation of deposits, clay type and its presence, and salt content were also studied as factors accompanied with curling (Bradley, 1933; Dow, 1964; Kindle, 1926; Minter, 1970; and Ward, 1923).

Mixtures of kaolinite with silica sand (graded to pass through sieve No. 20 and retain on sieve No. 30), pure kaolinite, and pure bentonite were studied in this research by

carrying out drying tests in the lab. The results of these experiments were compared with other results of Zielinski et al. (2014) and Kodikara et al. (2004). This research investigates curling phenomenon that takes place when a thin layer of soil experiences desiccation.

6.3 RESEARCH METHODOLOGY

To study curling deformation in soils, a number of desiccating tests on samples of pure kaolinite, silica sand, pure bentonite, and mixtures of kaolinite with silica sand of different percentages were carried out in the lab. Rectangular Perspex molds were used, each with volume of 65.84 cm^3 (15.9 cm length, 2.9 cm width, and 1.429 cm average thickness) as shown in figure 6.1.

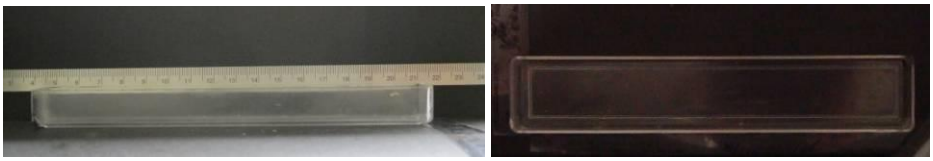

(a) Side view (b) Top view

Figure 6. 1. Rectangular Perspex mold.

A thin film of silicone grease was used to make the inside surface of these molds very smooth (decrease the adhesion as much as possible) to allow the soil samples shrink freely. All samples were dried in the lab where the temperature and relative humidity were around (23 ± 1) °C and (44 ± 5) % respectively. Furthermore, two cameras were used together in order to capture the behavior of the soil samples during drying in both

horizontal and vertical directions (cameras were placed at an angle of 90° with respect to the soil sample). This technique was proposed by Kikkawa et al. (2006) and Kitzhofer et al. (2010), but it is not a very well-known technique because the sample measurements become more complicated than using only one camera.

6.4 MATERIAL AND METHODS

Different mixtures of artificial soils were used: 85% kaolinite with 15% of silica sand prepared at water contents of (3×LL, 2.5×LL, and 2.75×LL), 80% kaolinite with 20% silica sand prepared at water contents of (3×LL and 2.5×LL), 90% kaolinite with 10% silica sand prepared at water content of 3×LL, 95% kaolinite with 5% silica sand prepared at water content of 3×LL, pure kaolinite with water contents of 3×LL and 5×LL, pure bentonite with water content of 5×LL, and pure silica sand with water content of 65%. The main focus in this chapter will be describing one set of experiments and comparing the results with the other tests (which are described in appendix 5).

Sixteen samples were prepared at the same time as shown in figure 6.2. Twelve of these samples were made up from a mixture of 85% kaolinite with 15% silica sand prepared at water content of 2.75×LL, and two of these samples were made up from pure silica sand and pure kaolinite prepared at water content of 65% and 5×LL respectively. The last two samples are described in the following steps: (1) the remaining mixture (85% kaolinite with 15% of silica sand at 2.75×LL) was placed in a big cylindrical mold of a diameter 5.9" (150 mm) and a total thickness of 1" (25.4 mm), (2) before adding the mixture, the

mold was divided into two parts of 0.5" (12.7 mm), (3) the two parts were fixed together by using a metal worm drive clamp with water resistant anti-slip tape (figure 6.3), (4) the cylindrical mold was filled with this mixture and left under the lab atmosphere for 24 hours, (5) the metal clamp and the tape were removed carefully and the sample was divided into two parts in two different pans, (6) one of the last two Perspex molds was filled with the soil from the upper part of the cylindrical mold and the other one was filled with the soil from the bottom part of this cylindrical mold, (7) the remaining soil from both parts was left under the lab atmosphere for around 1 week, (8) then it was carefully crushed and sieved. The intention was to check the grain size distribution of soil particles, and it revealed that most of the sand particles were settled at the bottom of the cylindrical mold. Soil of the upper part of the mold revealed the following fractions: 9.51% sand with 90.49% clay, and the remaining soil at the bottom of the mold was consisted of 22.13% sand with 77.87% clay. As a result, the behavior of the soil samples was significantly different in these two Perspex molds, as described later on.

6.5 EXPERIMENTAL SET-UP

The mixture was prepared by mixing 15% of silica sand and 85% of kaolinite with distilled water. The slurry was mixed carefully to ensure that the sand particles were distributed uniformly, and then the mixture was left inside a tightly sealed container for around 24 hours to ensure that the soil mixture is fully saturated and homogenized. The slurry at a water content close to 116.98% was distributed to twelve containers without any compactive effort and the initial dry density was around 0.637 Mg/m^3. The

remaining mixture was placed in the cylindrical mold (figure 6.3) for particle size distribution. The initial state of these molds are shown in figure 6.2. Additionally, photos were taken regularly to the sample and attached is so called the "reference sample", in both horizontal and vertical directions as shown in figure 6.4. Moreover, figure 6.5 shows the initial state of pure sand sample and pure kaolinite sample respectively.

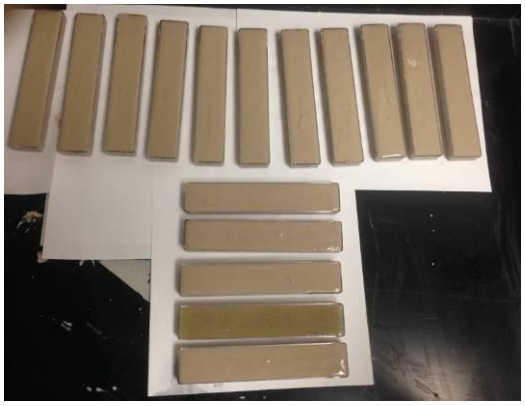

Figure 6. 2. Initial state of soil samples inside the Perspex molds.

Figure 6. 3. Cylindrical mold with a metal worm drive clamp and water resistant anti-slip tape.

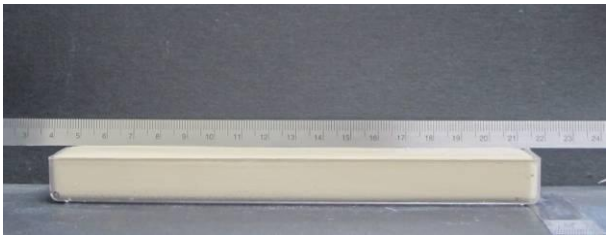

(a) Horizontal direction (side view of the sample).

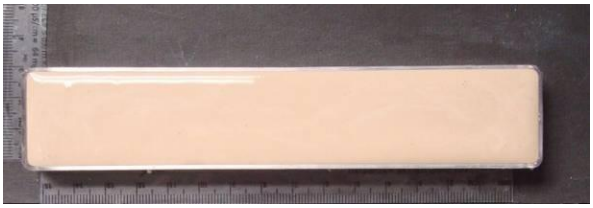

(b) Vertical direction (top view of the sample).
Figure 6. 4. The reference sample.

(a) Side view

(b) Top view

(c) Side view

(d) Top view

Figure 6. 5. (a) And (b) photos were taken to the initial state of pure silica sand sample, (c) and (d) photos were taken to initial state of pure kaolinite sample.

During drying, water content was measured continuously by taking one of these 12 samples each time and doing the following steps: (1) taking three samples from the upper layer (two from the sides and one from the middle), (2) after removing the upper layer, taking three samples from the bottom layer in the same way (figure 6.6), (3) these samples were left in the oven for 24 hours. In this way, one can obtain a general clue about the water content profile along the height of the sample. However, at a specific time this procedure was not practically possible because during water evaporation with time, the soil sample was becoming harder and it was not possible to divide the soil sample into two halves. At the end, only three water contents measurements were taken

(two from the sides and one from the middle of the sample). After all, it is clear that the difference in water content between the upper section and the bottom section is getting close eventually as shown in figure 6.8. It is worth mentioning, the total suction of these soil samples was measured every time with water content measurement by using WP4-T device.

(a) Taking samples from the upper layer of the mold.

(b) Removing the upper layer to take samples from the bottom.

Figure 6. 6. Taking samples for measuring the water content.

6.6 RESULTS

Particle size distribution and soil moisture content were the main factors considered to study the kinematics of curling in this research. However, development of curling in the soil mass has occurred due to different factors including development of stresses during desiccation of soils (Kodikara et al., 2004); this theory is discussed in the next section. Additionally, there are different factors which may affect the curling deformation in a

soil mass such as material type, material fabric, initial stresses, boundary conditions, rate of drying, and sample heterogeneities (Zielinski et al., 2014). In this research, a set of experiments was performed in order to understand the effect of particle size distribution and soil moisture content on the curling deformation of soil samples. Figure 6.7 shows the drying stages and curling development of the soil sample under the lab atmosphere.

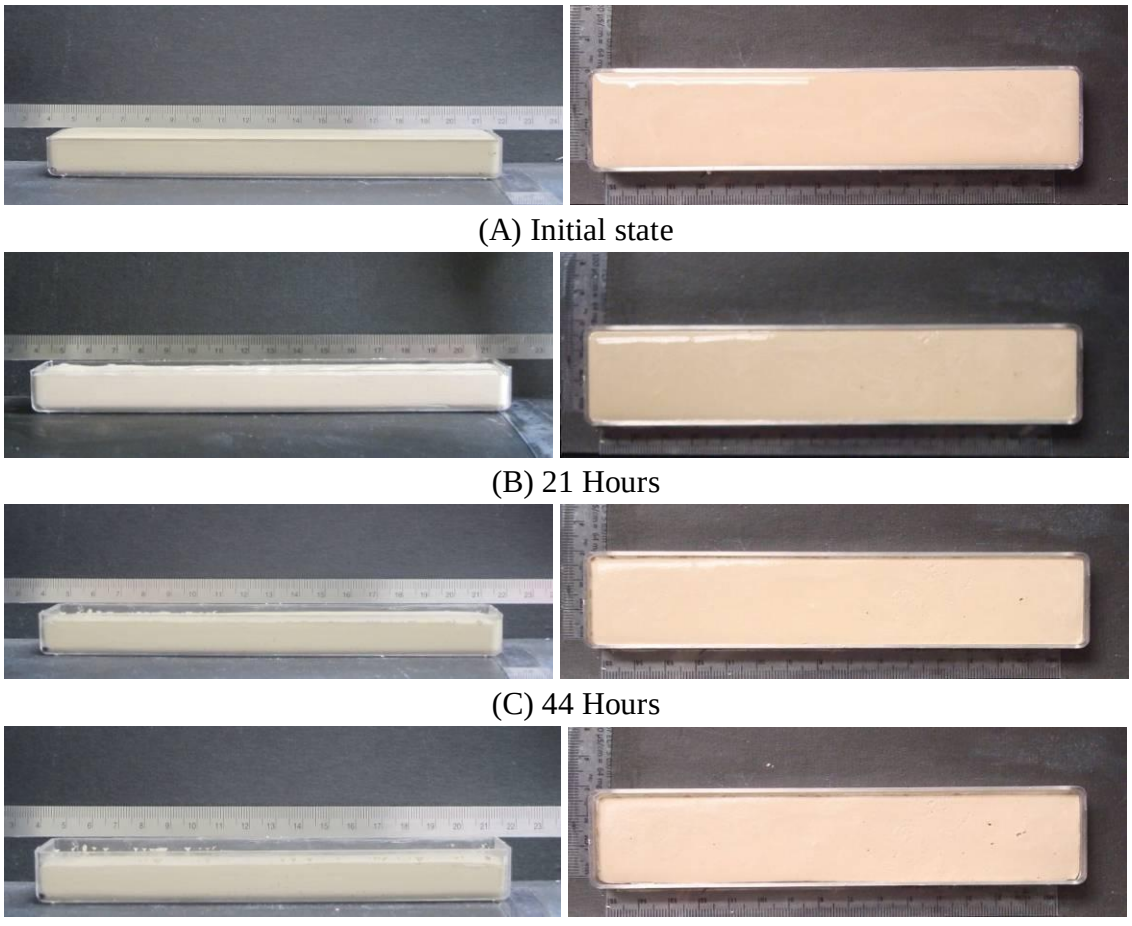

(A) Initial state

(B) 21 Hours

(C) 44 Hours

(D) 70 Hours

Figure 6. 7. Stages of curling development in a thin soil layer of 85% kaolinite and 15% silica sand which was prepared at 2.75×LL. Photos on the left side represent the side view of the sample and the ones on the right side represent the top view of this sample.

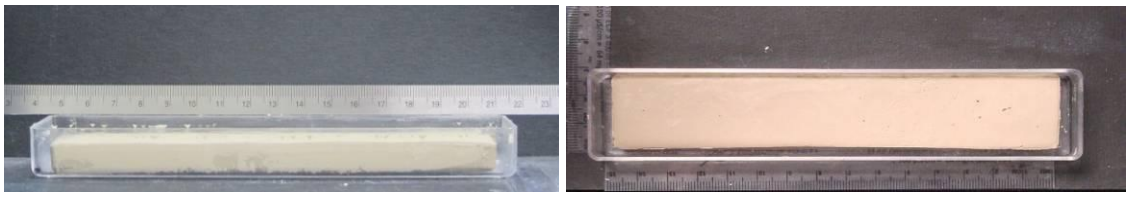

(E) 92 Hours

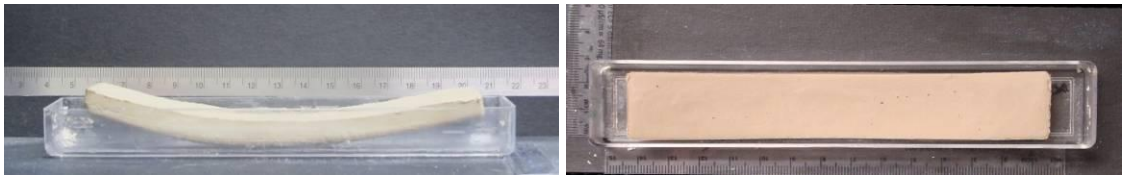

(F) 101 Hours

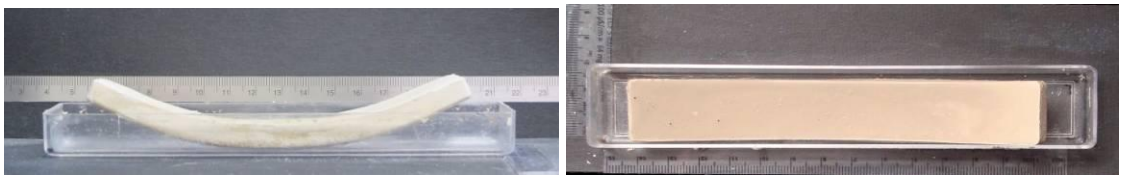

(G) 116 Hours

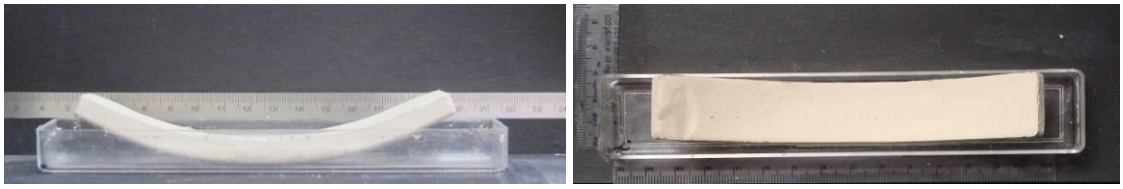

(H) 140 Hours

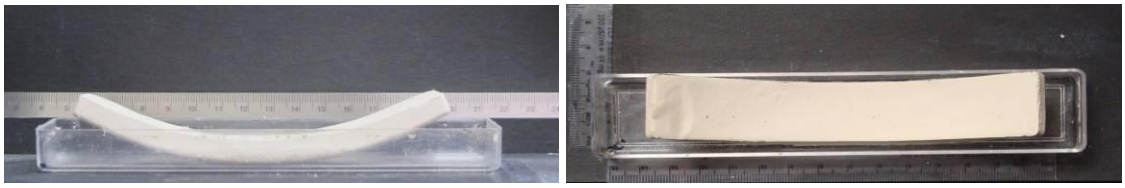

(I) 164 Hours

Figure 6. 7. Continued.

Table 6. 1. Main data collected during the test

Elapsed time (hours)	0	21	44	70	92	101	116	140	164
Specimen mass (g)	91.0	85.8	77.1	71.7	64.2	60.0	54.8	46.4	46.2
Temperature	23.3°	23.5°	23.5°	24.1°	23.7°	23.7°	23.6°	23°	23.2°
Humidity	39%	46%	48%	49%	51%	47%	42%	39%	38%
Suction (MPa)	0.00	0.07	0.59	14.23	50.54	65.9	84.8	116.6	116.6

Table 6. 1. Continued.

Elapsed time (hours)	0	21	44	70	92	101	116	140	164
Water loss (g)	0.0	5.2	13.8	19.3	26.8	31.0	36.2	44.6	44.7
Avg. w%	116.9	104.7	84.0	71.0	53.2	43.1	30.6	10.7	10.3
Sl %	1.01	0.90	0.72	0.61	0.46	0.37	0.26	0.09	0.09
Thickness (mm)	14.25	13.3	12.2	11.7	10.9	10.1	9.3	8.9	8.9
Specimen volume (cm^3)	65.84	61.5	55.1	43.1	36.5	33.8	31.1	29.8	29.8
Avg. w% (upper section)	116.9	99.2	80.7	69.1	51.0	41.8	27.8	9.8	7.6
Avg. w% (lower section)	116.9	103.5	87.85	74.34	54.09	44.0			

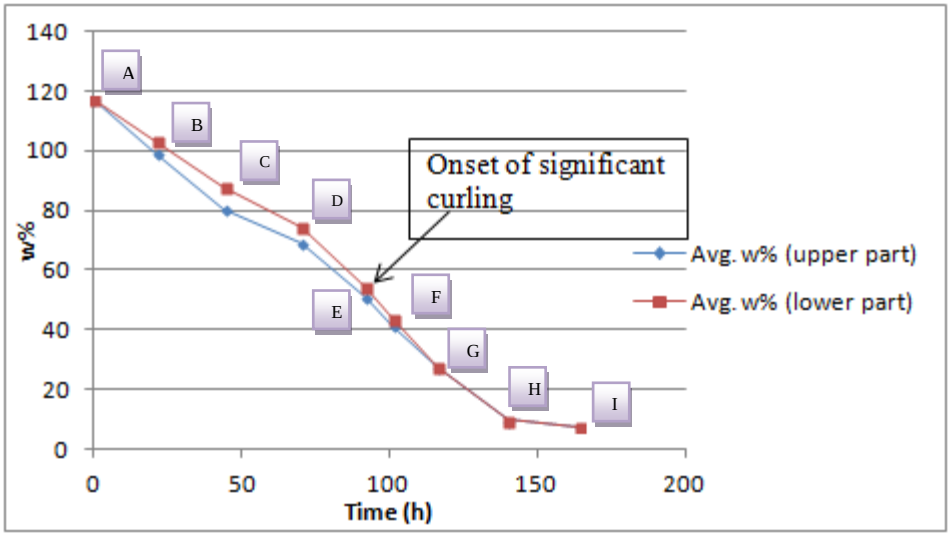

Figure 6. 8. Water content versus drying time for curling test to a thin soil layer of 85% kaolinite and 15% silica sand prepared at 2.75×LL.

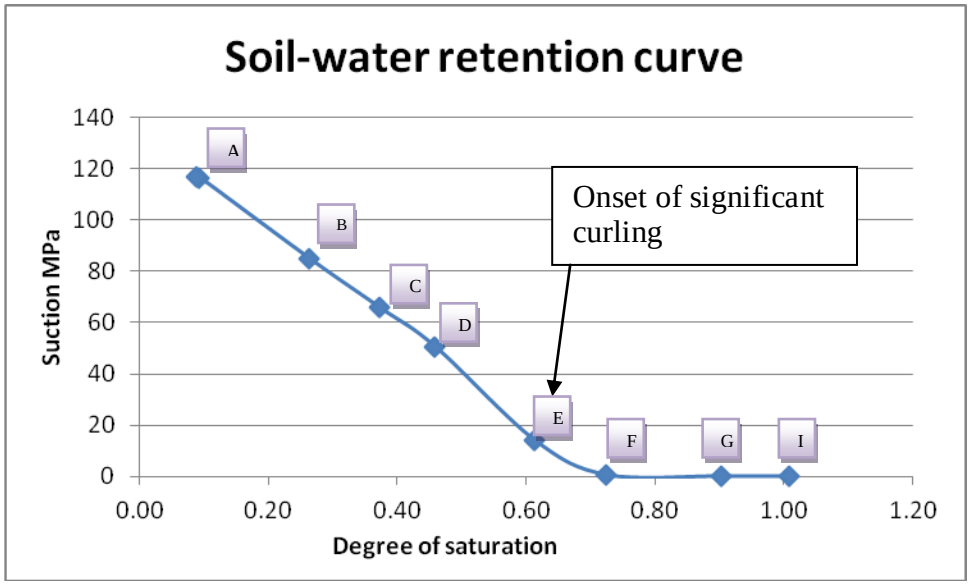

Figure 6. 9. Soil-water retention curve for curling test to a thin soil layer of 85% kaolinite and 15% silica sand prepared at 2.75×LL.

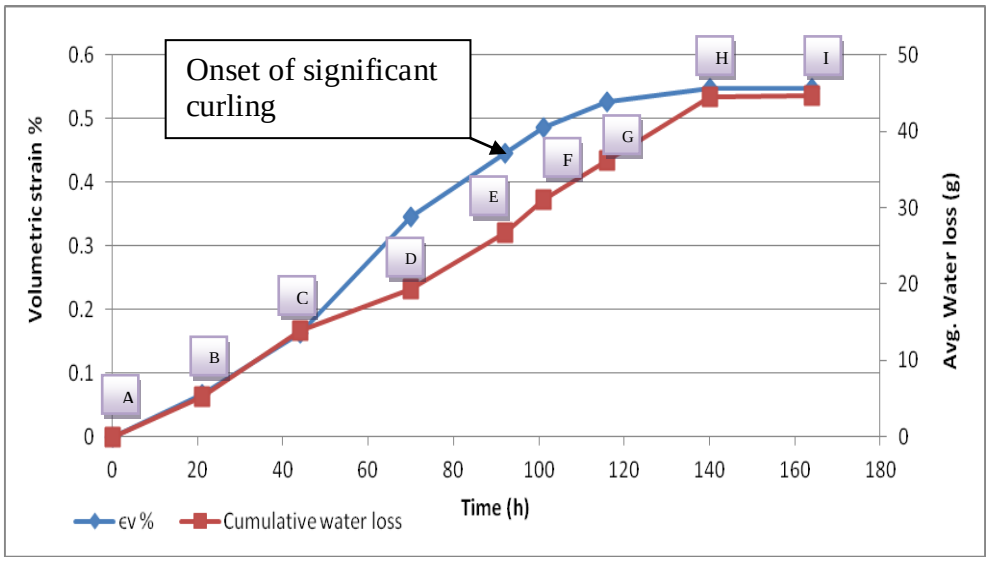

Figure 6. 10. Volumetric strain (%) and average water loss (g) vs. time (h).

As mentioned above, in order to investigate the effects of the sedimentation and soil moisture content, six other sets of experiments were performed with different mixtures: 85% kaolinite with 15% of silica sand was prepared at 3×LL and 2.5×LL, 80% kaolinite with 20% silica sand was prepared at 3×LL and 2.5×LL, 90% kaolinite with 10% silica sand was prepared at 3×LL, and 95% kaolinite with 5% silica sand was prepared at 3×LL. The final results of these tests are shown in figure 6.11.

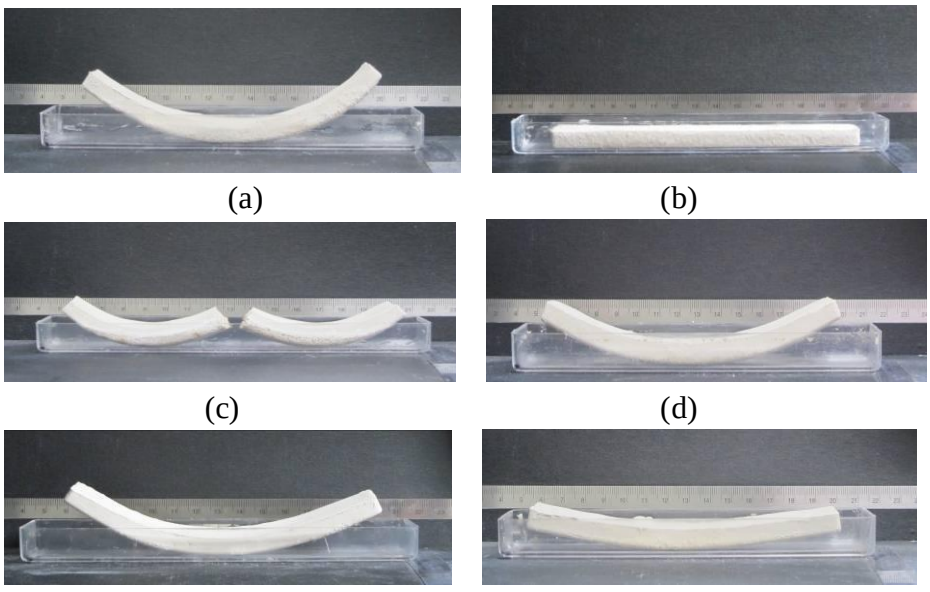

Figure 6. 11. Six different samples showing the differences in the rate of curling at the end of the tests; (a) 85% kaolinite with 15% of silica sand was prepared at 3×LL, (b) 85% kaolinite with 15% of silica sand was prepared at 2.5×LL, (c) 80% kaolinite with 20% silica sand was prepared at 3×LL, (d) 80% kaolinite with 20% silica sand was prepared at 2.5×LL, (e) 90% kaolinite with 10% silica sand was prepared at 3×LL, and (f) 95% kaolinite with 5% silica sand was prepared at 3×LL.

In the first two samples, soil moisture content was the main factor controlling soil surface curling. It was expected that preparing samples at high moisture content leads to

more gradual soil size distribution (Zielinski et al., 2014). As shown in figure 6.11 (a) and (b), the results are closely matched with what was expected; sample (a) experienced volumetric shrinkage and significant curling deformation (moving the edges of the sample upward during drying). However, the curling phenomenon in sample (b) was not significant in comparison with the volumetric shrinkage; this is probably due to a virtually uniform particle size distribution. Furthermore, sedimentation is more marked when comparing samples a, c, e, and f in figure 6.11; this is because they were prepared at the same moisture content (3×LL). Curling deformation was significantly increased with the percentage of sand particles. Since it has been proven that with high water content (e.g. 2.75×LL) the finer particles (kaolinite clay particles) overlaid coarse particles (silica sand particles), the third sample which was prepared with 20% of silica sand was broken from the middle (figure 6.11 (c)) after experiencing high curling deformation (moving the edges of the sample upward during drying), as shown in figure 6.12.

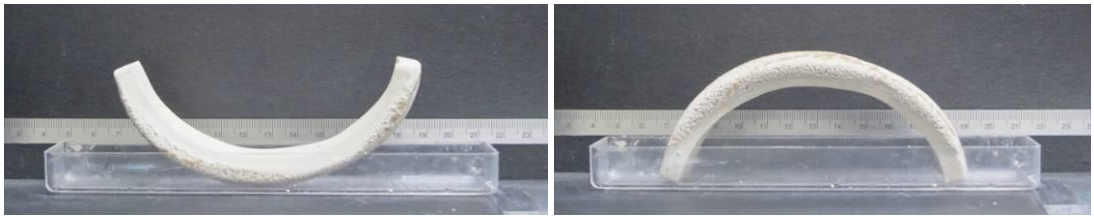

(a) (b)

Figure 6. 12. Curling deformation of the soil sample, 80% kaolinite with 20% silica sand and water content around 3×LL, at time of 101 hours; (a) showing the original sample which was concave up, and (b) flipping the original sample to show the sedimentation of sand particles.

As shown in figure 6.13 (b), sand particles were settled at the bottom of the sample; and while the edges were moving up, these particles were moving toward the center. As time progressed, the middle part of the sample became weaker while the edges moved up. Therefore, the sample was broken from the middle and the particle size distribution was clearly shown in figure 6.13 (a).

(a) Particles size distribution after breaking the sample.

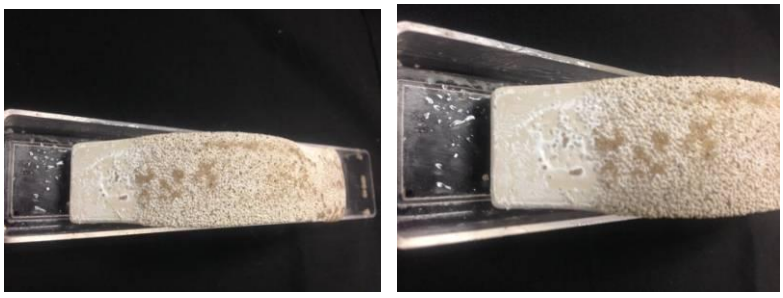

(b) Flipping the whole sample to show the grain size distribution of soil particles.

Figure 6. 13. Sedimentation of sand particles at the bottom of the mold.

As for the pure silica sand, one sample was prepared at 65% water content. As was expected, this sample only experienced a little reduction in volume during drying (figure 6.14).

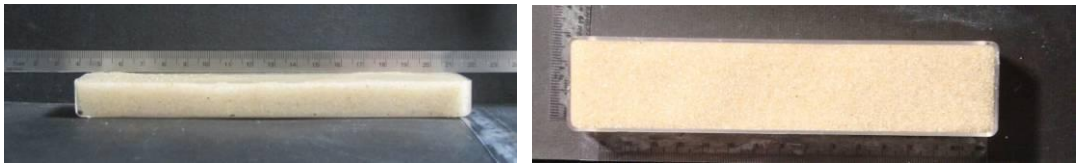

(a) Side view (b) Top view

Figure 6. 14. Pure silica sand was prepared at water content of 65%.

As for the pure kaolinite, two samples were prepared under two different water contents (3×LL and 5×LL). The first sample with 3×LL water content experienced shrinkage without curling during drying as shown in figure 6.15. However, the latter one experienced shrinking and curling deformation during drying as shown in figure 6.16. Overall, the amount of curling may be considered small (the sample moved up from both sides around 7 mm) in comparison with the mixture of kaolinite and silica sand with water content higher than 2.5×LL.

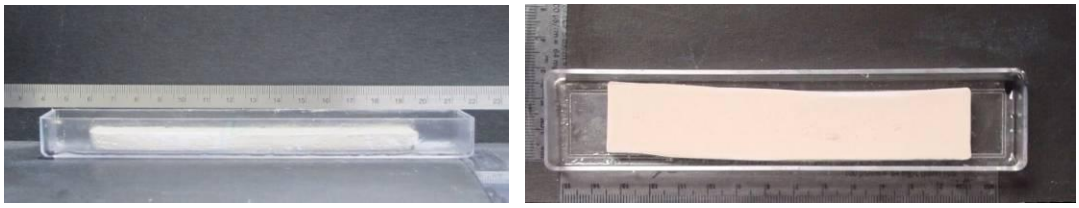

(a) Side view (b) Top view

Figure 6. 15. Pure kaolinite sample prepared at 3×LL.

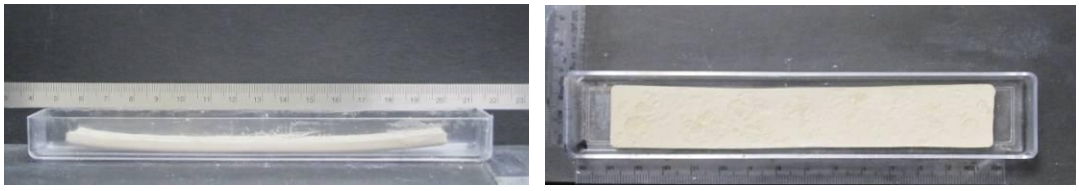

(a) Side view (b) Top view

Figure 6. 16. Pure kaolinite sample prepared at 5×LL.

Another sample was prepared with pure bentonite at water content around 5×LL. This sample experienced shrinkage without any curling deformation during drying as shown in figure 6.17.

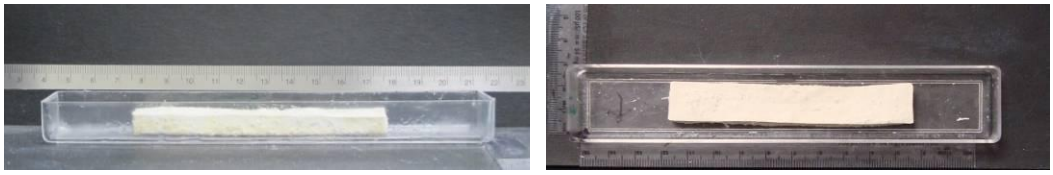

(a) Side view (b) Top view

Figure 6. 17. Pure bentonite prepared at 5×LL.

As for the last two samples (which were prepared by using the big cylindrical mold), the results are shown in figures 6.18 and 6.19. As mentioned above, after performing the sieve analysis test, it turned out the percentage of sand particles in the bottom section was around 22.13%; and at the time of preparing the sample, the water content was around 103% (2.44×LL). However, the percentage of the sand particles in the upper part of the mold was around 9.51%; and at the time of preparing the sample, the water content was around 99% (2.33×LL). Thus, micro-cracks were observed on the sample surface of the bottom part due to the large percentage of sand particles which created a rough contact at the bottom of the Perspex mold (figure 6.18 (b)). In contrast, due to the small percentage of sand particles in the sample of the upper part, a small non-uniform curling was observed (figure 6.19 (a)). The non-uniform curling is probably because of the non-uniform distribution of soil particles.

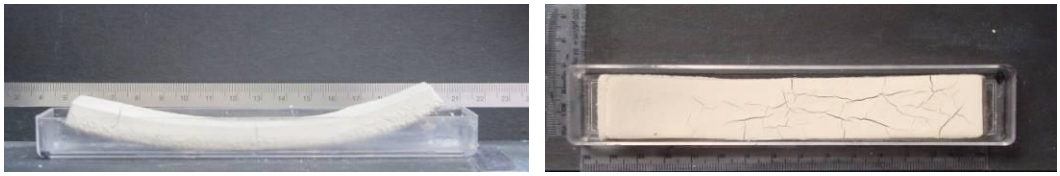

(a) Side view (b) Top view

Figure 6. 18. Sample prepared from the bottom part of the cylindrical mold.

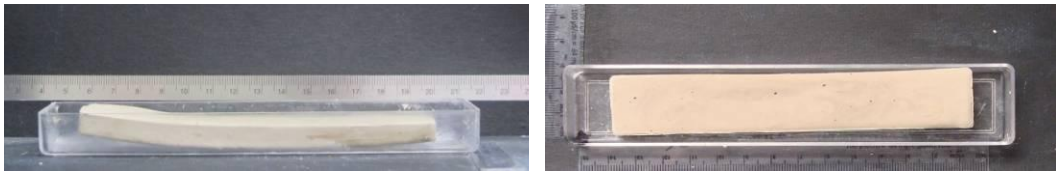

(a) Side view (b) Top view

Figure 6. 19. Sample prepared from the upper part of the cylindrical mold.

The same behaviors were observed with the mixture of 85% kaolinite and 15% of silica sand with initial water content of 3×LL. However, different behaviors were observed with the mixture of 85% kaolinite and 15% of silica sand with initial water content of 2.5×LL; samples from the lower and the upper sections experienced shrinkage without curling deformation, as shown in figure 6.20. On the other hand, the latter one, which was prepared with 80% kaolinite and 20% of silica sand with initial water content of 3×LL, behaved as following: the sample of the bottom part experienced shrinkage with curling deformation; however, the sample of the upper part experienced shrinkage without curling deformation. That probably goes back to the percentage of sand particles; after performing sieve analysis test, it turned out the percentage of sand particles at the bottom was around 37.21% and at the upper part was around 4.61%.

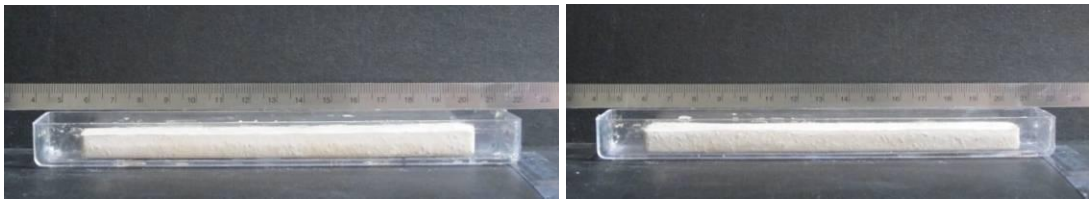

(a) Bottom part (b) Upper part

Figure 6. 20. Samples prepared using the big cylindrical mold with 85% kaolinite and 15% of silica sand at water content of 2.5×LL.

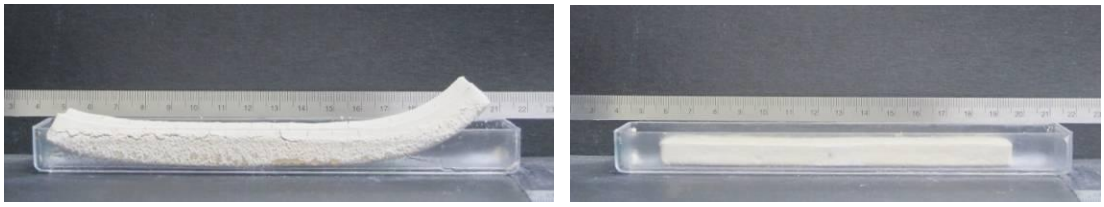

(a) Bottom part (b) Upper part

Figure 6. 21. Samples prepared using the big cylindrical mold with 80% kaolinite and 20% of silica sand at water content of 3×LL.

6.7 DISCUSSION AND CONCLUSION

The main aim of these experiments was for a better understanding the effect of material type and the initial water content on soil curling deformation. In this work, a total of eleven series of tests have been performed. It has been observed that particle size distribution has a significant effect on soil curling deformation; although, curling deformation was observed in a mixture of uniform soil particles (e.g. pure kaolinite prepared at 5× LL), it was not as significant as the one observed with a mixture of non-uniform soil particles (silica sand with kaolinite at high water content). Furthermore, particle size distribution of soil samples prepared at high water content (e.g. 2.75× LL and 3× LL) is obviously governed by sedimentation phenomenon at early stages of

drying. However, settlement of particles decreased as the soil water content decreased (Zielinski et al., 2014).

Figure 6.8 showed a representative drying curve obtained for a curling test of a thin soil layer of 85% kaolinite and 15% silica sand which was prepared at 2.75×LL. It is obvious that the moisture content of the upper part is lower than that for the lower part of the sample, which refers to drying which mainly took place at the top. In particular, at 44 hours, water content at the top was 80.7% and at the bottom section was 87.85%; however, these differences became smaller over time. According to Kodikara et al. (2004), the profile of the water content showed that the drying rate of the soil which is close to the surface was higher than the one below it; therefore, this observation is not beyond what was anticipated. Moreover, water content and soil suction were measured during the test, and it was observed that the soil sample has a significant suction under high water content (e.g. suction = 14.23 MPa while the water content was 71%) as shown in figure 6.9. This was consistent with the work of Kodikara et al. (2004), which showed that the soft soil was fully saturated at a considerable suction via Tempe cell tests. Fleureau et al. (1998) stated that the soft soil can be saturated till reaching suction around 20 MPa or sometimes above.

In order to describe soil curling deformation in terms of stresses, a theoretical explanation of Kodikara et al. (2004) is used. It has been assumed that during drying, a

soil could be considered under isotropic loading and nonlinear elasticity; thus, the change in stress could be related to the strain change in this equation:

$$\Delta\varepsilon_{sh} = -\frac{1}{(1-2\nu)}\Delta\sigma_{sh}\frac{E}{H}\Delta s$$

Where:

$\Delta\epsilon_{sh}$ is the shrinkage strain increment;

ν is the Poisson's ratio;

$\Delta\sigma_{sh}$ is the shrinkage stress increment;

E is the soil tangent modulus;

H is the tangent modulus related to the soil suction;

Δs is the suction.

It has been assumed that in early stages when the soil stress increased, $\Delta\epsilon_{sh}$ could be equal to zero. Therefore, the equation would end up with this form:

$$\Delta\sigma_{sh} = -\frac{1}{(1-2\nu)}\frac{E}{H}\Delta s$$

This tensile stress would become zero with time because there was no stress applied to the whole system in this case. In the meantime, shrinkage strain increases with a decrease in stress, and it ends up with this formula:

$$\Delta\varepsilon_{sh} = \frac{\Delta s}{H}$$

As shown in figure 6.22 (a), the stress and strain profiles consisted of different components which developed curling deformation in soil sample at early stages of drying (e.g. 92 hours with a thin soil layer of 85% kaolinite and 15% silica sand prepared at 2.75×LL). However, since the modulus of elasticity (E) is considerably small in soft soils (e.g. pure kaolinite prepared at 3×LL and 5×LL, and pure bentonite prepared at 5×LL), shrinkage deformation overcomes curling deformation because the latter one would be small while desiccating these soils (figures 6.15 and 6.17). Nevertheless, with the mixture of pure kaolinite which was prepared at 5×LL, small curling (moving up the edges of the sample) was observed at the end of drying path. At the end of drying, soil samples tried to reach water content equilibrium condition between the upper and the bottom sections; therefore, drying rate at the bottom increased to overcome the one above. Figure 6.22 (b) shows the results of the stress and strain profiles in this stage. Since the sample is already dry and hard in this stage, curling deformation overcomes the shrinkage deformation. This theory was clearly observed with the mixture of 80% kaolinite and 20% silica sand and the water content was 3×LL, the soil samples were broken at the end of drying (volumes of these samples were constant at this stage) due to curling deformation (moving up the edges of these samples) which led to weakening the middle part of these samples, as shown in figure 6.11 (c). Furthermore, depending on the type of the soil (e.g. elasticity modulus) in this stage, the level of stresses would be different between the upper and lower parts of the sample; therefore, the resulting curling may be concave-up or convex-up.

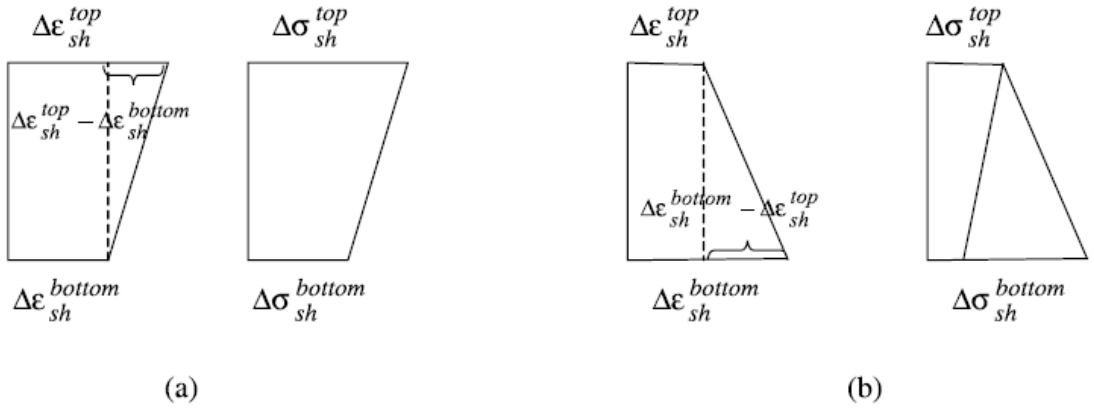

Figure 6. 22. Profiles of stress-strain of drying soils in case experiencing (a) concave-up, (b) convex-up (Kodikara et al., 2004).

CONCLUSION

7.1 INTRODUCTION

This chapter concludes the results of the tests performed throughout this study. Recommendations for future research are also presented at the end of this chapter. The aim of this work is to enhance the understanding of drying process in soils, considering both the phenomenon of initiation and propagation of desiccation cracks and also the development of shrinkage and curling deformation in soils upon desiccation. Interface shear strength parameters were studied in order to identify the effect of the textures of the bottom contact surface on the soil behavior under drying. The *image j* software was used to determine the severity of cracked area, width, length, and the shape of the cracks.

7.2 DESICCATION OF THIN SOIL LAYERS

A summary of the main tests described in chapters three and five is presented below. A total of two series of tests with circular samples under varying conditions were conducted providing qualitative and quantitative information about some parameters governing the process of soil cracking due to drying (e.g. bottom contact surface, osmotic suction, and total suction/relative humidity). Other eleven sets of tests with rectangular specimens of different mixtures and different water contents were performed to enhance the understanding of the main parameters controlling the curling deformation of soils due to drying. Furthermore, two sets of experiments had been carried out to investigate the effect of wetting-drying cycles of soil behavior.

In general, cracks were observed during the desiccation due to shrinkage of the soil as a result of a reduction of the sample moisture content. For instance, by using a grooved plate, soil samples tried to shrink while water evaporates, but these small grooves impeded the soil to shrink which induced tensile stresses inside the soil. Tensile stresses developed inside the soil sample due to the lateral restriction to shrinkage. The test performed in the direct shear device was to explore the strength of the sample at the time of slightly before development of cracks, and it turned out that the obtained shear stress was the maximum shear stress of this sample. From these results, it is possible to conclude that cracks started to develop once the tensile stress was equal to the tensile strength of the soil.

The effect of the suction (i.e. relative humidity) was investigated by designing an environmental chamber. The relative humidity inside the chamber was imposed by means of the salt solution $Ca(NO_3)_2.4H_2O$, 58.1%, which is corresponding to a suction of 75 MPa (it was calculated in the lab at 24.5 °C). It had been observed that by using a grooved plate, the crack intensity factor of the soil sample (kaolinite-porcelain) was roughly the same under both conditions. It could be concluded that the varying suction may not have an effect on the results, and also the cracks pattern did not differ that much. Nevertheless, it had been observed that by using a smooth plate, the amount of shrinkage of the soil sample was different; in other words, the one inside the desiccator did not experience radical shrinkage (only the thickness of the sample was changed).

The problems of the fungal growth and time were the two factors, which had been suggested for this deviation.

The effects of wetting-drying cycles on the behavior of thin soil layers were investigated in the lab to simulate seasonal climatic variations. It was observed that the iterations between wetting and drying caused the development of microcracks alongside with the originally existing major cracks in the mixture of kaolinite-bentonite. As for the pure kaolinite mixture, major cracks originally appearing were fully closed during wetting due to soil swelling and replaced by microcracks. The divergence of the behavior of these two samples reflects the effect of the soil type on the behavior of the soil during wetting-drying cycles. Since swelling was observed in both soil samples, attention should be paid to soil swelling during wetting path.

The effects of different soil mixtures and the water content on soil curling deformation had been studied. Although the initial water content of the soil sample is very important, it was observed that soil samples with uniform sized particles experienced no significant curling during drying. However, the curling was noticeable with soil samples have non-uniform size particles. For these samples, the ones prepared at high water content (e.g. 2.75×LL and 3×LL) showed more noticeable curling. That was because in these samples the sedimentation of particles leads the coarse particles to settle at the bottom and the fine ones settle at the top. Particle size distribution is controlled by soil water content and sedimentation at early stages of drying. The technique of using two digital cameras

to capture the 3D pattern of the soil sample provided very useful figures for understanding the difference in the behavior of soils under different conditions.

In this research, a comprehensive description of soil behavior under drying was obtained and presented by using *image j* software. Image analysis technique is a time-effective technique and it is available online. For precise measurements of cracks pattern, the lens of the digital camera should be placed by a stand above the soil sample. Special care should be taken to ensure the horizontality and central location of the lens above the soil sample. This can be achieved by using a small level to control the position of the camera.

Ultimately, the results are in line with those presented in existing literature. This work provides quantitative and qualitative information about the main factors controlling the behavior of thin soil layers under drying, which may consider as an essential concern to improve the modeling of soil behavior under desiccation.

7.3 INTERFACE DIRECT SHEAR TEST

In the present work, the conventional shear box was designed to study the soil-plate interface. Tests on fifty samples were carried out in the lab. Very interesting results were achieved from these tests. The experimental program and the results presented were focused on four parameters: the drainage conditions, the interface material, the initial water content, and the normal load. These parameters control the maximum shearing

resistance. In the drained condition, it had been observed that shear stresses of the soil-grooved surface interface were very close to the ones of the soil-soil interface, which means that the cracks may develop either from the bottom of the sample or on the surface. Since the adhesion of the soil-smooth surface interface was around zero, cracks did not develop in these samples during drying. In the undrained condition, it had been observed that the cohesion of the soil was greater than the adhesion of soil-plate interface. As for the internal friction angle, the one observed with the saturated soil-soil interface was higher than the ones observed with the soil-(grooved and smooth) interfaces; this observation was for both drained and undrained conditions. For a particular saturated sample (e.g. kaolinite-bentonite prepared at 90.1% water content) with a grooved plate interface, it could be concluded that the shear stresses increase while the sample drying until the cracks develop then they decrease with continuous drying.

7.4 RECOMMENDATIONS FOR FUTURE WORK

This section presents recommendation based on the work carried out in this study.

7.4.1 General Recommendations

- For better replication of the actual on-site conditions, large scale desiccation experiments should be performed.
- This work should be extended to include testing natural soils.
- This study would be further complemented by modeling of the soil behavior upon drying under different conditions.

7.4.2 Study-Specific Recommendations

- The effect of bottom contact surface should be studied to determine the effect of different levels of coarseness of the contact surfaces (plate-soil interface).
- More studies are required to investigate the influence of the shear rate on the strength of the soil; particularly, under very small shear rate (e.g. 0.005 mm/min).
- Since the artificial clay soil, which was used to performed the interface direct shear test, could not withstand high normal loads (e.g. higher than 5 Kg), further investigations of interface shear test with different types of soils (e.g. natural soils) and with high normal load should be carried out.
- The effect of temperature on the sample surface inside the desiccator (which is the main reason for growing a layer of mold on the sample surface) should be studied.

REFERENCES

Abu-Hejleh, A. N. and Znidarcic, D. (1995) Desiccation theory for soft cohesive soils, Journal Geotechnical Engineering, vol. 121.

Albrecht, B. A. and Benson, C. H. (2001) Effect of desiccation on compacted natural clays, ASCE, Journal of Geotechnical and Geoenvironmental Engineering, vol. 127 (1), 67-75.

Allen, J.R.L. (1982) On the curl of desiccation polygons, Sedimentary Geology, vol. 46, 23–31.

American Society for testing and Materials (ASTM) (2000) Annual Book of ASTM Standards, Sec. 4, vol. 04.08 and 04.09, West Conshohocken.

American Society for testing and Materials (ASTM) (2007) Standard Test Method for Direct Shear Test of Soils under Consolidated Drained Conditions, D 3080-98.

Andersen, J.V., Brechet, Y., and Jensen, H.J. (1994) Fracturing described by a spring-block model, Europhysics Letters, vol. 26, 13–18.

Aoki, K., Dong N. H., Kaneko T., and Kuriyama, S. (2002) Physically based simulation of cracks on drying 3D solid, In: Proceedings of the 10th Pacific Conference on Computer Graphics and Applications, Beijing, China, 9–11 October, pp. 467–468.

Aoki, K., Dong, N.H., and Kaneko, T. (2003) Representation method for cracks on drying 3D solid by physical model, Electronics and Communications in Japan Part 3, vol. 90(5), 50–59 (2007) (translated from Denshi Joho Tsushin Gakkai Ronbunshi, J86-D-II (12), 1756–1764).

Amarasiri, A., Kodikara, J., and Costa, S. (2011) Numerical modeling of desiccation cracking, international journal for numerical and analytical methods in geomechanics, vol. 35, 82–96.

Berney, E.S., Hodo, W.D., Peters, J.F., Myers, T.E., Olsen, R.S., and Sharp, M.K. (2008) Assessment of the effectiveness of clay soil covers as engineered barriers in waste disposal facilities with emphasis on modeling cracking behavior, Technical Report, Engineer research and development center, Tr-08-7. US Army Corps of Engineers, Engineer Research and Development Center.

Bowles, E. (1992) Engineering properties of soils and their measurement, Fourth Edition, McGraw-Hill, New York.

Bradley, W.H. (1933) Factors that determine the curvature of mud-cracked layers, American Journal of Sciences, vol. 26 (5), 55–71.

Bresler, E. (1973) Anion exclusion and coupling effects in nonsteady transport through unsaturated soils: I. Theory, Soil Science Society of America Proceedings, vol. 37, 663-669.

Brinker, C. J. and Scherer, G. W. (1990) Sol–gel science: the physics and chemistry of sol–gel processing, Boston: Academic Press.

Bro, A., Stewar, J., and Pradel, D. (2013) Estimating undrained strength of clays from direct shear testing at fast displacement Rates, in Geo-congress, Stability and Performance of Slopes and Embankments III, San Diago, CA, ASCE Geotechnical special publication, No. 231, C. L. Meedan, D. E. Pradel, M. A. Pando, and J. F. Labuz, Paper 5.

Bronswijk, J. (1988) Modeling of water balance, cracking and subsidence of clay soils, Journal of Hydrology, 97, 199-212 199. Elsevier Science Publishers B.V., Amsterdam.

Carter, M. (1983) Geotechnical Engineering Handbook, Chapman & Hall, New York. Dyvik, R., Berre, T., Lacasse, S., and Raadim, B. (1987), Comparison of truly undrained and constant volume direct simple shear tests, Geotechnique, vol. 37(1), 3-10.

Chao-Sheng T., Yu-Jun C., Bin S., Anh-Minh T., and Chun L. (2011) Desiccation and cracking behavior of clay layer from slurry state under wetting–drying cycles, Geoderma, 111–118.

Chertkov, V. and Ravina, I. (1999) Morphology of horizontal cracks in swelling soils1, Theoretical and Applied Fracture Mechanics, vol. 31(1), 19-29.

Chertkov, V. Y. (2002) Characteristic crack dimension of saturated drying soils: theory and applications, Faculty of Agricultural Engineering, Technion, Haifa 32000, Israel.

Chertkov, V.Y. (2000) Using surface crack spacing to predict crack network geometry in swelling soils, Soil Science Society of America Journal 64: 1918-1921.

Childs, E. C. (1969) An introduction to the physical basis of soil water phenomena, London: Wiley.

Colina, H. and Roux, S. (1999) Experimental model of cracking induced by drying shrinkage, The European Physical Journal, E1, 189-194.

Corte, A. and Higashi, A. (1960) Experimental research on desiccation cracks in soil, U. S. Army Snow Ice and Premafrost Research Establishment, Report No. 66, Corps of Engineers, Wilmette, Illinois, U. S. A.

Cui, Y.J., Sultan, N., and Delage, P. (2000) A thermomechanical model for clays, Canadian Geotechnical Journal, vol. 37 (3), 607–620.

Dasog, G., Acton, D., Mermut, A. and De Jong, E. (1988) Shrink-swell potential and cracking in clay soils of Saskatchewan, Canadian Journal of Soil Science, vol. 68, 251-260.

Decagon (1998-2003) WP4 Dewpoint PotentiaMeter, Operator's Manual, version 2.1.

Delage, P., Howat, M.D., and Cui, Y.J. (1998) The relationship between suction and swelling properties in a heavily compacted unsaturated clay, Engineering Geology, vol. 50, 31-48.

Deng, G. and Shen, Z.J. (2006) Numerical simulation of crack formation process in clays during drying and wetting, Geomechanics and Geoengineering, vol. 1 (1), 27–41.

Dineen K. and Burland J.B. (1995) A new approach to osmotically controlled oedometer testing, Proc. 1st Conference on Unsaturated Soils Unsat'95 2, 459-465, Paris, Balkema.

Dow, D.B. (1964) The effect of salinity on the formation of mud cracks, The Compass of Sigma Gamma Epsilon, vol. 41 162–166.

Drumm, E. C., Boles, D. R., and Wilson, G. V. (1997) Desiccation cracks result in preferential flow, Geotechnical news, June:22-25.

Dyer, M., Utili, S., and Zielinski, M. (2009) Field survey of desiccation fissuring of flood embankments, water management, vol. 162(3), 221-232.

Esteban, V. and Saez, J. (1988) A device to measure the swelling characteristics of rock samples with control of the suction up to very high values, ISRM Symposium on Rock Mechan- ics and Power Plants, Madrid, vol. 2.

Fang, H. Y. (1997) Introduction to environmental geotechnology, vol. 14 of New Directions in Civil Engineering. CRC Press.

Fakharian, K., and Evgin, E. (1996) An automated apparatus for three-dimensional monotonic and cyclic testing of interfaces, Geotechnical Testing Journal, vol. 19, No. 1, pp. 22-31.

Fleureau, J. M., Kheirbeksaoud, S., Soemitro, R., and Taibi, S. (1993) Behavior of clayey soils on drying wetting paths, Canadian Geotechnical Journal, vol. 302, 287-296.

Fredlund, D.G. and Xing, A. (1994) Equations for the soil-water characteristic curve, Canadian Geotechnical Journal, vol. 31(3), 521–532.

Geremew, Z., Audiguier, M., and Cojean, R. (2009) Analysis of the behaviour of a natural expansive soil under cyclic drying and wetting, Bulletin of Engineering Geology and the Environment, vol. 68 (3), 421–436.

Hallett, P.D., and Newson, T.A. (2005) Describing soil crack formation using elastic-plastic fracture mechanics, European Journal of Soil Science, vol. 56, 31– 38, doi:10.1111/j.1365-2389.2004.00652.x.

Hanzawa, H., Nutt, N., Lunne, T., Tang, Y.X., and Long M. (2007) A comparative study between the NGI direct simple shear apparatus and the Mikasa direct shear apparatus, Soils and Foundations, vol. 47 (1), 47-58.

Hartge, K. and Bachmann, J. (2000) Angles between cracks developed at primary shrinkage of fine grained soil Material, International Agrophysics, vol. 14, No. 1, pp. 43-51.

Herrera, M. C., Lizcano, A. and Santamarina, J. C. (2007) Colombian volcanic ash soils, In Characterization and engineering properties of natural soils, 2385-2409.

Holmes, D. M., Kumar, R. V. and Clegg, W. J. (2006) Cracking during lateral drying of alumina suspensions, Journal of American Ceramic Society, vol. 89, No. 6, 1908–1913.

Horgan, G. and Young, I. (2000) An empirical stochastic model for the geometry of two-dimensional crack growth in soil (with Discussion), Geoderma, vol. 96(4), 263-276.

Blatz, J., Cui, Y., and Oldecop, L. (2008) vapour equilibrium and osmotic technique for suction control, Journal Geotechnical and Geological Engineering, vol. 26, No. 6, 661–673.

Kassiff G. and Ben-Shalom A. (1971) Experimental relationship between swell pressure and suction, Géotechnique, vol. 21, 245-255.

Kayyal, M.K. (1995) Effect of the moisture evaporative stages on the development of shrinkage cracks in soil, Proceeding First International Conference on Unsaturated Soils, pp. 373–379.

Kemper, W.D., and Rollins, J.B. (1966) Osmotic efficiency coefficients across compacted clays, Soil Science Society of America Proceedings, vol. 30, 529-534.

Khoury, C. N. and Miller, G. A. (2012) Influence of hydraulic hysteresis on the shear strength of unsaturated soils and interfaces, ASTM Geotechnical Testing Journal, vol. 35(1).

Kikkawa, N., Nakata, Y., Hyodo, M., Murata, H., and Nisio, S. (2006) Three dimensional measurement of local strain using digital stereo photogrammetry in triaxial test, Geomechanics and Geotechnics of Particulate Media: Proceedings of International Symposium Geomechanics Geotechnics Particulate Media. Ube, Japan, 12–14 September 2006, pp. 61–67.

Kindle, E.M. (1923) Notes on mud crack and ripple mark in recent calcareous sediments, Journal of Geology, vol. 31 (2), 138–145.

Kitzhofer, J.,Westfeld, P., Pust, O., Nonn, T., Maas, H.G., and Brücker, C. (2010) Estimation of 3D deformation and rotation rate tensor from volumetric particle data via 3D least squares matching, Proceedings 15th International Symposium on Applications of Laser Techniques to Fluid Mechanical Lisbon, Portugal, 05–08 July, 2010.

Kleppe, J. H. and Olson, R. E. (1985) Desiccation cracking of soil barriers, ASTM International, 263.

Kodikara, J., Nahlawi, H., and Bouazza, A. (2004) Modelling of curling in desiccating clay, Canadian Geotechnical Journal, vol. 41, 560–566.

Konrad, J. M. and Ayad, R. (1997) An idealized framework for the analysis of cohesive soils undergoing desiccation, Canadian Geotechnical Journal, vol. 34(4), 477-488.

Lachenbruch, A. H. (1961) Depth and spacing of tension cracks, Journal of Geophysical Research, vol. 66, 4273-4292.

Lachenbruch, A. (1962) mechanics of thermal contraction cracks and ice-wedge polygons in permafrost, vol. 70. [Geological Society of America].

Laing, William A. (1978) Evaluation of image analysis techniques as applied to thermographs used in breast cancer detection, The University of Edinburgh, United Kingdom.

Lagerwerff J.V., Ogata G. and Eagle H.E. (1961) Control of osmotic pressure of culture solutions with polyethylene glycol, Science, vol. 133, 1486-1487.

Lakshmikantha, M. R. (2009) Experimental and theoretical analysis of cracking in drying soils, Ph.D. Thesis, Department of Geotechnical Engineering and Geosciences, Technical University of Catalonia, Barcelona, Spain.

Lambe, T.E. (1951) Soil testing for engineers, John Wiley & Sons, New York.
Liu, C. and Evett, J.B. (1997), Soil Properties, Testing, Measurement, and Evaluation, Third Edition, New Jersey, Prentice Hall.

Laribi, S., Audiguier, M., and Cojean, R. (2008) Assessing shrink/swell properties of two argillaceous soils from the Paris Basin: a comparison of cation exchange determination methods, Bulletin of Engineering Geology and the Environment, vol. 67 (3), 415–424.

Lecocq, N. and Vandewalle, N. (2002) Experimental study of cracking induced by desiccation in one-dimensional systems, The European physical journal-E EDP Sciences, Springer-Verlag, Societ Italiana di Fisica, 8 4, 445-452.

Lewis Richard J. (2007) Calcium Nitrate, Hawley's condensed chemical dictionary.

Li, J. H. and Zhang, J. (2010) Geometric parameters and REV of a crack network in soil, Computers and Geotechnics, vol. 37, 466–475.

Liu, C. and Evett, J. B. (1997) Soil Properties, Testing, Measurement, and Evaluation, Third Edition, New Jersey, Prentice Hall.

Liu, C., Wang, B.J., Shi, B., and Tang, C.S. (2008) The analysis method of morphological parameters of rock and soil crack based on image processing and recognition, Chinese Journal of Geotechnical Engineering, vol. 30 (9), 1383–1388.

Zhang, L. L., Zhang, J., Zhang, L. M., and Tang, W. H. (2011) Stability analysis of rainfall-induced slope failure, Proceedings of the ICE-Geotechnical Engineering, vol. 164 (5), 299-316.

Marcial, D., Delage, P., and Cui, Y.J. (2002) On the high stress compression of bentonites, Canadian Geotechnical Journal, vol. 39, 812-820.

Marinho F.A.M., Take A. and Tarantino A. (2008) Tensiometeric and axis translation techniques for suction measurement, Geotechnical and Geological Engineering, accepted for publication.

Metten, U. (1966) Desalination by reverse osmosis, M.I.T. Press, Cambridge, MA.

Miller, G. A., and Hamid, T. B. (2007) Interface direct shear testing of unsaturated soils, Geotechnical Testing Journal, vol. 30(3), Paper ID: GTJ13301; DOI:10.1520/GTJ1301.

Miller, C., Mi, H., and Yesiller, N. (1998) experimental analysis of desiccation crack propagation in clay liners, Journal of the American, Water Resources Association, vol. 34, No.3.

Minter, W.E.L. (1970) Origin of mud polygons that are concave downward, Journal of Sedimentary Petrology, vol. 40 (2), 755–764.

Mitchell, J. K. (1964) Shearing resistance of soils as a rate process, Journal of Soil Mechanics Foundation Engineering Division, ASCE, vol. 90(SM1), 29-61.

Mizuguchi, T., Nishimoto, A., Kitsunezaki, S., Yamazaki, Y., and Aoki, I. (2005) Directional crack propagation of granular water systems, Physical Review, E 71 (5), 056122.

Morris, P. H., Graham, J., and Williams, D. J. (1994) Crack depths in drying clays using fracture mechanics, Fracture Mechanics Applied to Geotechnical Engineering ASCE Geotechnical Special Publication, pages 40-53.

Morris, P. H., Graham, J., and Williams, D. J. (1992) Cracking in drying soils. Canadian Geotechnical Journal, vol. 29, 263-277.

Nahlawi, H. and Kodikara, J. (2002) Experimental observations on curling of desiccating clay, In Third International Conference on Unsaturated Soils, pages 5553-5556, Brazil. Recife. 2.1.

Naser Abu-Hejleh, A. and Znidarcic, D. (1995) Desiccation theory for soft cohesive soils, Journal Geotechnical Engineering, vol. 121, No. 6, 493–502.

Olsen, H. (1972) Liquid movement through kaolinite under hydraulic, electric, and osmotic gradients, American Association of Petroleum Geologists Bulletin, vol.56, 2022-2028.

O'Neil, M. (1962) Direct-shear test for effective strength parameters, Journal of Soil Mechanics and Foundation Division, ASCE, 88 (SM4), 109-137.

Ralph, J. (2014) The mineral and locality database, mindat.org.

Peron, H., (2008) Desiccation cracking of soils, Ph.D. Thesis, École Polytechnique Federal de Lausanne, Lausanne, Switzerland.

Peron, H., Hueckel, T., Laloul, L., and Hu, L.B. (2009) Fundamentals of desiccation cracking of fine-grained soils: experimental characterization and mechanisms identification, Canadian Geotechnical Journal, vol. 46, 1177-1201.

Persson, M. (2005) Image analysis in soil science, Department of Water Resources Engineering, Lund University.

Rodríguez, R. L., Sánchez, M. J., Ledesma, A., and Lloret, A. (2007) Experimental and numerical analysis of a mining waste desiccation, Canadian Geotechnical Journal, vol. 44.

Robinsonr, A. and Stokes,R .H. (1968) Electrolyte solutions. 2nd ed. Butterworths, London, United Kingdom.

Romero, E. (1999) Characterization and thermo-hydro-mechanical behaviour of unsaturated Boom clay: an experimental study, PhD Thesis, Polytechnical University of Catalunya, Barcelona, Spain.

Potyondy, J. G. (1961) Skin friction between various soils and construction materials, Géotechnique, vol. 11(4), 339–353.

Prat, P.C., Ledesma, A., and Lakshmikantha, M.R. (2006) Size effect in the cracking of drying soil, In: Gdoutos, E.E. (Ed.), Proceedings of the 16th European Conference of Fracture. Springer.

Prat, P. C., Ledesma, A., and Cabeza, L. (2002) Drying and cracking of soils: numerical modeling, in 8th Int. Conference on Numerical Models in Geomechanics NUMOG VIII, pages 705-711, Rome, Italy.

Sanchez, M. (2013) Transport phenomena in porous media, CVEN 673, Lecture Notes.

Scherer, G. W. (1990) Theory of drying, Journal of American Ceramic Society, vol. 73, No. 1, 3–14.

Serra, J. (1982) Image analysis and mathematical morphology, Academic Press, London.

Serra, J. (1988) Advances in mathematical morphology: Segmentation, vol 2. A.1, A.2.4.

Shibuya, S., Mitachi, T., and Tamate, S. (1997) Interpretation of direct shear box testing of sands as quasi-simple shear, Geotechnique, vol. 47, No. 4, pp. 769-790.

Shin, H._ and Santamarina, J. C. (2011) Desiccation cracks in saturated fine-grained soils: particle-level phenomena and effective-stress analysis, Geotechnique, vol. 61, No. 11, 961–972.

Shorlin, K., de Bruyn, J., Graham,M., and Morris,S. (2000) Development and geometry of isotropic and directional shrinkage crack patterns, Physical Review, E 61, 6950–6957.

Silvestri, V., Sarkis, G., Bekkouche, N. and Soulie, M. (1992) Evapotranspiration, trees and damage to foundations in sensitive clays, Canadian Geotechnical Conference, vol. 2, 533-538.

Smethurst, J. A., Clarke, D., and Powrie, W. (2006) Seasonal changes in pore water pressure in a grass-covered cut slope in London clay, Geotechnique, vol. 56, 523-537.

Statement of the Review Panel (1965) Engineering concepts of moisture equilibrium and moisture changes in soils, moisture equilibrium and moisture changes in soils beneath covered areas, Butterworths, Sidney, Australia, pp 7-21.

Stirling, R.A., Davie, C.T., and Glendinning, S. (2013) Numerical modeling of desiccation crack induced permeability, Newcastle University, Newcastle-upon-Tyne, UK.

Subba Rao, K. S., Allam, M. M., and Robinson, R. G. (2000) Drained shear strength of fine-grained soil-solid surface interfaces, Proceedings, Institution of Civil Engineering, Geotechnical Engineering, vol. 143, pp. 75-81.

Suits, L., Sheahan, T., Lakshmikantha, M., Prat, P. and Ledesma, A. (2009) Image analysis for the quantification of a developing crack network on a drying soil, Geotechnical Testing Journal, vol. 32(6), p.102216.

Takada, N. (1993) Mikasa's direct shear apparatus, test procedures and results, Geotechnical Testing Journal, vol. 16(3), 314-322.

Tang, C.S., Cui, Y.J., Tang, A.M., and Shi, B. (2010) Experimental evidence on the temperature dependence of desiccation cracking behavior of clayey soils, Engineering Geology, vol. 114, 261–266.

Tang, C., Shi, B., Liu, C., Zhao, L., and Wang, B. (2007) Influencing factors of geometrical structure of surface shrinkage cracks in clayey soils, Department of Earth Sciences, Nanjing University, 210093, China.

Tang, A. and Cui, Y. (2005) Controlling suction by the vapour equilibrium technique at different temperatures and its application in determining the water retention properties of MX80 clay, Canadian Geotechnical Journal, vol. 42, 1–10.

Tang, A., Ta, A., Cui, Y., and Thiriat, J. (2009a) Development of a large-scale infiltration tank for determination of the hydraulic properties of expansive clays, Geotechnical Testing Journal, vol. 32 (5), doi:10.1520/GTJ102187.

Tang, A., Vu, M., and Cui, Y. (2011) Effects of the maximum soil aggregates size and cyclic wetting–drying on the stiffness of a lime-treated clayey soil, Geotechnique, vol. 61 (5), 421–429.

Taylor, D.W. (1952) A direct shear test with drainage control, Symposium on Direct Shear Testing of Soils, ASTM Special Technical Publication No. 131, 63-74.

Ferreira, T. and Rasband, W. (2012) Image J. User Guide.

Towner, G. D. (1987b) The mechanics of cracking of drying clay, Journal of agricultural Engineering, Research, vol. 36, 115-124.

Tsubakihara, Y., Kishida, H., and Nishiyama, T. (1993) Friction between cohesive soils and steel, Soils and Foundations, vol. 33(2): 145–156.

Trabelsi, H., Jamei, M., Zenzri, H., and Olivella, S. (2011) Crack patterns in clayey soils: experiment sand modeling, International Journal for Numerical Analytical Methods in Geomechanics, vol. 36, 1410–1433.

Valentin, C. and Bresson, L.-M. (1992) Morphology, genesis and classification of surface crust in loamy and sandy soils, Geoderma, vol. 55 (3–4), 225–245.

Velde, B. (1999) Structure of surface cracks in soil and muds, Geoderma, vol. 93, 101-124. A.1.

Vogel, H., Hoffmann, H., Leopold, A., and Roth, K. (2005) Studies of crack dynamics in clay soil: II. A physically based model for crack formation, Geoderma, vol. 125(3-4), 213-223.

Ward, F. (1923) Note on mud cracks, American Journal of Sciences, vol. 6 (5), 308–309.

Weinberger, R. (1999) Initiation and growth of cracks during desiccation of stratified muddy sediments, Journal of Structural Geology, vol. 21, 379-386.

Wells, R., DiCarlo, D., Steenhuis, T., Parlange, J., Römkens, M., and Prasad, S. (2003) Infiltration and surface geometry features of a swelling soil following successive simulated rainstorms. Soil Science Society America Journal, vol. 67, 1344–1351.

Wikipedia, (2014) Effective stress, URL: http://en.wikipedia.org/wiki/Effective_stress.

Zarzycki, J., Prassas, M., and Phalippou, J. (1982) Synthesis of glasses from gels: The problem of monolithic gels, Journal of Materials Science, vol. 17, No. 11, 3371–3379.

Zieliński, M., Sentenac, P., Utili, S., and Dyer, M. (2010) Influence of the weather changes on the desiccation fissuring propagation and stability of flood embankments, Ph.D. Thesis, University of Strathclyde.

Zielinski, M., Sánchez, M., Romero, E., and Atique, A. (2014) Precise observation of soil surface curling, Geoderma, vol. 226–227, 85–93.

Zur B. (1966) Osmotic control the matrix soil water potential, Soil Science, vol. 102, 394-398.

APPENDIX 1

This appendix includes all the tests were done at the beginning of this research in order to decide which mixture would be used. Different soil mixtures with different water contents have been used and the results were somehow different.

Note: All percentages in terms of the sample mass.

A. KAOLINITE: PORCELAIN: BENTONITE (2: 4: 4) AND WATER 70%

To briefly describe this sample, kaolinite, porcelain, and bentonite were mixed with ratio of 2:4:4 respectively, and 70% of distilled water. Small mold used with a thickness of 1" and a diameter of 4", the bottom surface of the mold was smooth without using Vaseline. The sample left under the lab atmosphere for 72 hours. Figure A1.1 (a, b, and c) shows the result of this test after few minutes, 24 hours, and 72 hours from the time of setting up the experiment.

(a) (b) (c)

Figure A1.1. (a) Initial state, (b) after 24 hours, and (c) after 72 hours (partially dry)

B. KAOLINITE: PORCELAIN: BENTONITE (2: 4: 4) AND WATER 80%

This sample is identical to the previous one, except the amount of the initial water content changed to 80% instead of 70%. Figure A1.2 (a and b) shows the result of this test after 60 hours, and 600 hours from the time of setting up the experiment.

(a) (b)

Figure A.1.2 (a) After 60 hours and (b) after 164 hours.

C. KAOLINITE: PORCELAIN (5: 5) AND WATER 50%

This sample consists of kaolinite and porcelain, which were mixed with a ratio of 5:5 respectively and 50% of distilled water. Small mold with a thickness of 1" and a diameter of 4", the bottom surface of the mold was smooth without using Vaseline, and the sample left under the lab atmosphere. Figure A1.3 (a, b, and c) shows the result of this test after few minutes, 24 hours, and 72 hours from the time of setting up the experiment.

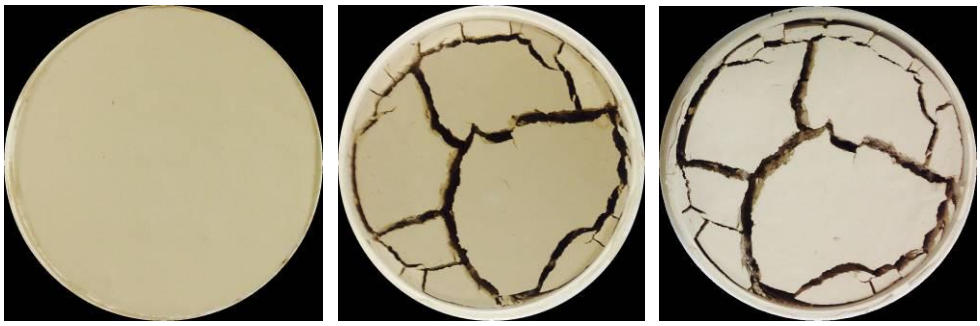

(a) (b) (c)

Figure A1.3 (a) Initial state, (b) after 24 hours, and (c) after 72 hours.

D. KAOLINITE: PORCELAIN (5: 5) AND WATER 50% (DIFFERENT MOLD)

This sample is identical to the previous one, but using different mold, which has a thickness of 2" and a diameter of 4'. However, the results looked different, the sample experienced only shrinkage. Figure A1.4 shows the result of this test after 72 hours from the time of setting up the experiment.

Figure A1.4 Sample state after 72 hours from the time of setting up the experiment.

E. PORCELAIN: BENTONITE (7: 3) AND WATER 70%

This sample consists of porcelain and bentonite, which mixed with a ratio of 7:3 respectively, and 70% of distilled water. Small mold used with a thickness of 1" and a

diameter of 4", the bottom surface of the mold was smooth without using Vaseline, and the sample left under the lab atmosphere. Figure A1.5 (a and b) shows the result of this test after 48 hours and 72 hours respectively from the time of setting up the experiment.

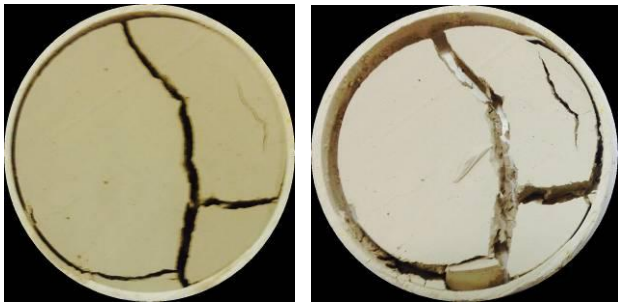

(a) (b)

Figure A1.5 (a) After 48 hours and (b) after 72 hours.

F. KAOLINITE: BENTONITE (7: 3) AND WATER 70%

This sample consists of kaolinite and bentonite which mixed with a ratio of 7:3 respectively, and 70% of distilled water. Small mold used with a thickness of 1" and a diameter of 4"; the bottom surface of the mold was smooth but without using Vaseline, and the sample left under the lab atmosphere. Figure A1.6 shows the result of this test after 72 hours from the time of setting up the experiment.

Figure A1.6 After 72 hours from the time of setting up the experiment.

G. KAOLINITE: BENTONITE (8: 2) AND WATER 70%

Basically, this sample is identical to the previous one, but the ratio of kaolinite to bentonite is 8:2 respectively. Figure A1.7 shows the result of this test after 72 hours from the time of setting up the experiment.

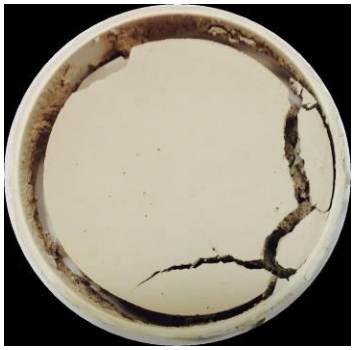

Figure A1.7 After 72 hours from the time of setting up the experiment.

H. KAOLINITE: PORCELAIN: BENTONITE (4: 2: 4) AND WATER 70%

This sample is identical to the first one, except the percentage of kaolinite and porcelain changed to 4:2 respectively. Figure A1.8 (a and b) shows the result of this test after 24 hours, and 72 hours from the time of setting up the experiment.

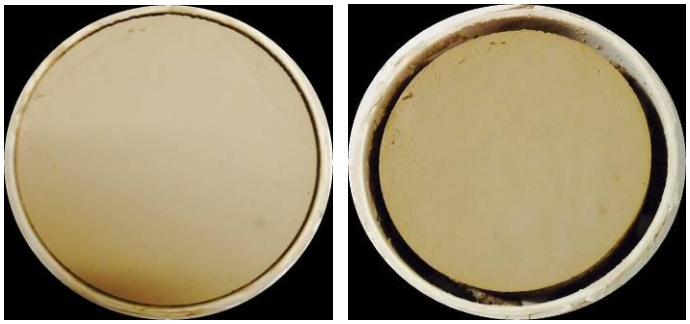

(a) (b)

Figure A1.8 (a) After 24 hours and (b) after 72 hours.

I. KAOLINITE 100% AND WATER 100%

This sample consists of pure kaolinite and 100% of distilled water. A big mold used with a thickness of 0.5" and a diameter of 5.9", the bottom contact surface of the mold has small grooves, and the sample left under the lab atmosphere. Figure A1.9 (a, b, and c) shows the results of this test after a few seconds, after 24 hours, and 72 hours from the time of setting up the experiment.

(a) (b) (c)

Figure A1.9 (a) Initial state, (b) after 24 hours, and (c) after 72 hours.

J. BENTONITE: KAOLINITE (3:7) AND WATER 120%

This sample consists of bentonite and kaolinite with a ratio of 3:7 respectively and 120% of distilled water. A big mold used with a thickness of 0.5" and a diameter of 5.9" (15 cm); the bottom surface of the mold has small grooves, and the sample left under the lab atmosphere. Figure A1.10 (a, b, and c) shows the results of this test after 24 hours, 48 hours, and 72 hours from the time of setting up the experiment.

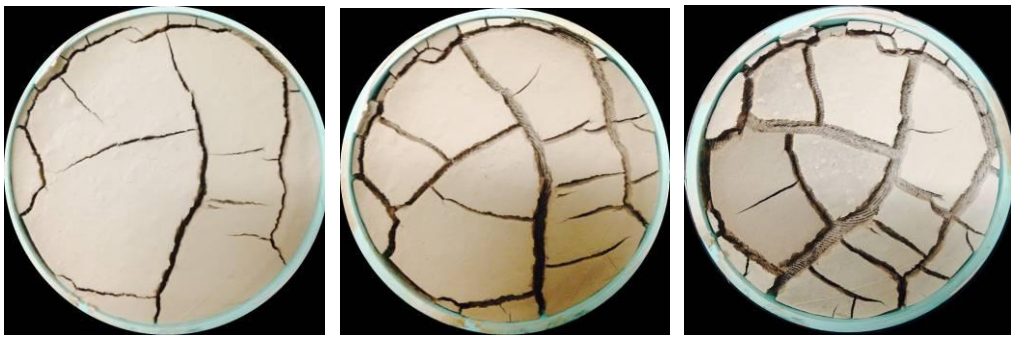

(a) (b) (c)

Figure A1.10 (a) After 24 hours, (b) after 48 hours, and (c) after 72 hours.

K. BENTONITE: KAOLINITE (3:7) AND WATER 85%

This sample is identical to the previous one, except the percentage of distilled water changed to 85%. Another thing is using a mold with a thickness of 1". However, the height of the sample was 0.5". Figure A1.11 shows the results of this test after 72 hours from the time of setting up the experiment.

Figure A1.11 Sample state after 72 hours from the time of setting up the experiment.

L. BENTONITE: KAOLINITE (4:6) AND WATER 120%

This sample consists of bentonite and kaolinite with a ratio of 4:6 respectively and 120% of distilled water. A big mold used with a thickness of 1". However, the height of the sample was 0.5"; the bottom surface of the mold has small grooves, and the sample left under the lab atmosphere. Figure A1.12 shows the result of this test after 72 hours from the time of setting up the experiment.

Figure A1.12 Sample state after 72 hours from the time of setting up the experiment.

M. PORCELAIN: KAOLINITE (8.7: 1.3) AND WATER 70%

This sample consists of porcelain and kaolinite with a ratio of 8.7:1.3 respectively and 70% of distilled water. A big mold used with a thickness of 0.5" and a diameter of 5.9" (5 cm); the bottom surface of the mold has small grooves, and the sample left under the lab atmosphere for 72 hours. Figure A1.13 (a, b, and c) shows the results of this test after few second, 24 hours, and 72 hours from the time of setting up the experiment.

(a) (b) (c)

Figure A.13 (a) Initial state, (b) after 24 hours, and (c) after 72 hours.

N. PORCELAIN: KAOLINITE (8.7: 1.3) AND WATER 70% (Different conditions)

This mixture is identical to the previous one, but it was under different conditions. A mold with a thickness of 1" used. However, the sample depth was 0.5" and the soil was exposed to a salt solution directly after setting up the experiment. Then the sample left under the lab atmosphere for 72 hours. Figure A1.14 (a, b, and c) shows the results of this test directly after exposed the sample to a salt solution, after 24 hours, and after 48 hours from the time of setting up the experiment.

(a) (b) (c)

Figure A1.14 (a) Initial state, (b) after 24 hours, and (c) after 48 hours.

APPENDIX 2

ANALYSES OF SEVERAL EXPERIMENTS HAVE BEEN DONE IN THE LAB

A- KAOLINITE: PORCELAIN: BENTONITE (2: 4: 4) AND WATER 70%

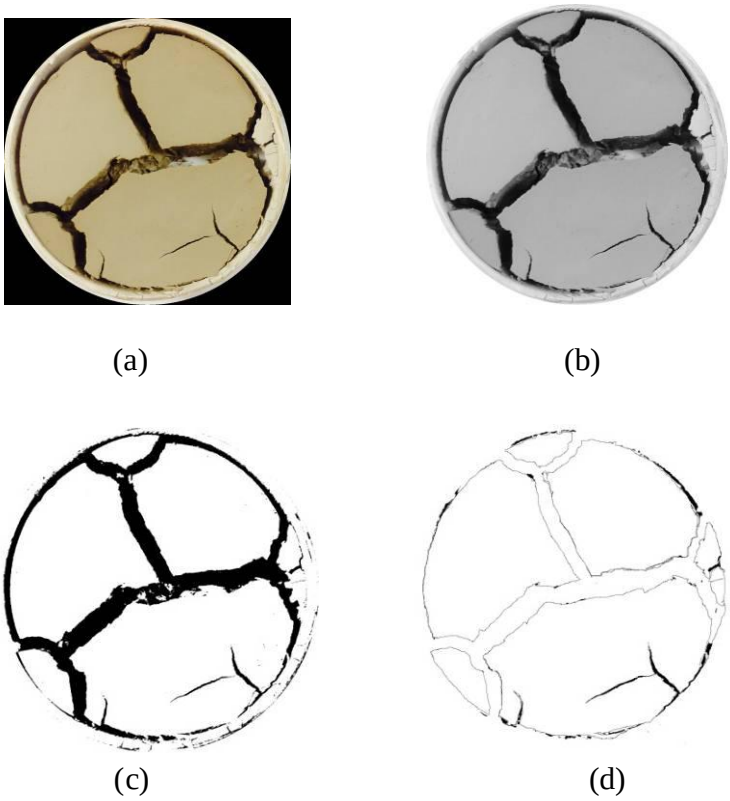

(a) (b)

(c) (d)

Figure A2.1. The main steps were done for the final stage image of this test, (a) original image, (b) gray scale image, (c) binary image, and (d) using threshold and outline options.

B- KAOLINITE: PORCELAIN: BENTONITE (2: 4: 4) AND WATER 80%

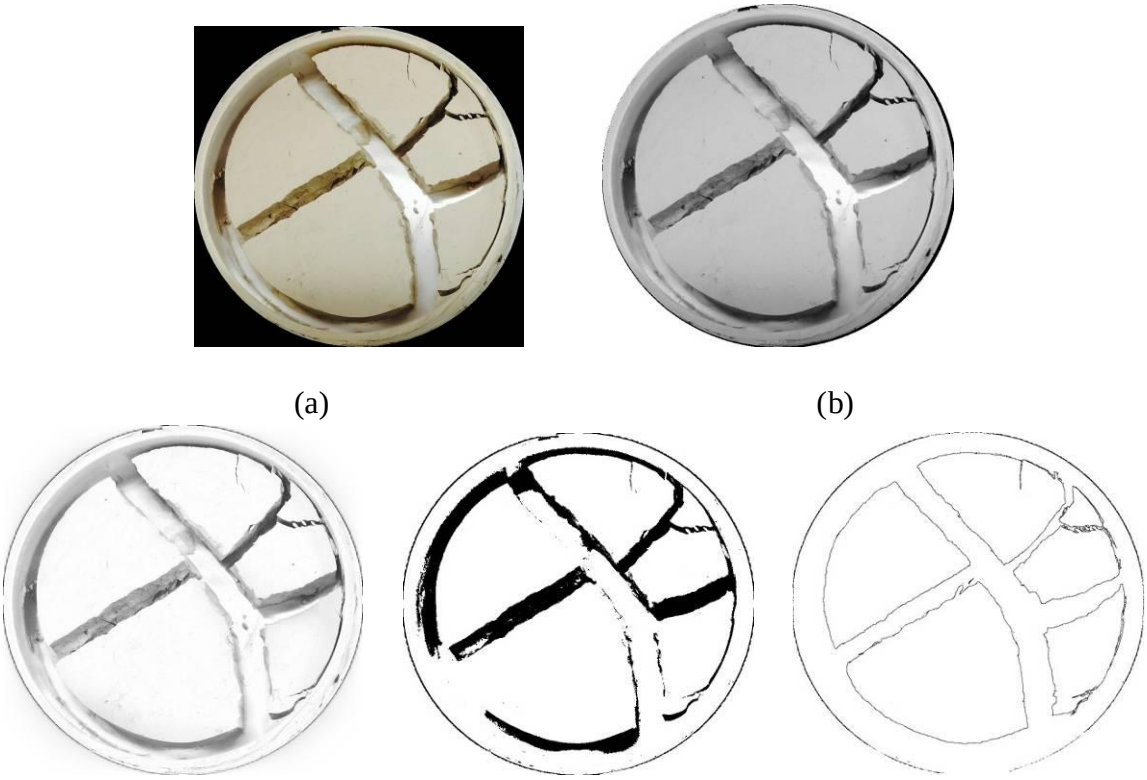

(a) (b)

(c) (d) (e)

Figure A2.2. The main steps were done for the final stage image of this test, (a) original image, (b) gray scale image, (c) subtract background, (d) binary image, and (e) using threshold and outline options.

Notice sometimes we may use subtract background option to reduce the noise and to adjust the intensity difference.

C- KAOLINITE: PORCELAIN (5: 5) AND WATER 50%

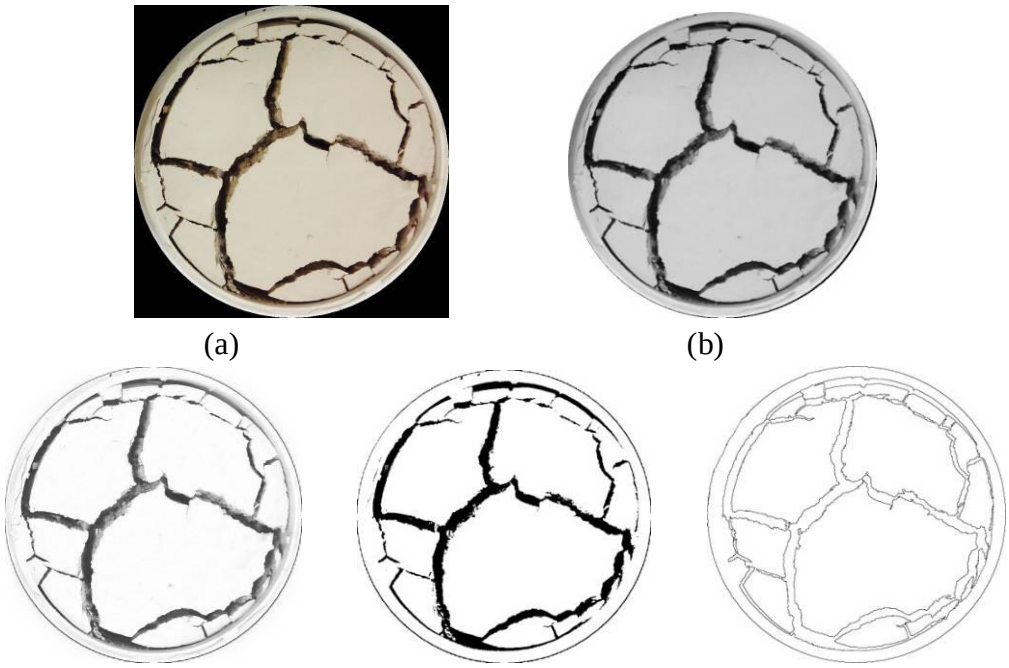

(a) (b)

(c) (d) (e)

Figure A2.3. The main steps were done for the final stage image of this test, (a) original image, (b) gray scale image, (c) subtract background, (d) binary image, and (e) using threshold and outline options.

D- KAOLINITE: PORCELAIN (5: 5) AND WATER 50% (DIFFERENT MOLD)

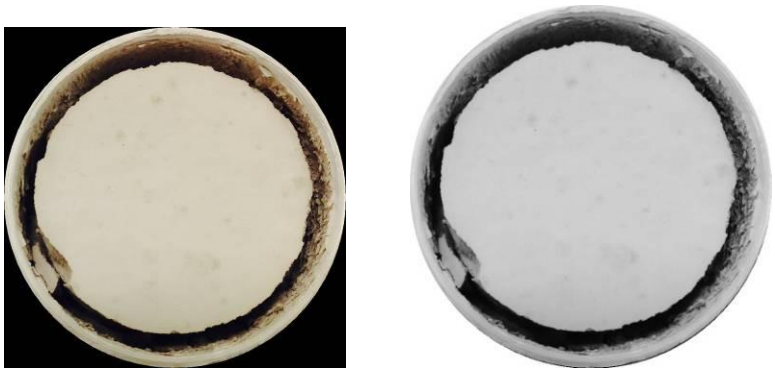

(a) (b)

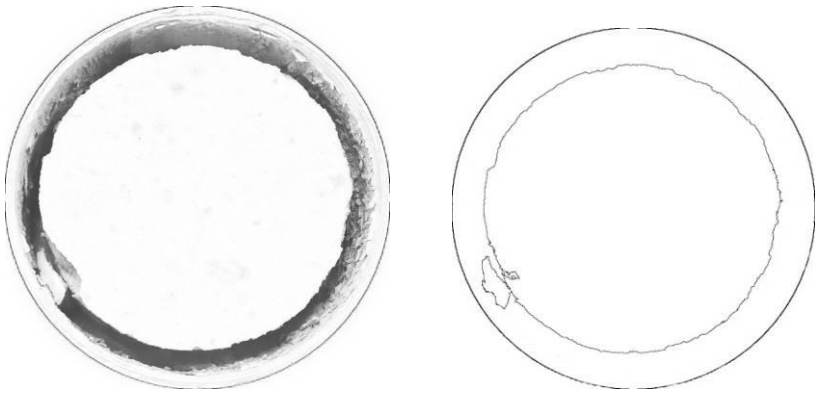

(c) (d)

Figure A2.4. The main steps were done for the final stage image of this test, (a) original image, (b) gray scale image, (c) subtract background, and (d) using threshold and outline options.

E- PORCELAIN: BENTONITE (7: 3) AND WATER 70%

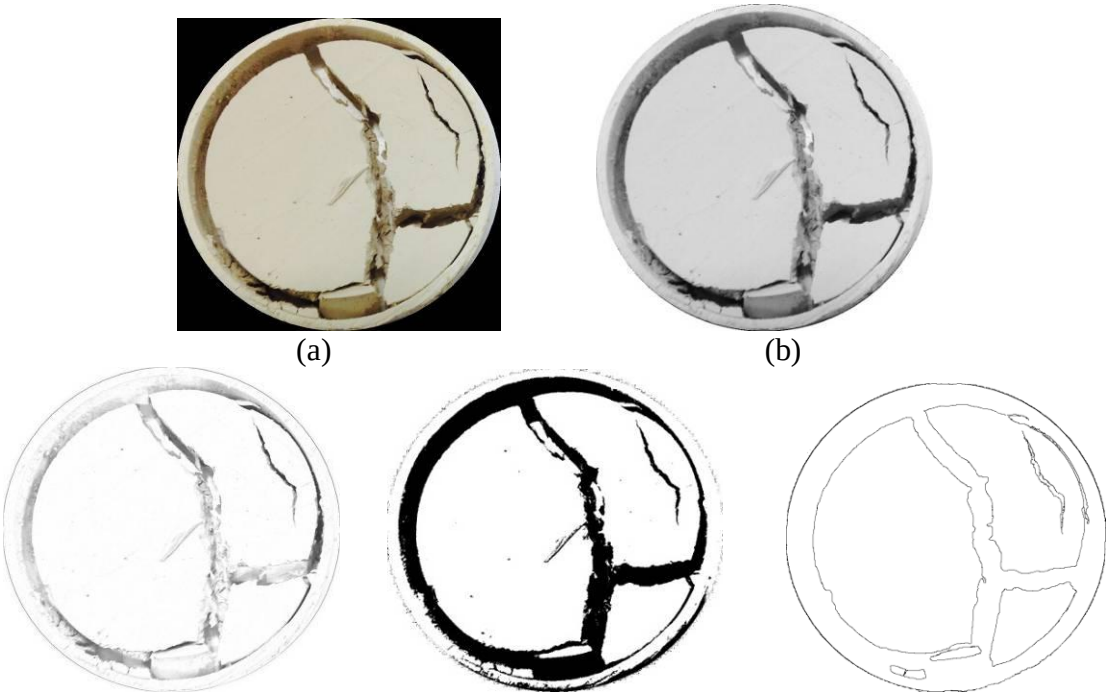

(a) (b)

(c) (d) (e)

Figure A2.5. The main steps were done for the final stage image of this test, (a) original image, (b) gray scale image, (c) subtract background, (d) binary image, and (e) using threshold and outline options.

F- KAOLINITE: BENTONITE (7: 3) AND WATER 70%

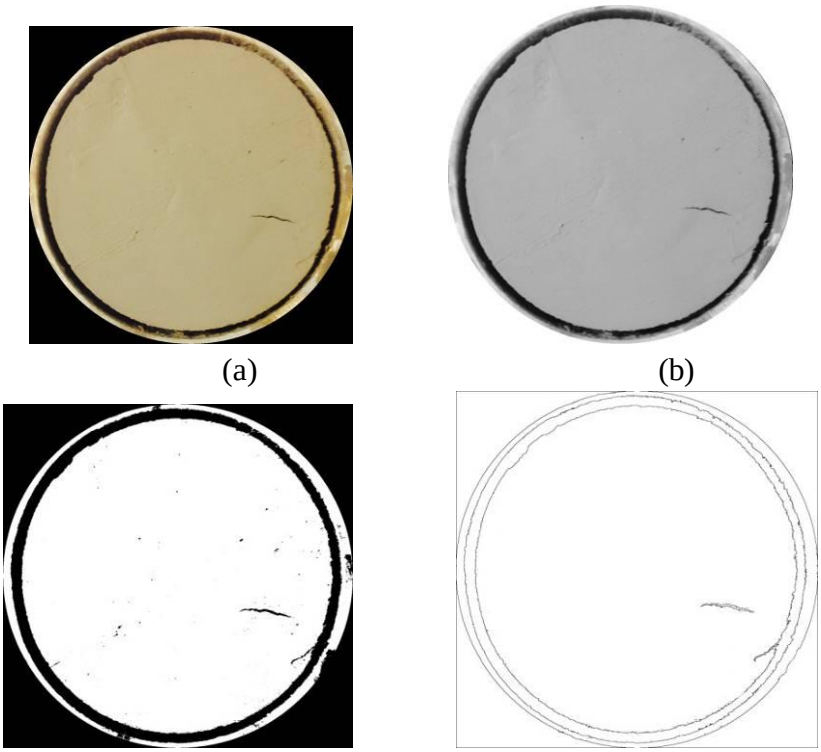

(a) (b)

(c) (d)

Figure A2.6. The main steps were done for the final stage image of this test, (a) original image, (b) gray scale image, (c) binary image, and (d) using threshold and outline options.

G- KAOLINITE: BENTONITE (8: 2) AND WATER 70%

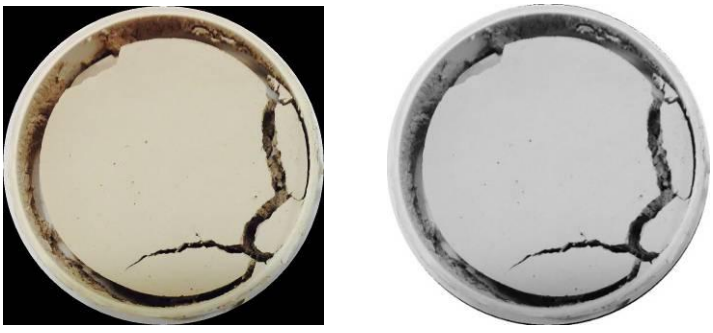

(a) (b)

(c) (d) (e)

Figure A2.7. The main steps were done for the final stage image of this test, (a) original image, (b) gray scale image, (c) subtract background, (d) binary image, and (e) using threshold and outline options.

H- KAOLINITE: PORCELAIN: BENTONITE (4 : 2 : 4) AND WATER 70%

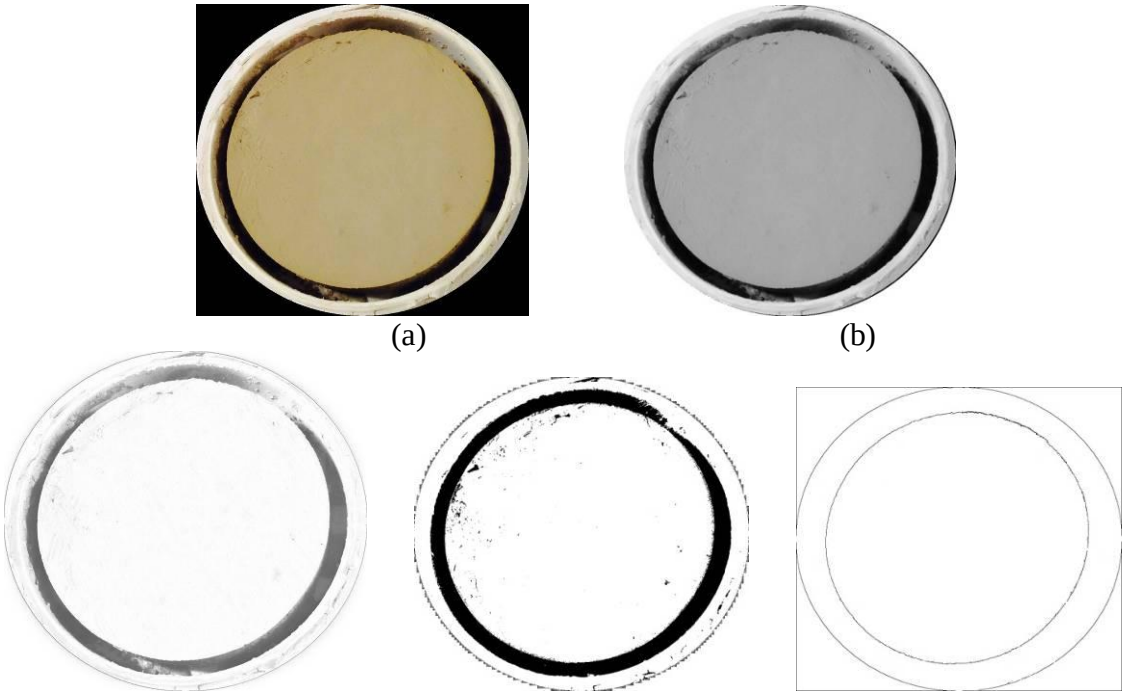

(a) (b)

(c) (d) (e)

Figure A2.8. The main steps were done for the final stage image of this test, (a) original image, (b) gray scale image, (c) subtract background, (d) binary image, and (e) using threshold and outline options.

I- KAOLINITE 100% AND WATER 100%

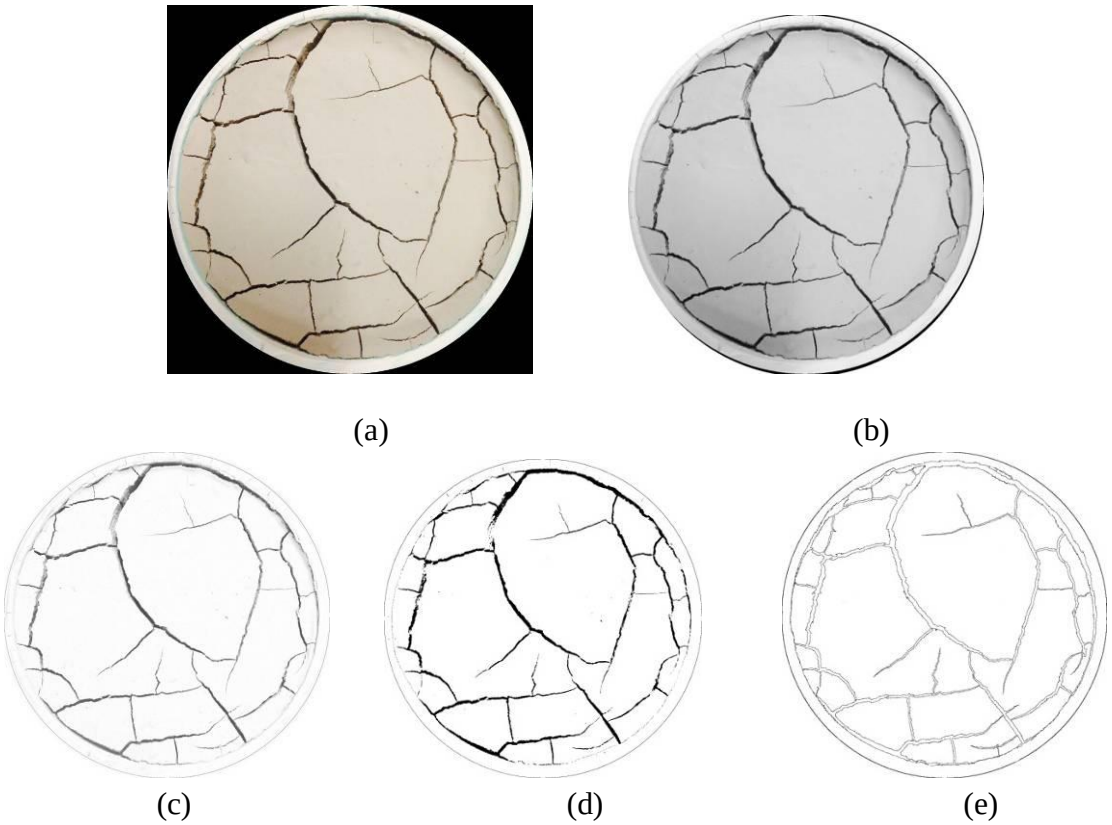

(a) (b)

(c) (d) (e)

Figure A2.9. The main steps were done for the final stage image of this test, (a) original image, (b) gray scale image, (c) subtract background, (d) binary image, and (e) using threshold and outline options.

J- BENTONITE: KAOLINITE (3:7) AND WATER 120%

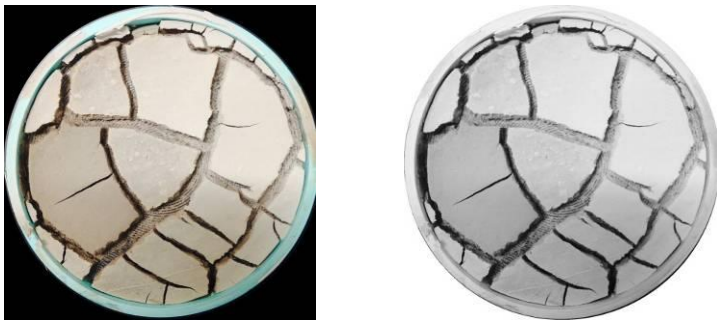

(a) (b)

(c) (d) (e)

Figure A2.10. The main steps were done for the final stage image of this test, (a) original image, (b) gray scale image, (c) subtract background, (d) binary image, and (e) using threshold and outline options.

K- BENTONITE: KAOLINITE (3:7) AND WATER 85%

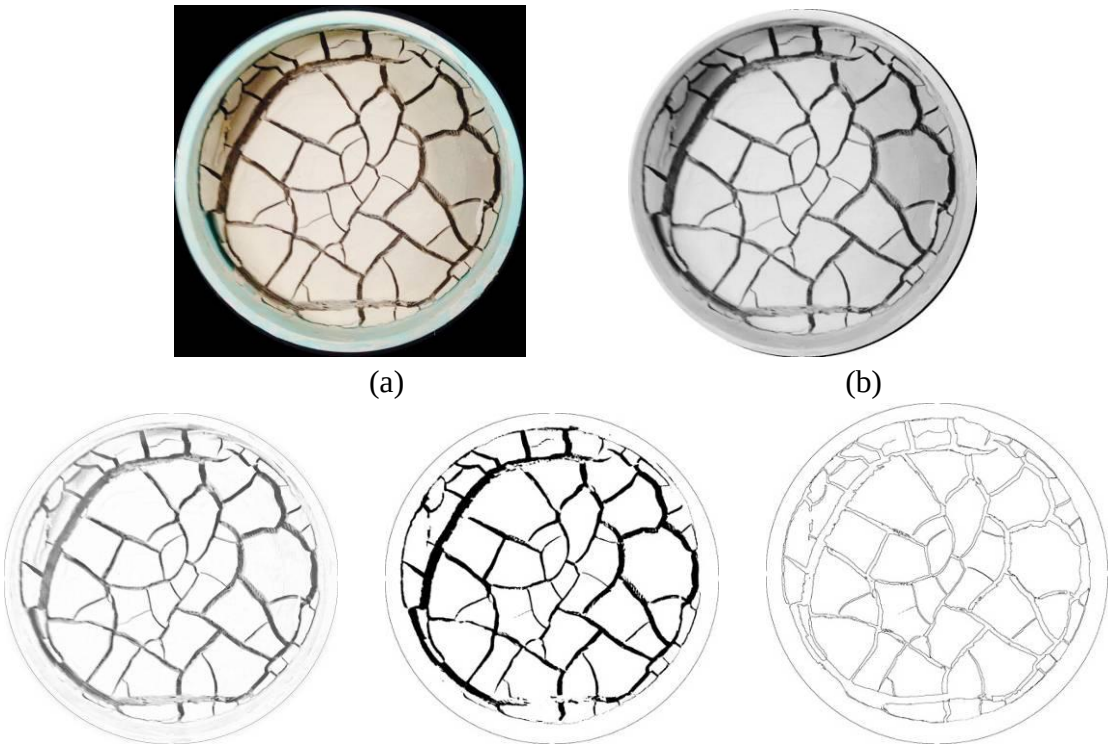

(a) (b)

(c) (d) (e)

Figure A2.11. The main steps were done for the final stage image of this test, (a) original image, (b) gray scale image, (c) subtract background, (d) binary image, and (e) using threshold and outline options.

L- BENTONITE: KAOLINITE (4:6) AND WATER 120%

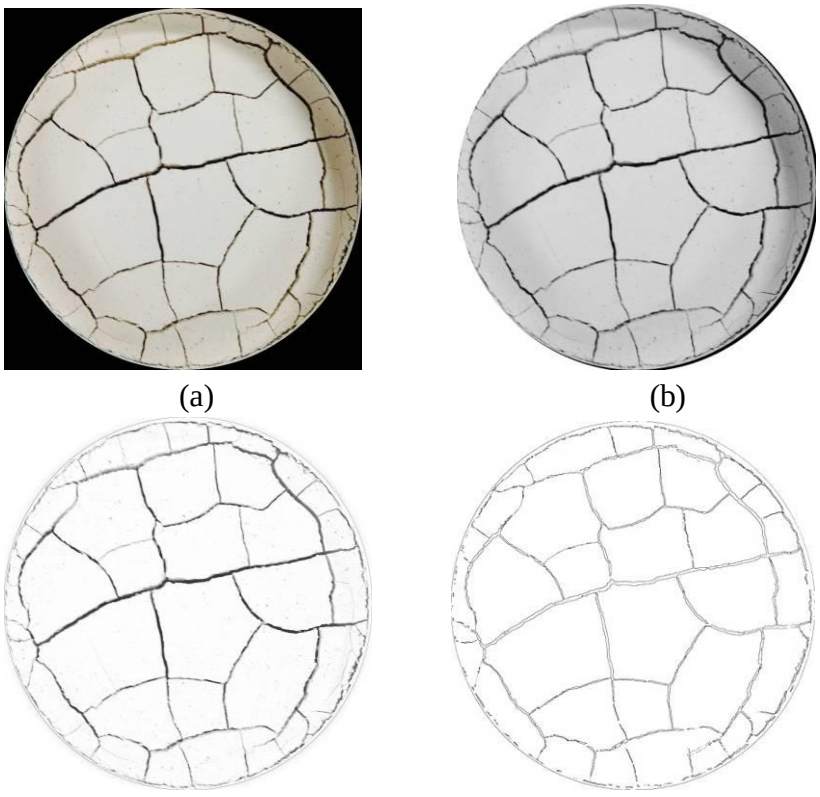

(a) (b)

(c) (d)

Figure A2.12. The main steps were done for the final stage image of this test, (a) original image, (b) gray scale image, (c) binary image, and (d) using threshold and outline options.

M- PORCELAIN: KAOLINITE (8.7 : 1.3) AND WATER 70%

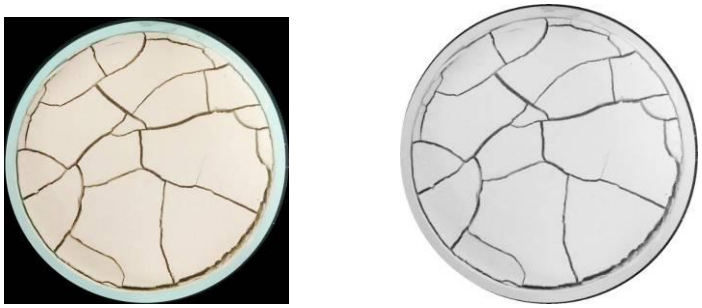

(a) (b)

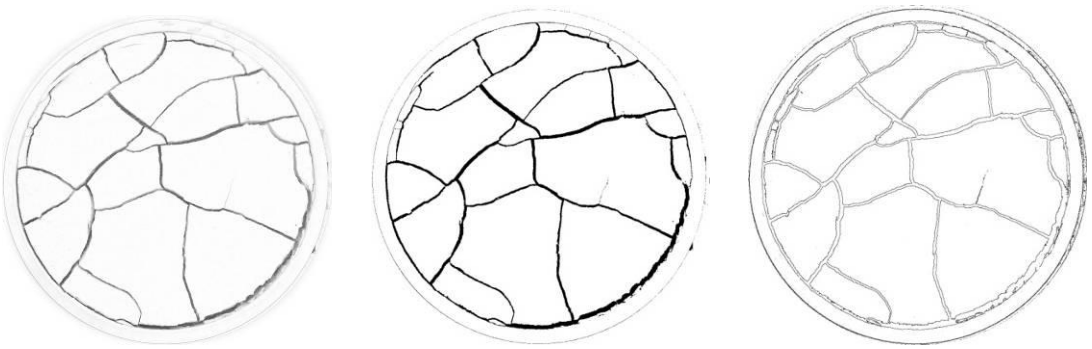

(c) (d) (e)

Figure A2.13. The main steps were done for the final stage image of this test, (a) original image, (b) gray scale image, (c) subtract background, (d) binary image, and (e) using threshold and outline options

N- PORCELAIN: KAOLINITE (8.7: 1.3) AND WATER 70% (Different conditions)

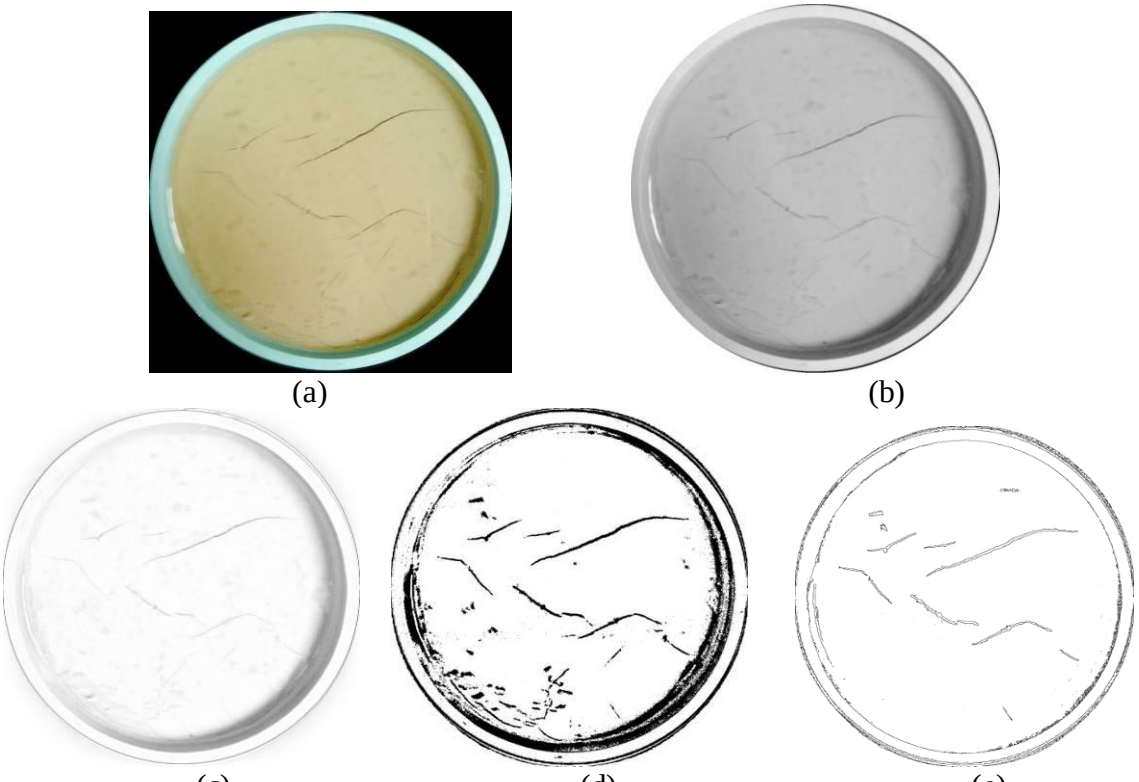

(a) (b)

(c) (d) (e)

Figure A2.14. The main steps were done for the final stage image of this test, (a) original image, (b) gray scale image, (c) subtract background, (d) binary image, and (e) using threshold and outline options.

Table A2.1. The geometry of the samples with some results from image analysis

Sample No.	Sample Area (mm^2)	Thickness (mm)	Sample Volume (cm^3)	Area of uncracked Material (mm^2)	Shrinkage area (mm^2)	Total Cracked area (mm^2)	CIF %	$(CIF)^{tot}$ %	Total length of each piece (mm)	Length per unit area (1/mm)	Avg. width of cracks (mm) (measured manually)	Avg. width of cracks (mm) (Eq.)*
A	9498.5	25.4	241.26	7127.282	462.038	1909.18	20.10	24.96	837	0.088	3.7	2.83
B	9498.5	25.4	241.26	5970.41	838.76	2689.33	28.31	37.14	727.3	0.077	5.33	4.85
C	9498.5	25.4	241.26	7404.898	372.27	1721.33	18.12	22.04	1099.29	0.116	2.5	1.90
D	*9498.5*	*25.4*	*241.26*	*7131.515*	*1844.44*	*522.545*	*5.50*	*24.92*	*318.15*	*0.033*	*8.74*	*7.44*
E	9498.5	25.4	241.26	6471.8	1488.6	1538.1	16.19	31.87	635	0.067	4.6	4.77
F	*9498.5*	*25.4*	*241.26*	*8423.7*	*752.54*	*12.1*	*0.13*	*8.05*	*312.177*	*0.033*	*3.61*	*2.45*
G	9498.5	25.4	241.26	6733.1	1307	1458.4	15.35	29.11	531.6	0.056	3.9	5.20
H	*9498.5*	*25.4*	*241.26*	*7412.2*	*1744.04*	*342.26*	*3.60*	*21.96*	*289.7*	*0.030*	*8.4*	*7.20*
I	17662.5	12.7	224.31	14106	247.9	3308.6	18.73	20.14	2379.2	0.135	2.29	1.49
J	17662.5	12.7	224.31	10668.472	255	6739.03	38.15	39.60	2409.5	0.136	4.3	2.90
K	17662.5	12.7	224.31	11629.05	193	5840.45	33.07	34.16	3778	0.214	2.9	1.60
L	17662.5	12.7	224.31	14291.566	81.1	3289.83	18.63	19.09	3430.9	0.194	2.1	0.98
M	17662.5	12.7	224.31	14083.18	301	3278.32	18.56	20.27	2197	0.124	1.7	1.63
N	*17662.5*	*12.7*	*224.31*	*17294.14*	*0*	*368.36*	*2.09*	*2.09*	*501*	*0.028*	*0.92*	*0.74*

Note: D, F, H, and N are almost un-cracked samples.

* The equation is:

$$Avg.widht\ of\ cracks = \frac{Total\ cracked\ area + Shrinkage\ area}{Total\ length\ of\ each\ piece}$$

Table A2.2. Crack intersection angles.

Sample → / Cell ↓	A	B	C	D	E	F	G	H	I	J	K	L	M	N
1	104	118.9	99.63	**104**	131.25	**171.6**	110.07	**0**	134.8	88.15	111.3	95.06	92.77	149.6
2	137.4	85.5	72.5		11.6		137.36		75.7	98.95	101.14	90.32	89.6	132.3
3	99.2	105.6	80.58		99.89		121.24		96.69	104.21	98.39	98.8	134.04	**141.5**
4	104	98.8	140.18		93.27		91.97		80.55	136.37	86.79	90.02	103.4	
5	91.6	138.4	130.2		148.03		73.6		102.3	81.2	102.53	86.75	97.94	
6	95.8	113.2	116.6		89.3		90		103.86	93.7	111.7	87.5	86.22	
7	130.3	88.3	117.1		96.86		130.8		112.5	93.8	99.7	130.56	76.9	
8	122.3	87.24	76.14		69.56		91.4		79.9	125.5	84.86	89.4	83.99	
9	90.8	77.99	84.9		**93.199**		**105.805**		87.7	92.35	91.47	96.3	118.4	
10	**108.1**	91.03	91.16						86.98	80.72	85.89	98.18	80.5	
11		74.3	104.1						91.29	102.3	83.66	86.9	106.4	
12		**98.013**	101.18						119.78	107.8	89.7	92.55	87.8	
13			107.3						83.66	115.23	97.2	84.86	103.7	
14			99.8						80.66	103.8	99.2	117.7	97.807	
15			95.29						104.89	90.5	86.3	104.9	95.52	
16			88.7						65.89	84.69	105.3	92.95	117	
17			86.25						130.7	129.3	90.7	91.32	89.4	
18			115.3						97.4	91.681	103.7	90.78	86.02	
19			82.47						112.1	78.69	99.8	100.1	89.204	

20			108.8						61.6	104.47	80.9	82.6	72.12	
21			**99.1167**						82.3	95.62	93.4	90.3	81.65	
22									81.88	99.0067	75.8	97.06	114.665	
23									**94.876**		80.8	93.7	**94.7143**	
24											91.4	94.13		
25											86.98	**95.114**		
26											85.135			
27											**93.221**			

Table A2. 2. Continued.

Note: the last number of each column represents the average value of intersection angles of that sample.

Table A2.3. Summary of intersection angles.

Range	0-80	80.1-100	100.1-180
No. of cells	42	117	75
Average value	68.32	90.16	116.23

APPENDIX 3

WETTING-DRYING CYCLES

KAOLINITE WITH BENTONITE

The 1st drying process.

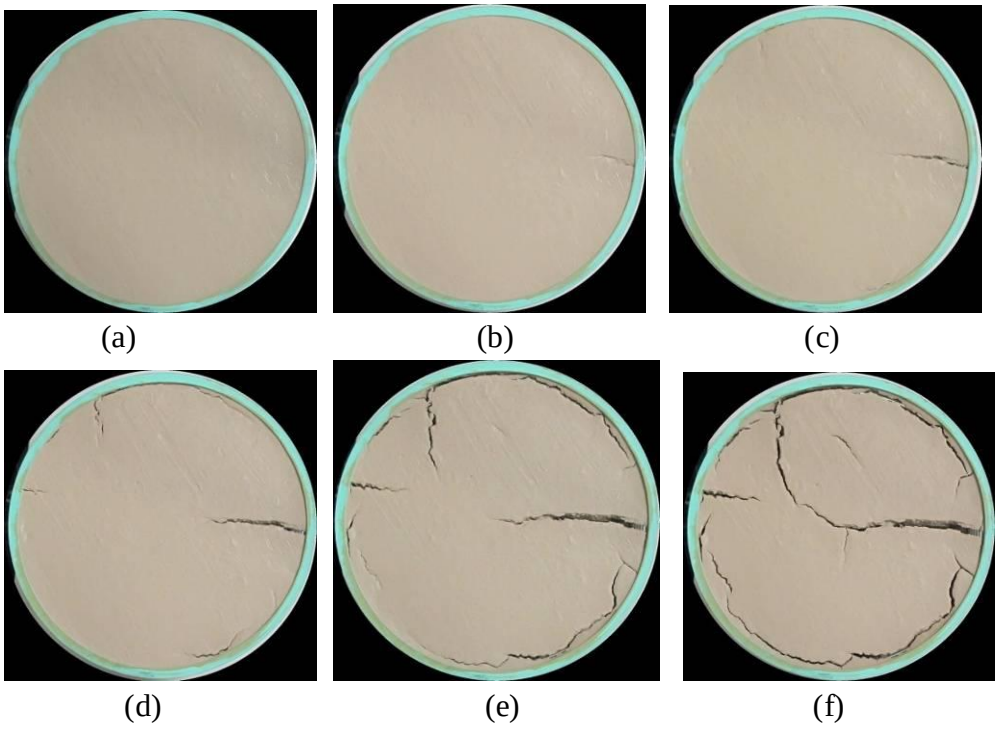

(a) (b) (c)

(d) (e) (f)

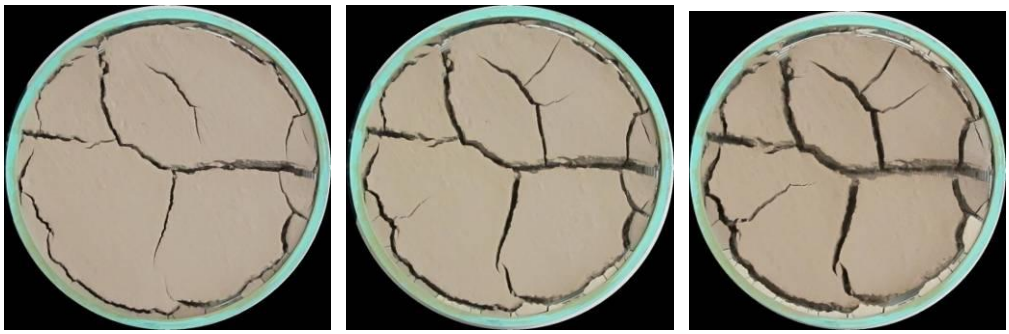

(g) (h) (i)

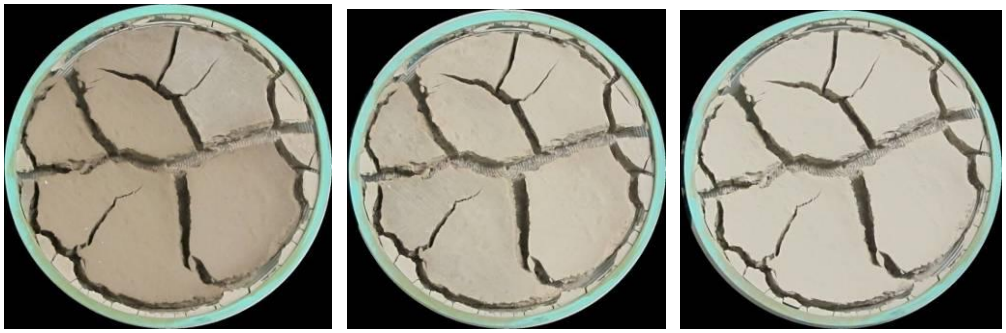

(j) (k) (l)

The 2nd wetting process.

(a) (b) (c)

(d) (e) (f)

The 2nd drying process

(a) (b) (c)

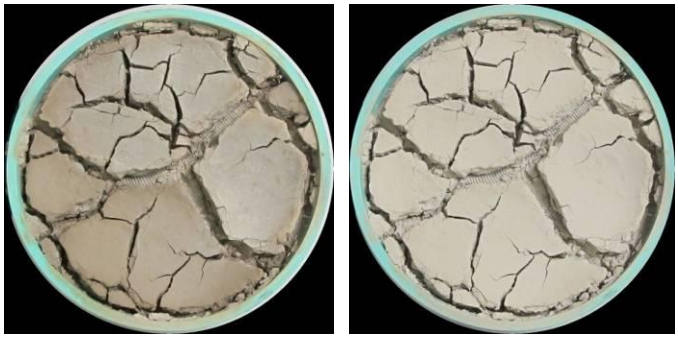

(d) (e)

The 3rd wetting process

(a) (b) (c)

The 3rd drying process.

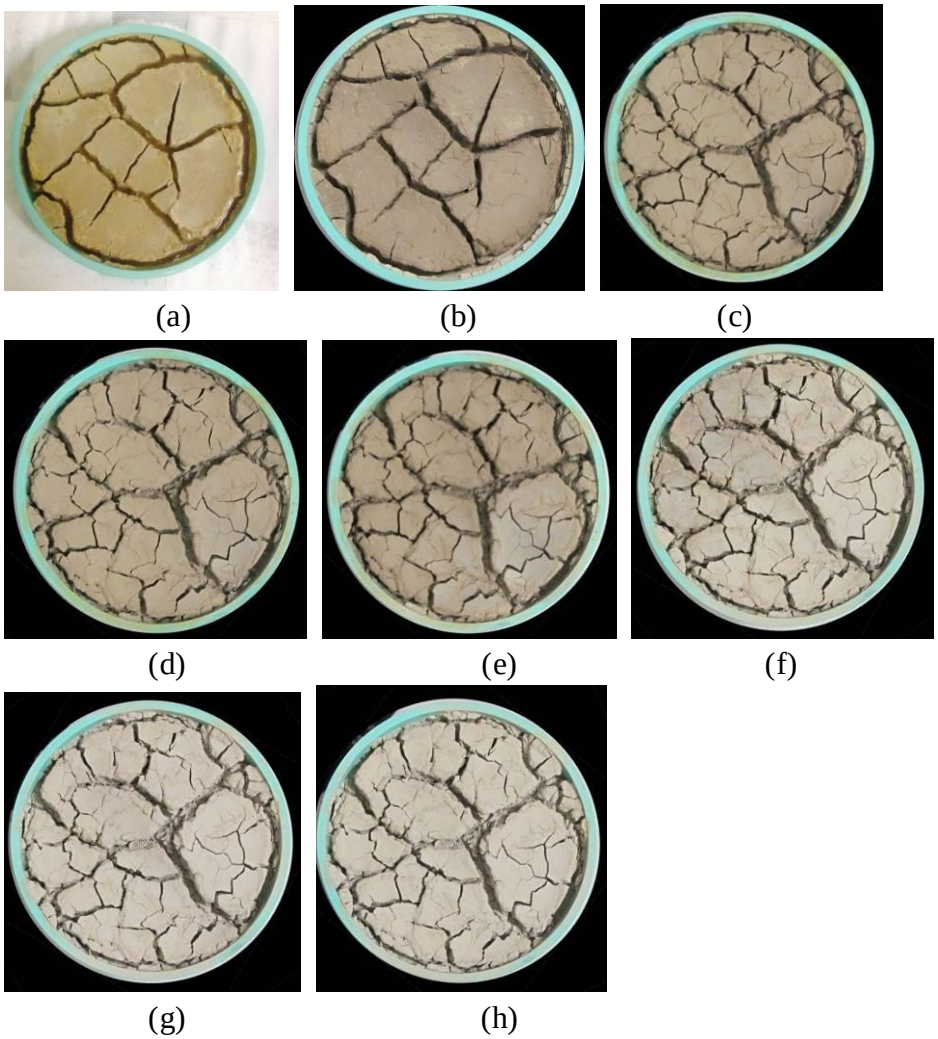

(a) (b) (c)

(d) (e) (f)

(g) (h)

The 4th wetting process

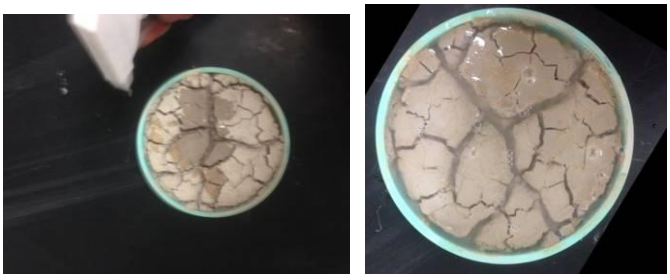

(a) (b)

The 4th drying process.

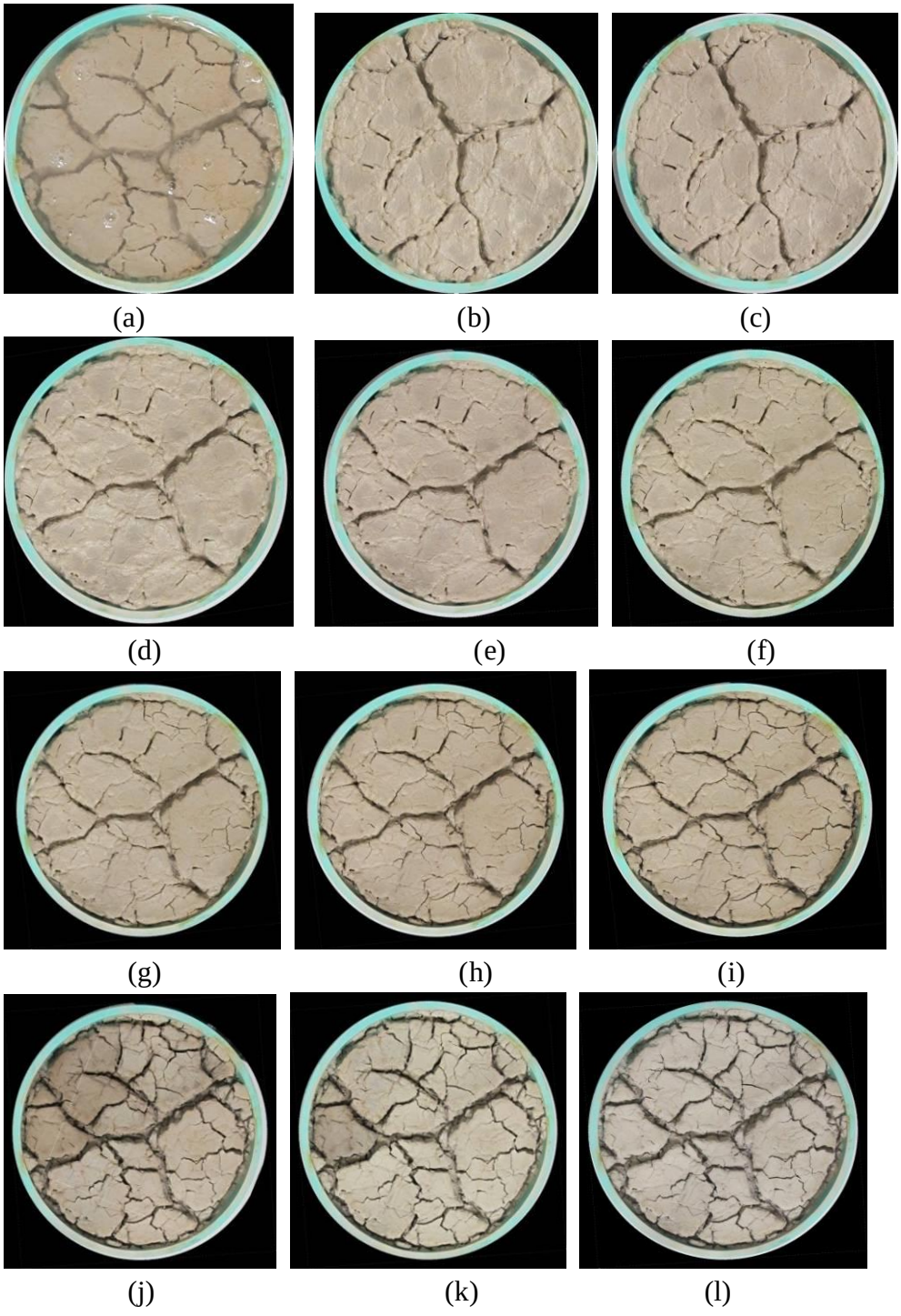

(a) (b) (c)

(d) (e) (f)

(g) (h) (i)

(j) (k) (l)

The 5th wetting process

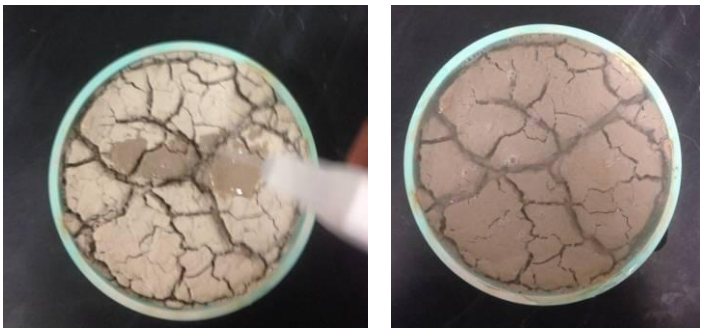

(a) (b)

The 5th drying process

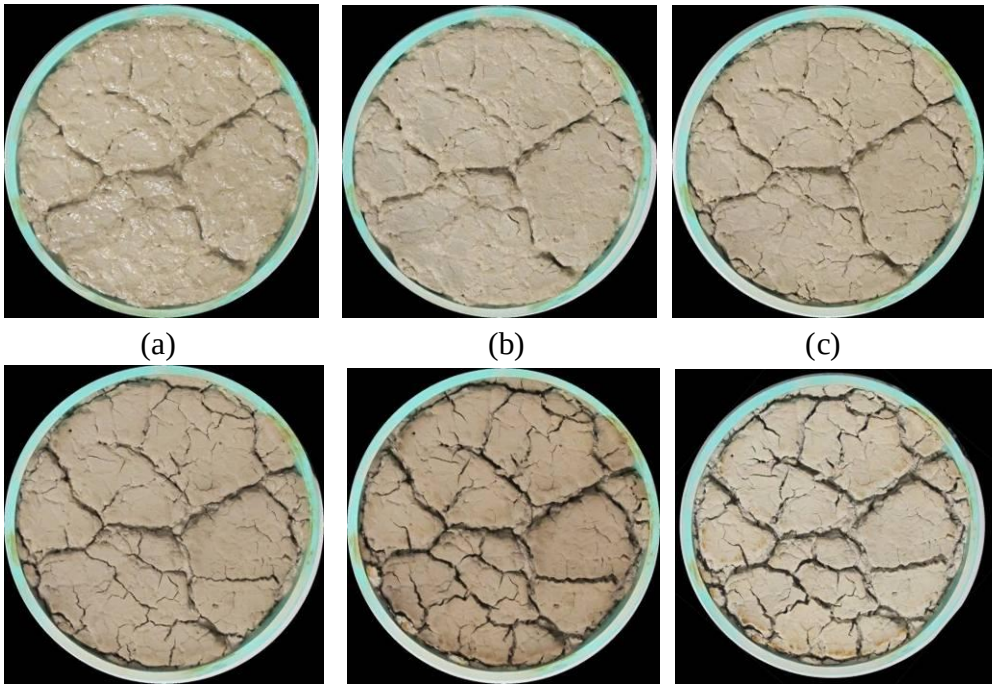

(a) (b) (c)

(d) (e) (f)

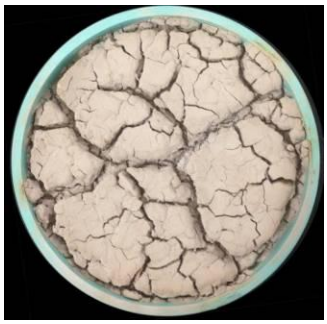

(g)

Table A3.1. Main parameters were obtained by using *image j* software, for only main cracks.

Time	After 1st drying	After 2nd wetting	After 2nd drying	After 3rd wetting	After 3rd drying	After 4th wetting	After 4th drying	After 5th wetting	After 5th drying
Initial sample area (mm2)	17662.5	12530.69	14834.2	9966.64	11088.9	9778.13	14537.5	8924.22	15236.2
Initial thickness (mm)	12.7	8.4	9.2	8.5	8.7	8.5	8.6	8.5	8.6
Initial sample volume (cm3)	224.31	105.26	136.47	84.72	96.47	83.11	125.02	75.86	131.03
Final thickness (mm)	8.4	9.2	8.5	8.7	8.5	8.6	8.5	8.6	8.5
Final sample volume (cm3)	105.26	136.47	84.72	96.47	83.11	125.02	75.86	131.03	77.38
% Change in sample volume (cm3)	0.53	**-0.30**	0.38	**-0.14**	0.14	**-0.50**	0.39	**-0.73**	0.41
Area of uncracked material (mm2)	12530.69	14834.16	9966.64	11088.99	9778.13	14537.54	8924.22	15236.19	9103.70
Shrinkage area (mm2)	600.82	123.04	948.55	417.87	668.14	194.87	820.75	163.98	714.94
Total Cracked area (mm2)	4530.99	2705.30	6747.31	6155.64	7216.23	2930.09	7917.53	2262.33	7843.86
CIF %	25.65	15.32	38.20	34.85	40.86	16.59	44.83	12.81	44.41
(CIF)tot%	29.05	16.01	43.57	37.22	44.64	17.69	49.47	13.74	48.46
Final W%	9.70	63.20	7.40	62.60	5.30	61.02	5.30	62.20	5.90
Final vertical strain (ΔH/H)	0.34	**-0.10**	0.08	**-0.02**	0.02	**-0.01**	0.01	**-0.01**	0.01

Table A3.2. Main parameters were obtained by using *image j* software, for final cracks (including fissures)

Time	After 1st drying	After 2nd wetting	After 2nd drying	After 3rd wetting	After 3rd drying	After 4th wetting	After 4th drying	After 5th wetting	After 5th drying
Initial sample area (mm2)	17662.5	12530.69	14624.2	6560.91	2897.27	1586.41	13837.24	304.71	14390.6
Initial thickness (mm)	12.7	8.4	9.2	8.5	8.7	8.5	8.6	8.5	8.6
Initial sample volume (cm3)	224.31	105.26	136.47	84.72	96.47	83.11	125.02	75.86	131.03
Final thickness (mm)	8.4	9.2	8.5	8.7	8.5	8.6	8.5	8.6	8.5
Final sample volume (cm3)	105.26	134.54	55.77	25.21	13.48	119.00	2.59	123.76	2.74
% Change in sample volume (cm3)	0.53	**-0.28**	0.59	**0.70**	0.86	**-0.43**	0.98	**-0.63**	0.98
Area of uncracked material (mm2)	12530.7	14624.16	6560.91	2897.27	1586.41	13837.24	304.71	14390.56	321.79
Shrinkage area (mm2)	600.82	123.04	948.55	417.87	668.14	194.87	820.75	163.98	714.94
Total Cracked area (mm2)	4530.99	2915.30	10153.1	14347.36	15653.7	3630.39	16537.04	3107.96	16625.8
CIF %	25.65	16.51	57.48	81.23	88.63	20.55	93.63	17.60	94.13
(CIF)tot%	29.05	17.20	62.85	83.60	92.41	21.66	98.27	18.52	98.18
Final W%	9.70	63.20	7.40	62.60	5.30	61.02	5.30	62.20	5.90
Final vertical strain (ΔH/H)	0.34	**-0.10**	0.08	**-0.02**	0.02	**-0.01**	0.01	**-0.01**	0.01

KAOLINITE ONLY WITH 100% OF WATER

The 1st drying process

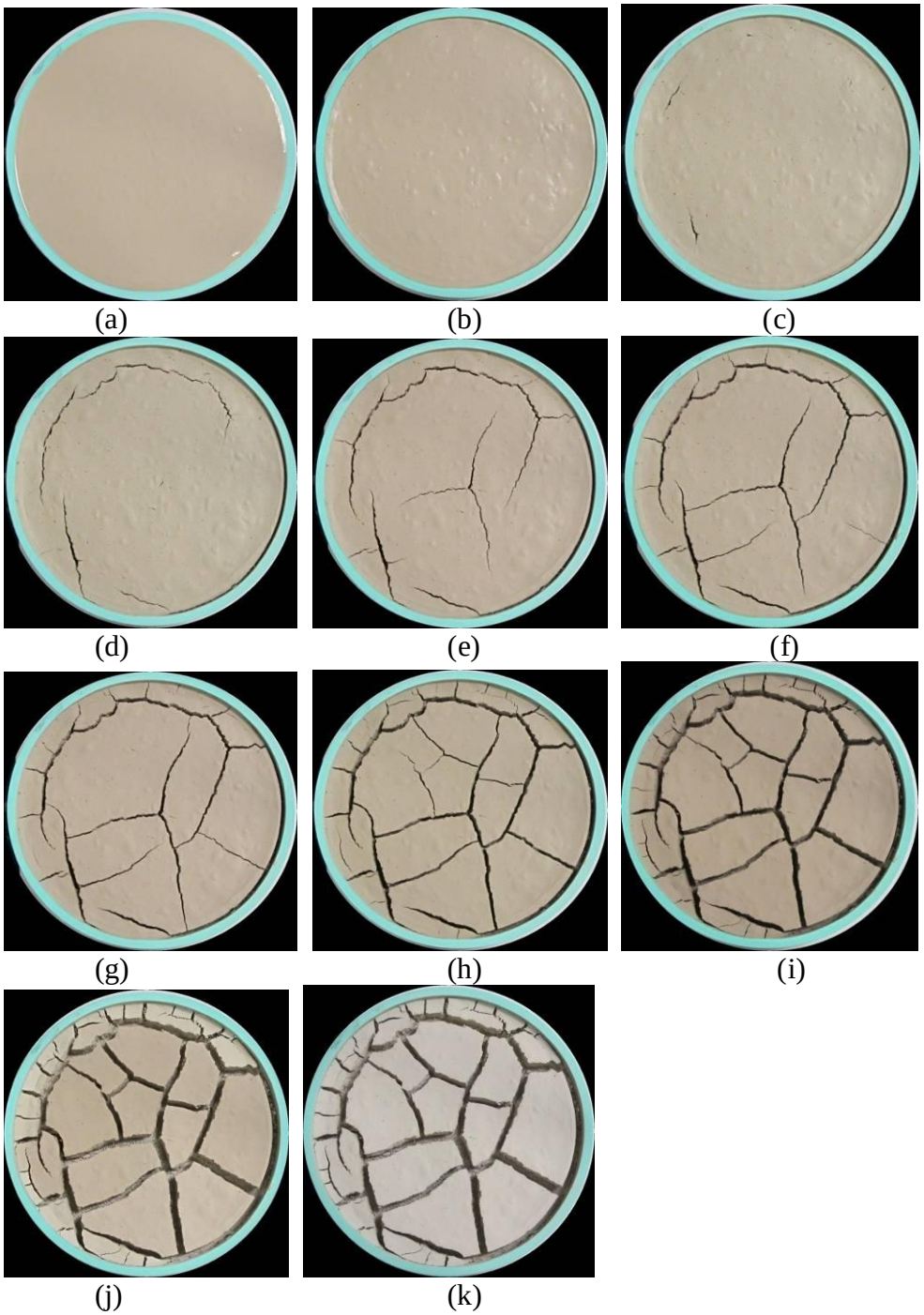

(a) (b) (c)

(d) (e) (f)

(g) (h) (i)

(j) (k)

The 2nd wetting- drying cycle

(a)

(b)

(c)

(e)

(f)

(g)

(h)

(i)

(j)

(k)

(l)

(m)

The 3rd wetting- drying cycle

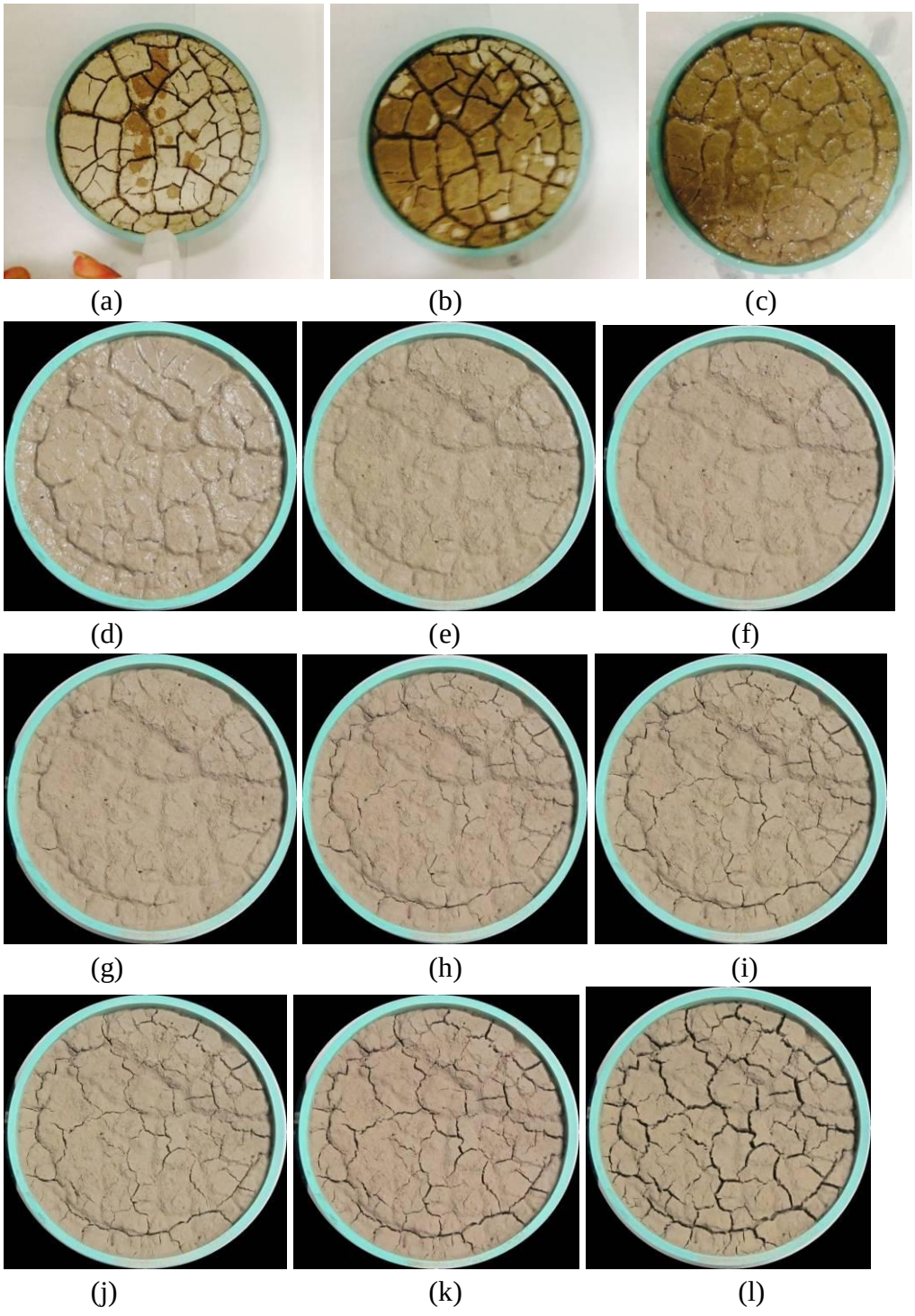

(a) (b) (c)

(d) (e) (f)

(g) (h) (i)

(j) (k) (l)

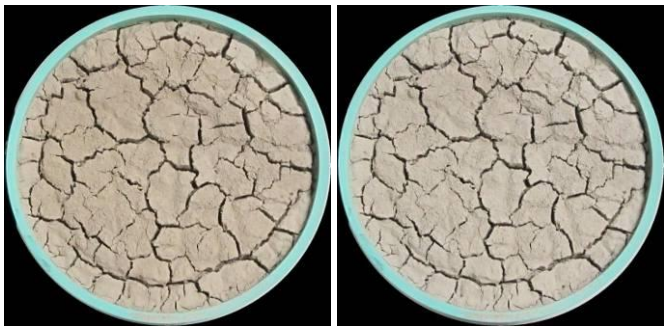

(m) (n)

The 4th wetting- drying cycle

(a) (b) (c)

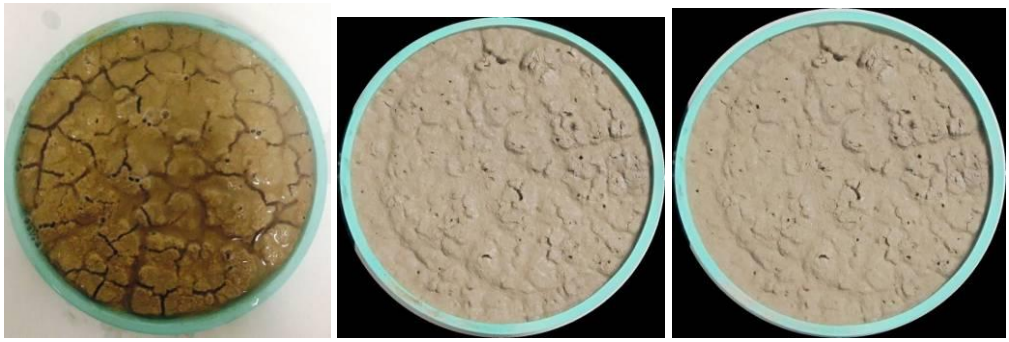

(d) (e) (f)

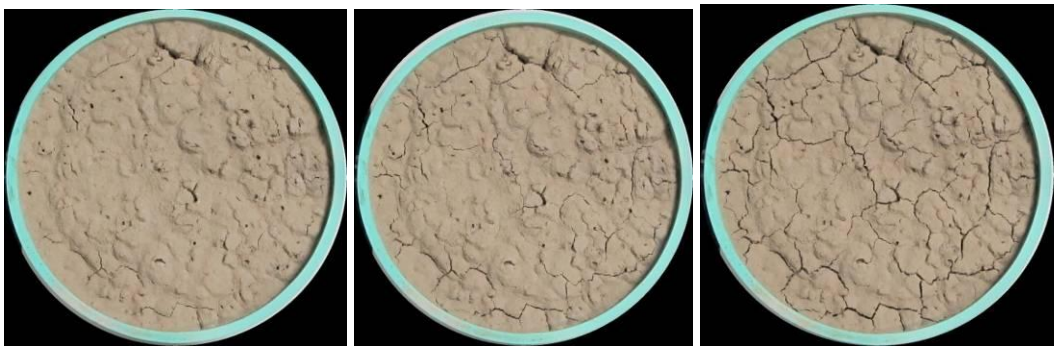

(g) (h) (i)

(j)

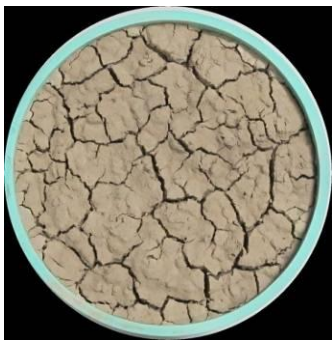

(k)

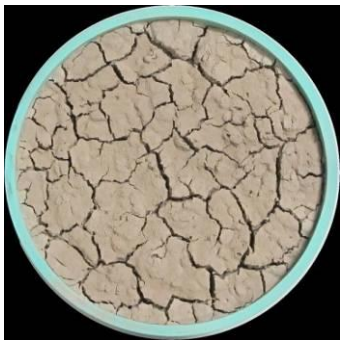

(l)

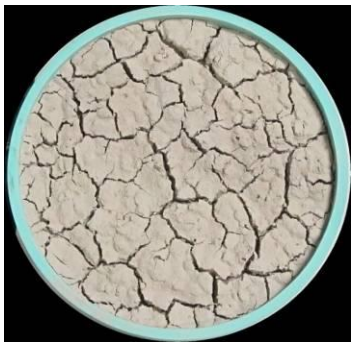

(m)

Table A3.3. Main parameters were obtained by using *image j* software, for only the main cracks

Time	After 1st drying	After 2nd wetting	After 2nd drying	After 3rd wetting	After 3rd drying	After 4th wetting	After 4th drying
Initial sample area (mm2)	17662.5	11526.59	17432.20	6417.96	17617.24	8213.15	17598.74
Initial thickness (mm)	12.7	8	9.1	8.5	8.7	8.5	8.7
Initial sample volume (cm3)	224.31	92.21	158.63	54.55	153.27	69.81	153.11
Final thickness (mm)	8	9.1	8.5	8.7	8.5	8.7	8.5
Final sample volume (cm3)	92.21	158.63	54.55	153.27	69.81	153.11	79.10
% Change in sample volume (cm3)	0.59	-0.72	0.66	-1.81	0.54	-1.19	0.48
Area of uncracked material (mm2)	11526.59	17432.20	6417.96	17617.24	8213.15	17598.74	9305.66
Shrinkage area (mm2)	593.87	132.06	593.87	0.00	0	0	0
Total Cracked area (mm2)	5542.04	98.24	10650.67	45.26	9449.36	63.76	8356.84
CIF %	31.38	0.56	61.10	0.26	53.64	0.36	47.31
(CIF)tot%	34.74	1.30	64.50	0.26	53.64	0.36	47.31
Final W%	7.32	53.20	0.13	53.40	0.34	49.20	0.86
Final vertical strain (ΔH/H)	0.37	**-0.14**	0.07	**-0.02**	0.02	**-0.02**	0.02

Table A3.4. Main parameters were obtained by using *image j* software, for final cracks (including fissures)

Time	After 1st drying	After 2nd wetting	After 2nd drying	After 3rd wetting	After 3rd drying	After 4th wetting	After 4th drying
Initial sample area (mm2)	17662.5	11526.5	17432.2	6249.96	17617.24	8045.15	17598.7
Initial thickness (mm)	12.7	8	9.1	8.5	8.7	8.5	8.7
Initial sample volume (cm3)	224.31	92.21	158.63	53.12	153.27	68.38	153.11
Final thickness (mm)	8	9.1	8.5	8.7	8.5	8.7	8.5
Final sample volume (cm3)	92.21	158.63	53.12	153.27	68.38	153.11	77.67
% Change in sample volume (cm3)	0.59	-0.72	0.67	-1.89	0.55	-1.24	0.49
Area of uncracked material (mm2)	11526.59	247.02	4617.77	16547.48	5542.04	15986.56	6138.48
Shrinkage area (mm2)	593.87	132.06	593.87	0.00	0.00	0.00	0.00
Total Cracked area (mm2)	5542.04	17283.4	12450.86	1115.03	12120.46	1675.94	11460.2
CIF %	31.38	97.85	70.49	6.31	68.62	9.49	65.12
(CIF)tot%	34.74	98.60	73.86	6.31	68.62	9.49	65.12
Final W%	7.32	53.20	0.13	53.40	0.34	49.20	0.86
Final vertical strain (ΔH/H)	0.37	**-0.14**	0.07	**-0.02**	0.02	**-0.02**	0.02

APPENDIX 4

INTERFACE DIRECT SHEAR TEST

❖ Undrained condition with shear rate of 0.5 mm/min

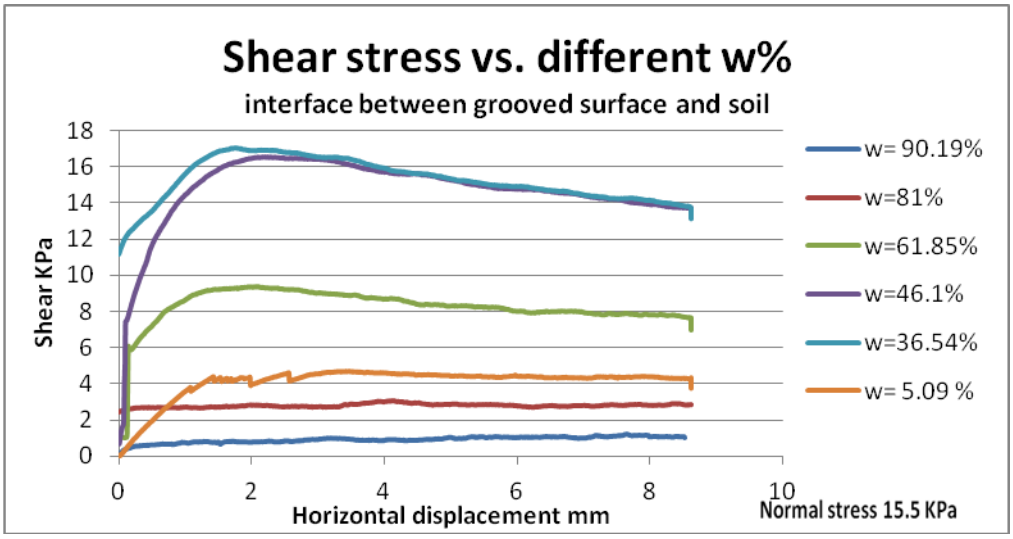

(a)

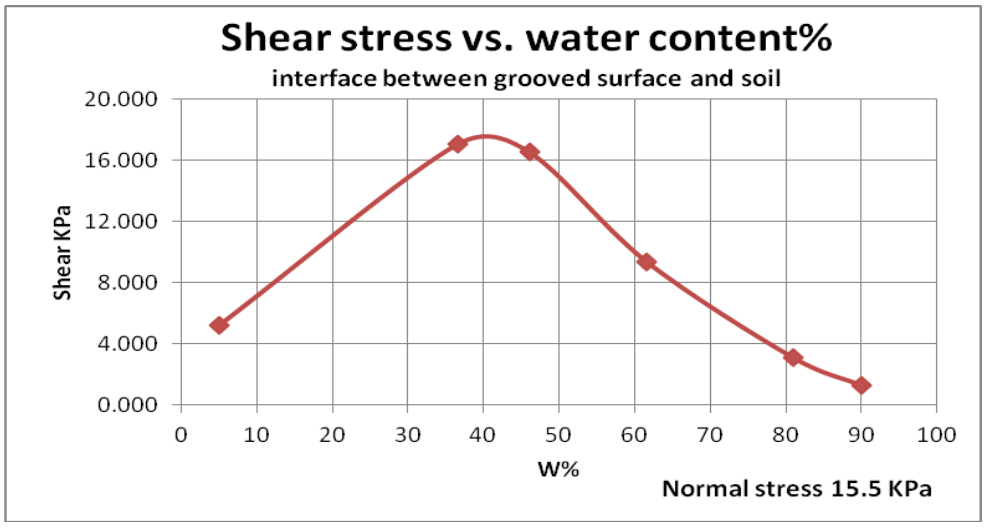

(b)

FigureA5.2. (a) Shear stress vs. displacement with different water contents, (b) maximum shear stress vs. w%.

❖ The behavior of clay with the straight line grooved surface interface studies in the lab under drained condition (shear rate = 0.018 mm/min)

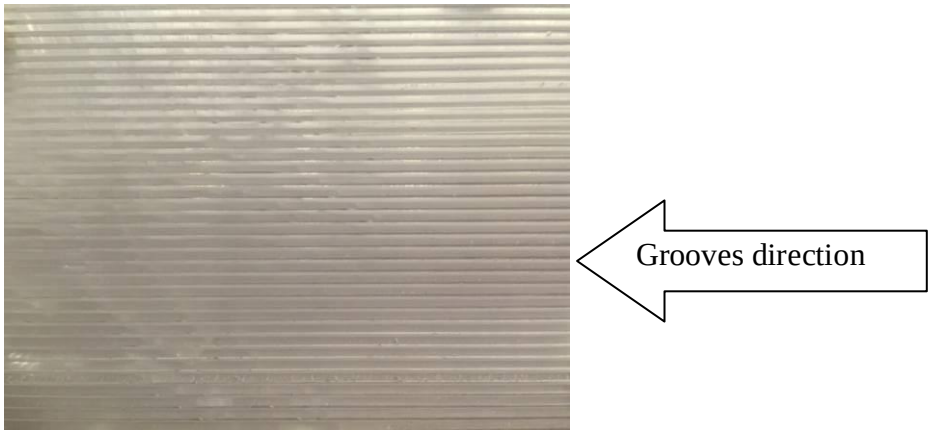

Figure A5. 3. Grooved Plate.

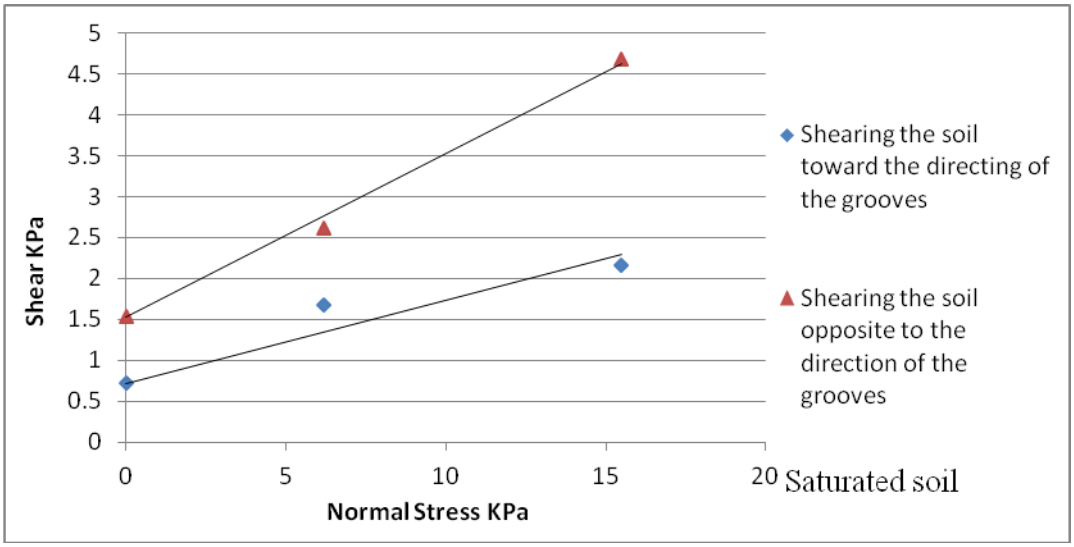

Figure A5.4. Failure envelopes of the interface shear tests (Soil- straight-line grooved plate).

Table A5. 1. Results of the interface shear tests (Soil- straight-line grooved plate)

	Shearing the soil toward the directing of the grooves	Shearing the soil opposite to the direction of the grooves
Adhesion KPa	0.72	1.53
Ø°	5.78	11.28

APPENDIX 5

- Shrinkage stages during drying (a mixture of 15% silica sand, 85% kaolinite, and water content of 2.5 × LL).

(a) Initial state

(b) 14 hours

(c) 37 hours

(d) 54.5 hours

(e) 61.7 hours

(f) 82 hours

(g) 91 hours

(h) 104 hours

(i) 118 hours

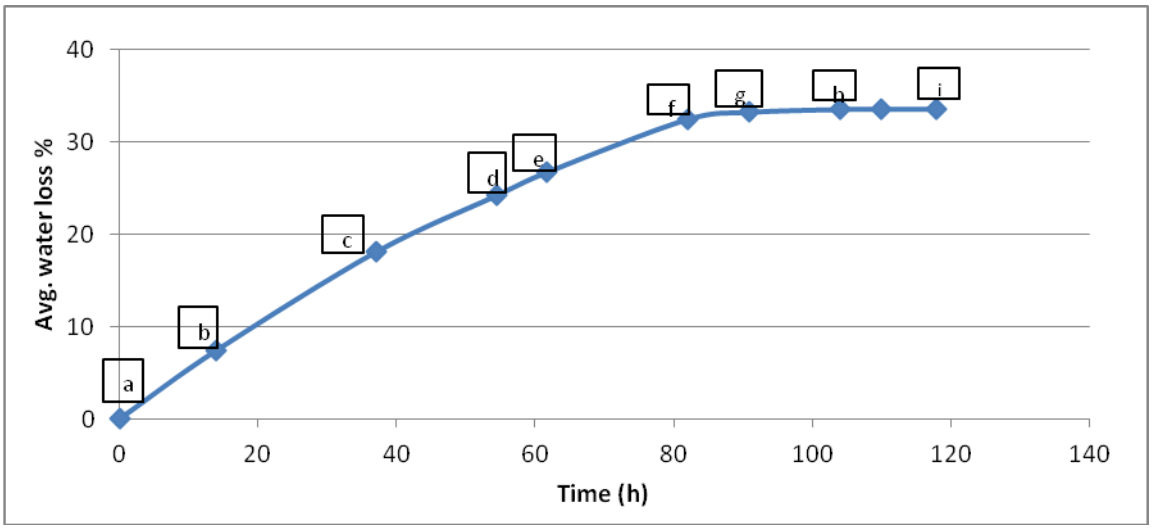

Figure A5.1. Average water loss versus time (a mixture of 15% silica sand, 85% kaolinite, and water content of 2.5 × LL)..

❖ Shrinkage stages during drying (a mixture of 85% kaolinite with 15% of silica sand was prepared at 3×LL)

(a) Initial state

(b) 21 hours

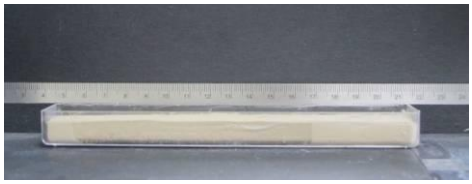

(c) 44 hours

(d) 70 hours

(e) 92 hours

(f) 101 hours

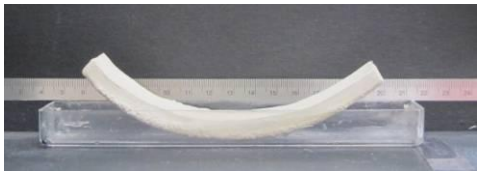

(g) 116 hours

(h) 140 hours

(i) 164 hours

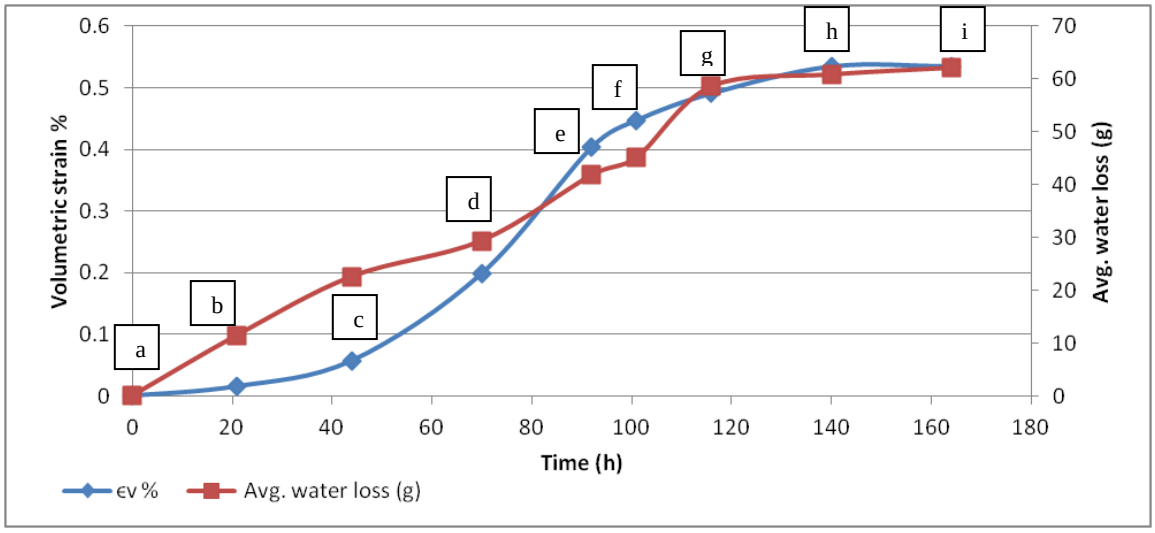

Figure A5.2. Volumetric strain and average water loss versus time (a mixture of 85% kaolinite with 15% of silica sand was prepared at 3×LL).

❖ Shrinkage stages during drying (a mixture of 80% kaolinite with 20% of silica sand was prepared at 2.5×LL)

(a) Initial state

(b) 21 hours

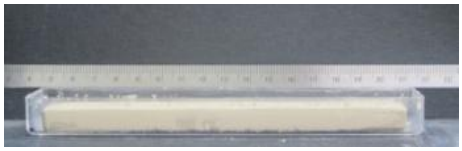

(c) 44 hours

(d) 70 hours

(e) 92 hours

(f) 101 hours

(g) 116 hours

(h) 140 hours

(i) 164 hours

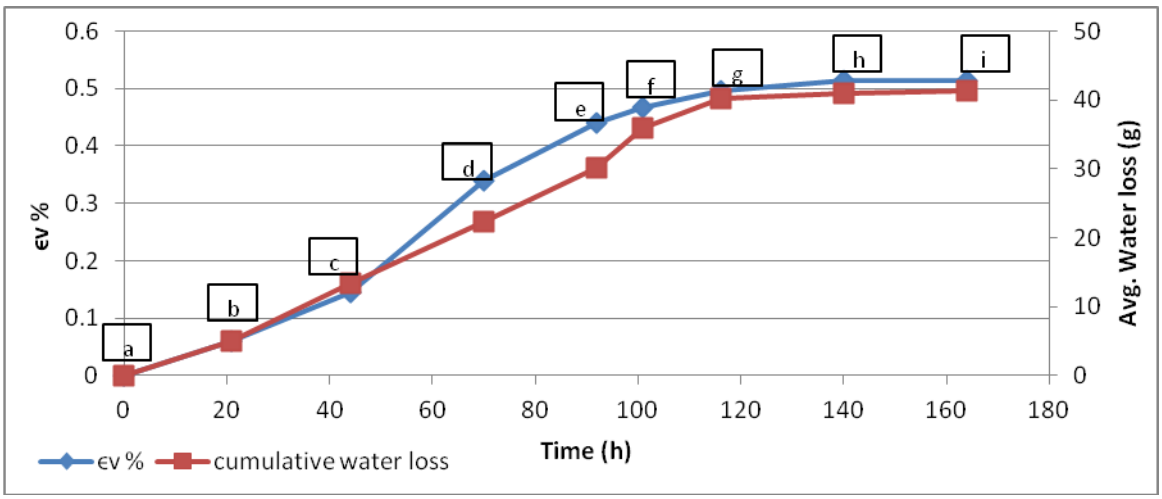

Figure A5.3. Volumetric strain and average water loss versus time (a mixture of 80% kaolinite with 20% of silica sand was prepared at 2.5×LL).

❖ Shrinkage stages during drying (a mixture of 80% kaolinite with 20% of silica sand was prepared at 3×LL)

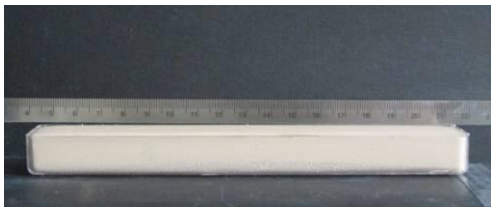

(a) Initial state

(b) 20 hours

(c) 46 Hours

(d) 70 hours

(e) 77 Hours

(f) 94 hours

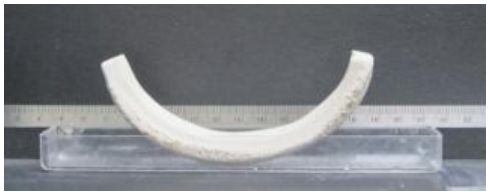

(g) 101 Hours

(h) 118 hours

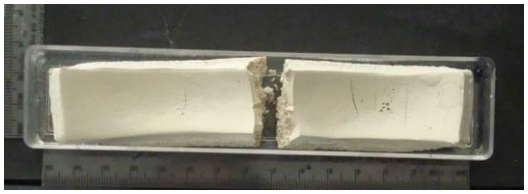

(i) 138 Hours

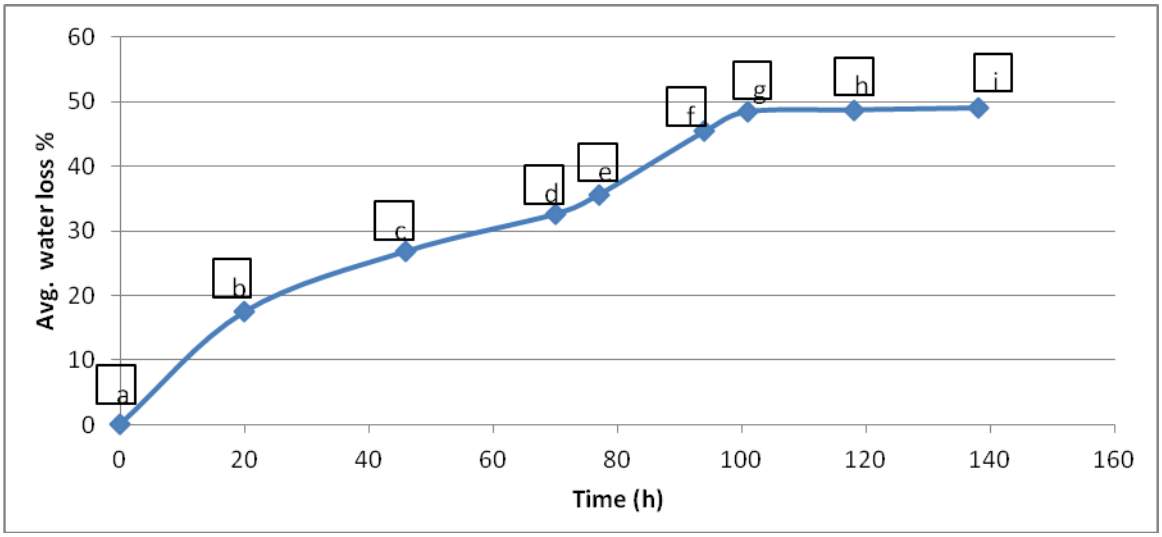

Figure A5.4. Volumetric strain and average water loss versus time (a mixture of 80% kaolinite with 20% of silica sand was prepared at 3×LL).

❖ Shrinkage stages during drying (a mixture of 90% kaolinite with10% of silica sand was prepared at 3×LL)

(a) Initial state

(b) 21 hours

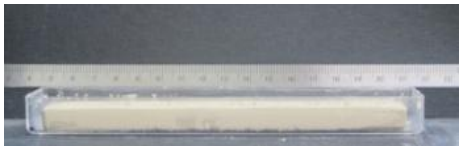

(c) 44 hours

(d) 70 hours

(e) 92 hours

(f) 101 hours

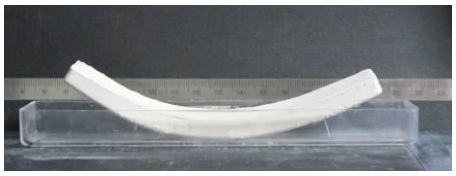

(g) 116 hours

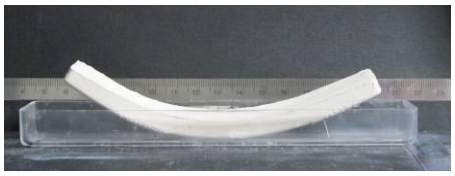

(h) 140 hours

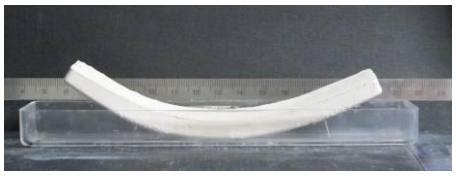

(i) 164 hours

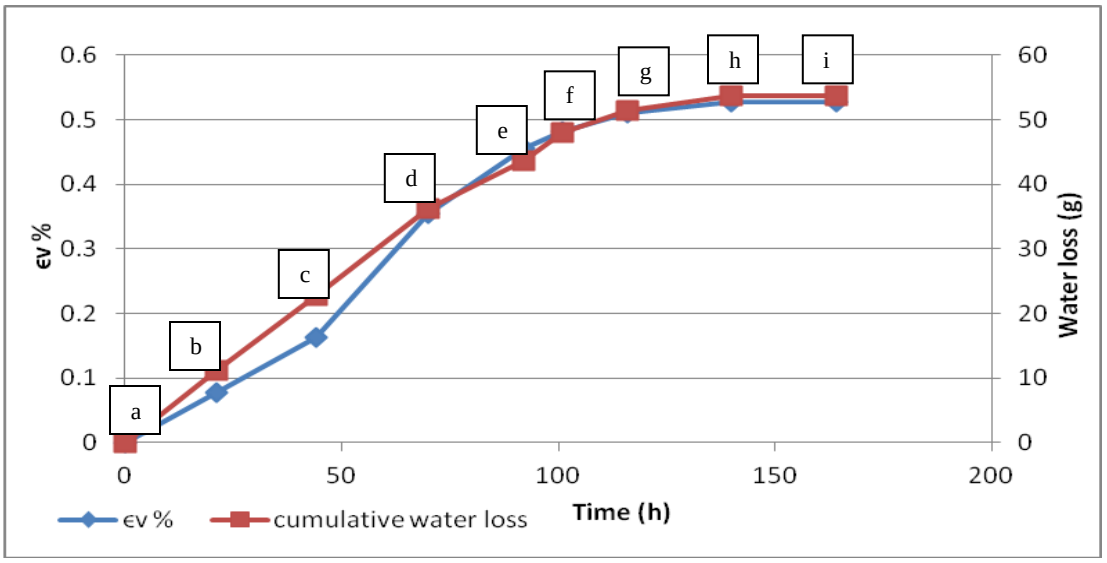

Figure A5.5. Volumetric strain and average water loss versus time (a mixture of 90% kaolinite with10% of silica sand was prepared at 3×LL).

- Shrinkage stages during drying (a mixture of 95% kaolinite with5% of silica sand was prepared at 3×LL)

(a) Initial state

(b) 21 hours

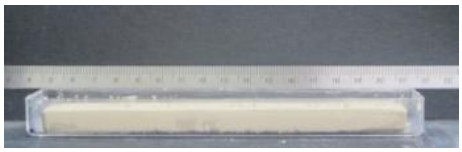

(c) 44 hours

(d) 70 hours

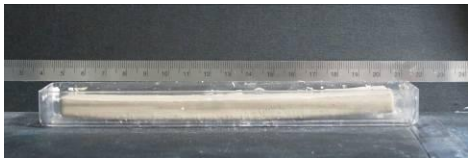

(e) 92 hours

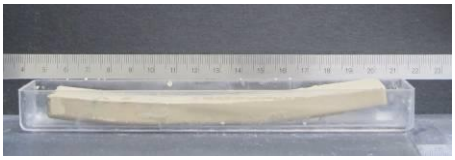

(f) 101 hours

(g) 116 hours

(h) 140 hours

(i) 164 hours

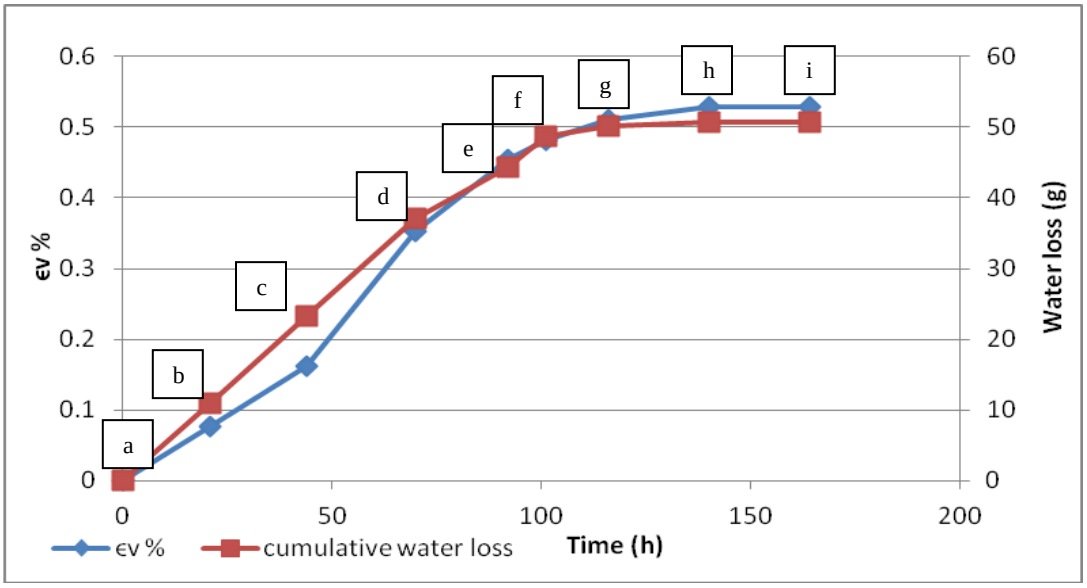

Figure A5.6. Volumetric strain and average water loss versus time (a mixture of 95% kaolinite with 5% of silica sand was prepared at 3×LL).